



**HAL**  
open science

# Spatiotemporal control of cooperation in yeast communities

Matthias Le Bec

► **To cite this version:**

Matthias Le Bec. Spatiotemporal control of cooperation in yeast communities. Mycology. Université Paris Cité, 2022. English. NNT: . tel-04062218

**HAL Id: tel-04062218**

**<https://hal.science/tel-04062218>**

Submitted on 7 Apr 2023

**HAL** is a multi-disciplinary open access archive for the deposit and dissemination of scientific research documents, whether they are published or not. The documents may come from teaching and research institutions in France or abroad, or from public or private research centers.

L'archive ouverte pluridisciplinaire **HAL**, est destinée au dépôt et à la diffusion de documents scientifiques de niveau recherche, publiés ou non, émanant des établissements d'enseignement et de recherche français ou étrangers, des laboratoires publics ou privés.



Distributed under a Creative Commons Attribution - NonCommercial - ShareAlike 4.0 International License

# Thèse

Pour obtenir le grade de **Docteur de l'Université Paris Cité**

Spécialité : **Sciences du vivant appliquées, biotechnologie et ingénierie des biosystèmes moléculaires**  
Ecole Doctorale Frontières de l'Innovation en Recherche et Éducation (ED 474) - Frontières du Vivant (FdV)

**Laboratoires Physico-Chimie Curie & Matière et Systèmes complexes**

# Spatiotemporal control of cooperation in yeast communities

Présentée par

**Matthias LE BEC**

Dirigée par **Pascal HERSEN**

Soutenue le 15 décembre 2022 devant le jury suivant :

**Mathieu Coppey** [rapporteur] (DR CNRS, Laboratoire Physico Chimie Curie, Paris)

**Robert Arkowitz** [rapporteur] (DR CNRS, Institut de Biologie Valrose – Université Côte d'Azur)

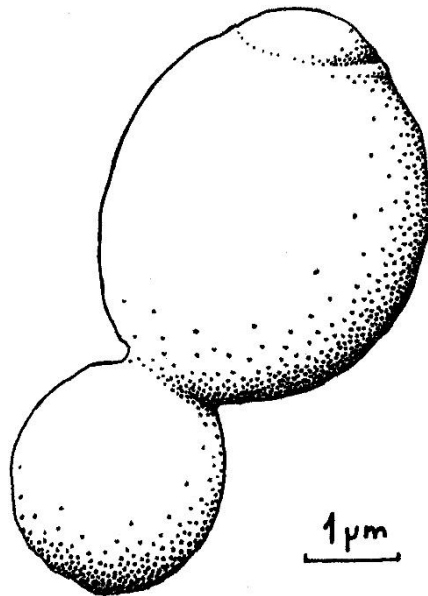
**Sébastien Léon** [examineur] (DR CNRS, Institut Jacques Monod - Université Paris Cité)

**Tâm Mignot** [examineur] (DR CNRS, Institut de Microbiologie de la Méditerranée - Aix-Marseille Université)

Pascal Hersen (DR CNRS, Laboratoire Physico Chimie Curie, Paris - Directeur de Thèse)







*Saccharomyces cerevisiae*

drawn from a scanning electron microscopy image made by the Lallemand company.



# Acknowledgements

I would like to thank my supervisor Pascal HERSEN for giving me the opportunity to work in his lab, for guiding my research while letting me take decisions, for his support and for sharing his valuable experience and expertise.

I would also like to thank the members of my Training Report Committee, Arnaud GAUTHIER and Sébastien LEON, who took the time to accompany me along these three years, both scientifically and professionally, importantly giving their insights on the profession of researcher which has broadened my perspectives.

I also had the chance to interact with Benoit SORRE and Karine GUEVORKIAN.

I would like to especially thank my co-workers, with whom I shared the daily joys and frustrations of experimental science. In addition to having been one of the most important sources of scientific interactions, they were also an incredible support for me during this period of emotional roller-coasters.

Among them I would like to thank in particular:

- Fabien DUVEAU for teaching me great knowledge both in fundamental and experimental microbiology, especially on our beloved *S. cerevisiae*.
- Céline CORDIER to run and organise all the experimental lab activities so smoothly. She is a true backbone for this team in many aspects and working together was very nice from start to finish.
- Sylvain POUZET to have shared this journey with me, it would have been so much more difficult without our quotidian jokes, scientific debates ideas and fun facts. Side by side, we grew up as scientists sharing our experiences along the way, trying to do our best and supporting each other during the occasional mental breakdowns.
- Alvaro BANDERAS for your enthusiasm for science, music and “the office”. Thanks for the frequent brainstorming sessions which allowed me to explore my work from a different angle.
- Lionel CHIRON for our collaboration, accompanied by great and various discussions on physics and technologies.
- Dimitrije MILUNOV for your unlimited sense of humour, and to have shared the modelling and equations-making process.
- Simon BARRAL for your calm and your jokes, and for helping me build my strains.
- I would also like to thank other non-permanents that work or have worked in the team: Gabriel, Kalina, Carine, Guillermo, Pierre-Louis, Vaibhav, Vincent, Hugo, Maud, Carolina and Jessie.

I am very grateful to have worked in such great scientific and human environments both at MSC and at the Physico-Chimie Curie laboratories.

I would also like to thank my family for supporting me throughout my academic career since the beginning, and for representing a solid anchor that I can always rely on. Thanks also to my friends, old friends from the "Sud-Ouest" and not-so-new friends from Chimie ParisTech and the fanfare Poulpe.

I would finally like to thank my companion Irina, whose unconditional and daily support was essential.

# Table of content

Acknowledgements.....	5
Abstract.....	9
Résumé.....	10
Scientific publications .....	11
Abbreviations and symbols.....	13
Introduction.....	15
1. Forewords.....	15
2. Diversity of microorganisms and their niches .....	17
3. Cooperation and division of labour in wild microbial communities.....	22
4. Control and engineer microbial communities.....	32
5. <i>Saccharomyces cerevisiae</i> and Sucrose .....	42
Chapter I – Engineering yeast for light-inducible control of cooperation.....	55
I.1. Optogenetics – Light sensitive transcription factor.....	55
I.2. Assemble DNA with Modular Cloning .....	60
I.3. Strains construction.....	62
I.4. Strains characterisation and optimisation .....	64
I.5. Residual sucrose utilisation .....	68
Chapter II – Microscopic spatial activation of SUC2 expression with light.....	71
II.1. Microfluidic device for microscopy observation.....	71
II.2. Image analysis - cell proliferation quantification.....	74
II.3. Spatial control of yeast growth in a microfluidic chamber.....	78
Chapter III - Pattern light on petri dishes with growth monitoring with the ‘ <i>OptoCube</i> ’ .....	85
III.1. OptoCube development .....	85
III.2. OptoCube performances characterisation .....	90
III.3. Modelling yeast growth on sucrose.....	96
III.4. Cooperators competition for sucrose.....	101
III.5. Cheaters competition for glucose.....	103
Chapter IV – Smart Microscopy, Cybersco.py: software for event-based, conditional microscopy ....	107
Conclusions and perspectives.....	121
Limitations.....	123
Perspectives.....	125
Résumé de thèse en français .....	133
References.....	139
Appendixes.....	155





# Abstract

Natural microbial communities can often be spatially structured, with different species that interact and grow in a heterogeneous manner. Even among clonal colonies, nutrient uptake, inhibitory chemicals excretion or chemical communication considerably affect the individual cell microenvironment leading to cell-to-cell phenotypic differentiation<sup>1,2</sup>. In both microbial ecology and evolution, spatial organization plays a key role in the population fate<sup>3-5</sup>. While recent works are progressing in the rational design of microbial communities<sup>6-9</sup>, there are few established methodologies to control, especially spatially, the functioning and development of microbial ecosystems.

*My PhD aims to get new insights in the role of spatial organisation in the interactions of microbial communities.*

To this end I designed and optimised a *Saccharomyces cerevisiae* yeast strain for **optogenetic control** of the **SUC2 invertase** production, allowing to induce the local production of **public goods** with blue light. I built a custom experimental device to create with light and observe through time **patterns of cooperator/cheater** cells and used it to investigate the influence of spatial organisation on the development of such consortia. I found that this cooperator/cheater consortium acts as a **spatial bandpass filter**, filtering out short spatial fluctuations of cheater/cooperator phenotypes but also large areas of identical phenotypes.

The results presented in this work show the importance of the **spatiotemporal structuration** in a cooperative system, due to **gradients** of diffusive molecules and **phenotypic heterogeneity** in the cell population. This represents a step toward better characterisations of microbial interaction **length scales** which can serve to deepen our understanding of natural microbiomes and to help designing synthetic ones.

**Keyword:** Synthetic biology, Optogenetics, *Saccharomyces cerevisiae*, Cooperation, Sucrose, Spatial Patterning, Microfluidics, Microbial communities

# Résumé

Les communautés microbiennes naturelles sont souvent structurées spatialement, avec différentes espèces qui interagissent et se développent de manière hétérogène. Même dans le cas des colonies clonales, le microenvironnement individuel des cellules est affecté par la consommation des nutriments, l'excrétion de molécules inhibitrices ou les communications chimiques, menant à une différenciation phénotypique entre les cellules<sup>1,2</sup>. Dans les domaines de l'écologie et de l'évolution microbienne, l'organisation spatiale joue un rôle déterminant dans le destin d'une population<sup>3-5</sup>. Malgré les récents travaux portant sur le design rationnel de communautés microbiennes<sup>6-9</sup>, il y a par contre peu de méthodologies établies pour contrôler, surtout dans l'espace, ces associations microbiennes.

*L'objectif de ma thèse est de mieux comprendre le rôle de l'organisation spatiale dans les interactions des communautés microbiennes.*

Pour se faire j'ai construit et optimisé une souche de levure *Saccharomyces cerevisiae* pour le **control optogénétique** de la production d'**invertase SUC2**, permettant d'induire la production locale de **bien commun** avec de la lumière bleue. J'ai construit un équipement expérimental sur mesure pour créer avec la lumière et observer au fil du temps des **patterns de cellules coopératrices/tricheuses** et je l'ai utilisé pour étudier l'influence de l'organisation spatiale sur le développement de ce genre de consortia. J'ai trouvé que ce consortium de coopérateur/tricheur se comporte comme un **filtre spatial passe-bande**, filtrant les fluctuations spatiales courtes de phénotypes coopérateur/tricheur mais aussi les larges régions de phénotypes identiques.

Les résultats présentés dans ce travail montrent l'importance de **la structuration spatiotemporelle** dans les systèmes coopératifs, due aux **gradients** de molécules diffusibles et à l'**hétérogénéité phénotypique** dans la population de cellules. Cela représente un pas vers une meilleure caractérisation des **échelles spatiales** des interactions microbiennes qui peut servir à approfondir notre compréhension des microbiomes naturels et à aider le design de microbiomes synthétiques.

**Mots-clés** : Biologie synthétique, Optogénétique, *Saccharomyces cerevisiae*, Coopération, Sucrose, Structure spatiale, Microfluidie, Communautés microbiennes

# Scientific publications

## First author:

**[in preparation] Spatio-temporal optogenetic control of yeast cooperation for sucrose catabolism**

M Le Bec, S Pouzet, C Cordier, S Barral, B Sorre, A Banderas, P Hersen.

**[published] Cybersco.py: software for event-based, conditional microscopy (2022)**

M Le Bec, L Chiron, C Cordier, S Pouzet, D Milunov, A Banderas, J Di Meglio, B Sorre, P Hersen – Scientific Reports **12**, 11579.

## Other scientific contributions:

**[published] Autonomous and assisted control for synthetic microbiology (2020)**

A Banderas, M Le Bec, C Cordier, P Hersen - International Journal of Molecular Sciences **21** (23), 9223.

**[published] The promise of optogenetics for bioproduction: dynamic control strategies and scale-up instruments (2020)**

S Pouzet, A Banderas, M Le Bec, T Lautier, G Truan, P Hersen - Bioengineering **7** (4), 151.

**[in revision (Front. Bioeng. Biotechnol.)] Optogenetic control of beta-carotene bioproduction in the yeast *Saccharomyces cerevisiae***

S Pouzet, J Cruz-Ramon, M Le Bec, C Cordier, A Banderas, S Barral, S Castano-Cerezo, T Lautier, G Truan and P Hersen.

**[in preparation] Optogenetic control of pheromone signalling in budding yeast**

A Banderas, M Hofmann, C Elizondo, M Le Bec, P Hersen.



# Abbreviations and symbols

- **Fitness:** the quantitative representation of an individual reproductive success, usually defined in comparison with a reference strain by performing competition experiments.
- **Hexoses:** Sugar molecules composed of six carbon atoms. In the context of sucrose hydrolysis, hexoses usually refer to glucose and fructose.
- **Microbiota:** the set of microorganisms found in a given environment
- **Microbiome:** the set of microorganisms and their genomes found in a given environment. Microbiome is thus more precise than microbiota: in addition to the list of species, the strains are accounted for.
- **Phenotypic variation:** among a population with identical genetics, there are variations in the expression of this genetic information, or phenotypes, between different cells.
- **DMD:** Digital Micro-mirror Device. It allows to project defined patterns of light by controlling its reflexion pixel by pixel.
- **DoL:** Division of labour. Defined and detailed in the introduction part 3.
- **ELM:** Engineered Living Material. Defined and detailed in the introduction part 4.
- **PIV:** Particle Image Velocimetry. Image analysis technic used to quantify cell growth. Detailed in the Chapter IV.2.
- **PDE:** Partial Differential Equation.



# Introduction

## 1. Forewords

I have always been quite fascinated by the existence of cooperative systems in nature and consider their functioning as an inspiration for human societies. Although the notion of cooperation can be seducing to explain the efficiency of a system, a quantitative exploration of the constraints and benefits of such strategies must be performed. The present work is an example of such investigation applied to the study of microorganism cooperative communities. The emergence of synthetic biology tools and concepts motivated me to investigate experimentally the engineering of cooperation of microbial systems.

I chose to study microorganisms for multiple reasons. They are growing fast, some species are easy to modify genetically, there is a furnished literature on microbial cooperation, and microorganisms represent a great potential for biotechnologies and bioproduction. Pascal HERSEN and I wanted, in the framework of this PhD, *to explore and get new insights in the role of spatial organisation in cooperating communities of microorganisms*. Initially, I was planning to study bidirectional cooperation systems, where two different strains would exchange nutrients or share essential tasks. The strategy would have consisted in controlling their spatial organisation (for example using light controlled cell adhesion), imposing various patterns to interrogate how space influences the consortium cooperation performances. Although potentially feasible, we decided to simplify the experimental system. Instead of controlling two different strains, we decided to control the phenotypic state of a single strain at selected locations. Specifically, we focused on a natural cooperation mechanism in the yeast *Saccharomyces cerevisiae*, the public goods release by the invertase SUC2 during sucrose hydrolysis, a system that has already been studied and characterised in well-mixed liquid cultures.

*During my PhD, I designed and optimised a Saccharomyces cerevisiae yeast strain for optogenetic control of the SUC2 invertase production, allowing to induce the local production of public goods at selected locations with blue light illumination. I built a custom experimental device to create with light, and observe through time, patterns of cooperator/cheater cells. I used this tool to investigate the influence of spatial organisation on the development of a cooperator/cheater consortium in yeast. I found that such a consortium acts as a spatial bandpass filter, filtering out short spatial fluctuations of cheater/cooperator phenotypes but also large areas of identical phenotypes.*

My work is mostly applied System Biology, aiming at answering how to experimentally control a multicomponent biological system predictably. I had to learn and work with a great diversity of experimental and theoretical skills: cloning, molecular biology,



population dynamics, evolution of cooperation, game theory, control theory, numerical simulation, coding, microfluidic fabrication, imaging, microscopy, instrumentation, and electronics. This interdisciplinary aspect is double-edged: combining multiple fields helps look afresh at already known phenomena and can yield novel scientific results<sup>10</sup>, but exploring scientific worlds with different terminologies and formalisms is also challenging. I am convinced that Science should be less compartmentalised, as the discipline's limits are likely subjective or artificial.

The present manuscript is organised as follows. I start by giving a brief and broad overview of the microbiology world and then discuss cooperative interactions in microbial communities, and how and why to engineer such systems. I end this introduction with a summary of the scientific literature on *S. cerevisiae* in relationship with sucrose utilisation. Then, I present my PhD work starting with the engineering and the characterisation of the yeast strains I designed to get an optogenetic control of invertase production. I then explore the spatial properties of the system at the microscopic scale using microfluidic tools. In the third Chapter, I present the tool I have developed to study the impact of spatial structuration in yeast communities at a larger scale. In this chapter, I describe the experimental results obtained by exploring the spatial properties of the light induced cooperator/cheater system and give details on the mathematical model and numerical simulations I set up. The last chapter describes the software we developed for "smart microscopy", a side project of my PhD. I finish this manuscript by summarizing my contributions and discussing the limits and the future of the scientific fields explored during my PhD.

## 2. Diversity of microorganisms and their niches

### “Microorganism” - what do microorganisms have in common?

Microorganisms or microbes represent a very diverse group of species<sup>i</sup>. It gathers all prokaryotes (unicellular) with some eukaryotes (unicellular and multicellular) (**Figure 1**). Their metabolic capabilities and functioning are also very diverse, as they can be chemoheterotrophs<sup>ii</sup> (saprophytes<sup>iii</sup>, pathogens, parasites, ...), photoheterotrophs<sup>iv</sup> (some bacteria), photoautotrophs<sup>v</sup> (cyanobacteria, microalgae) or chemoautotrophs<sup>vi</sup> (some archaea and bacteria, usually extremophiles). Microbes can have different sizes and extend over a large range of length scales, from hundreds of nanometers<sup>13</sup> for some bacteria and archaea to kilometers for filamentous fungi with, for example, a clonal mycelium network of *Armillaria ostoyae* spreading over ~10 km<sup>2</sup>, one of the largest single living organisms based on area reported<sup>14</sup>.

Microorganisms are found almost everywhere on earth, even in the most extreme habitats such as volcanic sites<sup>15,16</sup>, deep seafloor sediments<sup>17</sup> (~5km under sea level and 70m under the seafloor) and atmospheric water clouds<sup>18,19</sup>. We can identify two main microbe lifestyles: planktonic and sessile (*i.e.* immobile). They differ mainly by nutrient accessibility and cell crowding. Planktonic organisms are suspended in liquid, which is usually homogenized by mixing, reducing the variation of nutritive conditions in space. As a consequence, their fitness is not directly influenced by short-scale social interactions. In contrast, organisms that live in still environments (*e.g.* solid substrates) are almost always surrounded by multiple cells, from the same or different species. Sessile niche examples range from still liquid (pond), soil, submerged or open-air surfaces, organic tissues (pathogens, saprophytes, ...) to host organisms' digestive systems. The main characteristic shared between these niches is the absence of strong convective fluxes, which allows cells to stay together and form multicellular colonies. In these conditions, nutrients can reach the cell's microenvironment through diffusion.

---

<sup>i</sup> This manuscript lacks virology aspects, focusing on bacterial and fungal microbiology. It is still worth noting that most viruses do not have their own metabolism, which is viewed as if they have a negligible direct impact on the chemistry of their microenvironment. They can however impact greatly microbial systems indirectly<sup>11,12</sup>, notably by influencing their host metabolism, or provoking nutrient bursts when killing hosts.

<sup>ii</sup> Chemoheterotrophs are organisms that obtain their energy from a chemical reaction and use organic compounds as the source of carbon.

<sup>iii</sup> Saprophytes are organisms which obtain nutrients from dead organic matter or wastes.

<sup>iv</sup> Photoheterotrophs are organisms that use light for energy but cannot use carbon dioxide as their sole carbon source.

<sup>v</sup> Photoautotrophs are organisms that use light for energy and can use carbon dioxide as their sole carbon source.

<sup>vi</sup> Chemoautotrophs are organisms that obtain their energy from a chemical reaction and can use carbon dioxide as their sole carbon source.

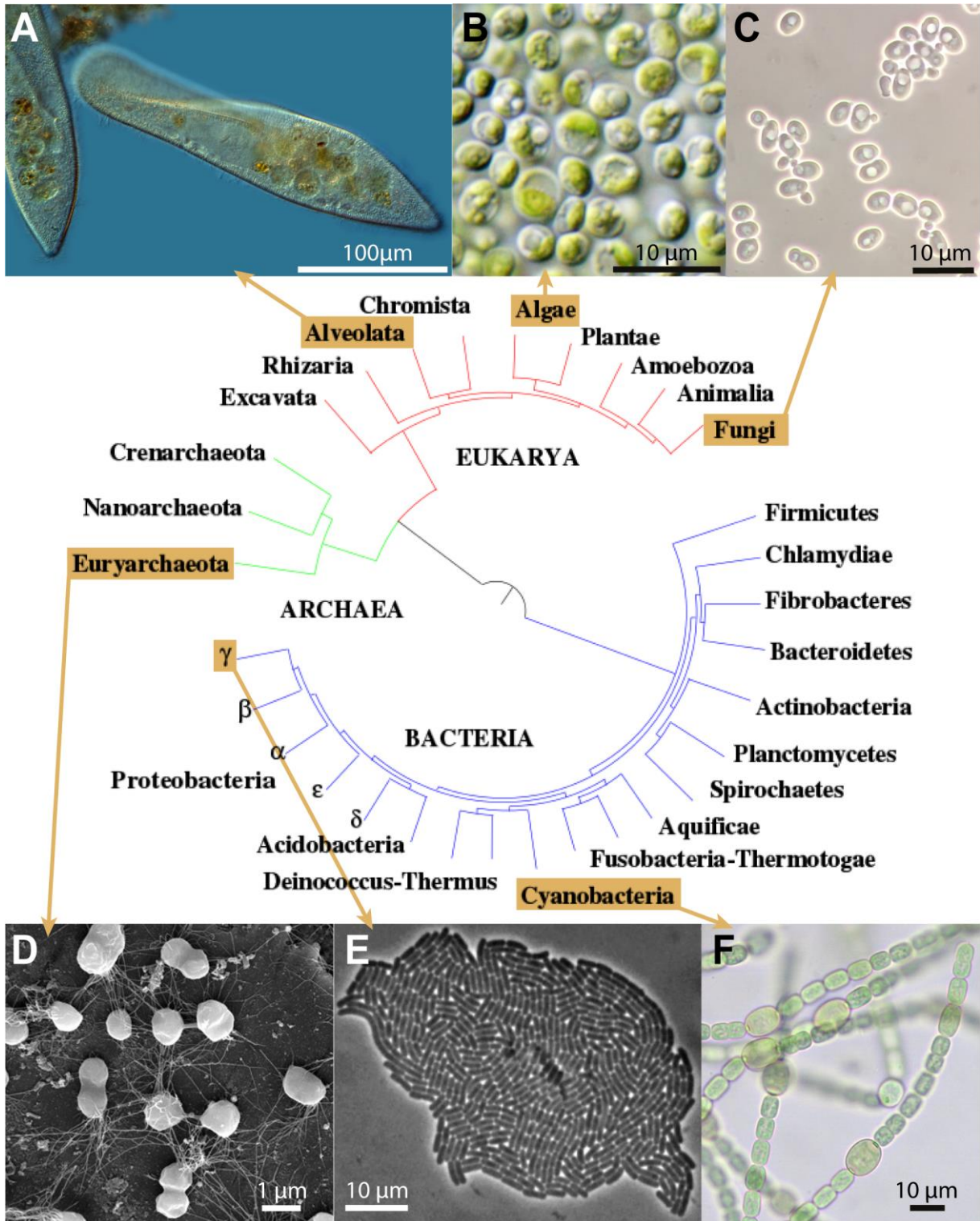


**Figure 1 – Microorganism phylogeny.** Contextualisation of various microorganisms in the tree of life representing evolutionary relationships between different phyla. (A) *Paramecium caudatum*<sup>20</sup>. (B) *Chlorella vulgaris*<sup>21</sup>. (C) *Saccharomyces cerevisiae*. (D) *Pyrococcus furiosus*<sup>22</sup>. (E) *Escherichia coli*<sup>23</sup>. (F) *Anabaena azollae*<sup>24</sup>.

In addition, some microbes are motile, exploring their environment to reproduce and/or to find nutrient sources. *Paramecium* can for example swim at  $\sim 2$  mm/s<sup>25</sup> whereas motile *E. coli* velocity peaks at around  $66 \mu\text{m/s}$ <sup>26</sup>. It is also worth noting that several microorganism species can go through both sessile and mobile lifestyles depending on their needs or their reproduction cycles<sup>27</sup>. Microbes that are not motile can still be dispersed by abiotic factors (rain, wind) or transported by motile organisms (insects or animals), allowing them to invade new regions. There are numerous examples<sup>28–30</sup> of microorganisms that attract motile organisms by producing odorant molecules. It has also been shown that *S. cerevisiae* can generate fluid flows when growing on viscous liquids by consuming nutrients and decreasing the local substrate density<sup>31,32</sup>.

### Sessility and diffusion

The **diffusion of molecules in solution** is a process governed by gradients of chemicals which are determined by the spatial positions of **sources** and **sinks** of chemicals. A source refers to the production of a molecule at a given location (for example a decaying organism or an organism releasing metabolic wastes). A sink refers to the removal of a molecule at a given location (examples are cell nutrient consumption or chemical degradation). A sessile microbial community is both a sink and a source of chemicals occurring at different locations and setting up landscapes of phenotypes and chemical gradients, with transitory or stationary profiles across the colony. The colony geometry, the chemical gradients and the colony metabolic state are linked.

Numerous bacteria and yeast grow as circular colonies on agar gel media, typically used for laboratory experiments. Starting from a single cell or few cells, successive mitotic divisions exponentially produce daughter cells which, by physical hindrance and surface tension, will spread and form a flat cone-shaped colony. Once the colony reaches a certain size, the nutrient consumption in its centre is greater than what can diffuse through the gel. This inter-competition marks the end of the exponential growth phase and the beginning of a linear, radial expansion<sup>33,34</sup>. Indeed, cells in the center of the colony cannot grow because they are starved: the colony can only grow at its periphery.

Observing the growth of a yeast community composed of two non-cooperating strains can highlight how radial growth can organise the colony in space, forming large radial stripes of clonal individuals<sup>35,36</sup> (**Figure 2.B**). In addition, M. Müller *et al.* (2014)<sup>36</sup> showed that when a mutualistic metabolic interaction between the strains was added to the system (exchange of amino acids), the resulting colony of such a consortium exhibited a different spatial organisation (**Figure 2.D**). The latter spatial organisation consisted of multiple clonal patches that never exceeded  $\sim 50 \mu\text{m}$ , corresponding to an optimized structure for nutrient exchange by diffusion. They also showed that when reducing the dependency of these strains on the

cooperative trait, the size of the patches increases gradually. This study nicely illustrates how the structure of a microbial consortium is determined by interdependent spatial parameters: colony geometry, nutrient availability and metabolic activity.

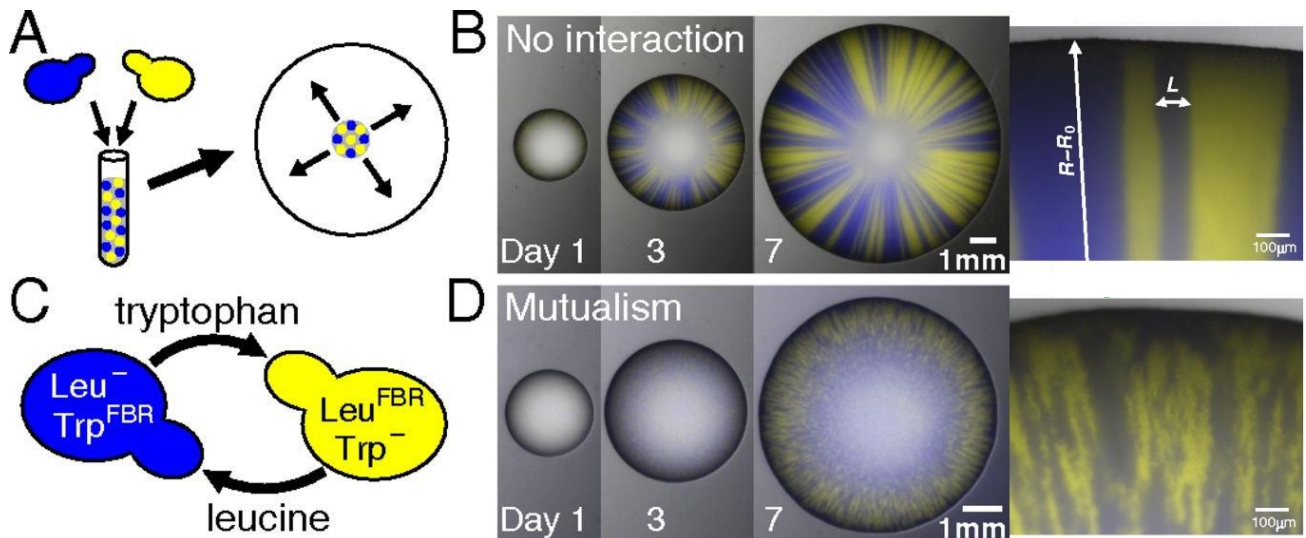


**Figure 2 - Spatial heterogeneity of yeast colonies growing on nutritive gels.** (A) Scheme of the plating protocol. (B) Fluorescent images of the colony expansion of two noninteracting yeast strains. (C) Scheme of the engineered mutualistic system: co-dependency for amino acid production (tryptophan and leucine). (D) Fluorescent images of the colony expansion of two cross-feeding yeast strains. Figure extracted from M. Müller *et al.* (2014)<sup>36</sup>.

Although a circular shape is common for small colonies (< 2 cm), larger colonies usually exhibit more complex morphologies. These morphologies typically emerge from a circular colony which experienced instabilities at their growing front, resulting in symmetry breakings. The emergence of asymmetry can be due to various mechanisms, one of which is diffusion-limited growth. For example, in *bacillus subtilis* colonies, diffusion-limited growth leads to dense-branching morphology patterns<sup>37</sup> with various shapes depending on the nutrient concentration (**Figure 3A**) and the gel stiffness. This is explained by growth inhibition due to the local depletion of nutrients at high cell density locations, restricting the cell growth to the tip of the colony branches. As a consequence, the colony morphology is related to various behaviours: growth repulsion between different colonies and directed growth toward nutrient sources. Such morphologies and behaviours can be obtained mathematically using reaction-diffusion equations<sup>37,38</sup> and taking into account only a few parameters (nutrient diffusivity, cell diffusivity and initial nutrient concentration).

I would also like to mention some of the morphologies found in *S. cerevisiae*, which can tune the physical properties of their colonies thanks to their adhesin proteins exhibited at the cells' external surface (FLO gene family). The resulting colony morphologies can differ quite strongly from spherical colonies (**Figure 3B, C, D**). Interestingly, such complex geometries are only triggered in certain nutritious conditions and ploidy states<sup>39</sup>.

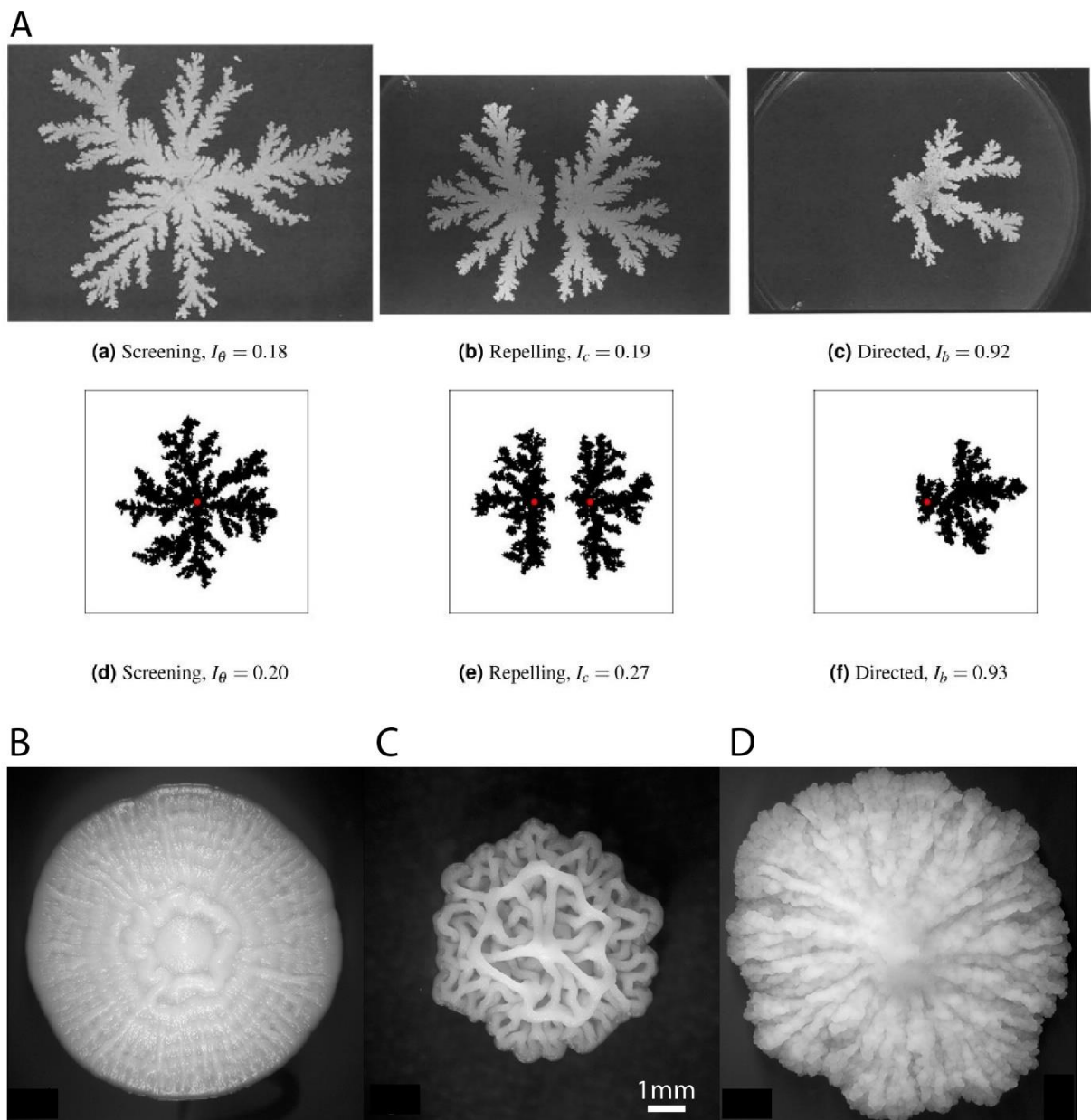


**Figure 3 – Microbial colony morphologies.** (A) Dense-branching morphology of *bacillus subtilis* colonies on gel media due to diffusion-limited growth. (a) Branching pattern with unbiased directions obtained when grown on a gel with homogeneous nutrient concentration. (b) Repelling pattern obtained when two colonies are inoculated close together. (c) Directed pattern obtained when nutrients are added asymmetrically to the right of the plate. (d), (e) and (f) are the corresponding simulation results for (a), (b) and (c) respectively.  $I_\theta$ : angular index of non-uniform growth, larger values indicate greater levels of non-uniform growth.  $I_c$ : index of repulsion, smaller than 0.5 when a gap forms, and greater than 0.5 when the colonies show a preference for growth towards each other.  $I_b$ : the proportion of cells on the right-hand side of the domain relative to the total number of cells. (B,C,D) Pictures of *S. cerevisiae* colonies for three strains with different morphologies. (B) “spokes” (with weak concentric rings in this case)(OS17, YEPLD, day 6). (C) “lacy” (YJM311 on YEPLD, day 6). (D) (E) mountainous (PMY348, 4% agar YEPD, day 6). Figure extracted from<sup>37,39</sup>.

### 3. Cooperation and division of labour in wild microbial communities

All living organisms are inherently competitive, favouring their own evolutionary success even (or especially) if it impairs their competitors. Yet, cooperation behaviours are widespread among the living world<sup>40,41</sup>, observed at different levels such as cooperation of: organelles in eukaryotic cells, cells in multicellular organisms, animals in complex societies... A cooperator is an entity that pays a fitness cost to produce a benefit for another entity's fitness. This formulation can seem counter-intuitive with regard to natural selection principles, and one might think that a cooperator should be outcompeted by "selfish", fitter, individuals. However, the emergence of cooperation can indeed be explained by natural selection, either relying on direct fitness benefits, indirect fitness benefits or both.

Direct fitness benefits are usually straightforward to grasp: the cooperative behaviour directly increases the fitness of its actors. For example, bacteria that produce and form a biofilm are less sensible to certain stresses<sup>4</sup>, thus directly increasing their own survival chance. However, indirect fitness benefits are less intuitive, as they concern the cooperation recipients, and I will focus mainly on these in the following parts.

#### Kin selection

Kin selection has been defined and described by Hamilton<sup>42,43</sup>: it is a process allowing the evolutionary emergence of cooperation that can happen through different mechanisms (e.g., kin discrimination and limited dispersal.). Importantly, he defined a rule describing the necessary conditions for kin selection: **altruistic cooperation can be favoured if the benefits to the recipient (b), weighted by the genetic relatedness of the recipient to the actor (r), outweigh the costs to the actor (c), or  $r \cdot b > c$** . The cost c represents the direct negative fitness consequences and  $r \cdot b$  the indirect fitness benefit. To better understand this, one must know that relatedness (r) is a statistical concept, describing the genetic similarity between two individuals, relative to the average similarity of all individuals in the population. Krebs (1987)<sup>44</sup> wrote the following sentence to better explain the importance of relatedness: *"The reason why relatedness is important in Hamilton's formula is because the coefficient of relatedness between two individuals is equivalent to the probability that they share a gene for altruism, not because they share a high proportion of other, non-altruistic genes."* However, focusing only on r can lead to misunderstandings since variations in b and c can be equally important. One important point is that relatedness matters mainly when genes underlying kin altruistic behaviour first emerge and become selected, whereas once it reaches fixation in the population, virtually all individuals will present the cooperative gene resulting in homogeneous relatedness in the population<sup>45</sup>.

Some recent misunderstandings in the literature<sup>46,47</sup> were confusing the scientific consensus on the limits of kin selection, and whether it is the only indirect process explaining the evolution of cooperation. It seems that kin selection is indeed the only process allowing the evolution of cooperation, as other concepts such as group selection are in fact referring to kin selection but analysed in another mathematical framework (multilevel selection).

Taken together, any cooperative system can emerge if it favours itself (the system), by favouring the cooperation recipients that have the highest probability to also cooperate. I will now give brief examples of kin selection mechanisms for the emergence of cooperation.

### *Reciprocity: Enforced cooperation*

Reciprocity mechanisms favour cooperation because they stabilise it but do not necessarily help it to emerge or spread in populations. They include both direct reciprocity where individuals prefer to help those who help them and indirect reciprocity where individuals help those that help others. These reciprocities can also be negative: cooperators can avoid or punish cheaters. The example of cleaner fish *Labroides dimidiatus* presents multiple of these processes: host reef fish will avoid cheaters (who feed on the host mucus instead of its ectoparasites), punish cheaters and switch partners when cheating occurs<sup>48,49</sup>.

### *Kin discrimination*

Kin discrimination mechanisms are possible when an individual can distinguish relatives from non-relatives and preferentially direct aid towards them. Kin discrimination can occur through the use of environmental or genetic cues. For example, bacteria extensively use genetic cues to favour kin selection using toxin-antitoxin systems, releasing a specific bacteriocin only they and their relatives can counter-act<sup>50</sup>.

The famous example of the Green Beard gene<sup>51</sup> is a particular case of kin discrimination: it represents an assortment mechanism, requiring a single gene — or a number of tightly linked genes — that both encodes the cooperative behaviour and causes cooperators to associate. For example in the yeast *Saccharomyces cerevisiae*, the FLO1 gene encodes cell-surface adhesins which allow preferential flocculation with FLO1 positive cells<sup>52</sup>. In addition, this gene is highly variable among strains such that non-relative cells secrete incompatible FLO1 proteins. Green Beard genes are also notably encountered for inter-species kin selection in bacteria as they can transfer plasmid genes horizontally<sup>53</sup>.

### *Limited dispersal*

Limited dispersal (sometimes referred to as population viscosity or structure) can generate high degrees of relatedness between interacting individuals because it tends to keep relatives together. This mechanism is critical in microorganisms<sup>54</sup>. Although limited dispersal can maintain relatives together to cooperate, it also forces them to compete for nutrients which can be deleterious. One way of seeing this concept is to consider that this concomitant



competition reduces the benefit (b) of helping relatives. As mentioned in the previous section, microbial dispersal and the resulting colony morphology depend on multiple factors, among which competition for nutrients is crucial. Thus again, microorganisms with limited dispersal need to find a trade-off between cooperation and competition to perform sustainably.

### Microorganism communication – microbial collective phenomena

Although most microbes are classified as unicellular organisms, they usually thrive within complex multicellular systems. Single cell fates depend strongly on the population organisation. As already described in the previous sections, competition for nutrient access is one of the most impactful cell-cell interaction encountered in microbial consortia. These collective interactions are usually very dependent on cell density, one of the most important parameters as it directly influences the global molecule production and consumption rates within the population. Thus, some microbes evolved means to sense local cell density to appropriately behave relative to the population state. This process, known as “Quorum Sensing”, is mostly performed through the sensing of secreted molecules, either microbial growth by-products or specific signalling molecules, called autoinducers. While there are evidence for inter-specific quorum sensing communication<sup>55,56</sup>, we will focus on the intra-specific one as it is more common.

Quorum sensing refers to behaviours that are only induced when a minimal population density is reached. This is performed by cells as follows: production and release of a signal molecule, accumulation of the signal in the microenvironment, sensing of the signal by specific receptors and downstream response. In practice, quorum sensing actually summarizes two antithetic components: population size (Quorum Sensing) and molecule renewal (Diffusion Sensing)<sup>57</sup>. Indeed, as quorum sensing systems rely on diffusible molecules, the experienced signal concentration can be reduced by chemical diffusion or liquid fluxes<sup>58</sup>. A unifying view of Quorum Sensing has been proposed as “Efficiency Sensing”<sup>59</sup>, measuring the combination of cell density, spatial distribution and diffusive/convective flux, whose function is to test the local efficiency of producing costly diffusible extracellular molecules.

In addition, the sensing and regulatory circuitry downstream of quorum sensing can be complex, mostly directed toward gene transcription regulation. The circuit’s outputs depend on the local signal concentration, quantitatively or as threshold detection (using a positive feedback), sometimes integrating multiple microbial signals, enabling to perform precise and complex biological functions in adequation with the current cell constraints. For example, the pathogenic *Vibrio cholerae* produces two different autoinducer molecules to regulate virulence factor production<sup>60</sup>, biofilm formation<sup>61</sup> and metabolic activity<sup>62</sup>. To do so they use four different receptors, whose redundancy could stabilise the system in case of receptor interference by exogenous molecules<sup>63</sup>. Similarly, the pathogenic *Pseudomonas*

*aeruginosa* uses two acyl-homoserine lactone signals (AHLs) to control virulence factor production, cell growth rate and motility. Interestingly, these *Pseudomonas* quorum sensing systems actually integrate several global regulators, allowing them to sense a broader range of environmental cues<sup>64</sup>. However, the autoinducer-receptor interactions are not necessarily very specific, for example in *Streptococcus pneumoniae* where evidence of eavesdropping (sense signals from other strains) and crosstalks (signal is sensed by other strains) have been reported<sup>65</sup>. This quorum sensing control bacteriocin production allowing these bacteria to manage competition between strains of the same species.

Quorum sensing can also serve to organise a biofilm in space. Different morphologies can be obtained depending on the system parameters (number of signals, diffusion rate, downstream processing). For example, simple simulations<sup>66</sup> show that a single signal system can lead to patterns that depend on the external shape of the colony (follow the contours) and a two signal system can lead to a shape independent pattern, while both are independent of the population size (**Figure 4**).

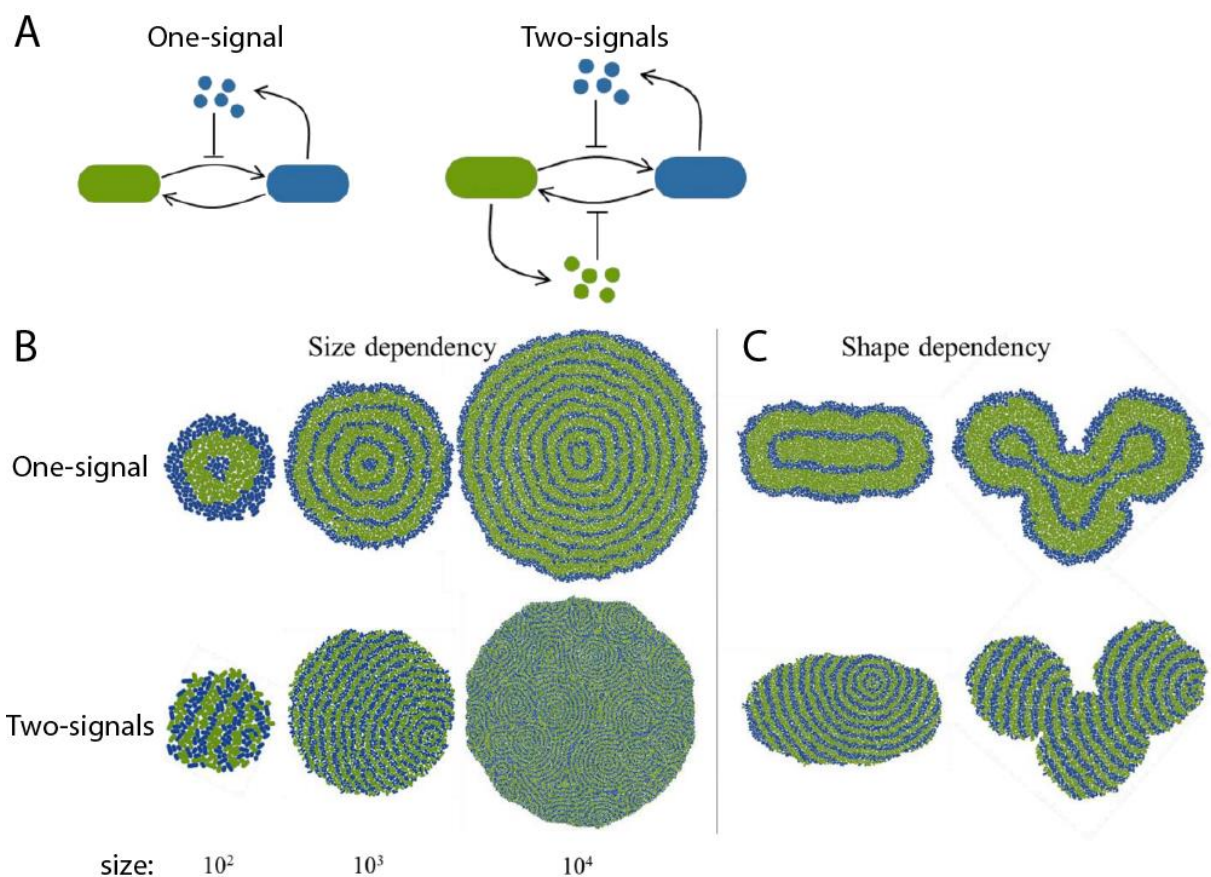


**Figure 4 – Simulation results for a one-signal and a two-signal quorum sensing system that control the state of bacteria cells (either blue or green).** (A) Network motif of the one and two-signal quorum sensing model. (B) Both systems lead to patterns independent of population size. (D) Only the one-signal system result in patterns which depend on the population shape. Results obtained using the agent-based model *gro* that simulates the growth and interaction of cells in a two-dimensional bacterial colony. Figure extracted from<sup>66</sup>.

We can also mention yeast sexual reproduction, which uses diffusive pheromones to communicate and trigger mating. In *Saccharomyces cerevisiae*, haploid cells can be either an a-cell or an alpha-cell, corresponding to their sex. Importantly, they can occasionally switch from one to the other sex. Mating occurs only between an a-cell and an alpha-cell, which produce sex-specific peptide pheromones: a-factor or alpha-factor respectively. These pheromones can be sensed by the opposite sex thanks to a cell surface receptor that triggers the mating pathway response: growth arrest, “shmooing” (protuberance formation), and cell mating. The role of the pheromones is to trigger mating only if the cell surrounding allows successful mating. Interestingly, the alpha-factor is degraded by a protease (Bar1) only produced by a-cell, whereas no such active degradation is observed for a-factor. While it is still debated, the asymmetry of this pheromone system suggests that each pheromone has a different function. Interestingly, the antagonist effect of one sex producing a pheromone and the other producing the corresponding protease can result in a sex-ratio detection (Figure 5).

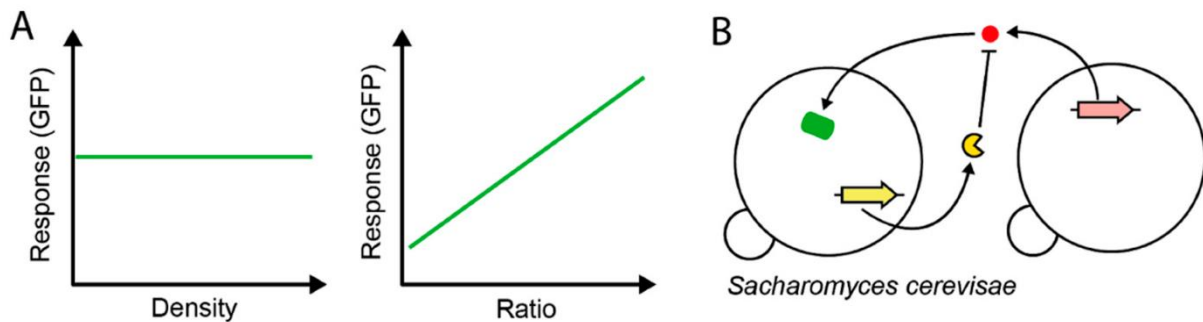


**Figure 5 - Relative sensing of population parameters.** (A) Theoretical perfect ratio sensing. The mean gene expression output of a reporter population (Response) is insensitive to changes in the total density of the co-culture, but sensitive to the relative abundance of the individual populations. (B) Intercellular signalling networks of *S. cerevisiae* mating. A stimulatory signal (red circle) accumulates in the media in proportion to the density of the signal emitter and stimulates green fluorescent protein (GFP) production. The concentration of the signal also depends on antagonistic activity, an extracellular protease (yellow), which balances out activation. Figure extracted from<sup>67</sup>

## Public goods

Public goods refer to a produced resource that is freely accessible to all individuals in a population. This cooperative trait is usually costly for the cells that produce the public goods, which makes such systems susceptible to cheater invasion. Indeed, game theory and experimental studies showed how public goods systems in microbes can be unstable when cheating occurs, leading to cooperator extinction. This is the case for the model of this PhD, the invertase excretion in yeast releases hexoses acting as public goods. Gore *et al.* (2019) studied this system of cooperation in liquid culture varying the cooperation cost and how efficiently this investment pays back to the cooperators<sup>68</sup>. They showed that for large cooperation cost or low efficiencies, cooperators were led to extinction (**Figure 6**).

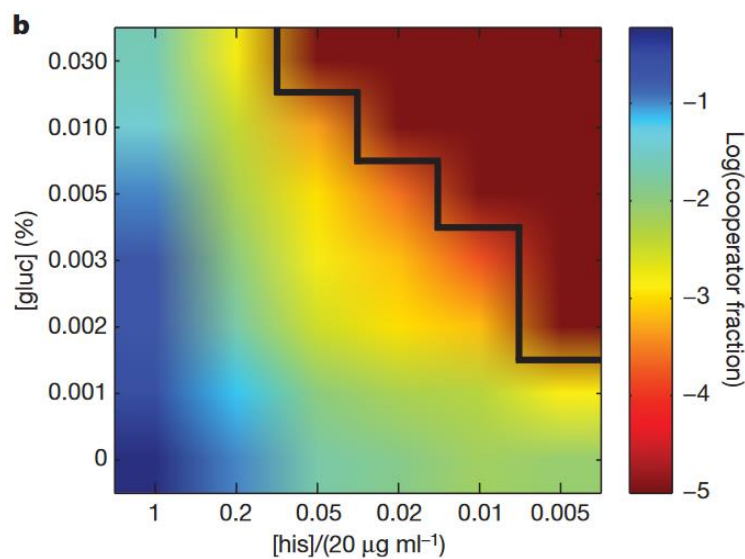


**Figure 6 - Outcome of competition experiments between cooperators and cheaters varying the cooperation cost ([his]) and the efficiency this investment pays back to the cooperators ([gluc]).** These results are obtained with co-cultures of a cooperator strain producing invertase and being auxotroph for histidine and a cheater strain prototroph for histidine. Reducing the histidine content of the media allows to reduce the cooperator growth rate and artificially increases the cooperation cost. Adding glucose in the media reduce the payback efficiency of cooperation and favour cheaters. The cooperator population can be led to extinction (solid black line denotes the extinction boundary). Figure extracted from Gore *et al.* (2019)<sup>68</sup>.

Public goods systems are nevertheless found in multiple microorganisms, notably inherent to saprophytic organisms and their extracellular biopolymer digestion. There are selection mechanisms that help to stabilise such cooperative behaviours<sup>54,69</sup>. As mentioned previously, limited dispersal is one of them, allowing to share public goods preferably with close relatives. Quorum sensing can also be used to conditionally trigger public goods production only when enough cooperating cells are present in their proximity. Another mechanism, categorized as kin discrimination, consists in adding more selectivity. For example, *Pseudomonas aeruginosa* scavenges iron ions by secreting chelating proteins

(siderophores). Once the siderophores are complexed with iron, they can be recognised specifically by cell-surface receptors, leading to their internalisation. The receptor specificity prevents non-relatives to use the siderophore stock, allowing to avoid cheating<sup>70</sup>. Another ubiquitous example of public goods is the production of extracellular matrix to form a biofilm. Cells share the burden of producing polysaccharide fibres so they can in turn benefit from the protective properties of the biofilm<sup>4</sup>. Other microorganisms produce antibiotic molecules in their vicinity to reduce interspecific competition. This is also a public good system, as any cell resistant to this antibiotic can benefit from its protection. We can also mention the extracellular production of biosurfactants, which allows to tune the cell motility and adhesive properties<sup>71</sup>.

### Division of labour

When looking at cooperation phenomena, one can use a functional view of the interaction networks, summarised by the term Division of labour. It helps decipher what kind of network allows synergetic effects between different members. Division of labour can be broadly defined as a separation of tasks among a population leading to synergistic advantages, and it can be found at many levels in biology:

- between differentiated cells of multicellular organisms,
- between individuals of unicellular or multicellular organisms of the same species,
- between individuals of different species.

The functions that are shared in a division of labour are varied: anabolic activity, catabolic activity, physical structure, sex (Soma/germline or eusocial insects), protection against the environment, predators or pathogens, etc... Classically, there are four main conditions that must be fulfilled for an ecological interaction to be classified as DoL<sup>72</sup>:

1. functional complementarity, (or more broadly: non-redundancy)
2. synergistic advantage (+/+),
3. negative frequency-dependent selection
4. positive assortment (gives spatial proximity)

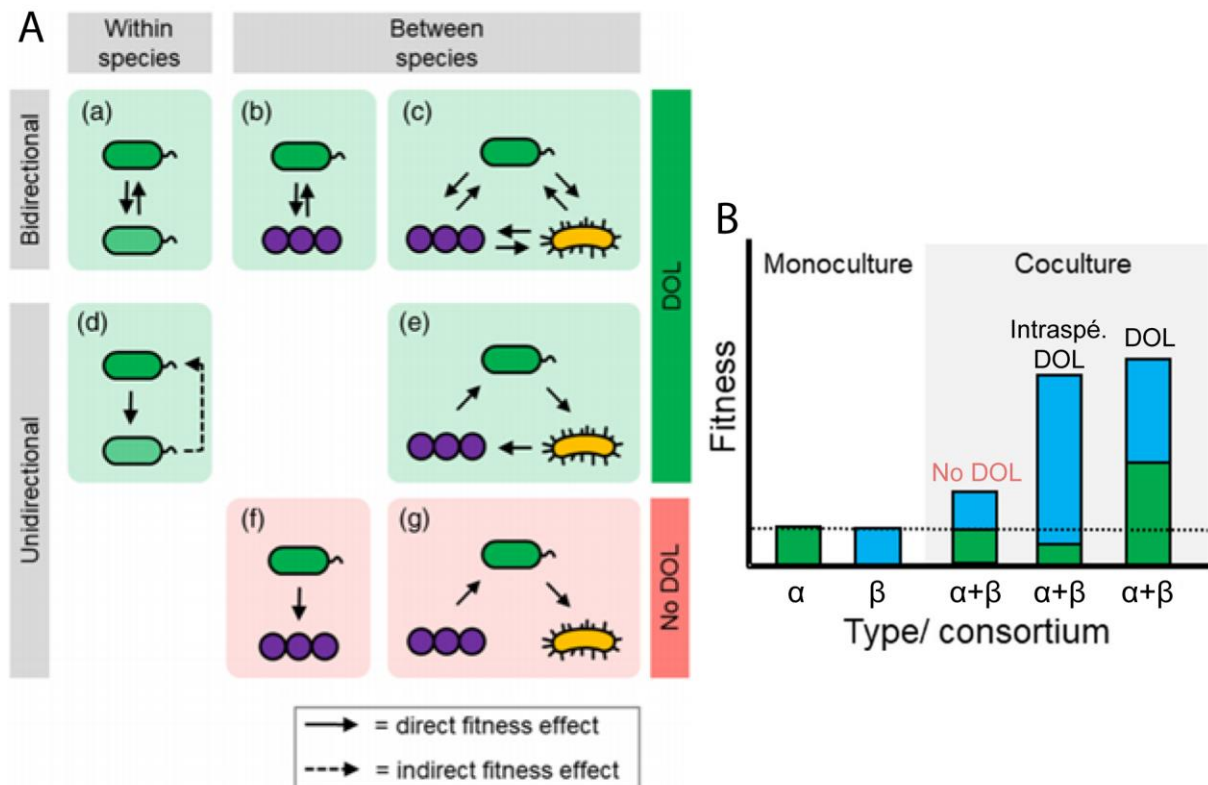


**Figure 7 – Microbial Division of Labour.** (A) Classification of pairwise and three-way interactions as DOL. (a) Mutually beneficial (reciprocal) interaction within two conspecific genotypes. (b) Mutually beneficial (reciprocal) interaction within two heterospecific genotypes. (c) Mutually beneficial (reciprocal) interaction between three different species. (d) Unidirectional interaction between two members of the same species. (e) Unidirectional interaction between three members of three different species. (f) Unidirectional interaction between two members of two different species. (g) Unidirectional (linear) interaction chain between members of three different species. (B) Synergistic interactions between two specialists  $\alpha$  and  $\beta$ . Figures extracted from<sup>72</sup>.

The **synergistic advantage** requires that all participants see their fitness increased compared to when they are alone (**Figure 7B**). If the interaction is intraspecific, this criterion changes as follows: the sum of all participants' fitness when cooperating should be higher than the sum when isolated. Indeed, a part of the population can reduce their own reproductive success to favour their relatives.

The **negative frequency dependant selection** is a criterion that ensures the stability of the population composition: the advantageous interaction would disappear if one partner overtakes the others. Another criterion ensuring the stability of the network is positive assortment: partners should present mechanism helping them getting and/or staying close together.

Examples of DoL in microbes are numerous, depicting a fascinating diversity of chemical reaction networks. The example of heterocystes in cyanobacteria (genus *Nostoc* and *Anabaena*) is quite striking for its metabolic complementarity<sup>73,74</sup>. These filamentous photosynthetic bacteria are like many cyanobacteria, able to fix atmospheric di-nitrogen in

addition to harnessing solar energy to fix carbon. But what makes heterocysts different, is that these functions are compartmentalized in different cells (DoL intraspecific see **Figure 7A.a**). Indeed, the nitrogenases being inhibited by oxygen, these chemical processes are incompatible. Most cyanobacteria encompass this problem by separating these functions temporally following a circadian cycle, which might be suboptimal. The heterocyst allows to perform both simultaneously, nitrogen fixation by the heterocysts perfusing the active photosynthetic cells of the filament with amino acids in exchange for sucrose. This requires an organised nutrient exchange, while maintaining two different and specific chemical conditions in the cells. Another good example of DoL in microbes is interspecific: the ubiquitous nitrogen cycle in soil bacteria (from urea or ammonia, to nitrite and finally to nitrate)<sup>75,76</sup> (**Figure 7A.c**).

DoL of metabolic processes is a beneficial strategy for microbial systems because it can help share the metabolic burden across cells and allows the compartmentalization of incompatible chemical reactions. Notably, this compartmentalization can (i) favour chemical reactions by tuning the thermodynamic equilibrium constant (law of mass action) by pumping-in reactants and pumping-out products, and (ii) improve reaction kinetics by pumping in reactants. All these advantages are very promising to improve the current microbial bioproduction for small molecules or proteins or develop new bioproduction processes. Consequently, DoL microbial interactions are becoming more and more studied, with the hope to be able to redirect them toward human society needs.

### Cellular differentiation in microbes

When studying cell specialisation in microbes, an interesting comparison can be made with developmental biology which studies the programs that allow a single cell to form an organised multicellular organism. Developmental programs are very robust, despite the complexity of multicellular organisms. Indeed, during development, numerous mechanisms need to be orchestrated in space and time: cell differentiation, cell division, cell migration, ... Such complex spatio-temporal control can be performed using various morphogens, diffusive signalling molecules secreted by cells, that are present heterogeneously across the embryo. Cells will thus experience a cocktail of signalling molecules, whose concentration values and dynamics will trigger specific cell differentiation programs. The resulting cellular structures are highly organized in space, with specialised cells that cooperate together to perform complex biological function. As an example, we provide in footnotes the development and functioning of the mammalian liver<sup>77,78vii</sup>.

---

<sup>vii</sup> The liver is an organ which consists in large exchange-surfaces, formed by numerous sinusoidal capillaries (blood vessels) and bile ducts, involved in various functions such as hormone, bile and albumin secretion, drug detoxification, cholesterol and urea metabolism and glycogen storage. This organ is composed of specialised cells: hepatocytes, cholangiocytes, endothelial cells (blood capillary), stellate and Kupffer cells (**Figure 8A**). The hepatocytes and cholangiocytes are the major cells constituting the liver and originate from definitive endodermal cells (**Figure 8B**). These definitive endodermal cells are

There are multiple similarities between multicellular organism development and sessile microbial colony development: spatial structures, division of labour, dynamical gradient of autoinducers (*i.e.* morphogens) and nutrients. Production of extracellular matrix can also be involved in both development processes, allowing to tune tissue physical properties. Although probably simpler in microbes (mammalian cells can tune the morphogen gradients using active transport, diffusion restriction and cell asymmetry<sup>80</sup>), the interdependence between cell activity and local concentration of molecules is quite similar. There are still strong differences between these systems, notably in the type of differentiation mechanisms. In addition, mammalian cell differentiation is mostly irreversible whereas microorganism phenotypes can usually change reversibly (property also found in plants). We could thus view a mature microbial colony as a multicellular individual born from a single (or few) cell, composed of specialised cells coordinated in space and time to cooperate, that can reproduce asexually, and possibly sexually for eucaryote microorganisms.

patterned with morphogen gradients (BMP, FGF, Wnt) during the early developmental stage, and can differentiate in various cell types accordingly to these gradients. When a specific spatio-temporal morphogen signalling is experienced, cells differentiate in hepatoblasts. Otherwise, the resulting cells are involved in the development of the pancreas, the intestine, the thyroid, or the lungs. The last differentiation step, from hepatoblasts in hepatocytes and cholangiocytes, is regulated by TGF $\beta$ , Notch, Wnt, BMP and FGF morphogens. Importantly, TGF $\beta$  expression is localised in the periportal region, resulting in TGF $\beta$  gradients with a peak of signalling activity around the portal mesenchyme. This allows to obtain a spatially resolved cell differentiation, forming biliary tubules close to the portal vein (Figure 8C). We can also note that an adult liver can exhibit regenerative properties to maintain healthy tissues, thanks to stem cells producing new hepatocytes and cholangiocytes<sup>79</sup>

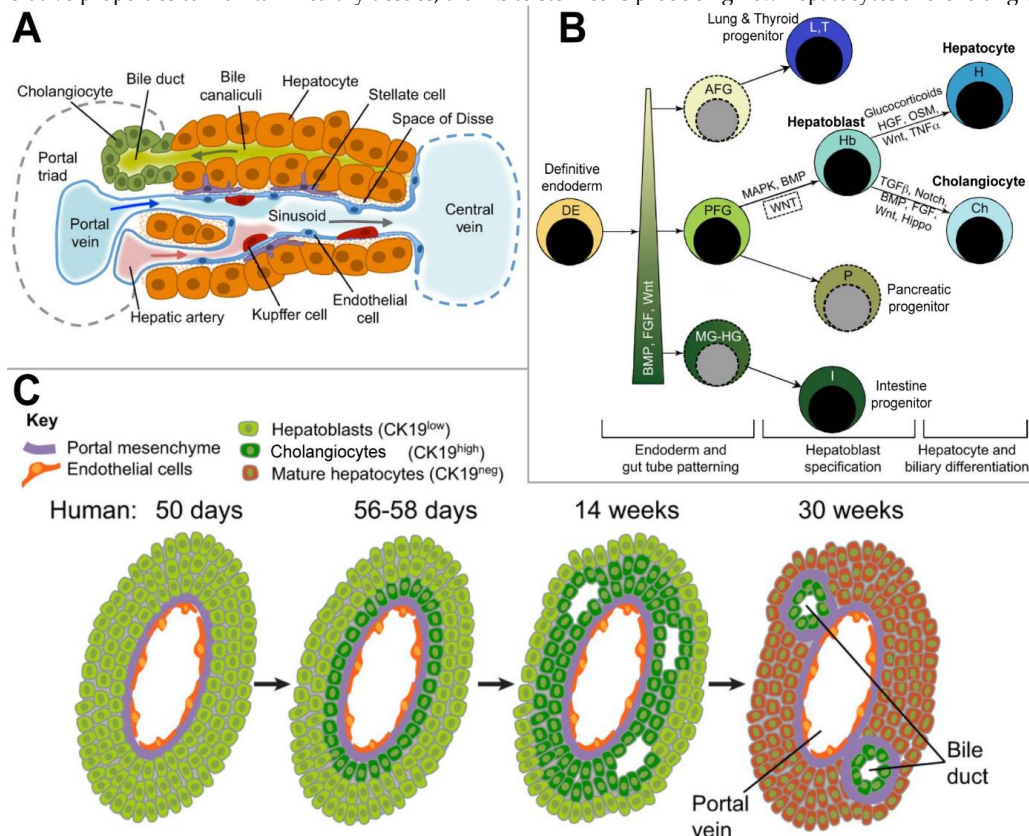


**Figure 8 – Mammalian liver development as a comparison example for microbial colony development.** (A) Scheme of the liver structure, composed of specialized cells cooperating to fulfil complex biological functions. (B) Cell differentiation in hepatogenesis and the corresponding morphogens. (C) Spatial patterning of cell differentiation to form functional morphologies. Figures adapted from<sup>77</sup>



## 4. Control and engineer microbial communities

As a logical progression of synthetic biology, there is a growing number of scientists willing to control and engineer multispecies microbial communities<sup>7,8,66,81-86</sup>. Such scientific goal can help to better grasp what are the key factors allowing to obtain a stable and predictable consortium composed of a complex interacting network. In addition, building on the potential benefits of division of labour, concrete applications for synthetic microbial consortia are envisioned, from biosensors, enhanced bioproduction to biomaterials fabrication.

Various parameters of microbial communities can be controlled, such as their growth, their metabolic activity and interactions or their communication. The tools useful for this purpose can vary depending on the type of community we aim to control, notably whether it is *in situ* or *in vitro*. While microbiology has been constantly developing its scope and technologies, the culture methods that are used the most today in the laboratory are not new: liquid broth and agar plate (the latter popularized in ~1890). The use of solid media culture presents many advantages, for example facilitating clone isolation. But it is still quite a simple culture setup. Indeed, our capacity to cultivate microbes in the laboratory is actually limited. The microorganisms that we are able to grow from a collected sample are called “the *culturome*”, whereas the broader diversity of the sample microbiome is usually assessed by detecting DNA or RNA sequences. The gap between *culturome* and detected microbiome exemplifies our current limitations to reproduce microbial niches and more generally to precisely manipulate microbial systems. This is probably due to multiple factors, such as oversimplification, technical limitations, extensive use of clonal cultures or use of single cell inoculation making density-dependent growth difficult or impairing essential interspecies interactions. There might also be a tendency to favour fast growing microorganisms with the use of nutrient-rich media<sup>87</sup>. Recently, various new technics have been explored, usually implementing a new degree of complexity. The most striking example is probably the development of microfluidic devices, composed of miniaturised culture chambers and tubing, allowing to customize complex 3D culture conditions with controlled flows of liquid media. The emergence of such methods in the past decade is refining our view of microbial landscapes and their spatial components<sup>2,88-91</sup>.

In the following, I will describe which natural microbiomes could be worth manipulating and give examples of synthetic microbial consortia designed for biofuel production.

## Manipulating natural microbiomes

Recent scientific efforts reveal how microbial communities control and/or engineering can help solve real-life problems, notably in human health. Humans are *holobionts*: hosts of thriving multispecies microbes. With the recent advances in “omics” assessments and “humanized” gnotobiotic<sup>viii</sup> animal models, research in microbiota has boomed. In particular, the importance of gut microbiota in human health has been brought to light at multiple levels (**Figure 9**). The human gut microbiome mainly performs the fermentation of non-digestible substrates (dietary fibres and endogenous intestinal mucus) supporting the growth of specialist microbes that produce short chain fatty acids (SCFAs) and gases. The major SCFAs produced are acetate, propionate, and butyrate, which have important roles for the host in glucose and cholesterol management, maintaining gut hypoxia, and satiety signalling. While gut microbiota heritability exists, the major factors influencing microbiota composition are environmental such as diet, drug treatments and household sharing<sup>92,93</sup>. Indeed, alimentation impacts the microbiome activity in addition to directly influencing nutrient uptake by dictating what nutrients are present in the gut. The diet imposes physical and chemical constraints on the gut microorganisms, shaping the microbial community diversity and abundance, in turn resulting in a certain metabolic landscape. For example, dietary fibres represent one of the main microbial nutrient sources and have been shown to be central to maintain good gut microbiota diversity<sup>94</sup>. There is a general association between diseases and low diversity gut microbiota, which indicates that microbial diversity is important for healthy and robust gut functioning. A wide range of health problems is correlated with gut microbiota dysbiosis such as obesity<sup>95</sup>, type 1<sup>96</sup> and 2 diabetes<sup>97</sup>, colorectal cancer<sup>98</sup>, inflammatory bowel disease<sup>99</sup>, coeliac disease<sup>100</sup>, arterial stiffness<sup>101</sup> and psoriatic arthritis<sup>102</sup>. It is however sometimes unclear if the microbiota has a causal role or is only symptomatic of a certain health condition.

---

<sup>viii</sup> Gnotobiotic refers to organisms with a fully known microbiome, sometimes referring to the absence of a microbiome.

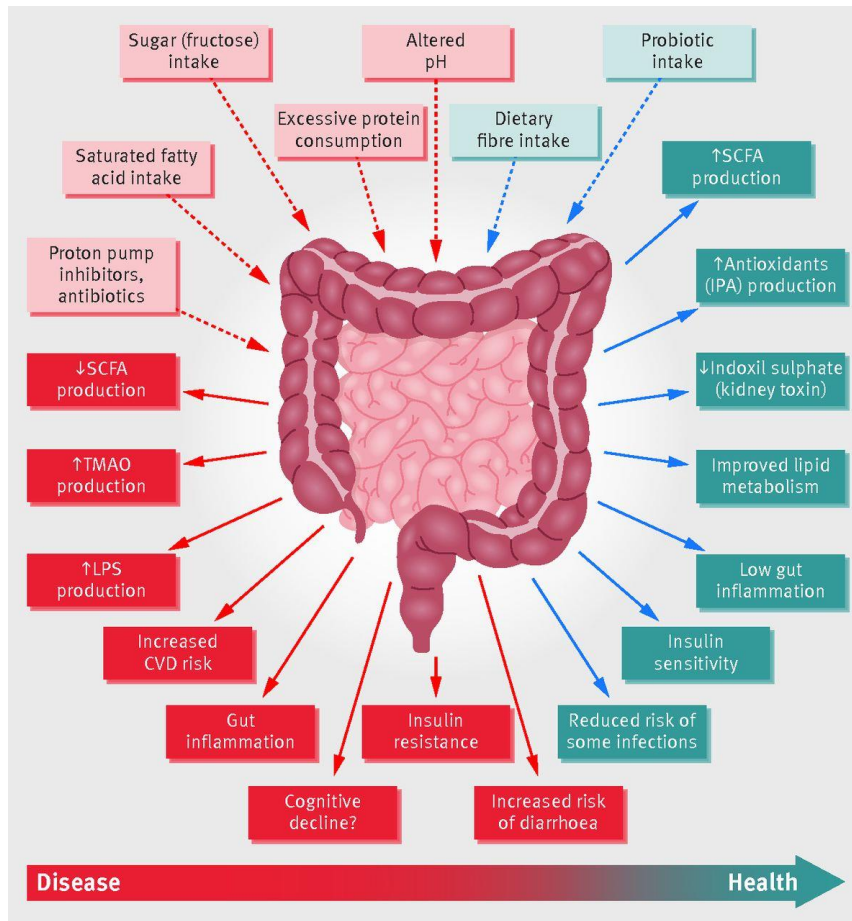


**Figure 9 - Schematic representation of the role of the human gut microbiota in health and diseases.** CVD=cardiovascular disease; IPA=indolepropionic acid; LPS=lipopolysaccharide; SCFA=short chain fatty acids; TMAO=trimethylamine N-oxide. Figure extracted from<sup>94</sup>.

Fecal microbiota transplantation (FMT) is one of the best examples of beneficial microbiota manipulation. It consists of sampling faeces from a donor with a healthy microbiota and implanting it in the colon of a patient. Importantly, it can be heterologous or autologous, where a patient’s own microbiota can be saved prior to its disruption and re-introduced later. The first reported case of fecal use in medicine date from the 4<sup>th</sup> century, described as an oral fecal administration for the treatment of food poisoning and diarrhea (“Zhou Hou Bei Ji Fang ” or “Handy Therapy for Emergencies”, Hong Ge<sup>103,104</sup>). There are now procedures to separate microbiota from stools and cryopreserve it, allowing for a rigorous selection of donors (testing for blood and enteric pathogens). It can then be administrated to the intestinal tract with precision using tube feeding. This procedure is both safe and efficient, and is now routinely used in cases of *Clostridium difficile* infection insensitive to drug treatments<sup>105,106</sup>, the current most common pathogen causing health care–associated infections in the United States. While the technic seems simple and crude, it allows to transfer both the diversity and composition of the microbiota, which are crucial to accelerate its rebalancing in the host’s gut. This technic can also be compared with probiotic treatments, being an oral ingestion of a rationally designed

microbial cocktail. Interestingly, such treatments do not necessarily impact the gut microbiota composition. It is even counterproductive as an antibiotic recovery strategy, actually delaying the renormalisation of microbiota activity (such as secondary bile acid metabolism) and mucosal host gene expression, whereas autologous FMT accelerates these processes<sup>107</sup>. Despite promising pre-clinical data, strong evidence of beneficial probiotic treatment for any disease in humans has not yet been established<sup>108-110</sup>. These results exemplify how human intervention to rebalance a microbiota can drastically vary in efficiency, with a nonintuitive tendency: using well controlled inoculum composed of strain isolates usually limit the achievable microbial diversity and in turn makes the consortium suboptimal or unadapted to the transplantation target.

The importance of human skin microbiomes has also been investigated<sup>111</sup>, which are - if unbalanced - associated with increased hair dandruff, skin infections (mycose, acnes, etc...), and eczema. Compared to the gut, human skin is overall nutrient-poor, cool, and dry, explaining the low skin microbiota biomass. Nonetheless, there are four main different types of skin microbial niches depending on the physico-chemical conditions: sebum rich (face, chest and back), moist (bend of elbow, back of knee and groin), dry (forearm and palm) and the feet. Lipophilic *Propionibacterium* species dominate sebaceous sites while *Staphylococcus* and *Corynebacterium* species prefer humid environments. For example, *Propionibacterium acnes* is able to proliferate in the sebaceous gland using proteases and lipases to degrade skin proteins and triglyceride lipids in sebum. This notably explains why we observe lower abundances of *P.acnes* in other mammals: their sebum is poor in triglyceride lipids<sup>112</sup>. In contrast to bacteria, the fungal community is the least abundant, with a similar composition across body location: dominated by the genus *Malassezia* except for the feet. Interestingly, skin microbial communities are found to be relatively stable over years, with sebaceous sites being the most stable and the feet the least.

Similarly, current agricultural research starts to emphasise the importance of rhizosphere and phyllosphere microbiota on plant health, and thus on agriculture productivity. It is now clear that the underground life inhabiting a given soil is crucial to obtain and maintain healthy and productive lands. We can for example mention the symbiotic associations of *Fabaceae* with bacteria in specialized organs, a.k.a. rhizobium or nodule, to fix atmospheric nitrogen. Importantly, mycorrhizal associations (plant root-filamentous fungi) can be very beneficial for plants, under unstressed or stressed conditions, by improving the plant inorganic nutrient uptake<sup>113</sup>. In the last decade, there is also a growing interest in the use of bio-fertilizers: inoculating beneficial microorganisms in crop soil<sup>114</sup>. Notably, there is a trend to shift from single-strain to microbial consortia inoculation.

More recently, leaf microbiota has also been shown to be of importance<sup>115</sup>, notably to reduce pathogen sensibility. Leaves constitute a fluctuating environment exposed to multiple stresses (light radiation, desiccation, ...) and with relatively poor nutrient availability. Microbes are found both at the surface (epiphytic) and the interior (endophytic) of leaves, colonising vertically (seed or pollen) or horizontally (air, soil, insects, ...). Phyllosphere microbiota are mainly composed of bacteria, followed by filamentous fungi and yeast, with few protists and bacteriophages - composition that has been found to change with the seasons. Microorganisms proliferating on the leaf surface can only do so as biofilm multicellular aggregates retaining moisture. There is a cuticle layer covering the leaf surface, acting as a protective barrier against pathogens and abiotic factors and allow to prevent desiccation. It is composed of a wide range of chemical compounds, mainly fatty acid polyesters (cutin) and wax supplemented with few polysaccharides. Leaf microbiota can enter and penetrate the leaf cuticle, typically through natural stomatal openings or wounds resulting from lytic enzymes and osmotic pressure. Plants have evolved recognition mechanisms to close their infected stomata, while pathogens have evolved mechanisms to prevent such stomatal defence. Inside leaves, apoplastic spaces are large intercellular spaces used to mediate gas exchange, but they are also a central phyllosphere microbiota niche, where humidity is the main factor controlling microbial occupancy. The establishment and abundance of these leaf microbial communities depend on numerous biotic and abiotic interactions. In addition, determining whether the effects of a given microorganism on the host plant are commensal, beneficial, or detrimental is not necessarily straightforward. For example, fungal mildew pathogens normally asymptomatic in various *Brassicaceae* species become active pathogens if *Albugo candida* (white rust) is already infecting the host. Commensal microbes may in fact be beneficial if they compete with detrimental species. Interestingly, different strains of the pathogenic fungus *Fusarium oxysporum* can act as microbial antagonists against other strains of the same species. Some other species produce Quorum Quenching (QQ) molecules which allow to suppress Quorum Sensing communication<sup>116</sup>, in turn reducing the virulence of various pathogens. Inoculating QQ producer species on plant leaf as an agricultural antibacterial agent constitute a promising strategy to replace harsh chemical treatments. The interactions between a plant's immunity and its leaf microbiota are not very well known, but there is evidence that pattern-triggered immunity (PTI, a general innate plant immunity) affect the endophytic microbiota<sup>117</sup>. An interesting example is the soil filamentous *Actinobacteria* (*Streptomycetes* sp.) which is able to activate plant biosynthesis of an antifungal compound (salicylic acid) and promote leaf defence responses against fungal pathogens<sup>118</sup>. Less is known concerning the effect of strain-specific resistance, also known as effector-triggered immunity (ETI), on microbiota composition.

Another microbial system of importance is rumen microbiota, which has been largely studied<sup>119–123</sup> for cattle and sheep production. Ruminant animals feed on cellulosic materials but, like all mammals, do not produce their own cellulase. The plant food is mainly composed of cellulose fibres (homopolymers of glucose) and hemicellulose (heteropolymers of glucose, mannose, xylose,...), molecules that only few organisms are able to digest: microbes. In turn, any animal digesting plant cellulose (ruminant, giant panda<sup>124</sup> or termites) can only do it thanks to the help of the metabolic capabilities of microbes, forming a symbiotic relationship. For ruminants, microbial abundance and diversity follow this order: bacteria, protozoa, archaea and fungi. The fermentation process takes place in a specialized digestive pocket called the rumen, containing the plant particle suspension that is frequently regurgitated, re-chewed, and re-swallowed. The main chain of chemical reactions taking place in the rumen can be simplified as follow: cellulose hydrolysis, anaerobic fermentation of soluble sugars, and finally secondary product fermentation producing methane. These three successive trophic levels are undertaken by different types of microbes, which interestingly are often functionally redundant (**Figure 10**). It is also worth noting that low-abundance taxa do not translate into less significant members of the microbial community: the key cellulolytic bacterium *F. succinogenes* represents only ~1% and methanogen archaea only ~1% of the microbial abundance<sup>120</sup>. These methanogen archea are also crucial for the functioning of the global food chain as they are “electron sinks”, notably consuming the dihydrogen produced by the primary fermentation. The worldwide cattle cheptel is ~1.4 billion animals (2010)<sup>125</sup> and represents a methane emission of ~1E14g per year (2019)<sup>125</sup>, in addition to its high water consumption and CO<sub>2</sub> emission, making this food industry one of the least eco-friendly. The understanding and optimisation of rumen fermentation could greatly improve the feed conversion ratio and reduce methane emission, a very potent greenhouse effect gas. To this end, multiple and various strategies of direct and indirect methanogen inhibition have been investigated such as the use of antimicrobial compounds, animal breeding or controlled microbial succession to the new-born calf. However, there are mixed results when comparing different studies, which can be a sign of unconsidered experimental complexity. Indeed, the number of microbe species, their functional diversity and redundancy, their numerous interactions, as well as the limited dispersal due to physical constraints make this system difficult to predict. The relevance of simplistic *in vitro* studies is also limited because lab-cultured microbial communities are lacking members compared to the sampled ones from rumen<sup>126,127</sup>. This field might benefit from enhanced control over *in vitro* parameters, such as spatial and/or temporal microbial organisation, which might help grow and study more realistic microbial communities in laboratory conditions.

Known core rumen isolates and their morphology	Morphology	Utilization						Production								
		Crystalline cellulose	Hemicellulose	Soluble sugars	Lactate	Succinate	Methanol	CO <sub>2</sub>	H <sub>2</sub>	Succinate	Lactate	Acetate	Propionate	Butyrate	Formate	Methane
<i>Treponema bryantii</i>	WWW			✓						✓	✓					
<i>Fibrobacter succinogenes</i>	rod	✓	✓	✓					✓	✓					✓	
<i>Methanosphaera stadtmaniae</i>	rod						✓	✓	✓							✓
<i>Methanobrevibacter ruminantium</i>	rod							✓	✓							✓
<i>Olsenella umbonata</i>	rod			✓						✓	✓					
<i>Bifidobacterium ruminale</i>	rod			✓						✓	✓					
<i>Pseudoscardovia suis</i>	rod			✓						✓	✓					
<i>Succinimonas amylolytica</i>	rod			✓						✓	✓	✓				✓
<i>Ruminobacter amylophilus</i>	rod			✓						✓	✓	✓				✓
<i>Succinivibrio dextrinosolvens</i>	rod			✓						✓	✓	✓				✓
<i>Prevotella ruminicola</i>	rod		✓	✓						✓	✓	✓	✓			✓
<i>Selenomonas ruminantium</i>	rod			✓	✓					✓	✓	✓	✓			✓
<i>Ruminococcus flavefaciens</i>	rod	✓	✓	✓	✓					✓	✓	✓				✓
<i>Oribacterium</i> sp. strain C9	rod			✓						✓	✓					
<i>Lachnospira multiparus</i>	rod			✓						✓	✓					✓
<i>Coprococcus</i> sp. Pe15	rod			✓	✓					✓	✓	✓				
<i>Lachnoclostridium clostridioforme</i>	rod			✓						✓	✓					
<i>Acetivibrio ruminis</i>	rod			✓						✓	✓	✓	✓			
<i>Butyrivibrio fibrisolvens</i> , <i>B. hungatei</i> , <i>B. proteoclasticus</i>	rod		✓	✓						✓	✓	✓			✓	
<i>Pseudobutyrvibrio xylanivorans</i>	rod		✓	✓						✓	✓				✓	
<i>Pseudobutyrvibrio ruminis</i>	rod			✓						✓	✓					
<i>Succinivibrio ruminis</i>	rod			✓						✓	✓	✓				
<i>Christensenella minuta</i>	rod			✓						✓	✓				✓	
<i>Anaeroplasma abactoclasticum</i>	rod			✓						✓	✓	✓	✓			✓

**Figure 10 - Overview of rumen microbiota composition.** This shows the diversity and the functional redundancy of such communities. Extracted from<sup>123</sup>

Recently, a new type of biomass-based energy is gaining weight: biogas (methane + CO<sub>2</sub>; ~60:40 to 80:20) production by agricultural waste anaerobic fermentation – a.k.a. Anaerobic Digestion or methanization. The fermentation feedstocks can be various but should have a low lignin content: ruminant manure, straw, silage, household waste, ... The main chemical reactions are similar to the rumen fermentation ones described above. The microbiota used to degrade this matter can be controlled and optimized for methane production but can also be already present in the feedstock and autonomously stable given that the fermentation temperature is relatively stable. Anaerobic digester microbiota has been found to vary quite strongly between batches, but some microbiota compositions have been identified to be better for methane production<sup>128</sup>. Nonetheless, the exact functioning of such microbiota is still unclear, and its composition assessment suffers from low reproducibility<sup>129</sup>. Working with batch or pseudo-continuous reactors, from individual to industrial scale, anaerobic digestion requires only a simple and passive purification process: filter out toxic hydrogen sulfide gases. While it is energy demanding, an optional step can be performed to concentrate the methane as the CO<sub>2</sub> contained in biogases is useless for combustion. Compared to electricity-based energy sources (wind, solar, nuclear, ...), one of the biggest advantages of gas is that it can easily be stored in addition to being readily usable through simple combustion.

Methanation is another type of microbial uses for biogas production. It corresponds to the last step of the methanization process, the conversion of dihydrogen H<sub>2</sub> and carbon dioxide CO<sub>2</sub> into methane, typically performed by archaea from *Methanoculleus* or *Methanothermobacter* genera. One of the requirements for this technology to be sustainable is to use the excess energy produced by uncontrolled renewable energy sources (sun and wind) to produce dihydrogen by water electrolysis. With the advantage of CO<sub>2</sub> fixation, methanation can be combined with methanization to increase the final methane purity output (also known as biogas upgrading). Interestingly, directly flowing H<sub>2</sub> in methanization reactors increases the pH, in turn altering the fermentation, which pushes the development of “ex-situ biomethanation”. This idea is to feed the methanization biogas output as well as dihydrogen to a second reactor, achieving ultra-pure methane production with no CO<sub>2</sub> emissions<sup>130</sup>.

**Altogether, these examples show the great potential for the understanding, manipulation, and creation of microbial consortia to solve central problems in human health and in the sustainability of food and energy production.**

### Synthetic microbial consortia for biofuel production

An example of application for synthetic microbial consortium is biofuel production. As previously mentioned, methanization is one of them, but I will discuss here liquid biofuel production such as ethanol or butanol. One of the main limitations with the current production of biofuel (mainly ethanol) is the requirement of fermentable sugars, typically based on starch, encroaching on alimentation feedstock. Using lignocellulosic feedstock instead is thus presented as a promising alternative as it is very abundant and non-food competitive. Notably, there are recent efforts in developing bioconversion systems, so-called Consolidated Bio-Processing (CBP), which consist in realising three bioconversion steps in one reactor: (i) cellulolytic enzyme production, (ii) hydrolysis of insoluble lignocellulosic particles into fermentable saccharides, (iii) fermentative biofuel production. It is worth noting that the main CBP bottleneck is usually the hydrolysis of the polymers, and many studies actually use pre-treated feedstock (typically using steam explosion). The CBP strategy, due to its multi-process aspect, is believed to greatly benefit from the use of complementary microbial communities. For example, a division of labour strategy could be engineered so the biopolymer hydrolysis and the fermentation would be undertaken by two different species. This has been tested<sup>131</sup> using the thermophilic *Thermoanaerobacterium thermosaccharolyticum* (M5) as a cellulolytic member with the solventogenic *Clostridium acetobutylicum* (NJ4) for butanol production (**Figure 11**). These strains are natural isolates and are already relatively specialised in the tasks they need to perform. The M5 strain is specialised in degrading xylan (a type of hemicellulose), releasing xylose in solution faster than they consume it as carbon source. It also produces a significant amount of acetate and butyrate. The NJ4 is specialized in producing high amount of butanol using xylose, acetate or butyrate as carbon sources. However, combining both



species in one culture is not as simple: their optimal incubation temperature is quite different. To solve this issue, the authors choose to perform a monoculture of M5 followed by a coculture (inoculating the NJ4 strain after 48h). This allows them to first degrade the biopolymers at 55°C, the ideal temperature for M5 performances, producing xylose acetate and butyrate. Then the temperature was lowered to the NJ4 preferred value (37°C) to allow it to optimally produce butanol. During the second phase, M5 does not grow well and is dominated by NJ4 after 144h, but the co-occurrence of the species has two synergetic effects: prevent xylose accumulation that normally inhibits xylanase and xylosidase activity; and butyrate presence when NJ4 is inoculated accelerate solventogenesis triggering.

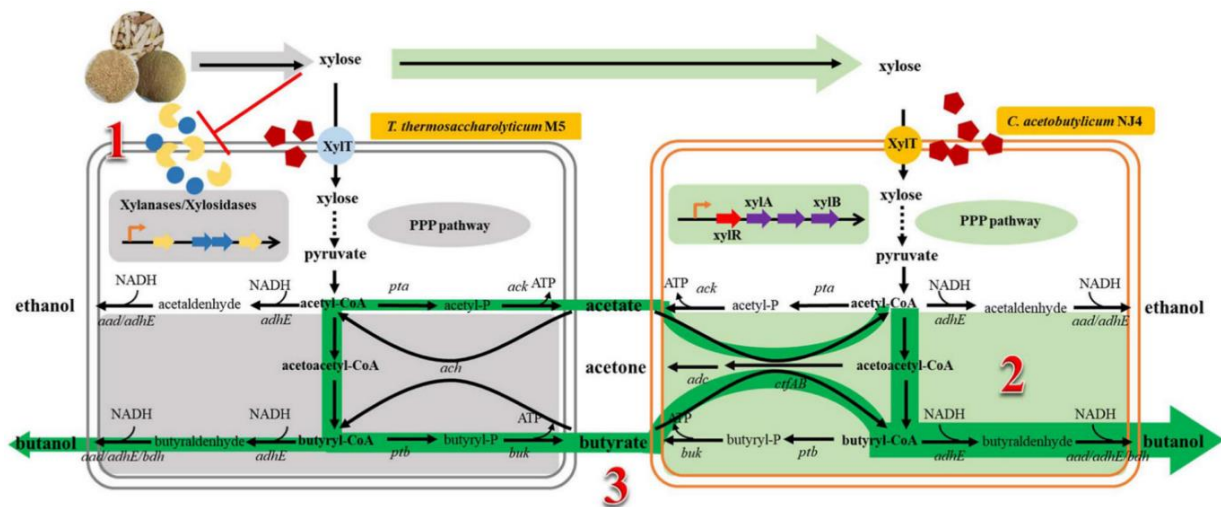


**Figure 11 - Consolidated Bio-Processing (CBP) for biofuel production.** Schematic illustration of the synergistic effects between strains M5 and NJ4 in the microbial consortium for butanol production from hemicellulose. CoA, coenzyme A; PPP, pentose phosphate. Extracted from<sup>131</sup>

Another interesting idea concerning cell factories is to incorporate a photosynthetic reaction in the workflow, to produce the carbon source in situ instead of using plant feedstock. Such phototroph systems would have the main advantage to require low feedstock input, allowing to achieve low cost bioproduction. This is notably inspired by lichens, symbiotic microbial organism realizing such phototroph-heterotroph interactions: carbon is provided by the photobiont (cyanobacteria or green algae) and supplied to one or multiple heterotrophs, typically fungi, which provide in return carbon dioxide, water, minerals and nutrients from their secondary metabolism, as well as protection from the environment. Pairing a phototroph microorganism for the carbon source with a heterotroph for the chemical bioproduction has for example be investigated with cyanobacteria and yeasts respectively. In this study<sup>132</sup>, the authors used the sucrose-secreting cyanobacterium *Synechococcus elongatus*, which was engineered to over-expressing the Escherichia coli gene *cscB* encoding for a sucrose symporter. As heterotroph, three different yeast species were tested. One of the main steps to achieve successful co-culture is to determine the culture media composition. For example, while yeast extract is the preferred nitrogen source for yeast growth, it strongly inhibits the cyanobacteria

one which does not need any nitrogen source. More precisely, exogenous amino acids are known to inhibit *Synechocystis* growth, and using yeast nitrogen base without amino acids allow to co-culture the yeasts and the cyanobacteria. Another possible problem is that the light exposure required for photosynthesis can be detrimental for heterotroph, not adapted to light radiation especially for UV. In their culture conditions, the illumination performed by cool-white fluorescent lamps did not show significant phototoxicity, but using the sun radiation instead would probably be detrimental. Another cyanobacteria requirement is a buffered culture pH which should be maintained around 7-8. Among the three yeast species tested, *S. cerevisiae* was found to be unable to grow on such low sucrose concentration (<0.5g/L) which might be due to the pH preventing acid catalysed hydrolysis of sucrose. In contrast, *R. glutinis* and *C. curvatus* did exhibit growth and sucrose utilisation. *R. glutinis* showed the most promising co-culture performances and was used to further investigate its potential. While both simple batch or semi-continuous co-culture strategies did not significantly enhance the final cyanobacteria biomass compared to the batch monoculture, they showed a 39% and 26% increase in total biomass and 54% and 60% in fatty acid production respectively. In addition, the presence of *R. glutinis* prevented reactive oxygen species (ROS) accumulation compared to the cyanobacteria monoculture, in turn elevating ROS growth inhibition. **Such microbial pair realise a successful artificial synergistic system composed of a prokaryotic photobiont and a eukaryotic heterotroph which could represent a potential sustainable platform for biofuels production using sunlight.** This study exemplifies the typical requirement to find common culture physico-chemical conditions which could accommodate all consortia members. Such technical requirements might be quite different when scaling up such systems for industrial bioproduction.

The yeast *Saccharomyces cerevisiae* has also proven to be a great platform for engineered microbial consortia, especially because scientists have studied this microorganism extensively. I will now focus on the particularities of this yeast, its relationship with sucrose and how this model organism can help us study spatially cooperating interactions.

## 5. *Saccharomyces cerevisiae* and Sucrose

### *Saccharomyces cerevisiae* overview

*Saccharomyces cerevisiae* is a unicellular ascomycetes fungus (commonly called yeast) which is considered ubiquitous in natural and domesticated habitats. This species can be found in decaying fruits, flower nectar, plant sap (wound), soil, tree bark, plant surface, insects and human gut microbiota, as well as in domesticated fermentative processes such as alcoholic beverage production, bread making or kombucha brewing. Indeed, due to its ability to metabolize various nutrient types, this yeast specie is a generalist that can adapt to changing microenvironment composition and structure.

These eucaryotes cells are not motile but can be planktonic or sessile. They notably tune their mobility by changing their adhesive properties, for example expressing certain adhesin proteins to flocculate as multicellular clumps and sediment. Their preferred ploidy state is diploid, state in which they proliferate asexually through mitosis. The sexual reproduction of this yeast occurs when they are starved: diploid cells undergo meiosis and produce haploid ascospores which can mate directly within the ascus or after dissemination.

Importantly, this microorganism specie has been a crucial model for biology research for multiple reasons. First, like many fermentative unicellular organisms, the *S. cerevisiae* dividing rate is fast (one division every 1h30) which allows to easily obtain millions of cells to perform experimentation with high statistical significance. Second, yeasts are eukaryotic which allows to investigate fundamental biology principles that also apply to mammalian cells. Finally, *S. cerevisiae* has the advantage of being both food-safe and industrially useful. It is worth noting that experimental model strains (or laboratory strains) of *Saccharomyces Cerevisiae* are usually maintained in haploidic state (HO locus dysfunction) to keep good genetic stability. In addition, such laboratory strains have been modified to obtain certain practical characteristics. To enable genetic modification using auxotrophic selection markers, the ability to synthesise certain mandatory amino acids has been removed from the yeast genome. The resulting cells can only grow if the amino acids are complemented in the culture media, or if a genetic modification has been made with an auxotrophic selection marker. Specifically, URA3, HIS3, LEU2, TRP1, and MET15 marker genes encode essential enzymes for de novo synthesis of the amino acids pyrimidine, L-histidine, L-leucine, L-tryptophan, and L-methionine, respectively<sup>133</sup>. While this strategy has been very practical in the past, the emergence of CRISPR/Cas9 technology made it relatively obsolete. During the selection for such yeast model strains, certain traits have also been selected either by inadvertence or for convenience. For example, one of the central model strains, S288C is non-flocculant due to a defect in the FLO8 gene, avoiding any filamentous growth or any cell-adhesion which can perturb single-cell isolation or planktonic liquid culture<sup>134,135</sup>. Nowadays, there are a handful

of *S. cerevisiae* model strains, the main ones being the BY4741<sup>136</sup> and W303 (“default” backgrounds), CENPK (typically for bioproduction studies) or Sigma1278b (typically for filamentous and flocculation studies).

### *Saccharomyces cerevisiae* carbon source

Yeast can metabolise a relatively large variety of carbon sources. We can cite glycerol, ethanol, maltose, but their preferred molecule is glucose. This means that when sufficient glucose is available, the cell will focus on it while inhibiting the metabolization of other carbon sources. The two different processes *S. Cerevisiae* use to metabolize these sugars are respiration and fermentation. While certain carbon sources can only be respired such as glycerol or ethanol, glucose and maltose can both be fermented or respired. These catabolic pathways mainly differ in their ATP yield, ATP production rate, oxygen requirements and CO<sub>2</sub> production: respiration is a slow but efficient process requiring oxygen and releasing low amounts of CO<sub>2</sub>, while fermentation is a fast but wasteful anaerobic process producing ethanol and high level of CO<sub>2</sub> (~2 ATP per glucose). Importantly, fermentation by-products still contain chemical energy: once glucose is depleted the produced ethanol can be in turn respired, adding ~10 ATP per glucose. The catabolic activity of the cells depends on the growth conditions:

- Absence of oxygen forces the flux toward fermentation
- Presence of oxygen with low glucose concentration lead to respirative catabolism
- Presence of oxygen with intermediate or high glucose concentration lead to fermentation in addition to respiration, phenomenon known as the Crabtree effect<sup>137</sup>

The main reason yeast preferably ferments glucose, even in presence of oxygen, is attributed to the gain in ATP production rate<sup>138</sup>. Indeed, microorganism competitive fitness is set by a trade-off between rate and yield<sup>139</sup>, which depend on the environmental conditions. In nutrient-rich media, typically the case for common yeast niches (fruits or nectar), this trade-off tends toward rates instead of yields, favouring fast growing metabolism to increase colonisation speed and in turn reduce competition. While the anti-microbial effects of ethanol might have provided additional benefits, it is believed that they are not necessary for explaining the emergence of the Crabtree effect.

The yeast respiration pathway is similar to most eukaryotes: after glycolysis, glucose is oxidized into CO<sub>2</sub> through the Tricarboxylic Acid Cycle (TCA) and mitochondria allow to transform the resulting NADH reduction potential in ATP molecules.

Fructose is another very commonly found sugar (mainly derived from sucrose hydrolysis, see below), and is most of the time considered as equivalent to glucose. Indeed, both are hexose, which can be imported by yeast using the same transporters (HXT), and fuel

glycolysis. However, discrepancies are observed between these similar sugars<sup>140</sup>. First, while glucose is 99.9% under its pyranose form, ~30% of fructose can be in the furanose form, conformation that does not correspond to the yeast transporter selectivity. Thus, this chemical property of fructose reduces the actual transport-competent concentration, in turn reducing fructose importation rate. Once imported, glucose needs an additional step (conversion of glucose-6-P into fructose-6-P) to enter glycolysis compared to fructose. Although these differences might be of importance in some conditions, we will consider fructose as an equivalent carbon source to glucose relative to yeast proliferation.

Sucrose is also a common carbon source for yeast, as this molecule is highly present in the biosphere due to its central role in plant physiology. Indeed, almost all plants use sucrose as a central carbon molecule. While photosynthesis produces glucose, plants directly transform it into sucrose as a storage and transport molecule. Bounding hexoses into a non-reducing disaccharide allow to condensate energy, to stabilise it for transport and to control its consumption by cells. Typically, photosynthetic cells (source tissues) perfuse sucrose through the phloem to non-photosynthetic tissues (sink tissues), where four different enzymes hydrolyse sucrose into hexoses to supply various metabolic pathways<sup>141</sup>. Phloem sap sugar composition is dominated by sucrose at ~2.3%w/v (glucose 0.7%w/v, fructose 0.4%w/v)<sup>142</sup>. Thus, any damage applied to a plant exposes a significant amount of sucrose to potential microbial infection, either vectored by the damaging factor (*e.g.* from animal microbiota) or post damaging. In addition, sucrose can represent a large proportion of the total sugar content of flower nectars or fruits<sup>143</sup>. Importantly, as *S. cerevisiae* cells are sessile, they need to be transported by various vectors to colonise a new nutrient-rich location. For example, it has been found that social wasps are a significative niche for *S. cerevisiae* cells, maintaining yeast cells viable in their gut during the winter and disseminating them before, during and after grape harvest<sup>144</sup> (while representing only 4% of the yeasts species found in the wasp gut microbiota). Similarly, *S. cerevisiae* cells have been reproducibly isolated from flies, fruit flies and honey-bees<sup>145</sup>.

To metabolise sucrose, yeast hydrolyses it into its monomers glucose and fructose, which are then metabolized through glycolysis, supplying both respiration and fermentation. Yeast possesses two different pathways for this to occur: (i) extracellular hydrolysis by invertase, followed by uptake, and (ii) uptake via sucrose-proton symport followed by intracellular hydrolysis (**Figure 12**).

These two strategies possess different characteristics: **the external hydrolysis induces the production of diffusible hexose which, as public goods,** favours interaction between individuals but also represent a potential fitness loss for the cell<sup>146</sup>. The internal hydrolysis process implies a lower ATP yield (from 4 ATP/sucrose molecule to 3) because of the proton symport ATP cost.

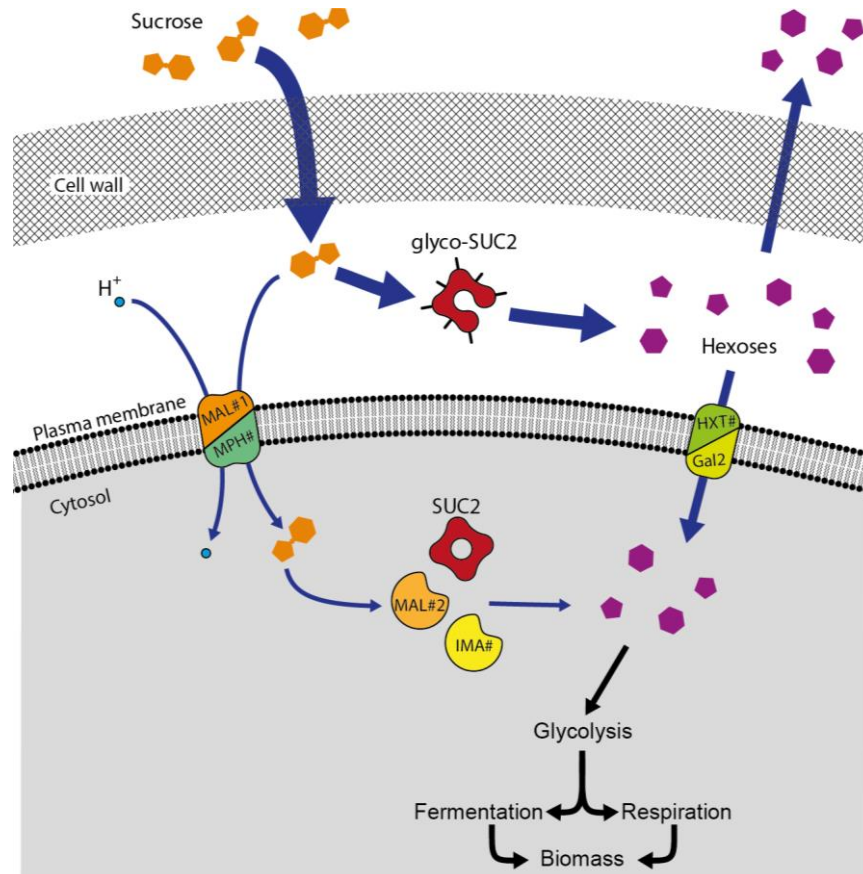


**Figure 12 – Scheme of sucrose metabolism in *S. cerevisiae*.** Sucrose can be hydrolysed into hexose either in the periplasm by glycosylated invertase (glyco-SUC2) followed by hexose import by hexose transporter (HXT#, Gal2) or in the cytosol by internal invertase (SUC2) or maltose related enzymes (MAL#2, IMA#) after being imported by maltose transporter (MAL#1, MPH#). Blue arrow's widths are indicative of the flux magnitude.

*Saccharomyces cerevisiae* predominantly uses the first mode of sucrose hydrolysis<sup>147,148</sup> : cells harbour invertase in their periplasm space, that hydrolyses sucrose into glucose and fructose, which are then transported into the cell by hexose transporters supplying both respiration and fermentation. *S. cerevisiae*'s invertase was already studied more than 100 years ago<sup>149,150</sup> and was the enzyme used by Michaelis and Menten for their classic paper '*Die Kinetik der Invertinwirkung*'<sup>151,152</sup>. This enzyme is named invertase because the hydrolysis of sucrose causes an inversion of optical rotation in the sugar solution (from positive to negative) which is relatively easy to measure.

## Evolutionary view of the SUC gene family

In *Saccharomyces cerevisiae*, the SUC gene family is composed of nine genes located on different chromosomes: SUC1 (VII), SUC2 (IX), SUC3 (II), SUC4 (XIII), SUC5 (IV), SUC7 (VIII), SUC8 (X), SUC9 (XIV) and SUC10 (XVI). All these genes are highly similar (92.3–95.6% identity to SUC2), and most of the mutations are synonymous C→T transitions<sup>153</sup>. Given the facts that (i) SUC2 is the only copy of SUC genes in other *Saccharomyces* species<sup>154,155</sup> and (ii) it is the only non-telomeric SUC gene<sup>155</sup>, SUC2 seems to be the ancestral gene. The origin of the subtelomeric copies of SUC genes in *S. cerevisiae* is probably only the result of its domestication<sup>153</sup>. I decided to work with the *S. cerevisiae* background BY4741 (S288C), which possesses only one active copy of the SUC2 gene<sup>154</sup>.

**Because of public goods production (hexoses), yeasts growing on sucrose and expressing SUC2 induce intercellular cooperative interactions.**

There are multiple factors that can explain the selection of extracellular production of invertase and its subsequent public good production. First, the sessile lifestyle allows (i) genetically relative cells to stay close together and (ii) the hexose diffusion to benefit preferentially neighbouring cells, which in turn allows cooperation to benefit cooperators. Second, this system is stabilized by negative frequency selection of the cheaters: if their proportion is too high, the resulting hexoses accessibility will be drastically reduced and so as their growth. This does not prevent cheaters to cheat but rather prevents cheaters to invade and replace the cooperator population. In addition, the invertase activity is not mandatory for yeast growth because of a positive feedback loop between two phenomena: (i) sucrose is inevitably hydrolysed in acidic liquids and (ii) microbial fermentation acidifies the culture liquid. And because yeast favours hexose metabolism, sucrose metabolism usually occurs during the late fermentation phase. The enzymatic hydrolysis is thus not mandatory, but rather a small investment to accelerate resource consumption and proliferation, which in turn allows to increase competitive strength and colonisation capacities. Altogether, while the extracellular invertase hydrolysis can be subject to cheating, especially in liquid culture, cooperators still benefit from the metabolic cost of producing SUC2 and cannot be led to extinction by cheaters.

Studies investigating a possible cooperation between different yeast strains to degrade sucrose found no evidence to support its existence, as no SUC-deficient cheaters were found among wild *Saccharomyces* yeasts<sup>156</sup>.

But the SUC2 system in yeast could be classified as a helper/reproducer system of Division of Labour (**Figure 7A.d**). Such architecture is only possible within a single specie: helpers are specialized in a cooperative task that reproducers do not have to perform to focus instead on their own role: proliferate. Here within the same strain of yeast, helpers would be

specialized in invertase production to release public goods (glucose and fructose) in their microenvironment, while the reproducers focus on dividing to increase the colonization rate. Even if helpers see their individual fitness decrease, this type of interaction is beneficial because the overall population fitness increases. It is stabilized by negative frequency selection of the reproducers (or cheaters) because if their proportion is too high, the resulting accessibility of sugar will be drastically reduced and so as their growth.

However, whether wild type yeast actually performs this DoL has not been shown yet. There is no study yet focusing on SUC2 phenotypic variation within a same yeast strain, which could reveal that not all individuals are participating the same amount in the production of invertase. Due to intrinsic biologic noise, it is probable that indeed some individuals exhibit a “cheater” behaviour, but in addition, heterogenous sugar availability in space could amplify and structure these phenotypic variations. We will see in this PhD that indeed, we observe a SUC2 heterogeneous expression in a multicellular colony which seems to correspond to the emerging hexose gradients (see ChapI.4).

This system has also been proposed to be one possible origin of multicellularity: some yeasts fail to fully separate after mitosis, resulting in flak-like structures maintained by the yeast cell wall. This yeast trait optimizes their use of public goods<sup>146,157</sup>, an advantage that can be selected with respect to kin selection (limited dispersal and kin discrimination).

### SUC2 expression – internal and external invertase

The SUC2 gene can be transcribed into two different mRNAs that differ in their 5' ends: with or without the coding sequence of the signal peptide responsible for its secretion (1.9 and 1.8 Kb, respectively). As a result, there exist two isoforms of invertase protein: external and internal (532 and 512 amino acids, respectively). The transcription for the mRNA coding for the external invertase is mainly regulated by the glucose availability: when its concentration is above 2.5–3.2 g/L, the SUC2 promoter is repressed due to transcription factors (SFL1, MIG1/2, RGT1) binding to the SUC2 promoter<sup>158,159</sup>. In low glucose or fructose concentration (around 1 g/L), the expression is “derepressed”, and it is 5- to 10- fold higher than in the absence of hexose<sup>160</sup>. Despite significant improvements in our knowledge regarding the molecular mechanisms involved in the repression of SUC expression, the transcriptional activator of this gene is still unknown<sup>159</sup>, but chromatin change has been shown to be of importance for SUC2 induction<sup>161</sup> (histone acetyltransferases facilitate SWI/SNF's binding to SUC2 promoter). The non-glycosylated internal invertase is constitutively weakly expressed, with no apparent regulation mechanism. This would suggest that there are two transcription initiation sites regulated by two different promoters, but the putative sequences have not been clearly identified. Due to the low-affinity sucrose symporters, few sucrose molecules are imported so the internal isoform of the invertase plays a minor role in sucrose metabolism.



The different SUC2 promoter regulations are approximately represented in **Figure 13** based on the expression level values measured and published in<sup>146,160,162,163</sup>.

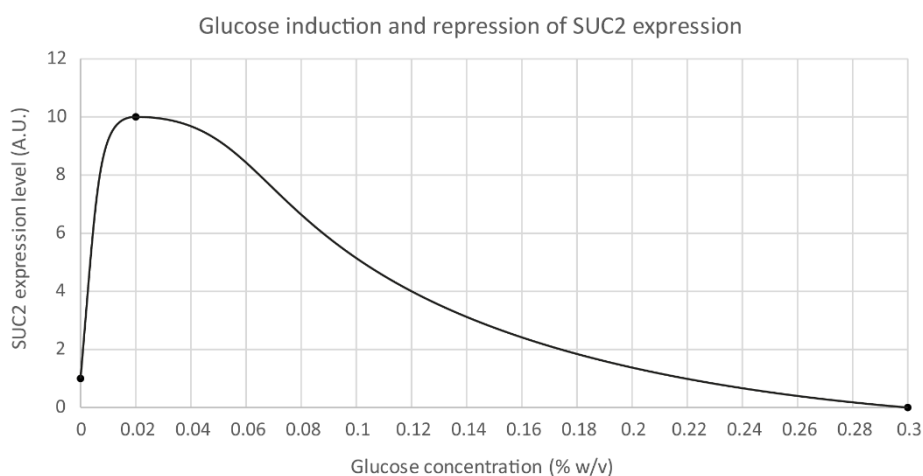


**Figure 13 – Approximative representation of SUC2 expression regulation by glucose concentration.** Based on experimental values extracted from<sup>146,160,162,163</sup>.

### Enzymatic properties

The SUC2 invertase is a  $\beta$ -D-fructosidase (or  $\beta$ -D-fructofuranosidase): it catalyses the hydrolysis of the glycosidic bond  $\alpha$ -D-glucose-(1 $\rightarrow$ 2)- $\beta$ -D-fructose<sup>164</sup> (**Figure 14**). Invertase belongs to the enzyme family GH32 (Glycoside Hydrolases) which has a characteristic N-terminal 5-fold  $\beta$ -propeller catalytic domain surrounding a central negatively charged active site cavity, and an additional  $\beta$ -sandwich domain appended to the catalytic domain (**Figure 15A**). An aspartate located close to the N-terminus acts as the catalytic nucleophile and a glutamate acts as the general acid/base catalyst<sup>165</sup> (for the reaction mechanism see **Figure 16**).

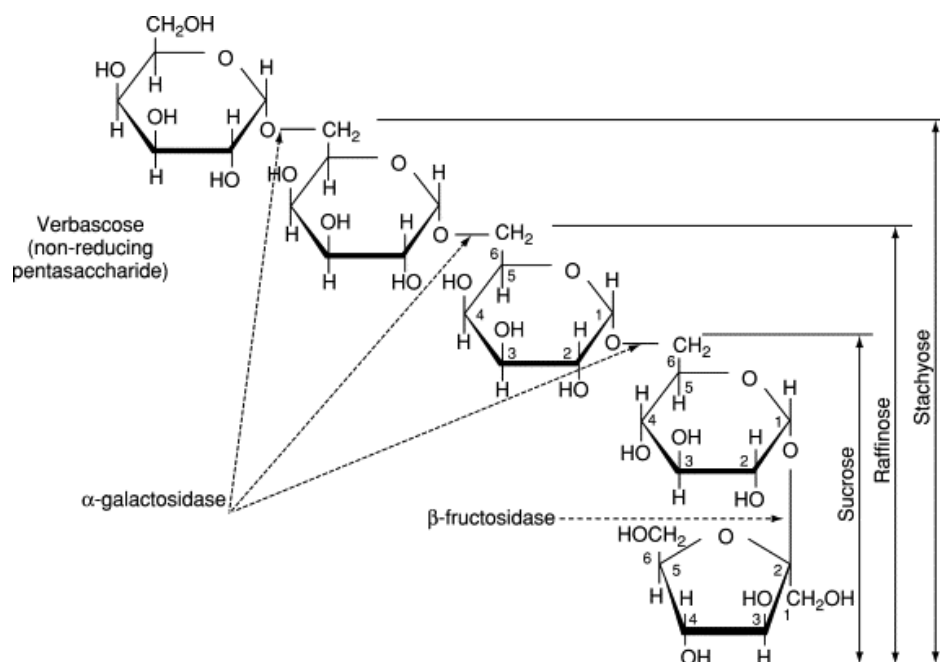


**Figure 14 – The different types of Invertase substrate.** Figures extracted from<sup>164</sup>

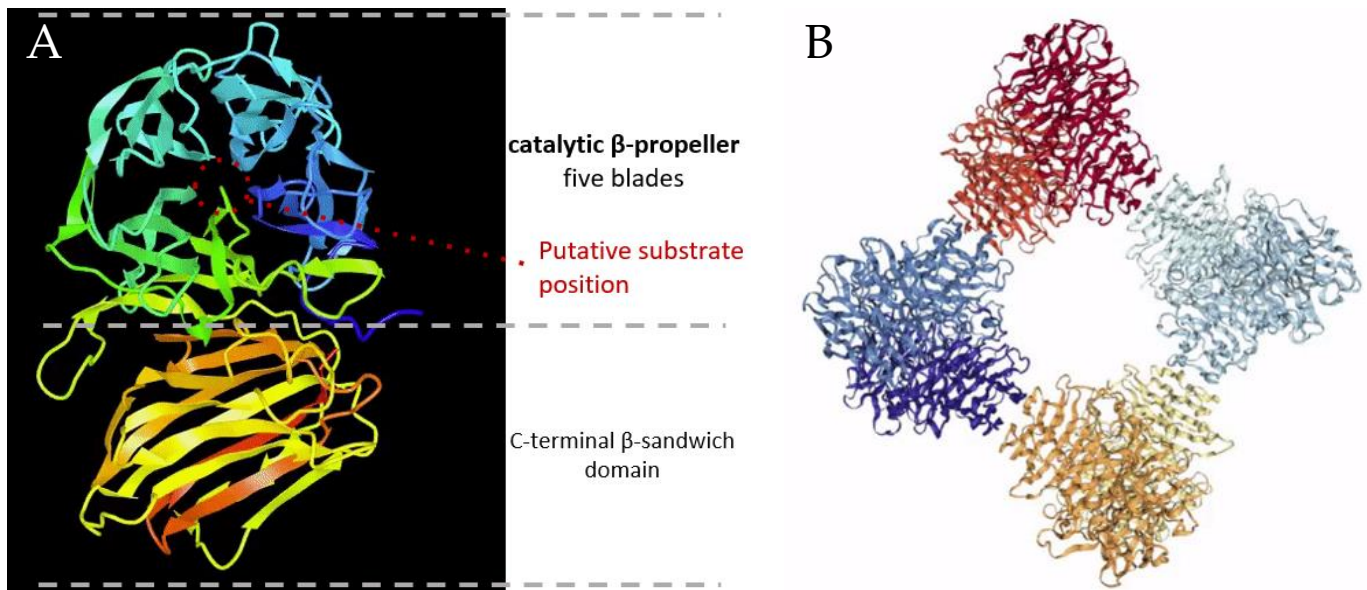


**Figure 15 - Three-dimensional Structure of Saccharomyces Invertase.** (A) the monomer (B) the octamer. Figures extracted from<sup>165</sup>

The monomer is composed of 512 residues (58.5 kDa), but the invertase is mostly observed in the form of a tetramer of dimers, equivalent to an octamer (428 kDa -  $130 \times 130 \times 110 \text{ \AA}$ ) represented in **Figure 15B**. The optimal conditions for its enzymatic activity are pH=5,5 and T=55-60°C<sup>166</sup>. At pH=5.0 and T=37°C, the values for  $K_{cat}$  and  $K_m$  have been determined as  $4700 \text{ s}^{-1}$  (for monomers) and 26 mM respectively. This enzyme is also highly N-glycosylated (mainly with variable sized mannose oligosaccharides<sup>167</sup>), which increases thermal stability<sup>168</sup>, prevents protease degradation<sup>169</sup>, maintains its oligomeric structure<sup>170,171</sup> and might increase the enzyme residence time in the periplasmic space<sup>172</sup>.

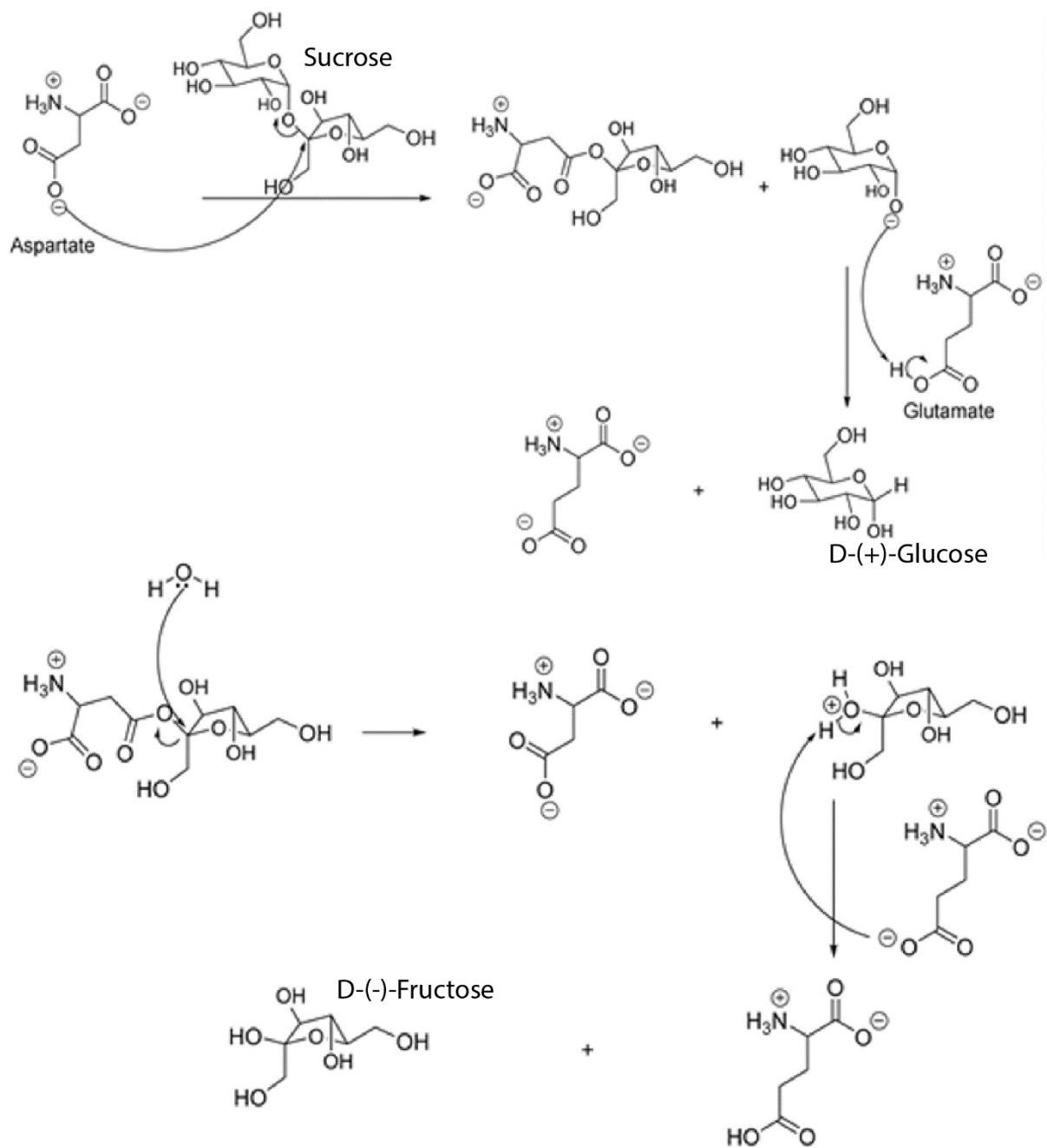


**Figure 16 – Mechanistic view of the invertase enzymatic activity.** The carboxylate group of the side chain of aspartate acts as nucleophile, while the carboxylic group of the glutamate amino acid acts as an acid (donor of the proton), and the conjugate base acts also as a nucleophile in the next reaction. Figure extracted from<sup>173</sup>

## Engineered yeast sucrose utilisation

Engineer yeast sucrose metabolism can be an efficient way to control the metabolic carbon flux and thus the yeast metabolic yield. Sucrose internal hydrolysis leads to a lower ATP yield (3 ATP/sucrose molecule instead of 4 for the external hydrolysis) because of the proton symport ATP cost. This in turn favours ethanol production over biomass production<sup>174,175</sup>. While the external hydrolysis is dominant in wild type yeast<sup>147,148</sup>, note that several research teams have genetically engineered *Saccharomyces cerevisiae* for sucrose metabolism to only take place internally. One engineered strain was designed to harness the lower ATP yield in anaerobic fermentation, which confirmed the theoretical prediction that it would favour ethanol production over biomass production<sup>175</sup>. In contrast, another strain was developed to exhibit a slow sucrose uptake rate, favouring respiration over fermentation, leading to higher metabolic yield for biomass production<sup>176</sup>.

## Maltose pathway's unspecific activity

As with many other examples of metabolic pathways, the invertase coded by the gene SUC2 is not the only enzyme implied in sucrose metabolism in *S. cerevisiae*. Indeed, because of the similarities between the molecule of sucrose (glucose- $\alpha$ (1 $\rightarrow$ 2) $\beta$ -fructose) and maltose (glucose- $\alpha$ (1 $\rightarrow$ 4)glucose) or isomaltose (glucose- $\alpha$ (1 $\rightarrow$ 6)glucose), some enzymes involved in the maltose and isomaltose metabolism exhibit a non-negligible enzymatic activity for sucrose. While the IMA group (isomaltase) is composed of 5 hydrolysing enzymes, the gene family MAL are composed of 6 complex loci found in subtelomeric regions of different chromosomes. Each locus is composed of 3 types of proteins: a transporter (1), a hydrolysing enzyme (2) and a transcription factor (3). Any given protein of these families is named as follows: MAL31 is the transporter of the locus number 3. Among these six proton-coupled symporters, MAL11 (or ATG1) is the most active on sucrose. Interestingly, some of the SUCx and MALx loci reveal to be linked together (locus proximity and non-coding flanking homologies) suggesting an evolutionary relationship between the two loci<sup>177</sup>. In addition, there are two other transporters MPH2&MPH3 (highly similar maltose permease) which exhibit some activity on sucrose.

To better understand the relative importance of these enzymes on yeast growth on sucrose, Marques et al. (2017)<sup>178</sup> engineered yeast strains so that there is not any sucrose utilisation left. They designed and successfully implement two different strategies: (i) remove any kind of hydrolysing enzyme (SUC2;MALx2;IMAx) or (ii) remove the invertase and all sucrose transporter (SUC2;MALx1;MPH2&3).

This unspecific activity of the maltose pathways on sucrose metabolism was not significant in the yeast background I used

I have introduced this manuscript giving a broad view of microbiology to then focus on microbial interactions, detailing the particularities of cooperation and division of labour. For sessile microbial populations, it is now clear that space is a major determinant of their fates. However, quantitative investigations on the spatiality of such systems are yet rare in microbiology literature. Indeed, it is sometimes difficult to estimate and measure the ranges of actions of microbial interactions as they depend on interlinked components: the colony geometry, its metabolic organisation and local nutrient availabilities. In-depth analysis of such spatial components could be of interest for the use of cooperation and division of labour in engineered microbiomes to improve current applications and develop future ones.

During my PhD, I used the *S. cerevisiae* cooperative system for sucrose metabolism as a model and propose an exploration of its spatial properties. My aim was to determine what types of spatial constraints apply to this public goods system and quantify the typical lengths that characterise it.

The envisioned strategy was to generate patterned cooperator/cheater consortia with imposed spatial organisations to investigate their impact on the population growth. To this end, we chose to use light to control invertase production in space, which requires to develop multiple tools. First, a strain for optogenetic control of SUC2 expression must be engineered, optimised and characterised to successfully control the cooperative state of the yeast cells. Then, illumination devices should be set up to project precise light patterns onto yeast culture recipients which prevent convection fluxes and only allow diffusion regimes, mimicking a sessile lifestyle.

I will now present my work, starting with the genetic engineering of multiple yeast strains and the characterisation of their growth in well-mixed liquid cultures. I then will describe how I investigated two different scales of spatial patterning of the cooperator/cheater consortium, first at the microscopic scale with the help of microfluidic tools, and then “zoom-out” at the millimeter to centimeter scale using the ‘*OptoCube*’, a custom device I built for simultaneous light projection and yeast growth monitoring on agar gels.





# Chapter I – Engineering yeast for light-inducible control of cooperation

Cells possess various biological sensors (chemical, light, pressure, ...), some of which are now well identified and characterised (mainly proteins and inducible promoter sequences), allowing the design of controllable (or inducible) synthetic biological systems. Chemical control systems have been commonly used in numerous and various studies, but media renewal is usually required to stop the induction and they are not very convenient to control and shape spatial patterns in microbial colonies. Optical control, a.k.a. optogenetics, is mostly based on photosensitive proteins that change their conformation upon illumination. The use of light has multiple advantages – high resolution in space and time, low cost, easy remote control and induction release – making it one of the best candidates to control biological spatial patterns.

## I.1. Optogenetics – Light sensitive transcription factor

The first optogenetic tools were developed at the dawn of the 21<sup>st</sup> century to study neuronal activity. Early attempts were quite complex, either using a heterologous photosensitive pathway from *Drosophila*<sup>179</sup> or using photocaged inhibitor and their corresponding heterologous ion channels<sup>180</sup>. The first single-component optogenetic tool reported was a photosensitive ion channel found in the green alga *Chlamydomonas*<sup>181</sup>, which when heterologously expressed in neurons can trigger cations fluxes and thus neuronal activity upon blue light illumination<sup>182</sup>. Since then, a broad range of light-sensitive tools have been developed, taking advantage of the growing library of natural photosensitive proteins characterised and protein engineering knowledge (**Figure 17**). It is thus possible to combine multiple optogenetic systems in one cell given that their activation wavelengths are sufficiently distinct<sup>183,184</sup>. Such optogenetic tools are nowadays used in various fields of biology, as they can virtually be used in any protein-producing organism. Notably, there are several systems that require certain cofactors for proper functioning, which can be either autologously produced by the organism or added to the nutrient solution (but can be expensive and/or toxic).



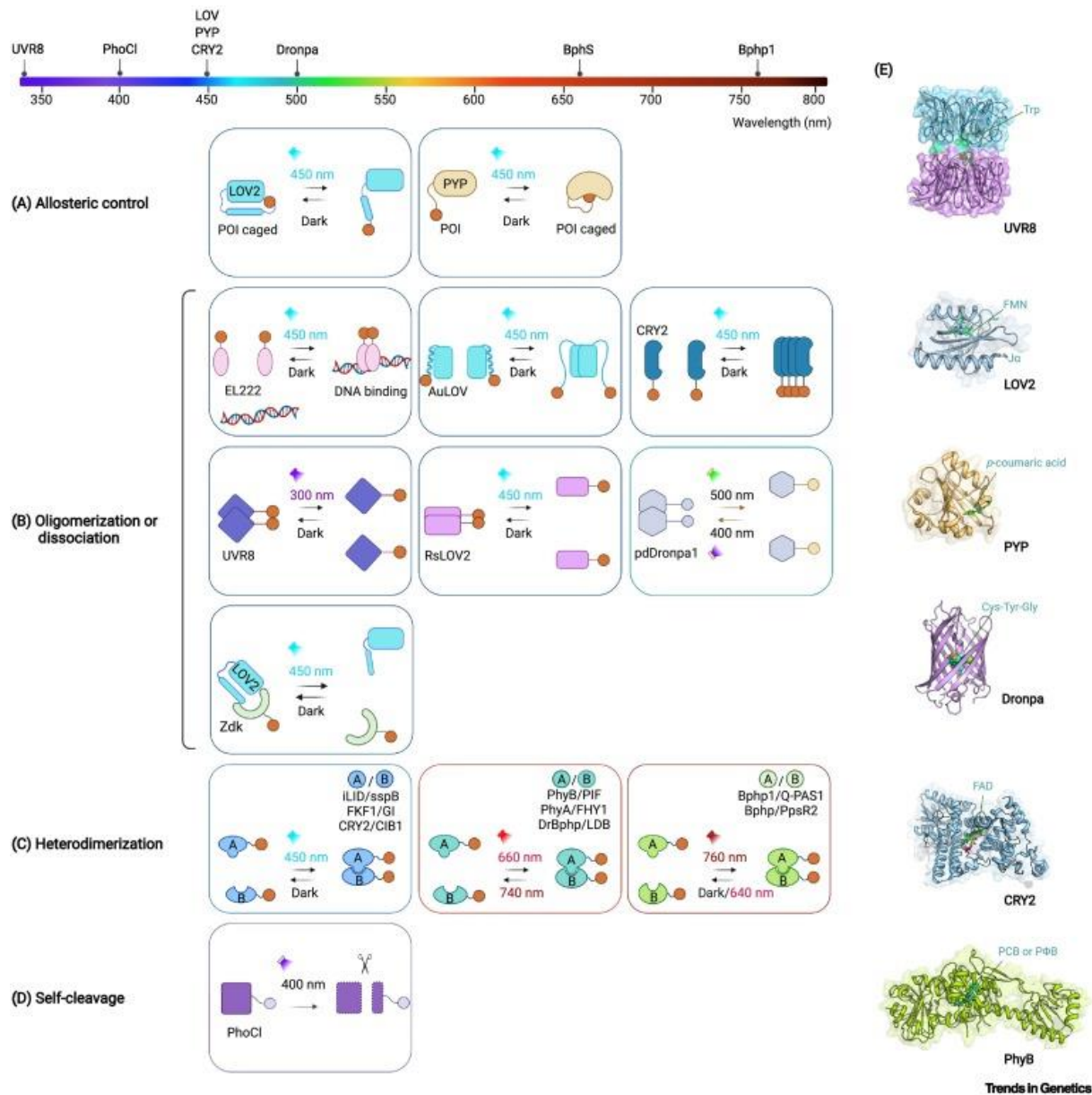


**Figure 17 - Representative photosensory modules and optogenetic engineering strategies.** (A) Photoswitchable allosteric control can be achieved by tagging or insertion of LOV2 or PYP into protein of interests (POIs), such as transcription factors, signalling proteins, and anti-CRISPR proteins. (B) Light-induced changes in oligomeric states, as seen in EL222, AuLOV, CRY2, UVR8, and pdDronpa1, are utilized to control protein–DNA or protein–target interactions for transcriptional regulation. Similarly, light-dependent dissociable systems, such as LOV2 Trap and Release of Protein (LOVTRAP), have been developed to photo-reverse protein–protein association. (C) Optical dimerizers that respond to light emitting at different wavelengths. Most commonly used combinations are indicated in the right corner. The A/B components of each pair can be modular engineered into proteins of interest to assemble functional transcriptional complexes, genome-engineering enzymes, or recombinases. (D) PhoCl engineered as a self-cleavable protein in response to light stimulation at 400 nm, which can be incorporated into POIs to conditionally inactivate their function with near UV light. (E) Three-dimensional structures of typical photosensory modules, with the light-absorbing cofactors or chromophores shown in sticks. Figure extracted from<sup>185</sup>

We can for example mention the CRY2/CIBN system: the photosensitive CRY2 protein change conformation upon blue light illumination, inducing its binding to its CIBN partner, forming a reversible heterodimer. This system requires FAD cofactor to be functional, molecule present in almost all organisms given its importance for redox-active enzymes. Such optogenetic protein pair has been used to engineer various light induced functions such as cell adhesion<sup>186</sup>, gene transcription<sup>187</sup>, DNA editing<sup>188</sup> or protein localisation. For the latter, CIBN can for example be anchored to the cell membrane intern surface, allowing to recruit locally the light activated CRY2 proteins<sup>189</sup>. By fusing CRY2 with GEF proteins, this light induced protein recruitment can be used to regulate locally GTPase protein activity, in turn allowing to control mammalian cell motility<sup>190</sup>. One of the drawbacks of such heterodimer systems is the requirement to produce each member in equal amounts., typically optimized by promoter strength tuning. There are also optogenetic systems which combine a light sensitive protein with various versions of Cas9 protein, to achieve high specificity DNA targeting and/or DNA editing<sup>185</sup>. Similarly, optogenetics has been used to control recombinase activity with light, allowing to induce gene knock-out and synthetic circuit rewiring with single-cell precision<sup>185</sup>.

In our case, we use an already established system for optogenetic control of transcription in yeast to obtain reproducible light-inducible gene expression. We choose the EL222 system<sup>191</sup> which is composed of a photosensitive LOV domain, attached to a DNA-binding HTH<sup>ix</sup> domain, that changes conformation upon blue light illumination (450-470nm) leading to homodimerization. Only this dimer form can bind to a specific 12 bp DNA sequence. We used the pC120 promoter<sup>192</sup> containing 5 repeats of this sequence, with the addition of a TATA box minimal promoter. To improve its efficiency in eukaryotes, a VP16 transcriptional activation domain (AD) and a nuclear localization signal (NLS) sequence have been added<sup>192</sup>. The final construct allows to activate quantitatively the transcription downstream of pC120 promoters upon blue light illumination. In our hands, this EL222 system proved to have better induction properties compared to its predecessor CRY2/CIB1

Using light as an induction system implies certain experimental constraints. First, ambient light can obviously uncontrollably induce the system when the cells are manipulated. While this is true, the problem can be avoided in multiple ways: making sure all the incubation locations are in the dark, reducing the duration of the cell manipulation, reducing the ambient light to a low level (just enough so the experimentalist can see) or using coloured light far from the optogenetic specific wavelength (typically red light for EL222). Also, while using light instead of chemical inducers alleviate the problem of chemical toxicity, it can still be harmful to cells. Indeed, when light interacts with biomolecules, the absorbed energy induces various chemical reactions that can impair cell function. This phototoxicity is considered to be mainly due to light induced Reactive Oxygen Species (ROS) production<sup>193</sup>. This depends on the

---

<sup>ix</sup> helix-turn-helix

exposition duration, light intensity and wavelength. The shorter wavelengths being more energetic, light below 500 nm (blue and UV) is particularly detrimental<sup>194</sup>. Another important aspect is that optogenetic systems can be activated by fluorescence measuring devices. Typically, blue light optogenetic system should not be used with GFP reporter proteins to quantify the resulting optogenetic induction as the measurement and the induction are affected by the same light wavelength. Attention should also be taken for the fluorescent excitation filter used in the measuring device. As an example, YFP fluorescence signal is typically measured with an excitation filter which produces light from 490nm to 510nm. This light could activate EL222 proteins whose absorption spectra is between 300nm and 500nm. Using instead a 509nm to 519nm excitation filter (normally used for lasers) allowed me to image YFP under an epifluorescent microscope without activating the optogenetic system.

Depending on experimental constraints, various illumination devices have been proposed in the literature. For example, *in vivo* neural activation on living mice brain requires the device to be portable and miniaturized. For *in vitro* stimulation, different culture recipients can be upgraded to obtain a time control illumination, as I did during my PhD (**Figure 18**). I mainly used the OptoBox (described below) for bulk stimulation, an epifluorescent microscope for single cells stimulation, and the so-called '*OptoCube*' for spatially resolved macroscale illumination patterning (more information on the OptoCube in **Chapter III**).

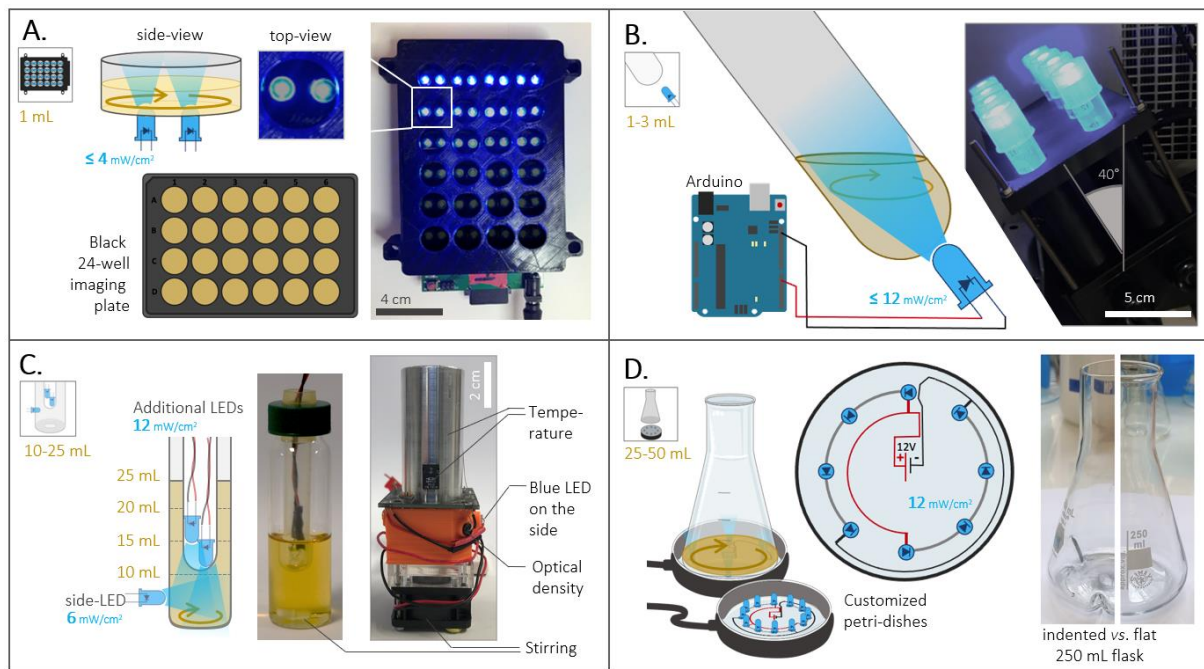


**Figure 18 - Four optogenetic devices allowing for various culture volumes and conditions.** (A) Light-plate apparatus<sup>195</sup> (a.k.a. the “OptoBox”) illuminates independently 1 mL cultures in 24-well plate. Two LEDs (0 to 4 mW/cm<sup>2</sup>) illuminate the culture from below and are programmed via a custom software. (B) The OptoTubes illuminate standard 14 mL culture tubes with a LED (0 to 12 mW/cm<sup>2</sup>) placed at their bottom. It is programmed with an Arduino. (C) The eVOLVER system<sup>196</sup>, uses a DIY “sleeve” (right) where a glass vial (center) can be inserted. For each of the eVOLVER unit, temperature, stirring and illumination conditions can be controlled. In addition, optical density can be monitored. The glass vial’s lid was adapted to accommodate for more light input (side-LED: 6 mW/cm<sup>2</sup> + additional LEDs: 12 mW/cm<sup>2</sup> each). (D) The OptoFlask, is a custom-made stand containing various number of LEDs placed circularly (12 mW/cm<sup>2</sup> each), on top of which a flask (flat or indented) can be placed. Devices placed in a shaking incubator. LED wavelength  $\lambda=460\text{nm}$ . Figure extracted from Pouzet et al. 2022 [under revision].

## I.2. Assemble DNA with Modular Cloning

Genetic circuits are composed of DNA sequences, or genetic parts. These parts are organized in a specific order depending on their function, which I will also refer to as 'type'. The canonical example is an expression cassette composed of three types of part in the order promoter > coding sequence > terminator. Other types of genetic parts include signal peptide for protein secretion, protein degradation tag, RNA degradation tag, plasmid origin of replication, ... Given that the genetic parts are placed in the right order, one can change the sequence of a part without affecting the function of its neighbours although it is not always as predictable.

Building on these facts, Modular Cloning technics (MoClo) have been proposed to facilitate the construction of functional genetic circuits. Based on type IIS restriction enzymes cutting DNA outside of their recognition sites (*a.k.a.* GoldenGate assembly), the MoClo is a library of genetic parts that can be assembled in a modular fashion. While the use of GoldenGate assembly can theoretically allow any type of combinatorial assembly, it is more efficient to use a simple and standardized architecture to organise how the parts should be assembled. A MoClo is usually organised in plasmids of three different levels: 0, 1 and 2 (**Figure 19**). Level 0 plasmids contain a single genetic part carried by a generic vector plasmid. Level 1 plasmids are constructed using multiple level 0 plasmids, extracting each genetic part to form a functional plasmid containing one expression cassette. Level 2 plasmids are constructed using multiple level 1 plasmids, extracting each expression cassette to form a functional plasmid containing multiple expression cassettes. Once constructed, any level plasmids are transformed in *E.coli* cells to screen for correct assemblies, isolate them and amplify their quantity. They can then be used either as functional plasmids to be transformed into the organism of interest or serve as DNA templates for PCR whose product can be used as repair fragments for CRISPR/Cas9 genomic insertions.

I used the Modular Cloning system adapted for yeast<sup>197</sup> to assemble custom expression cassettes which I then integrated into the yeast genome. We bought the YTK MoClo kit from addgene (Kit #1000000061) and supplemented it with my own parts. Precisely, I built level 0 plasmids for the following parts: pC120, SUC2, P2A, p2RGal and multiple HairPin parts (see below). I notably had to include a silent mutation in the SUC2 sequence to remove an undesired restriction site. The use of the MoClo was particularly useful to integrate multiple hairpin sequences with various degradation rate<sup>198</sup> and to build the corresponding expression cassette library. This allowed to test multiple designs at once to find which hairpin sequence performs the best for the invertase system.

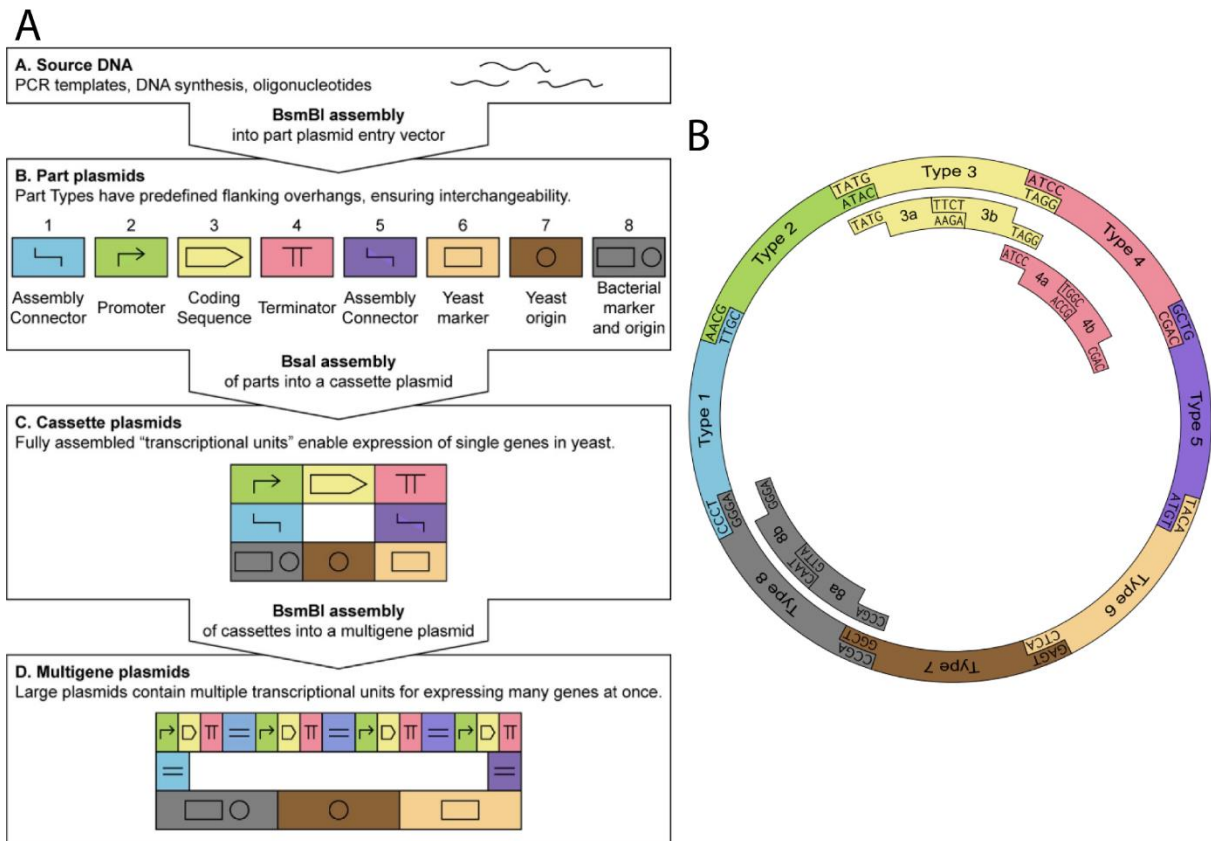


**Figure 19 – Modular Cloning (MoClo) in yeast.** (A) MoClo workflow and the different levels: part (level 0), Cassette (level 1) and Multigene (level 2). (B) Details of a level 1 plasmid showcasing the possible assemblies of multiple coding sequences in one expression cassette. Figure extracted from<sup>197</sup>

### I.3. Strains construction

To obtain the strains used in this work, all genetic parts have been integrated into the genomic DNA of the yeast using CRISPR/Cas9 or selection markers to ensure the stability of the construct. Using CRISPR/Cas9 was very efficient and allows to obtain scarless genetic modification with only one selection marker prerequisite (the transformation of the CRISPR/Cas9 expression plasmid use URA selection marker). I started by integrating two parts that will be present in all my strains: a nuclear fluorescent marker mApple-HTB2 and an EL222 expression cassette. The former is a convenient tool for microscopy image analysis and constitutive fluorescence reference. The latter should not have any effect by itself (without its corresponding inducible promoter). To allow better comparisons between the strains, I consider the resulting strain as **WT**. I then deleted the endogenous SUC2 gene to abolish internal and external invertase production. The resulting strain **ΔSUC2** should have a drastically reduced growth in sucrose.

By introducing a SUC2 gene under the control of the inducible promoter **pC120** in the ΔSUC2 strain, we should be able to control the invertase production quantitatively using blue light. To monitor the actual invertase production, I added at the C-terminal end a fluorescent protein tag (mVenus) with two different designs. Both are constructed with the invertase signal peptide located just after the promoter to ensure proper excretion of the protein, but they differ by the linker between SUC2 and mVenus. One of them is a classical **fusion** protein (**yPH470**), while the second possesses a 22 amino-acid long self-cleaving peptide<sup>199</sup> as linker called **P2A** (**yPH471**). The latter allows to split the resulting protein post-translationally, which results in an equimolar production of invertase and mVenus. This was anticipated to solve a potential impairment of the tagged protein functioning by the classical fusion design.

I also constructed a **Reporter** strain which should allow to monitor endogenous SUC2 expression profile in yeast population.

We choose the fluorescent proteins in order to independently activate the optogenetic system (EL222~460nm), quantify the invertase production (mVenus~515nm) and image yeast nucleus (mApple~570nm). This required to carefully choose the fluorescence filter for mVenus, making sure that the excitation bandwidth was not below 500nm to avoid unintentional optogenetic activation of the EL222 system. The resulting strains are represented in **Figure 20**. More detailed information on the protocols used, the strain and plasmid lists can be found in appendixes. I will present in the next section the characterisation and optimisation process of these strains, which will result in two additional strains: yPH536 and yPH540.

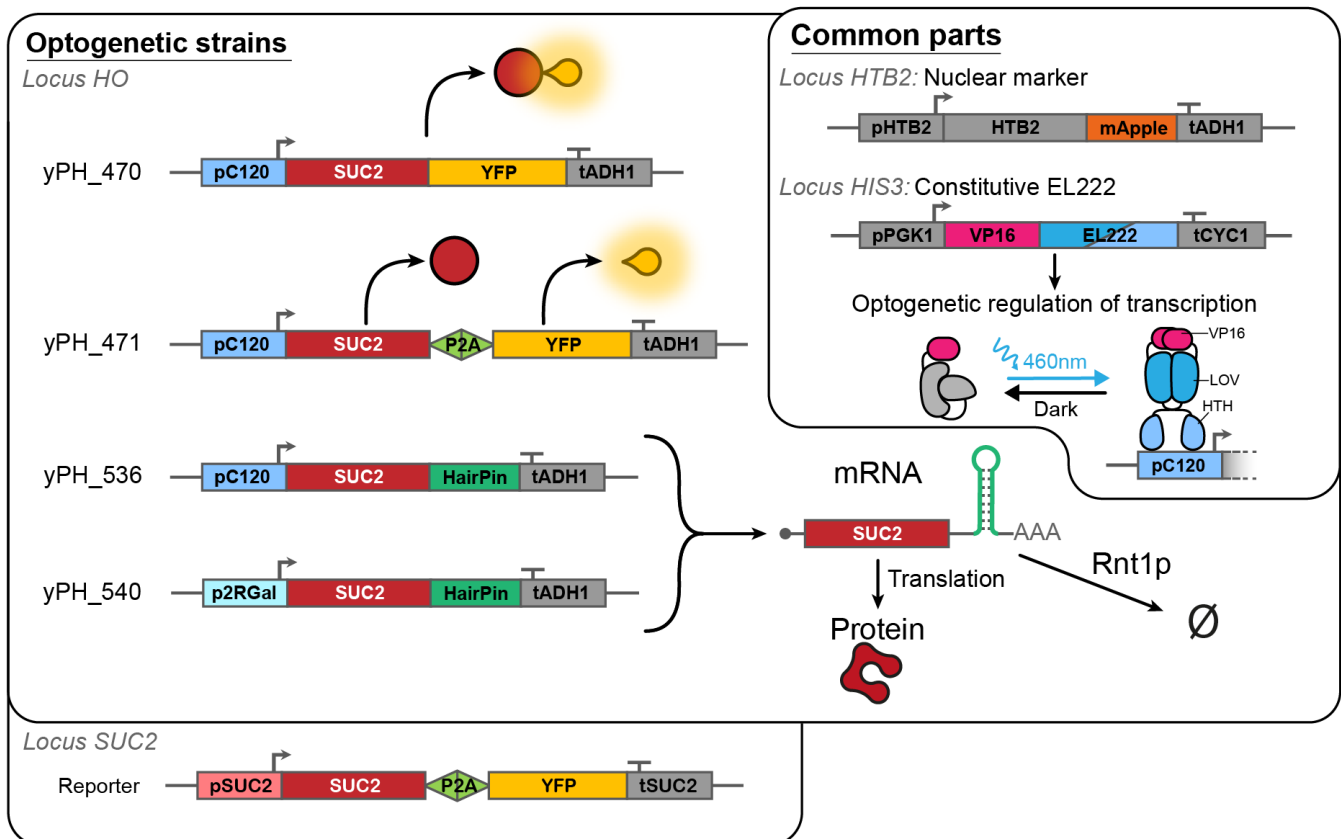


**Figure 20 – Yeast strains built and used during my PhD.** All strains have a mApple nuclear marker and a constitutive EL222 expression cassette. yPH470, 471, 536 and 540 are optogenetic strains producing invertase SUC2 upon blue light illumination. yPH470 has a classical fusion protein construct tagging SUC2 with YFP (mVenus). yPH471 construct also allow to monitor SUC2 expression but with the help of a P2A sequence so the invertase and YFP protein separate during translation. yPH536 and yPH540 constructs allow to reduce the SUC2 expression using a HairPin tag for mRNA enhanced degradation (by Rnt1p ribonuclease), but do not possess fluorescent marker. yPH540 has a weaker optogenetic promoter (p2RGal) than pC120. The reporter strain construct allows to monitor SUC2 wildtype expression (native promoter and locus) using a P2A sequence and a YFP.



## I.4. Strains characterisation and optimisation

I characterised the strains by measuring cell invertase activity (**Figure 21A**) and YFP fluorescence (**Figure 21B,C**) after a 2h enzyme production phase. This production phase was performed in a 24-well plate using a homemade Light Plate Apparatus<sup>195</sup> to control blue light illumination (**Figure 18**). To compare our strains to the WT expression level of invertase, the production phase was done in 0.05% glucose liquid media so that the native SUC2 promoter was derepressed. Extracellular enzymatic activity was measured directly on living cells using a glucose quantification assay kit and normalised by the total amount of protein using Bradford assay. As expected, WT and  $\Delta$ SUC2 strains are not responsive to light induction, and both light-inducible SUC2 strains (yPH\_470 and yPH\_471) show a clear increase in invertase activity upon blue light stimulation. Using a 2.8 mW/cm<sup>2</sup> light source, yPH\_470 and yPH\_471 produced an enzymatic activity of 40% and 310% of the WT respectively. Interestingly, the yPH\_470 strain only reached ~13% of the invertase activity measured for the yPH\_471 strain, despite having the same promoter. Cytosolic fluorescence levels show a similar trend in which the yPH\_470 value is ~20% of the yPH\_471 value. These results suggest an impaired invertase production when the enzyme is fused to a fluorescent reporter (yPH\_470), which is likely due to protein quality control in the early secretory pathway<sup>200,201</sup>. This shows the importance of using a P2A sequence to monitor gene expression in our case.

I then investigated how invertase activity influences yeast growth in sucrose in batch culture upon illumination. I performed these experiments in the same way as before: 2h invertase production phase in 0,05% glucose followed by monitoring growth in 1% sucrose. I then estimated invertase production in the presence or absence of illumination by using the maximal growth rate as a proxy (**Figure 21D**). We observe that the  $\Delta$ SUC2 strain showed slow growth in sucrose, with a maximal rate at ~30% of the WT. This could be due to the presence of maltose symporters with residual activity for sucrose<sup>202</sup>, but we did not observe any difference when the corresponding genes MAL11, MAL31 and MPH2-3 were deleted. We thus attributed this residual growth to the previously mentioned slow degradation of sucrose by acid-catalysed hydrolysis<sup>203</sup>, which is probably amplified by the media acidification due to yeast fermentation. This is discussed in more detail in the next section.

In addition, we observed that even in the absence of blue light illumination, the light-inducible SUC2 strains were growing faster than the  $\Delta$ SUC2. This likely corresponds to the known basal expression leaking out of the pC120 promoter<sup>204</sup>, enhanced by the long lifetime of the Suc2p protein (no activity loss measured after 48h of incubation at 30°C between pH 4 and 6)<sup>205-207</sup>. Therefore, although a straightforward strain construction did work, it did not give an optimal control over Suc2p production. Indeed, the basal activity of the pC120 promoter was already high enough for cells to progressively accumulate Suc2p in the cell wall, resulting in a significant growth rate in the dark (**Figure 21D**). To overcome this difficulty, we

undertook two strategies: (i) reduce the promoter leakage and (ii) reduce the SUC2 mRNA lifespan. This was done (i) by replacing the minimal promoter of the pC120 promoter<sup>204</sup> and reducing the number of repeated binding domains from five to two (=p2RGal), and (ii) by adding a hairpin mRNA degradation tag at the 3' end<sup>198</sup>. We constructed the DNA sequences using the previously described Modular Cloning technics, and we integrated them into the yeast genome using CRISPR/Cas9 (see methods in annexes). The resulting strains are yPH\_536 (hairpin) and yPH\_540 (p2RGal + hairpin) and their behaviours are shown in **Figure 21D,E**.

We expected that our strategies to reduce invertase production in the dark will not critically reduce growth for the illuminated conditions because we observed that when activated, the yPH\_471 strain produced more invertase than what is required to support yeast growth on sucrose (**Figure 21A,D**). Our results showed that both strains have reduced growth rates in the dark compared to our first construct (yPH\_471). However, while the yPH\_536 has a comparable growth rate to the WT and yPH\_471 when illuminated, the yPH\_540 maximal growth rate is diminished to 61% of the WT (**Figure 21D**). Therefore, the hairpin degradation tag was an efficient strategy to reduce the residual growth in the dark while showing a clear increase in growth rate upon illumination. As the difference in SUC2 expression between light and dark conditions of the yPH\_536 strain is the highest, I choose to focus on this strain for the rest of our study.

In august 2021, a study was published reporting the use of optogenetics to produce the sucrose invertase Suc2p in *S. cerevisiae*. This study is based on the CRY2/CIB1 optogenetic system<sup>208</sup>, which in contrast with the EL222 system is insufficient to recover the WT growth on sucrose. They notably showed the formation of ring-like patterns, due to cooperators activating the growth of cheaters by producing hexose while simultaneously inhibiting the growth of cheaters by competing for amino acids. Nevertheless, we think our work can serve as a complement, offering a more quantitative investigation of the spatial behaviour of such cooperator/cheater systems.

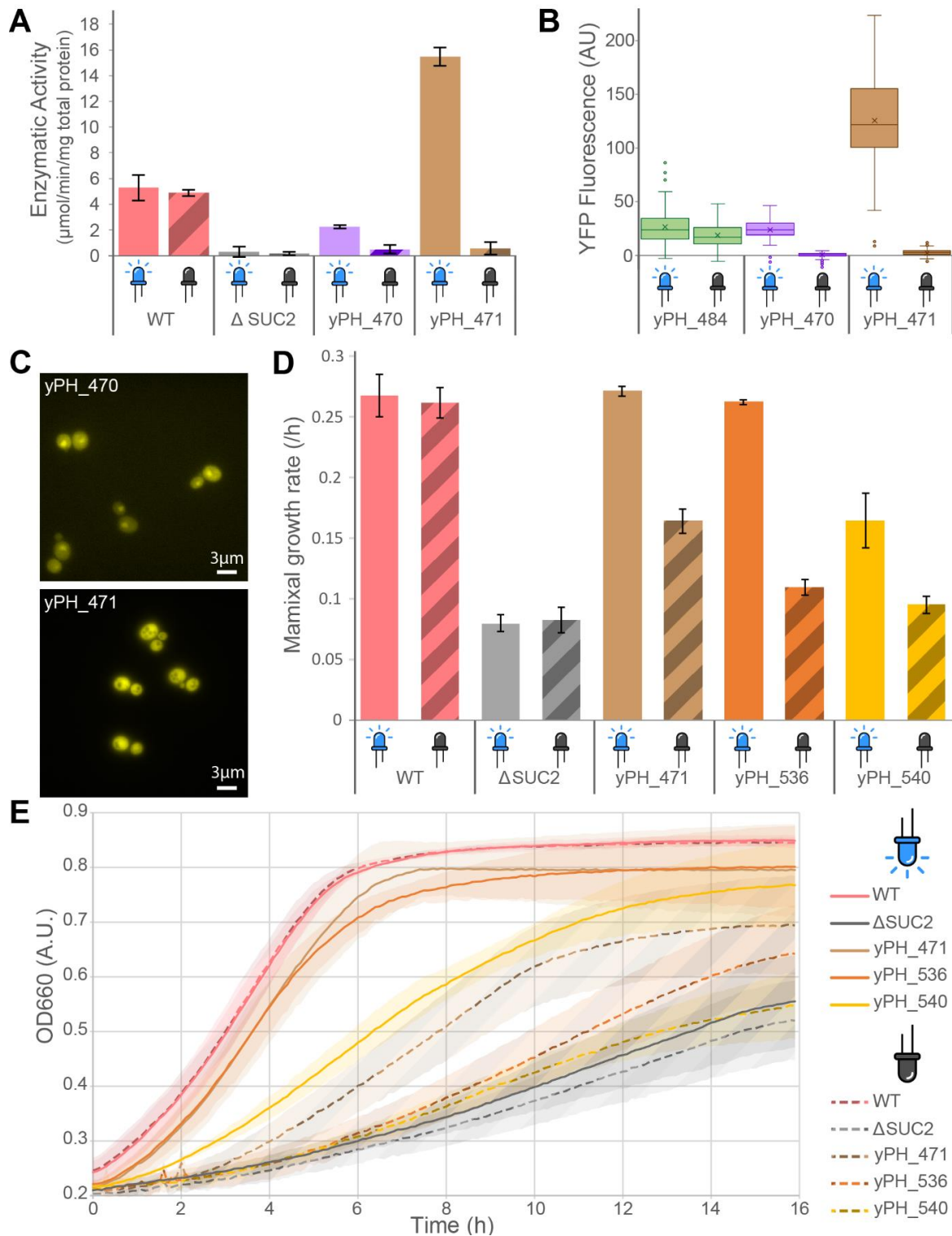


**Figure 21 – Strains characterisation.** (A) Yeast enzymatic activity induced upon illumination, measured with a glucose enzymatic assay. (B) Corresponding fluorescence quantification of microscopy images on  $43 < n < 134$ . (yPH484 is a reporter for WT expression of SUC2), (C) Microscopy images of YFP fluorescence of illuminated cells, (D) Maximal growth rate in SC 1% sucrose, retrieved from growth curves in (E) obtained with a plate-reader. The yPH\_536 display the best dynamic range for inducible growth on sucrose. Data were obtained after 2 h of invertase production: yeast cells were illuminated with continuous blue light ( $2.8\text{mW}/\text{cm}^2$ ) or kept in the dark using the Light-Plate Apparatus in media with 0.05% glucose. Error bars of panel (A) and (D) represent  $\pm$  the standard deviation for 3 technical replicates.

To better grasp the wildtype spatiotemporal SUC2 expression in yeast communities, I built a fluorescent reporter strain of SUC2 native expression without impairing the resulting invertase activity. I imaged colonies of the SUC2-reporter strain growing on agar petri dishes at 24h, 40h and 64h after inoculation. I used a fluorescence microscope to capture the Venus signal from SUC2 expression, as well as the constitutive mApple signal which is used to normalize by cell density. I also vary the sucrose concentration to 0.1% and 1%. Retrieving the glucose concentration from SUC2 expression is however not straightforward because the SUC2 expression level is not monotonic with respect to glucose concentration (**Figure 13**). For the colony growing on low sucrose concentration (**Figure 22A,B**), the SUC2 expression profile is established within the first 24h of growth to then increase overall without changing its shape. We can note that the resulting ring of maximal SUC2 expression is located at the periphery, where the sucrose concentration should also be the highest, optimizing the energy investment in invertase production. For the colony growing on high sucrose concentration (**Figure 22C,D**), the SUC2 expression profile seems overall stable in time, which could correspond to a steady state between hexose release and hexose consumption.

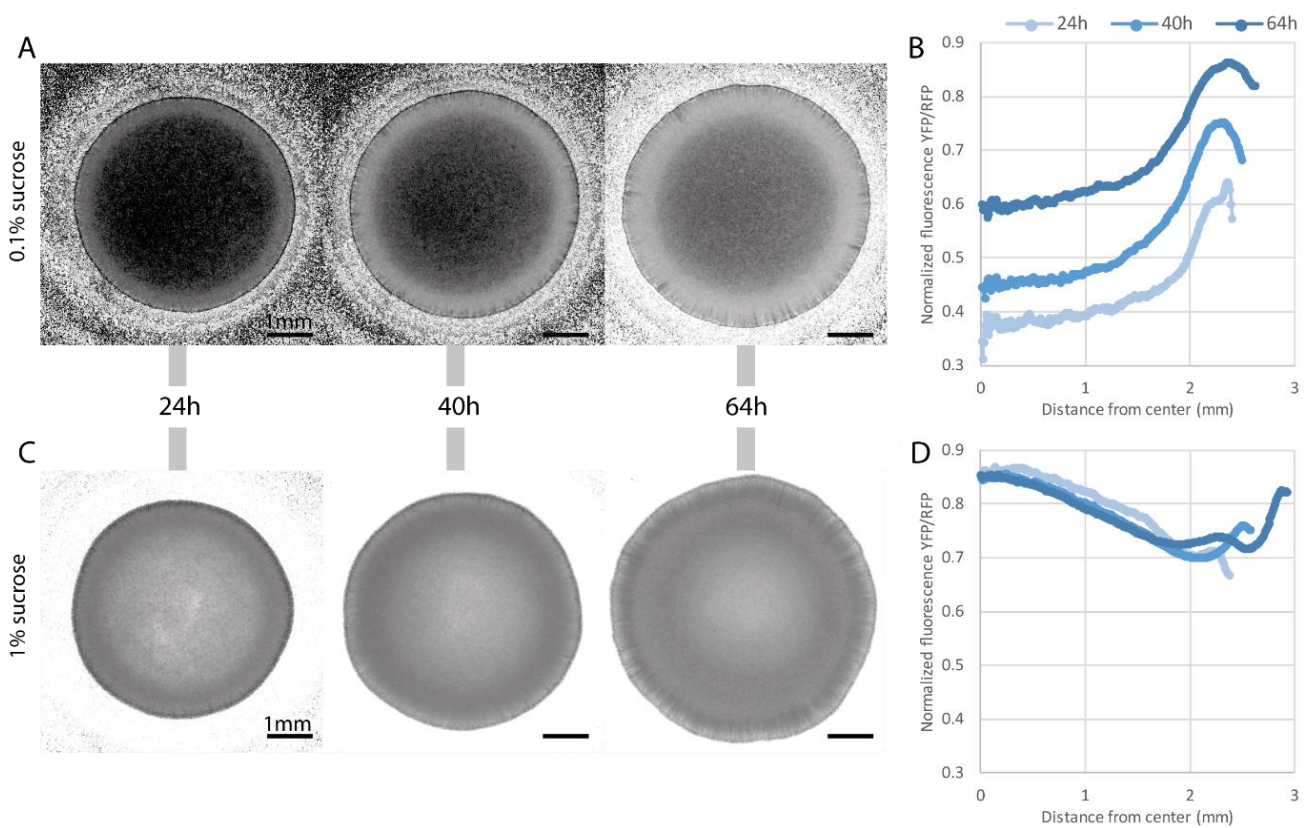


**Figure 22 – Spatiotemporal native SUC2 expression profiles in yeast colony.** Two colonies were monitored growing on SC agar at 0.1% (A, B) or 1% (C, D) sucrose at 24h, 40h and 64h after inoculation. (A) and (C) are the normalized fluorescence images YFP/RFP to remove the influence of cell density on fluorescence levels. (B) and (D) represent the evolution of the image radial profiles in time.

## I.5. Residual sucrose utilisation

Sucrose is a disaccharide composed of an alpha glucose and a beta fructose molecule, linked by an alpha glycosidic bond. When sucrose is dissolved in water, solvent molecules can hydrolyse the glycosidic bond releasing glucose and fructose. As previously mentioned, this reaction can be catalysed by the invertase, but can also be catalysed by protons (or more precisely by hydronium  $H_3O^+$ ). The reaction kinetic is of the first order and depends on hydronium concentration, which by definition is proportional to the negative power of ten of the solution pH<sup>209</sup>. The reaction can be written as follow:

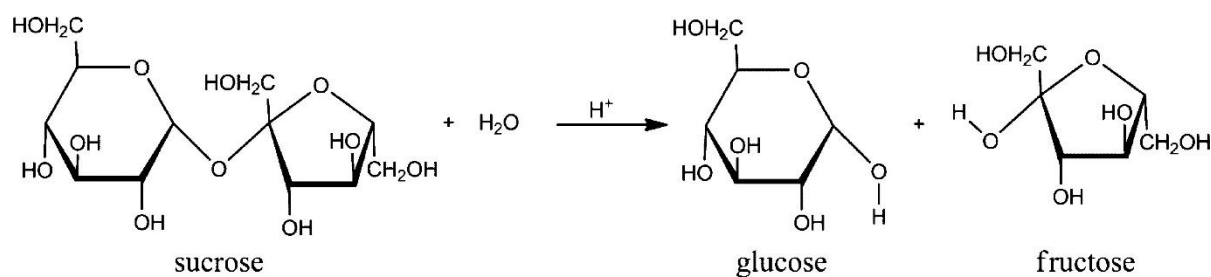


**Figure 23 – Acid catalysed sucrose hydrolysis chemical reaction.** Figure extracted from<sup>210</sup>

Following Arrhenius law, this reaction is also accelerated at high temperatures. These facts have been notably used by industries to produce “inverted syrup” (glucose + fructose) from sucrose: acid hydrolysis (pH~2) at mild temperatures (~60-80°C, higher temperature would degrade the produced hexoses). However, because such physico-chemical conditions also produce unwanted molecules that impair the taste and colour of the syrup, the use of yeast invertase is nowadays predominant. There are also alternative catalysts, notably immobilized and thus recoverable, that have been shown to be efficient for sucrose hydrolysis<sup>211</sup>.

Acid-catalyzed hydrolysis of sucrose was one of the first described catalytic reactions, and was commonly used to study general chemistry laws, leading to ground-breaking works such as one of the first quantitative studies of chemical kinetics<sup>212</sup> or the classic Arrhenius law<sup>213</sup>. While there is a large amount of study using this reaction as model, the exact reaction mechanism was still not clearly established in the literature until recently.

The reaction happens as follows: protonation to the oxygen of the glycosidic bond, glycosidic bond cleavage, and the resulting carbocation is finally hydrated by water nucleophile attack. The rate-determining step of this reaction is the glycosidic bond cleavage. The main uncertainty relies on the exact point of bond cleavage: fructosyl-side or glucosyl-side. Experimental data suggest a fructosyl oxygen bond fission<sup>214</sup>. This is not straightforward to measure as the rapid anomerization reactions of fructose and glucose in acidic solutions prevent the detection of the initial (and intermediary) products. A recent theoretical study using density functional theory calculations showed that “the fructosyl-oxygen bond cleavage is

slightly more favorable than the glucosyl-oxygen one, not kinetically but thermodynamically”<sup>210</sup>. Thus, while both cleavages occur primarily, the concomitant isomerisation reaction between the two carbocation transition states finally favour the products resulting from fructosyl oxygen bond cleavage (alpha-D-glucose and a fructosyl carboxonium ion).

To avoid the presence of residual glucose in culture media, any sucrose media must be prepared fresh, and any sucrose stock solution should be stored at a pH above 8 and at a low temperature to prevent its hydrolysis. However, yeast culture media are slightly acidic (pH~5). In addition, yeasts acidify their microenvironment while growing, by secreting organic acids and pumping out protons, and attempting to buffer yeast culture media pH impairs yeast growth and does not prevent media acidification<sup>215</sup>. There is thus uncontrollable sucrose hydrolysis during yeast growth, which we will call residual sucrose utilisation.

We can estimate the acid catalysed sucrose hydrolysis using the following equations:

$$\frac{[S]}{[S_0]} = e^{(-k_{exp}t)}$$

with

$$k_{exp} = A \times e^{\left(\frac{-E_a}{RT}\right)} \times 10^{-pH}$$

Using the parameters  $A = 1.15 \times 10^{15} \text{ mol}^{-1} \cdot \text{L} \cdot \text{s}^{-1}$  and  $E_a = 1.08 \times 10^5 \text{ J/mol}$ .

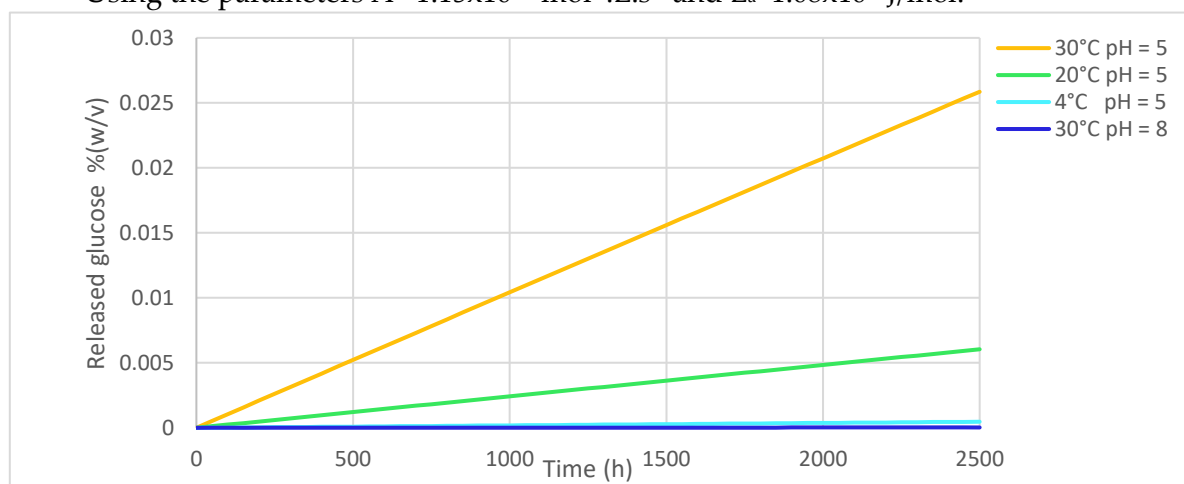


**Figure 24 – Computed glucose released from acid catalysis of a 1% sucrose solution stored at different conditions of temperature and pH. To properly store a sucrose stock solution it is best to increase the pH up to 8, and/or keep it at 4°C.**

Examples of computed glucose released for acid catalysed sucrose hydrolysis can be found in **Figure 24**. I verified experimentally such estimation for two SC 1% sucrose unbuffered solutions with a pH measured at 5, one stored for 90h at 30°C and the second for 2500h at 20°C. Using a glucose enzymatic assay, I obtained a release of 0.002% and 0.012% w/v of glucose respectively, twice the amount predicted by the computation in **Figure 24** of 0.001% and 0.006% w/v of glucose.



# Chapter II – Microscopic spatial activation of SUC2 expression with light

## II.1. Microfluidic device for microscopy observation

Microscopic observations allow to acquire single-cell information and are thus very powerful for quantitative biology. For yeast observation, microfluidic devices are a good solution to perform long time lapses as they allow to perfuse culture chambers with liquid media, while forcing cells to form colonies in monolayer to facilitate imaging. These devices are usually made of a Polydimethylsiloxane (PDMS), polymer with good casting and optic properties, as well as gas permeability which is crucial for microbial proliferation.

It is still worth noting that performing a microfluidic experiment can sometimes be a delicate and tedious task.

### Microfluidic chip designs

I worked with two main microfluidic chip designs for continuous culture of yeast, which differ in their nutrient availability. They are both composed of (i) thin chambers to trap and observe yeast cells as a monolayer and (ii) large flow channels for culture media renewal. The liquid flows in the large channels are controlled by a peristaltic pump, and their leaching into the chambers is prevented by fluid resistance due to the small volume of the chambers. The goal is to obtain a fully diffusive regime in the chamber for microbial growth, which is mostly reached in our microfluidic chip designs. The geometry of the “Yeast mother machine”<sup>90</sup> (**Figure 25A**) is designed with a dead-end to induce the formation of monodirectional gradients from the source to the sink (respectively Flow Channel -> Yeasts for nutrients, Yeasts -> Flow Channel for metabolic wastes). The second design<sup>216</sup> (**Figure 25B**) was thought to reduce these microenvironment heterogeneities, using two flow channels and a square chamber, enhancing diffusive fluxes between the chambers and the channels. Indeed, the H-shaped chip allows to get quasi-homogenous chemical conditions in the chambers with active perfusion and removal of toxic wastes. However, once the chamber is filled with cells, radial and bidirectional gradients may form.



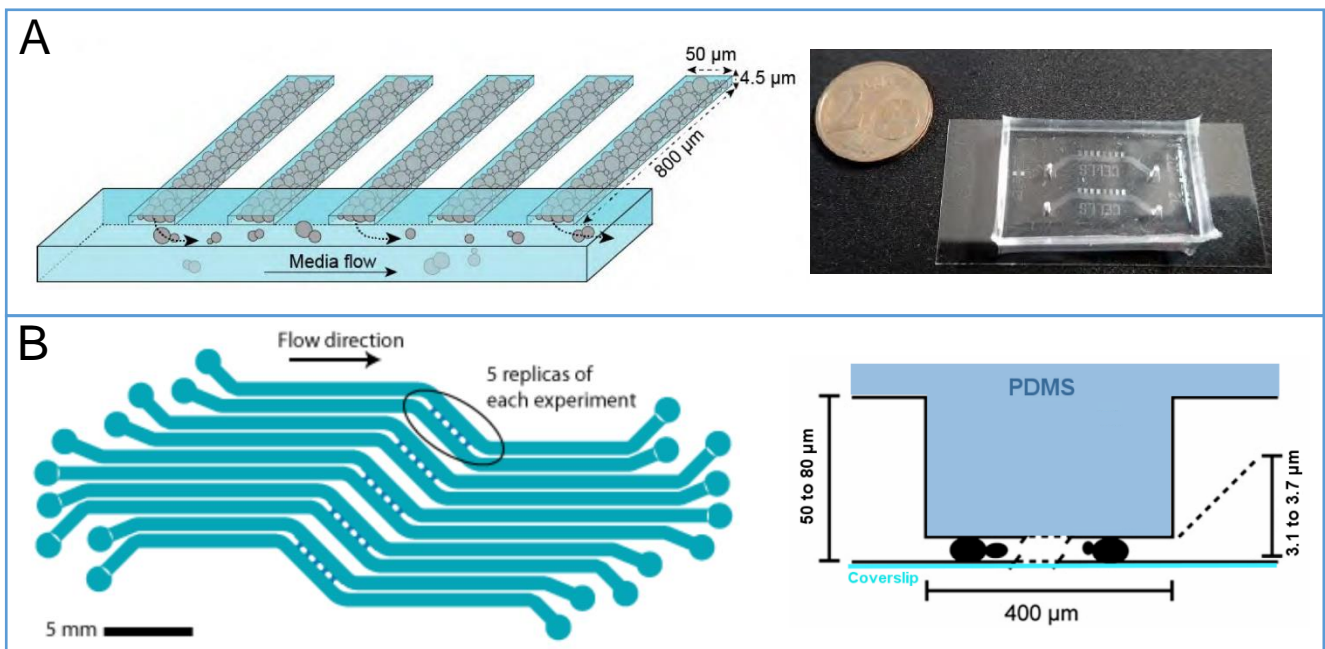


**Figure 25 - Microfluidic chip designs.** Both designs are composed of thin chambers to trap and observe yeast cells as a monolayer, connected to large flow channels for culture media renewal. (A) "Yeast mother machine" or Monodirectional gradient chip<sup>90</sup>. This elongated dead-end chamber design constrains the yeast growth in one direction and allows the formation of gradients along the same axis. (B) H-shaped chip<sup>216</sup>. The chambers are 400 $\mu$ m squares connected on two sides to two flow channels to improve liquid renewal. Liquid flows typically used are 50 to 100  $\mu$ L/min per flow channel using a peristaltic pump.

### Microfluidic fabrication

To obtain a customized PDMS microfluidic chip, three main steps are required: (1) chip design, (2) mould making (wafers) and (3) chip making. I mostly only perform the two last steps, reusing already existing chip designs. During my PhD, the techniques I used to fabricate the microfluidic chips are the soft photolithography using photopolymerising resin (x and y spatial resolution of  $\sim$ 3-5 $\mu$ m) for step (2) and PDMS casting with plasma adhesion to glass cover for step (3). Detailed protocols for these steps can be found in the appendixes.

Typically an experiment starts by loading the cells in the microfluidic chamber using syringes to force a cell suspension to flow through the chamber. For dead-end designs, a centrifugation step is necessary to load the cells. The microfluidic chip can be mounted on a microscope stage adapter and held with paper scotch. The chip can then be connected to a tubing and pumping system, which was previously washed with ethanol for sterility and filtered distilled water to remove any potential residual salt. Importantly all liquid media that will be flowed in the microfluidic system must be filtered for two reasons: to avoid dust which could obstruct a microfluidic feature and to sterilise the media without producing fluorescent molecules typically obtained with autoclaving. Computer controlled fluidic valves can also be

added to the tubing circuits to switch culture media dynamically, one example of use can be found in **Chapter IV Figure 3** of the paper<sup>217</sup>. The tubing connection needs to be tight enough so no air can enter the circuit, which could cause flow perturbations. In my case, I solved almost all air bubble problems I encountered by making some junctions tighter (between metal tubes and PDMS).

Microfluidic devices allow me to interrogate a cooperator/cheater consortium of yeast at the single cell resolution using localised light stimulation. The resulting time-lapse will present heterogeneous growth in the cell population which must be analysed to reveal the public good production and diffusion. I will detail some of the possible ways one can measure yeast growth in microfluidic devices.

## II.2. Image analysis - cell proliferation quantification

I will now present the image analysis I used to quantify cell proliferation in microfluidic devices.

### Cell counting

To quantify cell proliferation in a microfluidic device, one can infer from time lapses images how many mothers gave birth to how many daughters in a defined time.

#### *Spot detection*

A simple but robust image analysis to count cell is spot detection. By fitting Gaussian curves, these algorithms easily detect any fluorescence spots for various intensities and sizes. I used TrackMate which is an ImageJ plugin that allows spot detection, as well as spot tracking. Thanks to the mApple nuclear marker of the strains I made, it was possible to localize and count precisely yeast cells in real-time, even in packed 2D microcolonies. This method is quite robust to spot size and focus variations. To use this method, one must acquire the entire chamber to be able to count all cells present and born in the chamber for the entire duration of the time lapse. We can thus recover the global growth rate of each microfluidic chamber by linear fit of the log transform (**Figure 26**).

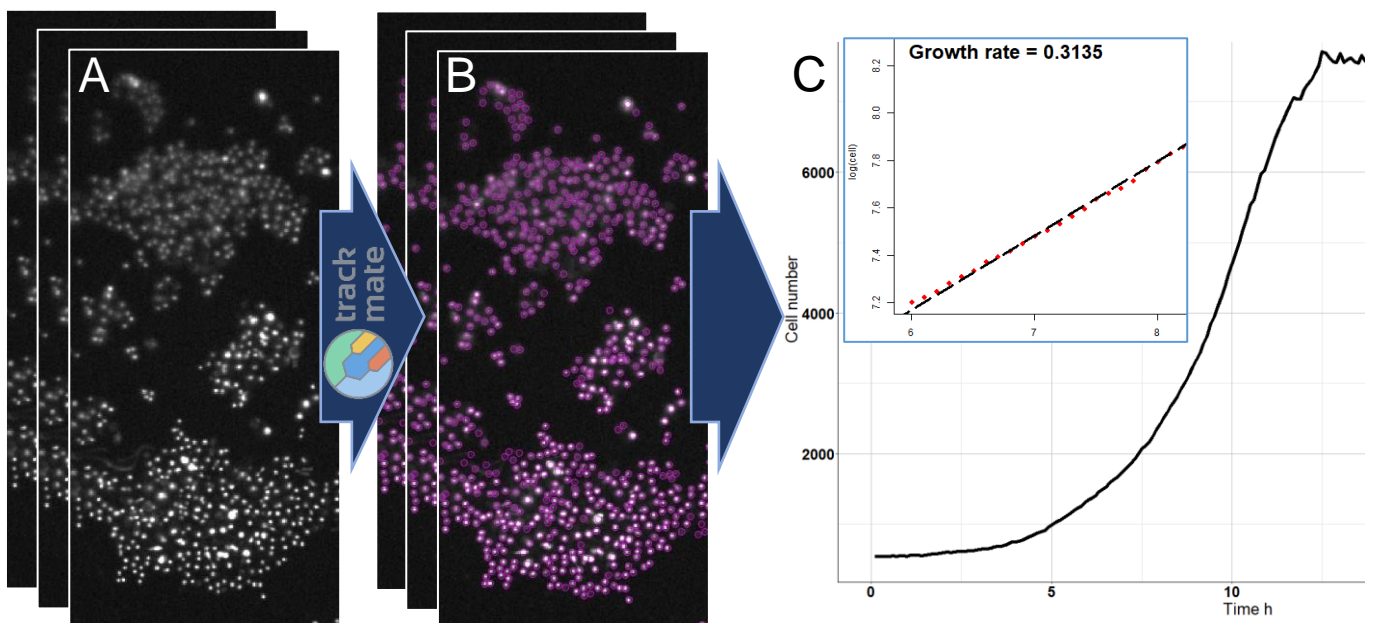


**Figure 26 – Image analysis workflow.** (A) Fluorescence image of yeast nuclear marker. (B) Output of TrackMate spot detection. We can note that it is robust: detects out-of-focus nuclei, superposed nuclei, and removes non-circular shapes (C) Growth curve obtained from time-lapse data, inset represents the log transform used for growth rate determination.

### Machine Learning segmentation

Supervised machine learning algorithms have shown to be very efficient for various types of cell segmentation. We also use such methods to segment yeast cells from bright field images. To obtain such image analysis, one must first record a set of typical examples of input images that will be used to train the machine learning model. The second part of the image training set is the corresponding segmented cell masks you would wish as output. These can be obtained with the help of thresholded fluorescence images or by hand drawing. We found that only tenths of images-masks pairs were sufficient to obtain a robust yeast segmentation algorithm, notably thanks to data augmentation strategies. The training computing itself does not last very long (5 to 30min) and the segmentation of one image takes about 0.1 to 1s. A example of machine learning segmentation for yeast cells is shown in **Figure 27**. A simple post-process morphological operator is applied to separate fused cell masks: erosion followed by dilatation. The resulting masks are finally used to count particles.

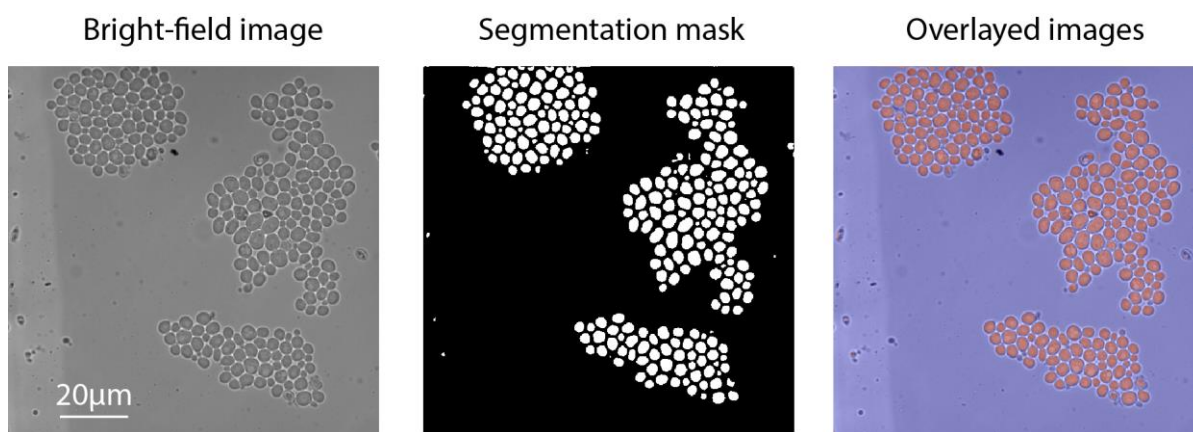


**Figure 27 – Machine learning used for yeast cell segmentation.** The model is first trained with bright-field images of yeast with the corresponding mask. Once trained the model allows to obtain a mask of the cell segmented. The overlaid images show the precision of the method.

This method was used in the Cybersco.py paper included in **Chaptet IV**, for example to investigate the impact of the number of yeast cells on the dynamics of recovery of cell division following a metabolic switch from glucose to sucrose. *“To test this assumption, cells growing in a microfluidic chamber were counted in real-time and, as soon as the number of cells in the chamber reached a given value ( $N = 100, 500$  or  $2000$ ; **Figure. 5**), CyberSco.Py switched the perfusion from glucose to sucrose by triggering a microfluidic valve.[...] We observed that the duration of the lag phase decreased as the size of the population in the microfluidic chamber at the time of the metabolic shift increased, indicating faster production and accumulation of the enzymatic products within larger yeast populations, and hence a better adaptability of large yeast populations to sucrose metabolic shifts.”<sup>217</sup>*

## Measure cell growth

The simplest method to quantify cell growth requires to keep all mothers and born daughters in the field of view, so that the total population is monitored for the entire time lapse duration. This will allow to directly recover a growth curve for the entire microfluidic chamber (**Figure 26**). This however does not allow to retrieve spatial variation of cell growth.

### *Cell tracking*

Other methods to measure cell growth require instead a cell tracking algorithm which is used to compute the entering and exiting flux of cells in a monitored area, allowing to recover the number of mothers and born daughters in a defined area at every timepoint. This could theoretically allow to obtain spatially resolved data of cell growth, by subdividing the field of view in a grid of windows where the entering and exiting cells are computed. However, tracking algorithms require low cell movement between two timepoints to work, which can be difficult to obtain for large growing yeast colonies. Indeed, when proliferating, cells push each other making their displacement additive, resulting in high velocities. Importantly, while there are some simple tracking methods which yield relatively long trajectories, they are still error-prone which prevents proper lineage reconstruction. Even if the tracking algorithm makes relatively few errors when analysing two images, the probability that a cell is correctly tracked for the entire duration of the timelapse may be quite low. An example of tracking results using TrackMate can be found in **Figure 29**.

### *Particle Image Velocimetry and divergence*

An alternative to estimate cell proliferation is to infer local displacement by using for example Particle Image velocimetry (PIV) methods. There is indeed a direct relationship between the spatial variations of cell velocity and the local growth rate of cells ( $\mu = \text{div}(\mathbf{V})$ ). Only this last method was used to get a quantitative view of the spatial variation of cell proliferation when a small subset of a population of light-inducible SUC2 yeast was illuminated (**Figure 28**).

This method is typically used in fluid mechanics to quantitatively measure flow characteristics in space and time. It allows to recover a velocity field between two images by computing the time cross-correlation of small interrogation windows. The quality of the velocity field depends on the chosen interrogation window size: too small will only measure pixel noise, too big will lose smaller scale spatial variations. In our case of expanding cells, we could retrieve the local growth map from velocities through derivation along the spatial dimensions (divergence operator). Indeed, as previously mentioned, cell displacement is an “additive process”, or more precisely an integrative function of local cell growth.

I performed the PIV analysis using the open-source JPIV software (<https://github.com/eguvep/jpiv/> ; <https://eguvep.github.io/jpiv/index.html>). Five bright-field images were used to compute one velocity vector field using correlation functions sum. We do not display the negative values for the divergence map as they do not inform us on cell growth (only positive values) but are the result of the still pixels in the area without cells at the border of the microcolonies.

## II.3. Spatial control of yeast growth in a microfluidic chamber

As a first example of spatial light control of yeast growth through production of Suc2p, we tested the strain yPH\_536 in a microfluidic system<sup>216</sup> (Figure 28) observed under a microscope. At such small scales (cells are growing as a monolayer in a chamber of 400 x 400  $\mu\text{m}^2$ ) we expected that hexoses released by a few Suc2p producing cells will be quickly available by diffusion to non-producing cells at the opposite side of the chamber. Indeed, a simple estimate from a diffusion-reaction equation<sup>x</sup> indicates that the typical length scale over which the concentration decreases from a point source in steady state is 65  $\mu\text{m}$  for 0.1% glucose and 165  $\mu\text{m}$  for 1% glucose. We let cells grow in 2% glucose before starving them with 0% glucose for 1h and switching to a 1% sucrose carbon source. We then used a Digital Micro-mirror Device (Mosaic3 from Andor) to activate with blue light (460nm LED at 20% intensity through a filter cube (EX) 470nm/40; 200 ms exposure time every 6min) a small patch of ~400 cells (rectangle of 50x350 $\mu\text{m}$ ) while performing time lapse microscopy (Figure 28). The images are acquired every 6 min in bright field and were analysed by Particle Image Velocimetry (PIV) as mentioned in the previous chapter. We obtained a vector field of cell displacement representing the cumulative effect of local cell growth (Figure 28D). Computing the divergence ( $\delta V_x/\delta x + \delta V_y/\delta y$ ) of this vector field gives an estimate of the local growth rate (Figure 28E,F). While cells kept in the dark did not exhibit significant growth (Figure 28F), we observed that growth was mostly initiated from the illuminated area (Figure 28D,E), demonstrating that indeed cells were producing hexoses in this area. We observe that the cheater cells located at the opposite side of the chamber relative to the illuminated area were also growing but only after some lag time (2-4h) and at a slower pace (0.01-0.02/h compared to 0.02-0.04/h for the illuminated cells) (Figure 28E), suggesting that they used hexoses diffusing away from the growing cooperative area. While this experiment demonstrates our capacity to initiate growth by illuminating small portions of a yeast population, and therefore defining regions of cooperators (illuminated) or cheater (in the dark) phenotypes, cell growth inexorably pushed cooperators away from the illuminated area (Figure 29 and 30). And, because of the long lifetime of Suc2p in the cell wall (compared to the cell motions), they conserved for some time their capacity to produce hexoses, in turn blurring the spatial frontiers between cooperators and cheaters.

---

<sup>x</sup> given by  $\sqrt{DC/q}$ , where D is the diffusion coefficient of the metabolite of interest, C its concentration and q the rate at which it is imported by cells. To compute this typical length scale, we estimate q for a dense monolayer of yeast using equation (4) (see Chapter III.3.).

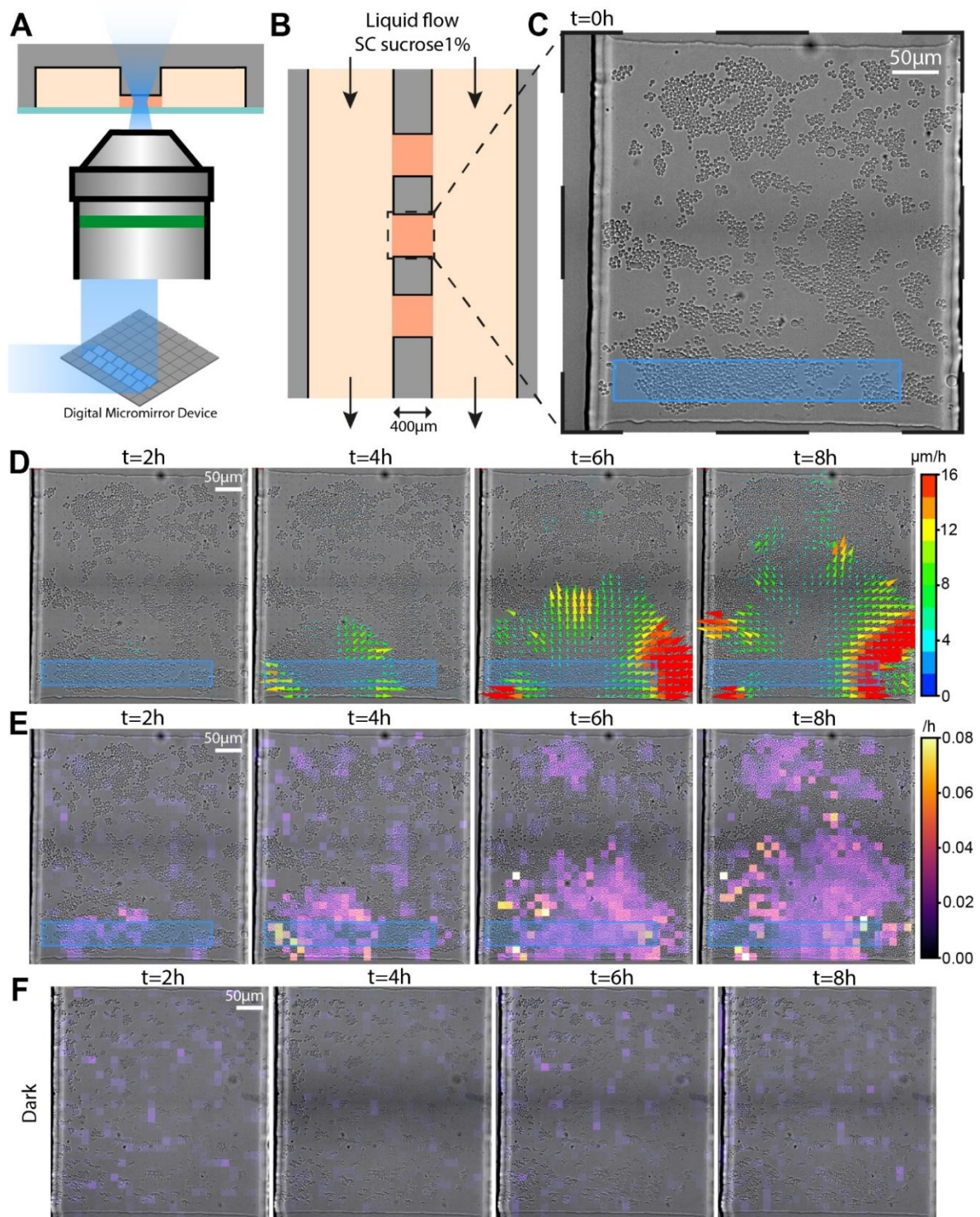


**Figure 28 - Spatial control of yeast growth in a microfluidic chamber.** (A) Scheme of the side-view and (B) the top-view of the microfluidic chip. Chambers have a dimension of  $400 \times 400 \times 3.5 \mu\text{m}$  and are perfused with liquid media through two large side channels. (C) Bright-field image of the chamber filled with hundreds of yeast cells of yPH536 strain. The blue rectangle represents the area illuminated by the Mosaic (DMD) at 460nm for 200ms every 6min. (D) Time-series of bright-field images with a PIV analysis vector map overlaid showing cell displacements due to cell division. (E) The corresponding divergence map overlaid as a proxy for local cell growth (spatial derivative). (F) Divergence map of a non-illuminated chamber.



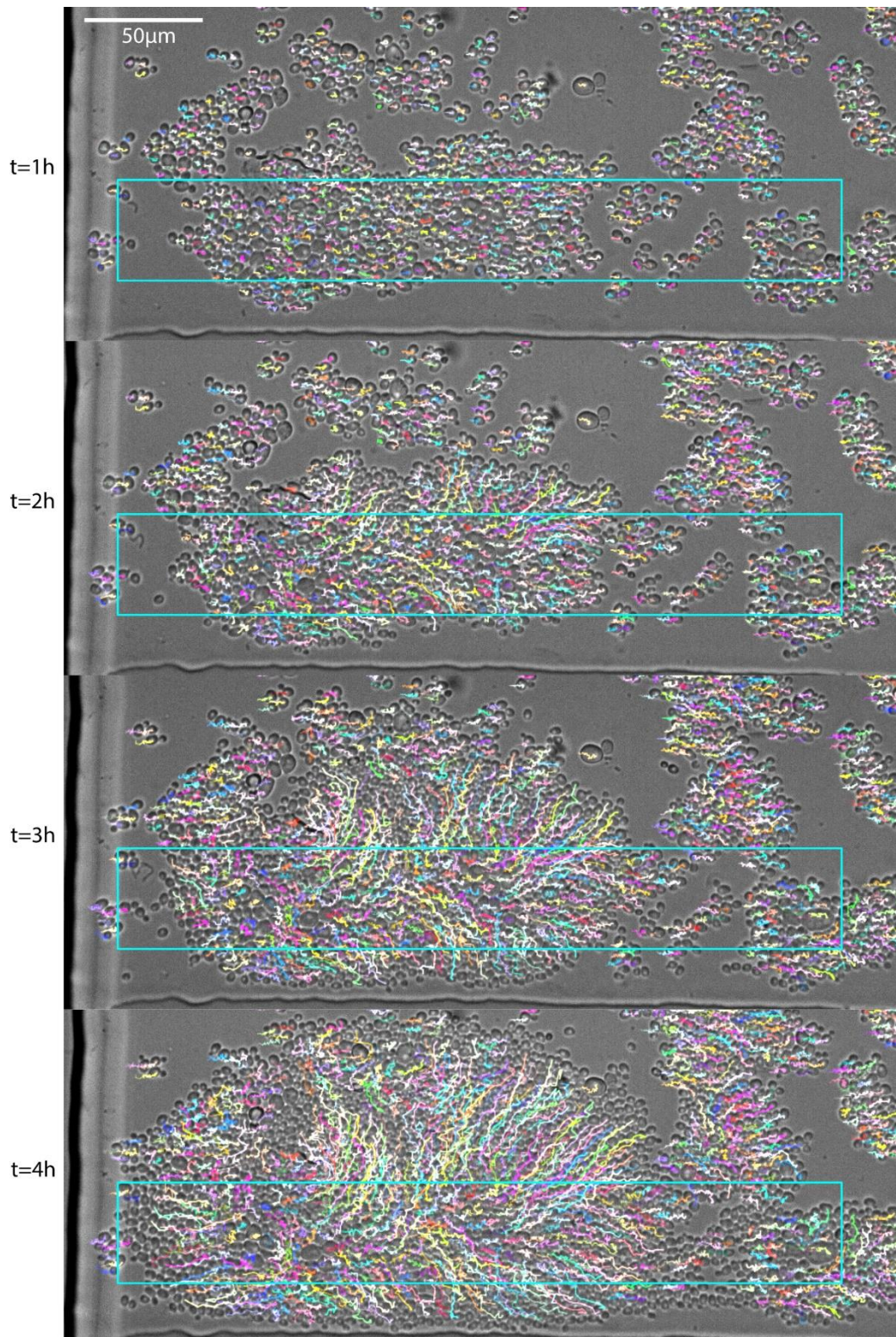


**Figure 29 – Tracking of yeast cells (yPH536) in a microfluidic chamber with localized light illumination** (same experiment as Figure 35). Tracking was performed with TrackMate plugin<sup>218</sup> in ImageJ. Only the trajectories starting at t=0 and with high quality are plotted to better visualize them. The blue rectangle represents the area illuminated by the Mosaic (DMD) at 460nm for 200ms every 6min. Cells starting in the illuminated area can be pushed away from it.

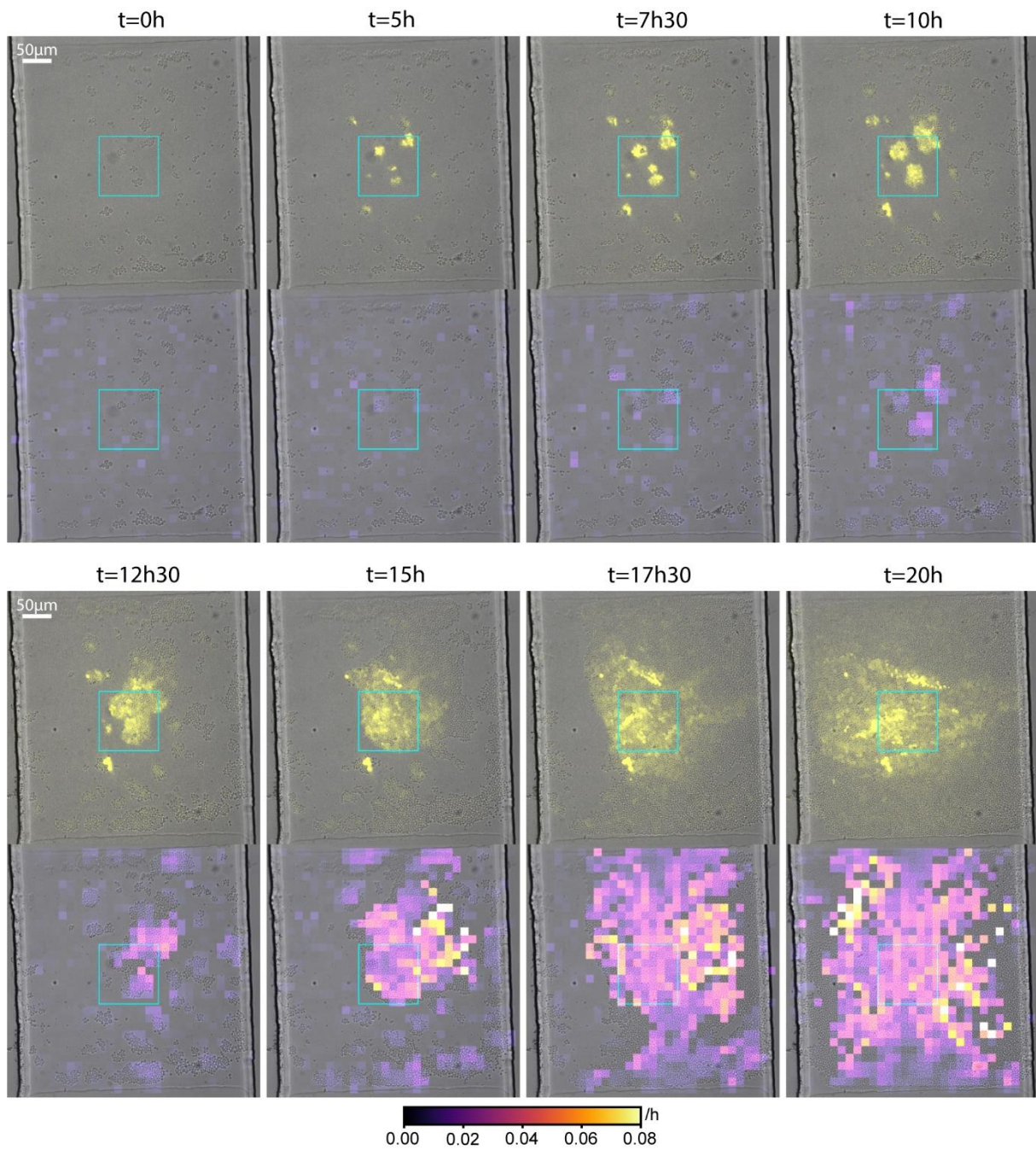


**Figure 30 – Spatial control of yeast growth (yPH471) in a microfluidic chamber perfused with SC sucrose 1% and with localized light illumination.** Time-series of (top) bright-field images with mVenus YFP fluorescence overlaid showing cooperatively cell displacements due to cell division, and (bottom) the corresponding divergence map overlaid as a proxy for local cell growth (spatial derivative). The blue square represents the area illuminated by the Mosaic (DMD) at 460nm (intensity 20%) for 250ms every 6min.

The above microscopic and microfluidic investigation allows to realize that the studied sucrose metabolism involves spatial interactions which can exceed hundreds of micrometers. I therefore chose to study this system at a larger scale, toward the millimeter and centimeter scales.





# Chapter III - Pattern light on petri dishes with growth monitoring with the 'OptoCube'

To investigate the impact of heterogeneous SUC2 expression on yeast growth at larger scale, I developed a custom tool, the 'OptoCube', to apply spatially resolved optogenetic activation while being able to monitor yeast growth on agar gel media.

The final version of the OptoCube is a static incubator equipped for illuminating petri dishes with light patterns and recording time-lapses of microbial growth on agar-plates (**Figure 32A**). This setup, described in detail in the appendixes, gives many possibilities in terms of light patterning with high spatial and temporal resolution ( $\sim 0.1$  mm,  $\sim 1$  s) compared to the dimensions and dynamics of microbial colonies ( $> 1$  mm,  $> 1$  hour). The light patterning is performed by a projector (or Digital Micro-mirror Device : DMD), controlled by a microcontroller board (Arduino Uno) using a digital pin, and is synchronized with the image acquisition through serial communication with the computer. Up to 15 small or 6 standard petri dishes can be simultaneously monitored for days.

## III.1. OptoCube development

To perform simultaneous light patterning and time-lapse recording of agar-plate yeast growth, I performed several optimizations and built several versions of the OptoCube. More precisely, I focused my efforts on making the imaging part as precise and reproducible as possible. I tried the following methods: V1 measure of reflectance with a camera, V2 measure of absorbance with a camera and V3 measure of reflectance with a flat-bed scanner (**Figure 31**). Cameras were not ideal as they tend to collect heterogeneous light intensities depending on the position of the sample in the field of view. I found the best imaging system to be the scanner as it gives super high-resolution images (4800x4800 dpi<sup>2</sup>) while having homogeneous light illumination. I use VueScan software on a Windows computer to control the scanner as it proposed a built-in time-lapse feature.

More scanner parameters could be tuned with the use of a Raspberry Pi, like the LED's colour used to perform the scanning imaging. An open-source package (Scanner Access Now Easy) is available to control a large range of scanners with Linux OS, even though it is not necessarily up to date or easy to set-up.

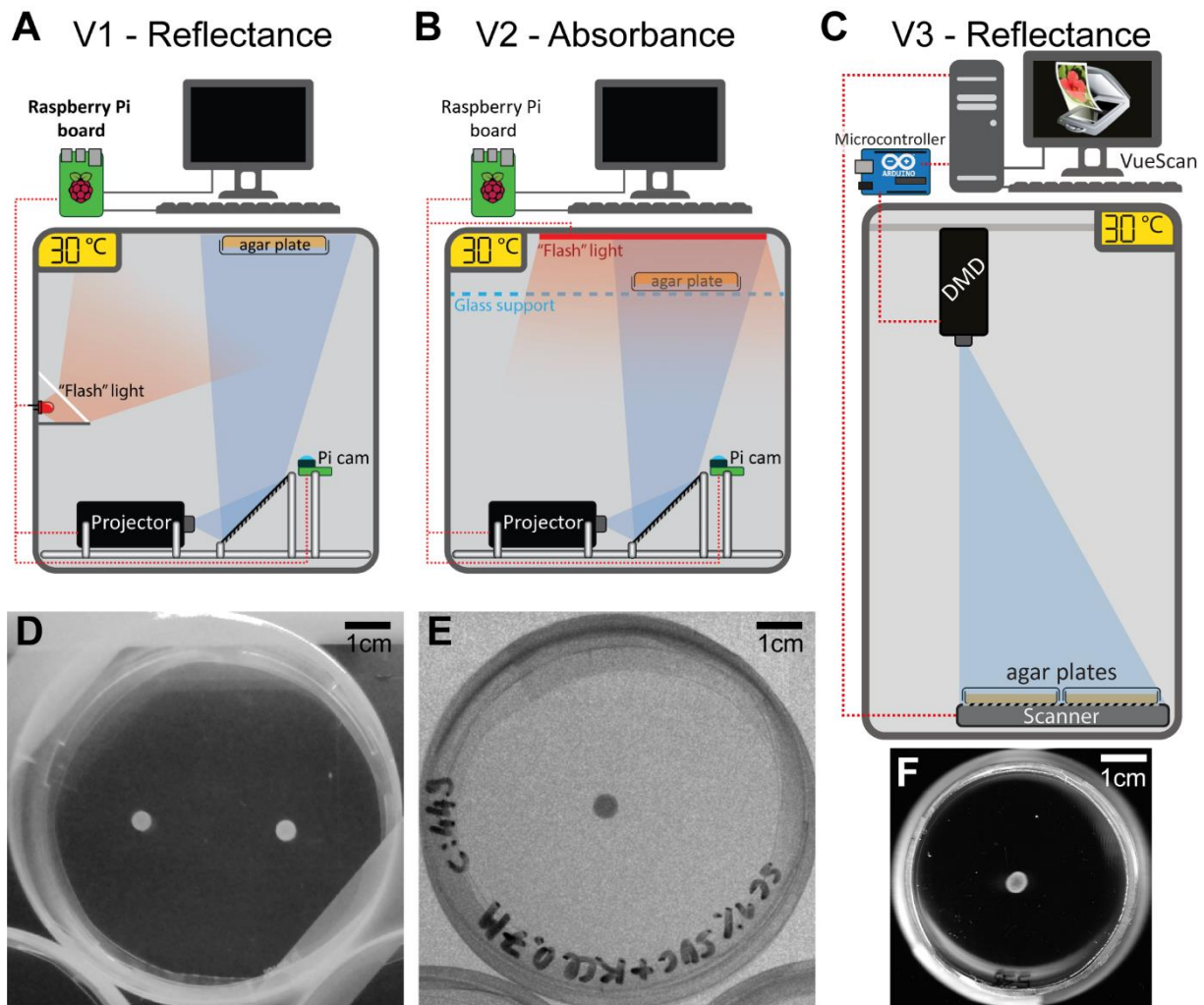


**Figure 31 – OptoCube evolution during development.** (A) Version 1 measure reflectance using a Raspberry Pi camera and a strip led as “flash” light. (B) Version 2 measure absorbance using a Raspberry Pi camera and a repurposed computer screen as “flash” light. (C) Version 3 measure reflectance using a flat-bed scanner. Example of pictures obtained with Optocube V1 (D), V2 (E) and V3 (F).

I designed a specific protocol to start the experiment with a reproducible, homogeneous lawn of yeast over the entire petri-dish surface by overlaying a soft-agarose layer (0.67mm) containing yeast poured on top of a nutritive layer (**Figure 32C**). Cells embedded in the gel will proliferate and form spherical microcolonies (**Figure 32B**) while being trapped, avoiding uncontrolled cell displacement over long distances. This differs from the classical method to grow isolated colonies at the surface of the gel, where cell proliferation induces their displacement away from the colony center. While the OptoCube allows to monitor isolated colony growth, it might be less precise and saturate for dense and large colonies. Also, I did not investigate in depth yeast sucrose metabolism for isolated colonies.

Choosing instead to start from a homogeneous lawn of cells allowed to increase competition for hexoses, configuration where invertase activity is determinant for yeast growth. This resulted in a thin (~2.35 mm) and translucent gel facilitating scanner imaging. Given the gel's thickness, diffusion equilibrates concentrations much faster in this dimension compared to the lateral ones. I simulated diffusion in a 1D finite segment with boundary conditions {point source ; reflective wall} , showing that it takes 5 h to fully equilibrate a segment of 2.35mm where it takes over 1 000 h for 53mm (diameter of a small petri dish).

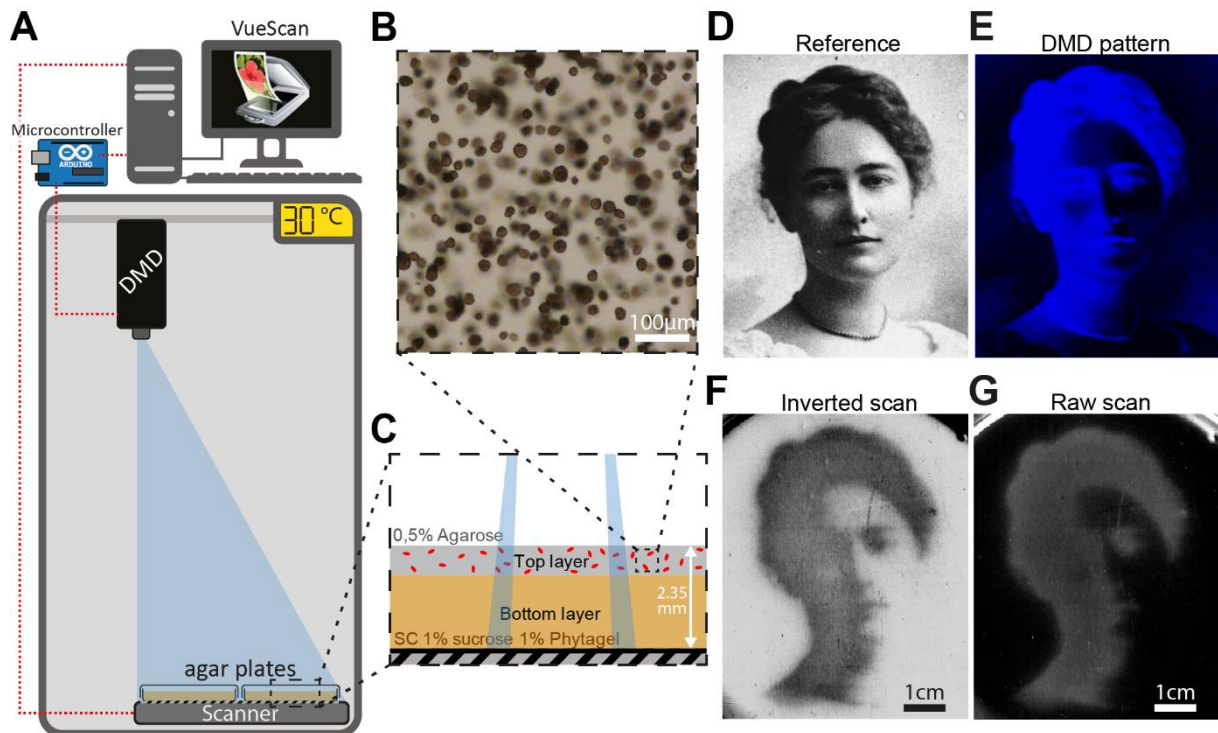


**Figure 32 - OptoCube home-made device for simultaneous optogenetic spatial patterning and yeast growth monitoring in solid media.** (A) Scheme of the *OptoCube* and its components: a DMD and a flat-bed scanner inside a temperature-controlled incubator, controlled by a computer and a microcontroller. The light intensities of the DMD pattern range from 0.0014 mW/cm<sup>2</sup> to 1.13mW/cm<sup>2</sup>. (see Materials and Methods and supplementary information) (B) Microscopy image of grown yeast microcolonies embedded in 0.5% agarose gel. (C) Scheme of bi-layered agar plate with a homogeneous lawn of yeast covering the entire plate. (D) Reference image of Maud Menten, as a tribute to her works on the Michaelis-Menten enzymatic kinetic equation using the invertase as model<sup>151</sup>. (E) Blue light pattern projected by the DMD. (F) Inverted image of the resulting yeast growth after 45 h of illumination using the *yPH\_536* strain. (G) Raw scan of the corresponding. Background subtraction was done using the first image in the timelapse.

The light intensities of the DMD pattern range from 0.0014 mW/cm<sup>2</sup> to 1.13mW/cm<sup>2</sup>. Indeed, there is a DMD leakage which prevents to get ideal non-illuminated area. We will discuss in the next section that 0.0014 mW /cm<sup>2</sup> is arguably low enough to consider dark regions as cheaters for sucrose metabolism.



Building an OptoCube is relatively cheap (~1 000 to 10 000€) and easy, the main expense being the commercial temperature-controlled incubator. One could also build a DIY incubator with thermal regulation, but it might induce heterogeneous temperature around the sample which tend to favour condensation on the petri dish lid. The DMD could also be replaced by a cheap video projector, but it might be less performant for its intensity range and its leaking. The flatbed scanner model can also be changed as many models are supported by the VueScan software or can be controlled through another software. For the model we used, a Canon LIDE400, I had to open the glass cover and apply black tape on some parts of the bottom which are reflecting surfaces (this prevent undesired optogenetic activation reflection artefacts). Other Arduino-like microcontrollers could be used instead of the classical Arduino UNO.

As a demonstration of the OptoCube's capabilities to optogenetically control light-inducible SUC2 expression and yeast growth in space, I sent patterned illumination directly onto a yPH\_536 lawn growing on top of a 1% sucrose gel (**Figure 32D-G**). I used this opportunity to pay a small tribute to Maud Menten, who worked on the famous Michaelis-Menten enzymatic kinetic equation using the invertase as model<sup>151</sup>. I observed that cell growth was mostly occurring inside illuminated areas. As expected, the image produced at the surface of the gel was not as well resolved as the initial image. This blurring effect is the result of the noise in microcolony spatial distribution, the light scattering (although it was small, see **Figure 29**), but most importantly the results of metabolic interactions, cells without illumination behaving as cheaters and growing thanks to hexoses diffusion away from the reference pattern. Other examples of yeast growth patterns I obtained using various patterns of illumination are shown in **Figure 33**.

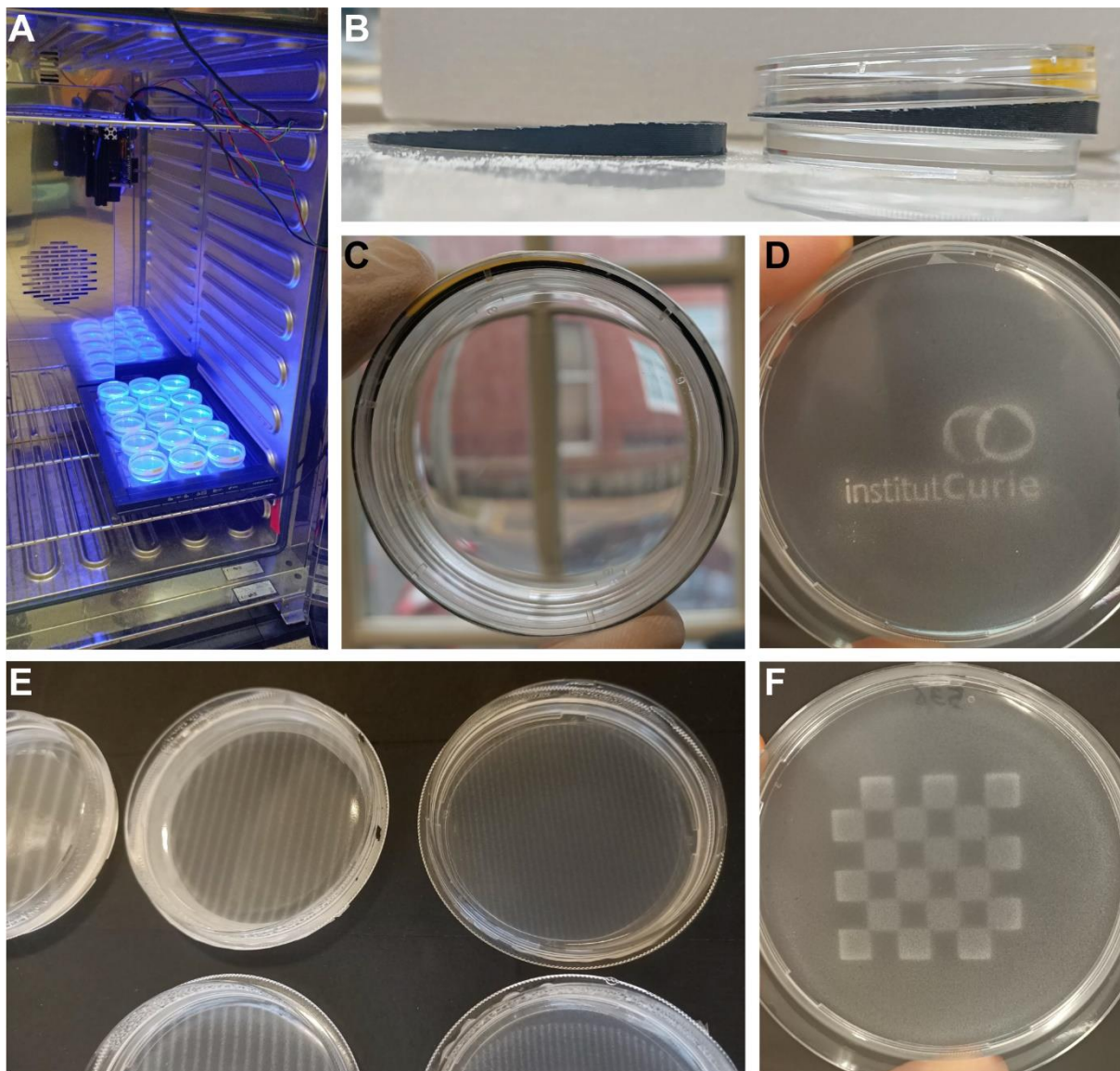


**Figure 33 – Pictures of the OptoCube device and patterned agar plates.** All represented plates are 6 cm of outer diameter. (A) Inside of the OptoCube with the DMD homogeneously illuminating 15 plates. (B) 3D printed part to tilt the lid to 5°. (C) Plate containing a two-layer gel with homogeneous yeast inoculation, highly transparent just after plating. (D-F) Examples of plates showing yeast growth after exposure to various patterns of illumination (Institut Curie logo, stripes and squares).

### III.2. OptoCube performances characterisation

To evaluate the performance of the OptoCube and ensure the quality of the recorded data, I performed various control experiments.

I built a calibration curve (**Figure 34**) to convert the pixel intensity measured by the scanner into cell density in colony-forming unit per milliliter (CFU/mL). To do so, I plated yeast cultures with various cell densities and measured the corresponding pixel intensity with the scanner. The resulting calibration curve was fitted with a Hill function that will be used to convert the raw scanner data into biologically relevant ones.

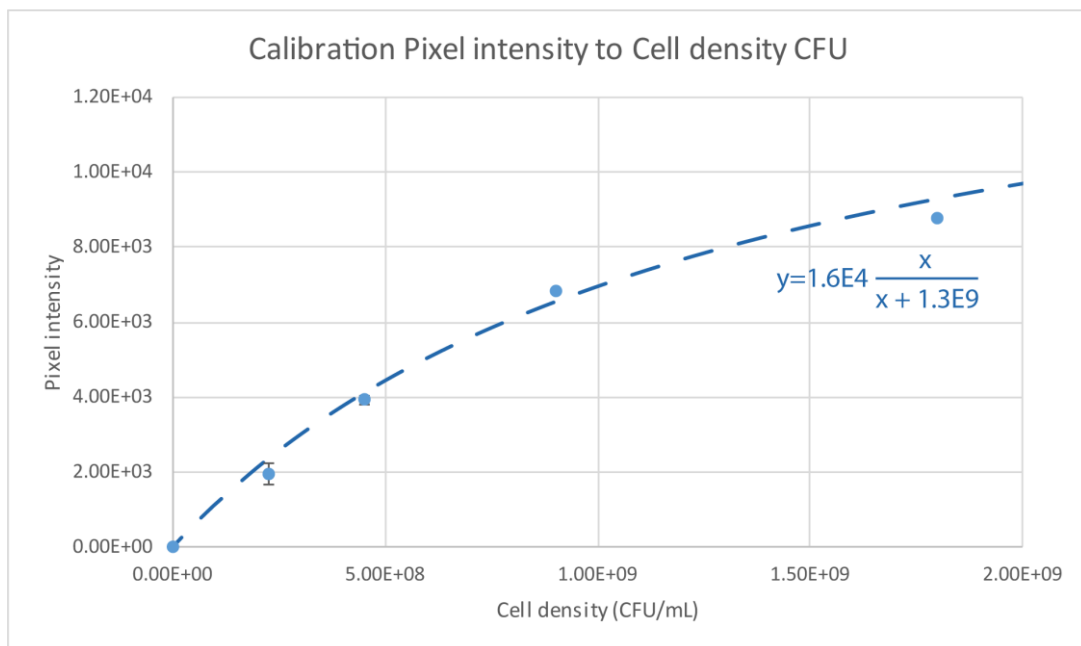


**Figure 34 – Scanner calibration for cell density measurement.** The fit is plotted as a dashed line, representing the Hill function  $y = 1.6E4 * (x / (x + 1.3E9))$ . Error bars represent standard deviation of duplicates.

I also controlled that the light illumination does not induce significant phototoxicity (**Figure 35**) which was the case for all the intensities I used.

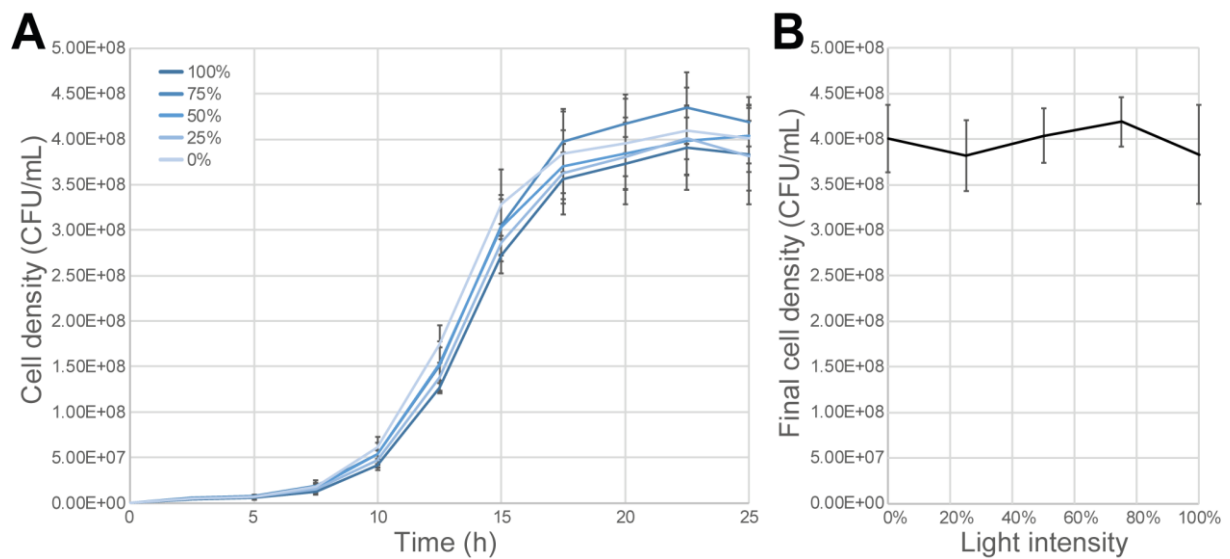


**Figure 35 – Light toxicity controls.** I stimulated the entire surface of the agar plates covered with yPH\_449 strain (WT) varying the light intensity from 0 to 100%. (A) Growth curves. (B) Dependence of the final pixel intensity on the light intensity at  $t=25h$ . No significant phototoxicity can be measured. Lines represent mean of triplicate and error bars represent  $\pm$  standard deviation.

Importantly, I measured the sharpness of the DMD light pattern (**Figure 36**). Indeed, because light is scattered when hitting the gel surface, the frontier of the projected light pattern is not perfectly sharp. This phenomenon is difficult to quantify precisely, so instead of measuring the light I preferred to measure the biologically relevant value instead. To do so, I used an optogenetic yeast strain that produces YFP fluorescence when illuminated, acting as a light reporter. The resulting fluorescence was then measured using a macroscope and used to quantify the light pattern sharpness. **The sharpness can be estimated at  $67\mu m$**  using the spatial parameter of the fitted sigmoid function.

Finally, I investigated how the drying of the gel impacted yeast growth (**Figure 37**). Indeed, because of the low thickness of the gel, the surface/volume ratio is high which resulted in strong water evaporation. Despite using multiple layers of parafilm to prevent desiccation, prolonged incubation in the OptoCube at  $30^{\circ}C$  does induce gel drying. As a consequence, plates stimulated after 24h of incubation or more did not respond as well as the plate stimulated from the beginning. This might also be in part due to residual sucrose hydrolysis by acid catalysis. All OptoCube experiments were done in the same conditions and all agar plates were made freshly, ensuring consistency between the experiments.

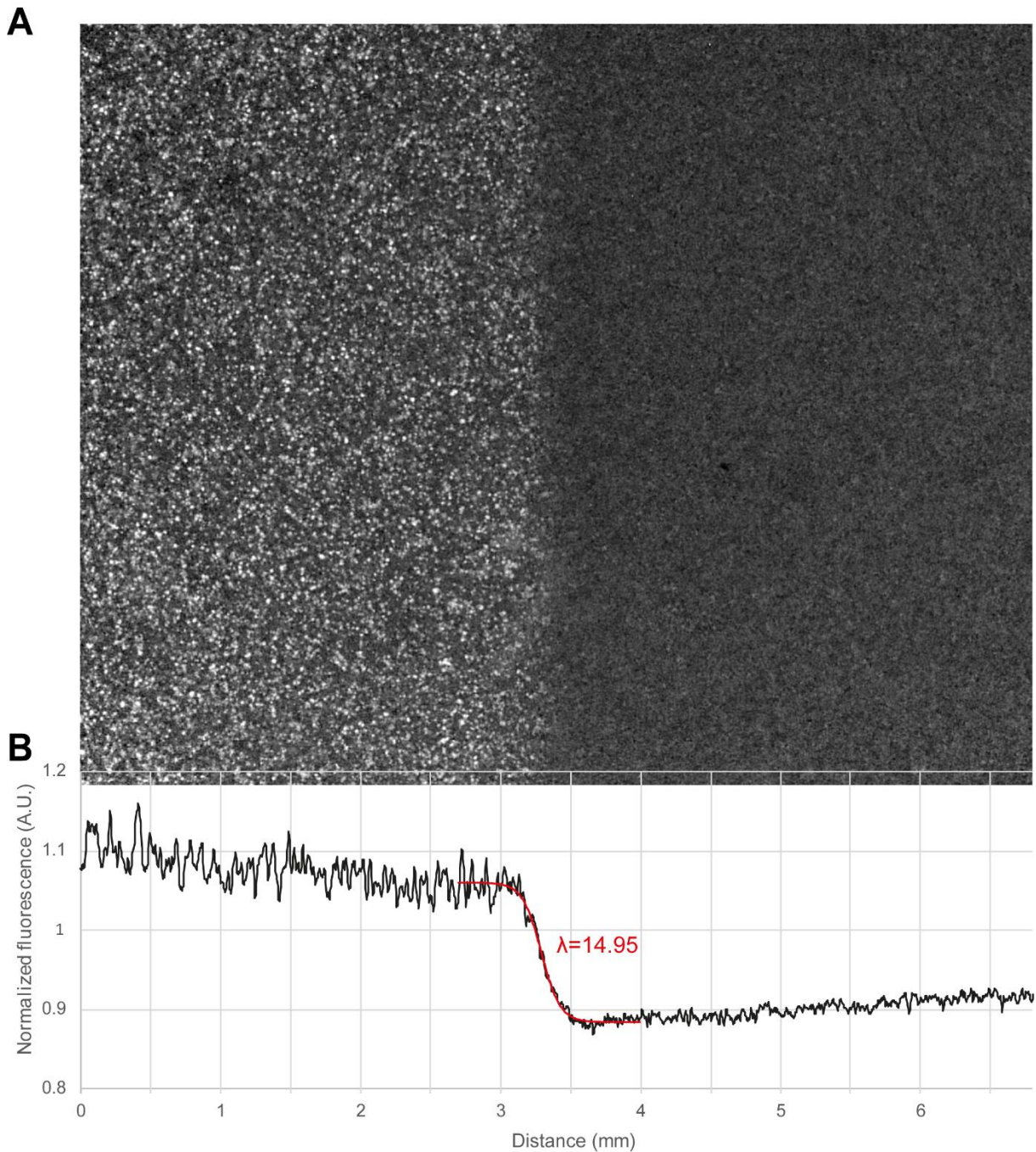


**Figure 36 – OptoCube light pattern sharpness.** I applied a light pattern with a sharp transition between 100% to 0% of intensity for 24h on a bilayered agar plate, with the top layer containing an optogenetic yeast strain that produces Venus protein upon blue light illumination (yPH459). (A) Macroscopic normalized fluorescent image of the light pattern transition and (B) the resulting fluorescent profile along the horizontal axis. The normalization was done by dividing by the fluorescent image of a non-illuminated plate. The red line represents the fitted function: sigmoid function with parameter  $\lambda=14.95$ , with  $y=1/(1+\exp(-\lambda x))$ . This gives the following spatial parameter  $1/\lambda=0.067\text{mm}$ .

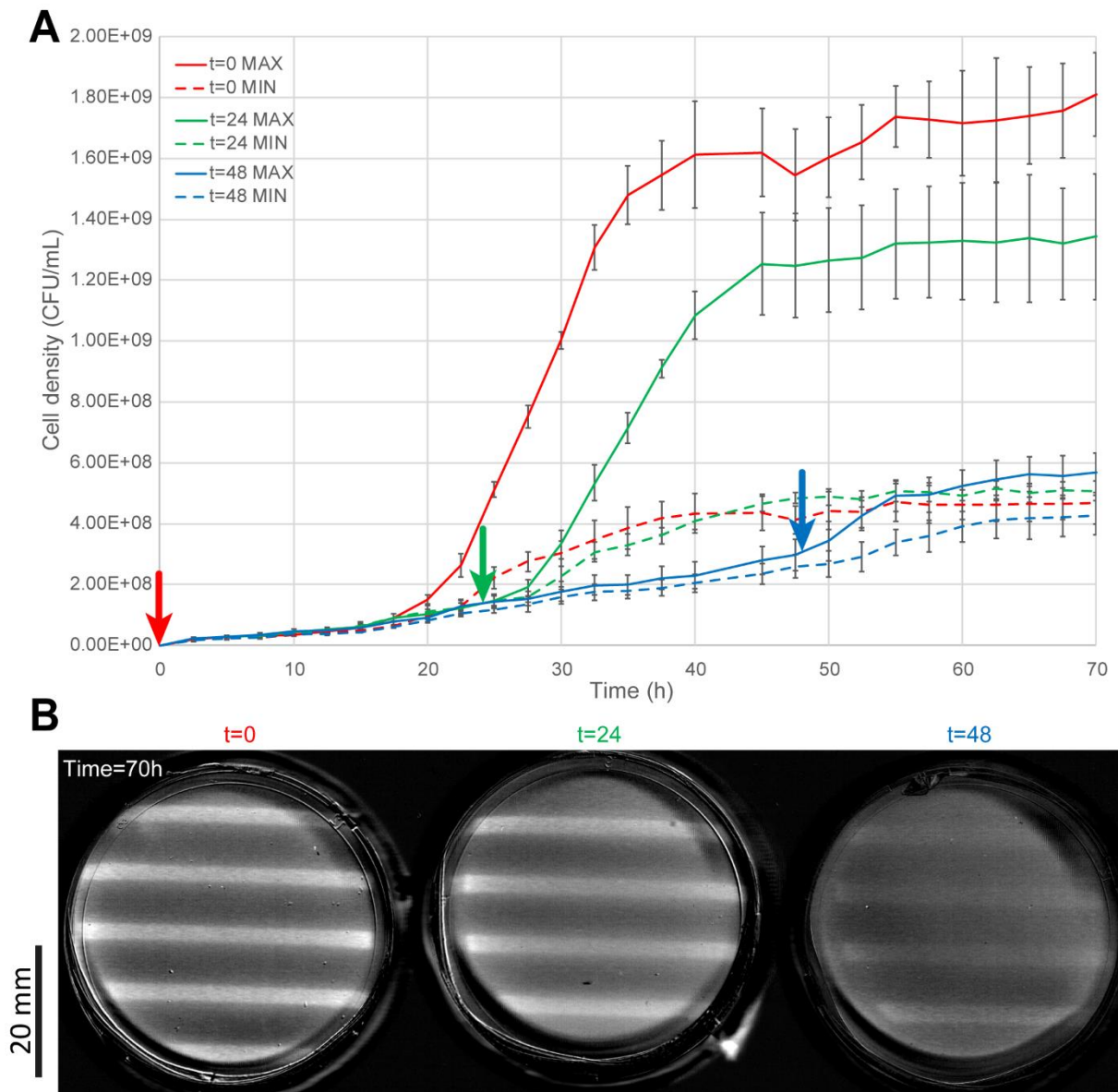


**Figure 37 – Gel drying after prolonged incubation in the OptoCube at 30°C.** I stimulated agar plates covered with yPH536 strain using the same pattern (blue lines alternated with dark region, wavelength=5.6mm, Light:Dark area ratio=25%:75%, Light intensity=100%) at different times. We observe that plates stimulated after 24h of incubation or more do not respond as much as the plate stimulated from the beginning. Values are mean of three extremums per plate, error bars represent  $\pm$  standard deviation.

I also characterised the growth of the different strains under homogeneous light illumination over the entire petri dish (**Figure 38**). We recovered equivalent behaviours between strains as in liquid cultures (**Figure 21D,E**). We can note that for all strains, the maximal growth rate measured was increased in agar compared to liquid, from 0.27 to 0.37/h for the WT and from 0.07 to 0.13/h for the  $\Delta$ SUC2 strain. For the growth in agar; we observed that the yPH536 strains growth curve obtained in dark conditions is quite similar to the  $\Delta$ SUC2 strain. The maximal growth rate of yPH536 and  $\Delta$ SUC2 were 37% and 27% respectively compared to the illuminated yPH536. This increase for the optogenetic strain is due to two phenomena mentioned previously: the promoter leakage and the DMD leakage. Nonetheless, we argue that **the non-illuminated yPH536 cells can still be considered as cheaters for sucrose metabolism compared to illuminated cells.**

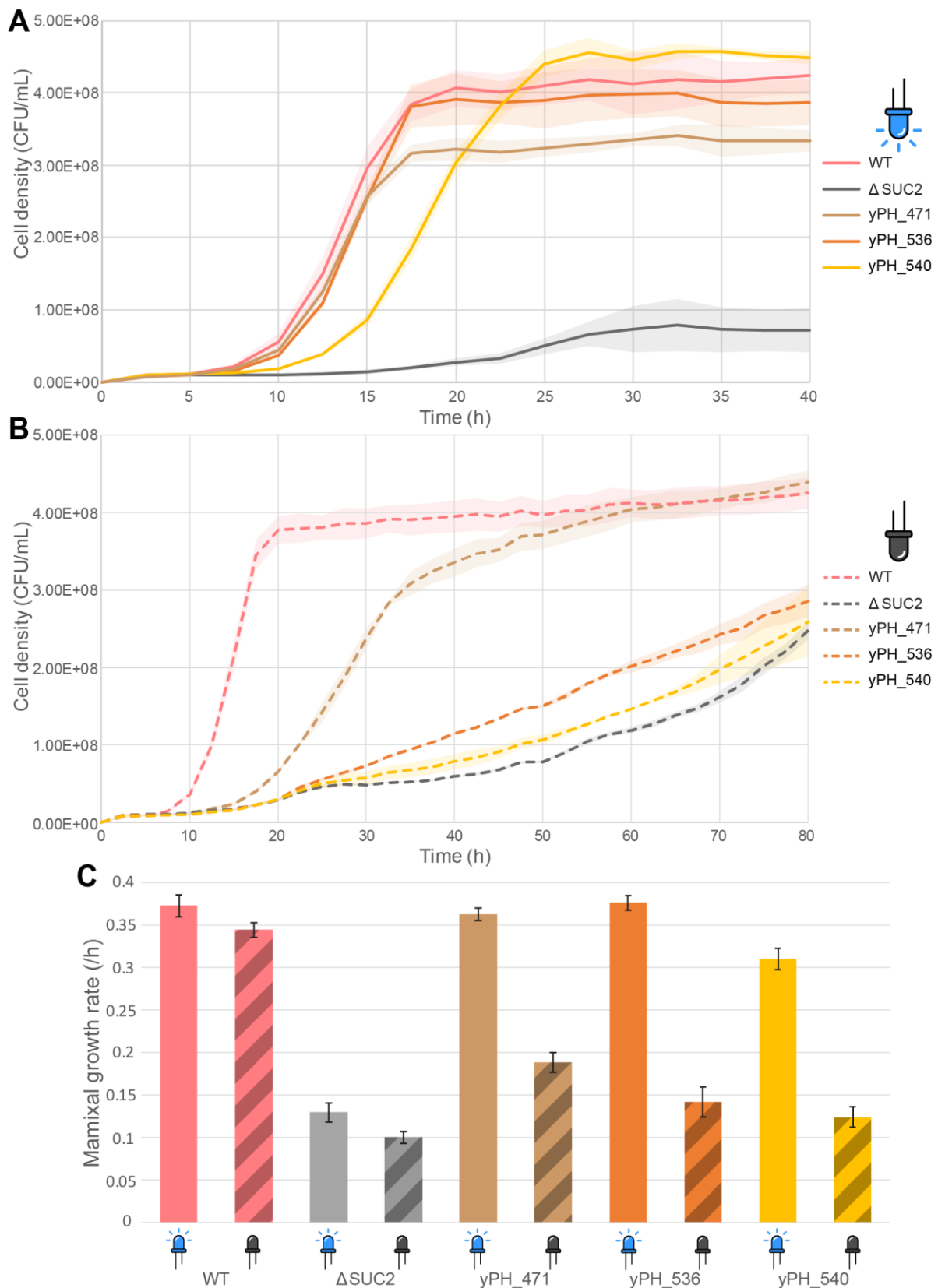


**Figure 38 – OptoCube growth curves of the different strains with homogeneous illumination.** Growth curves in 1% sucrose with continuous light stimulation at 0% (A) or 100% (B) intensity in the OptoCube. Lines represent mean of triplicate and areas represent  $\pm$  standard deviation. Extracted maximal growth rates are shown in (C), mean of triplicate and error bars represent  $\pm$  standard deviation.



### III.3. Modelling yeast growth on sucrose

I built a model of the yeast growth on sucrose to better understand the role of key physical and chemical elements at play. I choose to reduce the system's number of dimensions assuming two symmetries axis:  $y$  and  $z$ . To simplify our analysis, I chose for my experiments to apply light patterns invariant in the  $y$  direction. If we assume that the central part of the plate is not affected by its boundary conditions, we can approximate that our system is invariant in  $Y$ . The geometry of the gel allows us to assume that diffusion in the  $z$  axis happens very fast compared to the diffusion in  $x$  and  $y$  direction:  $\Delta Z = 2.35\text{mm} \ll \Delta X = \Delta Y = 53\text{mm}$ . I thus model the diffusion and yeast growth variations along the  $x$  axis only (**Figure 39**). The top and bottom gel layer initial concentrations are meant by the dimension reduction.

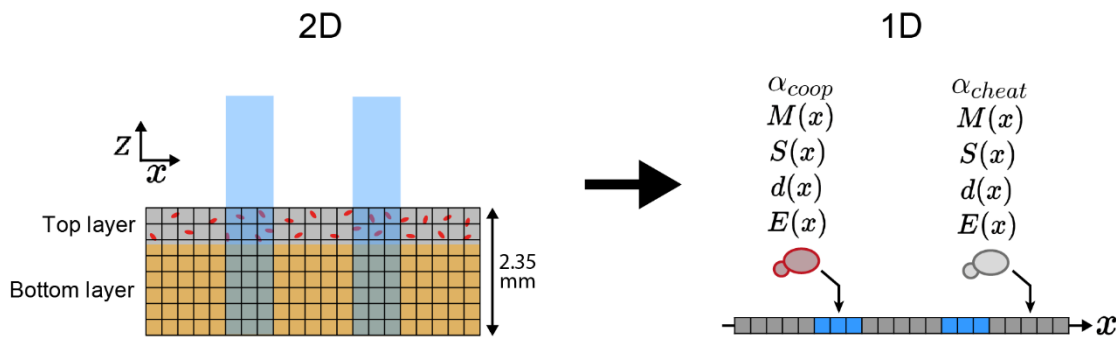


**Figure 39 – Schematic view of the model dimensional reduction.** The system is invariant in  $y$ , and we assume that diffusion in the  $z$  direction is instantaneous compared to diffusion in the other directions.

The model uses partial differential equations (PDEs) and is based on a previous work<sup>146</sup>, using Michaelis–Menten kinetics for enzymatic reactions—namely, invertase catalysis for sucrose hydrolysis Eq(3) and high and low affinity glucose transporters for yeast hexose consumption Eq(4)—and Monod equation for the growth rate dependency on hexoses concentration Eq(6). Crucially, the model accounts for sugar diffusion in space using the concentration gradients. The resulting set of equations is detailed below, and the model parameters (taken from the literature for most of them) can be found in Table 1. The model does not take other nutrient concentrations (notably nitrogen sources) into account, assuming that they were not limiting. The model does not account for ethanol respiration nor for the gel drying. Importantly, I took most of the model parameters retrieved from the literature. Indeed, I did not aim to “fit” our model but rather to outline the effects of key mechanisms and check to what extent data from the literature were enough to recover most of the observed dynamics. I therefore manually tuned only three parameters: the invertase production rates  $\alpha_{coop}$ ,  $\alpha_{cheat}$  and the maximal growth rate  $\mu_{max}$  so that the numerical simulations reproduced best both the dynamic and the final density of the corresponding experiments (light dose response and spatial wavelength experiments, **Figure 41** and **Figure 43**). I found that  $\alpha_{coop}=1.8\text{E}-24$  and  $\alpha_{cheat}=1.5\text{E}-25$  mol/s/cell, and  $\mu_{max}=0.27/\text{h}$  were the best parameters values. The set of equations was numerically solved using a PDE solver in Python and taking advantage of the symmetries

of the problem to reduce computation cost. Overall, the resulting simulated yeast density dynamics are in good agreement with the experimental results (see **Figure 41** and **Figure 43**). It is worth noting that such equations can be extended to 2D or 3D systems but will be more computationally costly.

$$\frac{dS}{dt}(x) = D_S \frac{d^2 S}{dx^2} - I(x) \quad (1)$$

$$\frac{dM}{dt}(x) = D_M \frac{d^2 M}{dx^2} + 2I(x) - Q(x) \quad (2)$$

$$I(x) = E(x) K_{cat} \frac{S}{K_m^E + S} \quad (3)$$

$$Q(x) = \left( V_{max}^1 \frac{M}{K_m^1 + M} + V_{max}^2 \frac{M}{K_m^2 + M} \right) d_{cell}(x) \quad (4)$$

$$\frac{dE}{dt}(x) = \alpha \frac{M}{K_\alpha + M} d_{cell}(x) \quad (5)$$

$$\frac{d(d_{cell})}{dt}(x) = \mu_{max} \frac{M}{K_s + M} d_{cell}(x) - r_{death} d_{cell}(x) \quad (6)$$

with

$$\frac{d(d_{cell})}{dx} = 0 \quad (7)$$

The model is used to simulate different configurations of yeast growth on sucrose. To solve the PDE we use a python package called scikit-fdiff (<https://scikit-fdiff.readthedocs.io>). We chose the Crank-Nicholson scheme to compute the diffusion of molecules across a discretized space. We use a simulation hook to compute non-linear terms and prevent negative values. The discretization of the time and space dimensions has been carefully chosen to respect the following order of magnitude:

$$\Delta t \ll \frac{\Delta x^2}{D_M}$$

Values were typically  $\Delta t = 2$  sec and  $\Delta x = 1e-4$  m.

Variable	Description	Unit	Initial value	Source	Reference
M	Hexose concentration	[M]	1e-8	Fixed experimentally	
S	Sucrose concentration	[M]	0.029	Fixed experimentally	
E	Invertase per pixel	[M]	1e-35	Fixed experimentally	
$\alpha$	Enzyme production rate	[mol/s/cell]	1.8e-24 or 1.5e-25	Fit	
d	Cell density	[cell/L]	2.85e9	Fixed experimentally	
I	Invertase activity	[M/s]	/	/	
Q	Hexose consumption	[M/s]	/	/	
$D_S$	Diffusion coef of sucrose	[m <sup>2</sup> /s]	6.1e-10	Fixed experimentally	[3]
$D_M$	Diffusion coef of hexose	[m <sup>2</sup> /s]	7.6e-10	Fixed experimentally	[3]
$K_{cat}$	Kcat of monomeric Invertase	[/s]	4700	Fixed experimentally	[1]
$\mu_{max}$	Maximal growth rate	[/s]	7.5e-5	Fit	
$r_{death}$	Death rate	[/s]	0	/	
$V_{max}^1$	Maximal consumption rate	[mol/s/cell]	4.175e-17	Fixed experimentally	[2]
$V_{max}^2$	Maximal consumption rate	[mol/s/cell]	2.6e-17	Fixed experimentally	[2]
$K_m^1$	Affinity constant for hexose	[M]	0,0008	Fixed experimentally	[2]
$K_m^2$	Affinity constant for hexose	[M]	0,021	Fixed experimentally	[2]
$K_s$	Monod constant	[M]	0,00012	Fixed experimentally	[4]
$K_m^E$	Km of Invertase	[M]	0,026	Fixed experimentally	[1]
$K_\alpha$	Hill coef for Invertase production	[M]	1e-5	User defined	

Table 1 - Model parameters summary

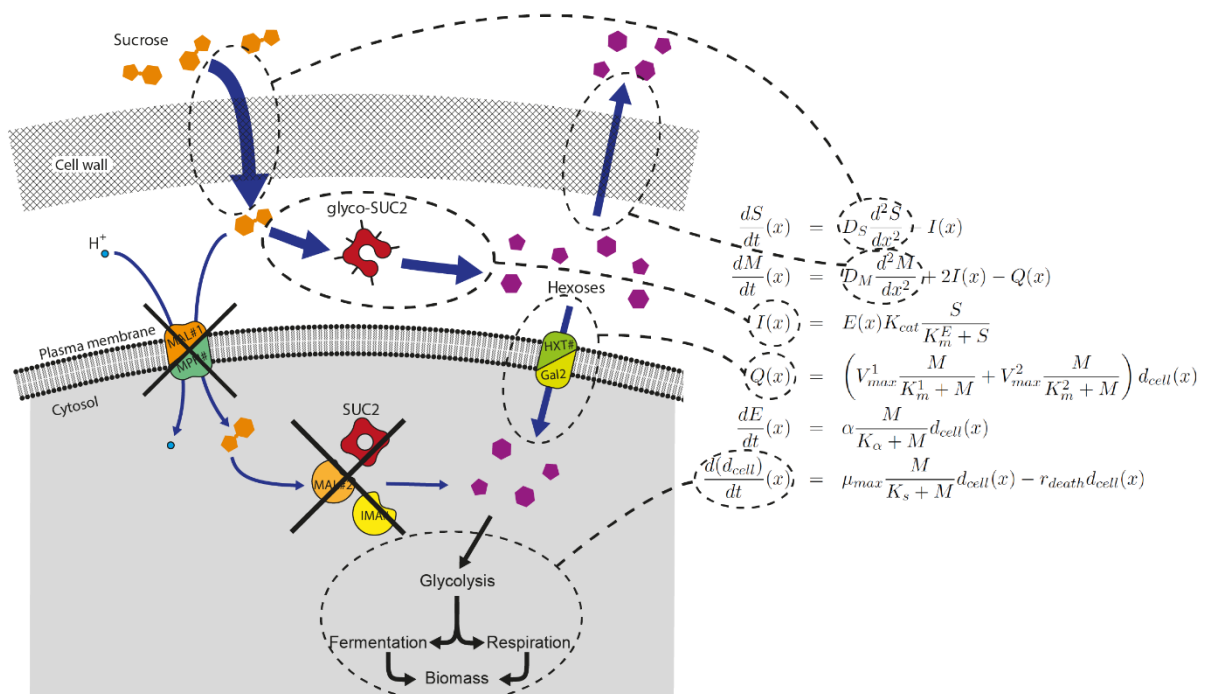
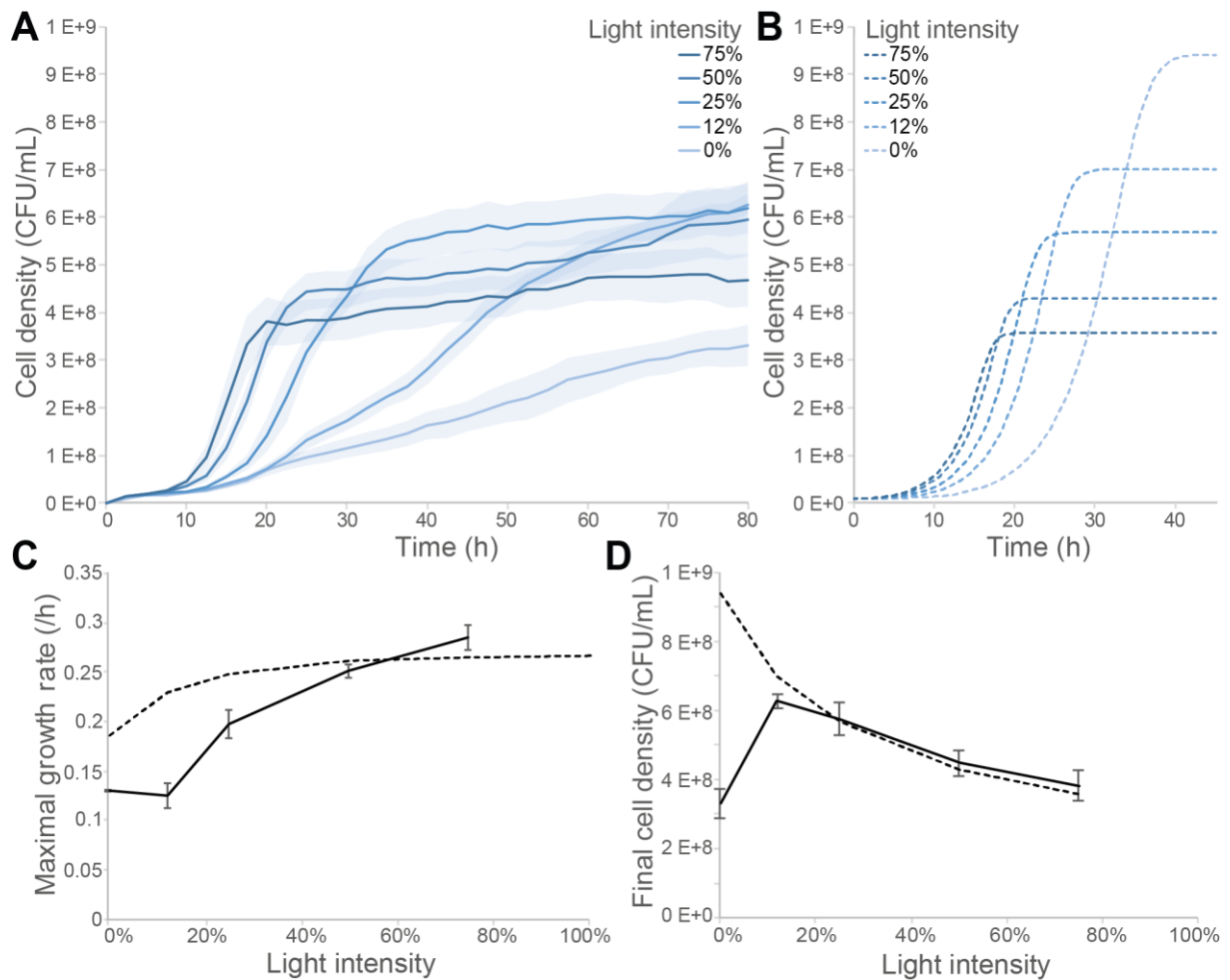


Figure 40 – *Saccharomyces Cerevisiae* sucrose pathway and the corresponding equations used to model the system.

To exemplify how the model behave compared to the experimental results, I investigated how invertase production rate influences the growth dynamic of yeast on sucrose without introducing any spatial pattern. I thus performed a light-dose response of the yPH\_536 strain using homogeneous and constant light stimulation (**Figure 41**). The resulting growth curves (**Figure 41A**) were used to extract the maximal recorded growth rates (**Figure 41C**) and the final cell densities at stationary phase (**Figure 41D**). Varying light intensity, we were able to tune the maximal growth rate from 0.12 to 0.27/h (**Figure 41C**). We also observed that the final density of yeast cells depended on how fast they consumed the sucrose stock (**Figure 41D**). The reduced final density for high SUC2 expression may be due to the Crabtree effect known to reduce yeast metabolic yield at high glucose concentration<sup>137</sup>. Indeed, hexoses accumulate more when there is an excess of invertase, leading to fermentative growth, whereas a limited invertase production prevents hexose accumulation and favours respiration. The corresponding simulated growth curves (**Figure 41B**) recover the experimental final densities (**Figure 41D**) but did not fully fit the experimental growth rate, especially for slow dynamics (**Figure 41C**). We note that when we did not illuminate cells, the final density was significantly lower, suggesting that growth was impaired due to gel drying prior to total nutrient consumption (**Figure 37**).



**Figure 41 - Light-dose response of the optogenetic strain yPH\_536 in the *OptoCube* with homogeneous light illumination.** (A) Experimental growth curves. (B) Corresponding simulated growth curves. (C) Maximal growth rate retrieved from growth curves represented in (A). (D) Dependence of the final cell density on the light intensity. For each experimental growth curve, I used the cell density value reached at the onset of stationary phase, where cell growth starts decelerating. We suspect this late slow increase in cell density to be due to ethanol respiration, which is not accounted for in our model. The corresponding simulated growth curves do not fully fit the experimental data, especially for slow dynamics, but allow to recover the experimental final density. When yeasts are not light activated, their final density is significantly lower because growth was stopped due to gel drying prior to total nutrient consumption (Figure 37). Solid lines represent experimental results, dashed lines represent simulated ones. Light blue area and error bars represent  $\pm$  the standard deviation for 3 technical replicates

### III.4. Cooperators competition for sucrose

To investigate how the size of the cooperator subpopulation affects the growth of the entire population, I projected a line of blue light of various widths, centred on a petri plate with a homogeneous lawn of yPH\_536 (**Figure 42A**). I then measured the mean final cell density profile of each plate's surface at t=85 h when yeast growth stopped (**Figure 42B**). We observed an exponential decay for cell density at the border between illuminated and non-illuminated areas showing hexoses diffusing away from the cooperators which allow the nearby cheaters to grow. To evaluate how cooperator and cheater populations share the available sugars, we plotted the final cell density values at the centre of the line (cooperator) and away from the line (cheaters) depending on the line width (**Figure 42C**).

We observed that increasing the illumination line width decreased the cooperators' final cell density while it increased the cheaters one. For thin lines of light, cooperator final densities are high because once the sucrose is locally depleted, there is sucrose diffusion supporting more cooperator growth. With increasing line width, the portion of sucrose diffusion reaching the centre of the line decrease, leading to smaller final densities: this evidences that there is a cooperator competition for sucrose within illuminated areas. This phenomenon leads to final cell density profiles with their highest values at the frontier of the line instead of the centre (**Figure 42B**). This morphology is similar to the ring pattern formed in colonies of non-motile microorganisms, which exhibit a localised growth at the colony edge resulting in a linear radial growth<sup>219–222</sup>. To better understand the process, we simulated one of these experiments (5.6mm wide blue line). **Figure 42D** represents the obtained sucrose and hexose concentrations and cell density profiles after 15 and 25 hours of illumination. These time-points illustrate two different types of hexose profiles. First when hexose consumption is lower than invertase activity, hexose accumulates at the cooperator location promoting their growth. This high local density will increase both hexose consumption and sucrose hydrolysis, depleting sucrose locally which in turn drastically reduces hexose production at the centre of the cooperator area. Any sucrose left in the cheater area will diffuse toward the cooperator area and be degraded at its frontiers.

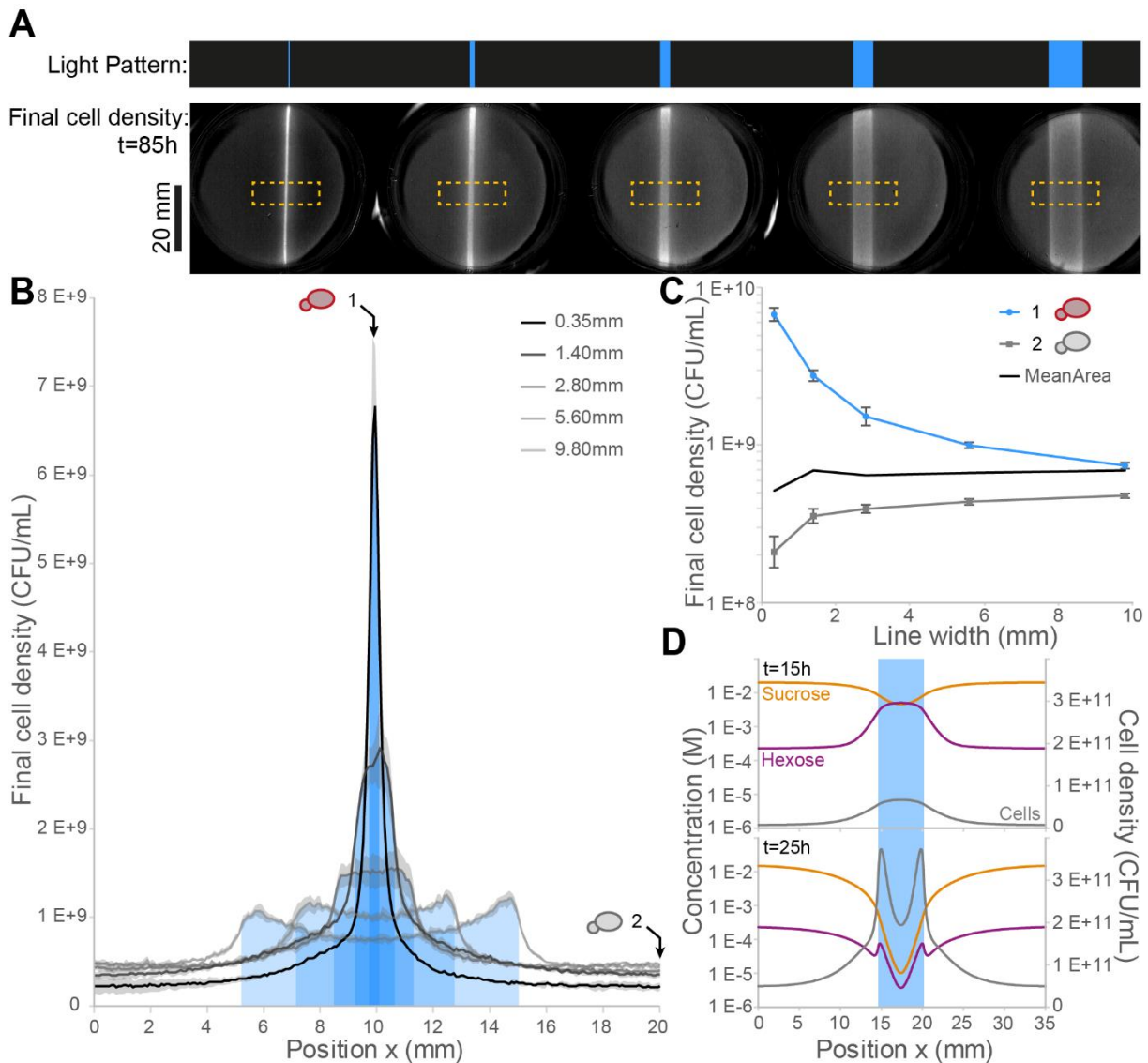


**Figure 42. Effect of cooperator population size on their fitness.** (A) DMD light pattern and the corresponding scan of the plate after 85 h of growth. Background subtraction was done using the first image in the timelapse. (B) Cell density profiles of a selected area (dashed orange square) at t=85 h. (C) Dependence of final cell density on the line width for the centre of the line (1) ; x=10mm) and far away from the line (2) ; x=20mm). The mean final density over the entire selected area was also plotted (MeanArea). (D) Simulated concentration and cell density profiles of the experiment with a 5.6 mm wide blue line, at t=15 h and t=25 h. First, hexose accumulation at the cooperator location promotes their growth, which then induces hexose exhaustion due to local depletion of sucrose. This cooperator competition for sucrose leads to final cell density profiles with their highest values at the frontiers of the line instead of the centre. Concentration values are plotted on logarithmic scale. Light grey areas and error bars represent  $\pm$  the standard deviation for 3 technical replicates.

### III.5. Cheaters competition for glucose

We then investigated the influence of the spatial organisation of a cooperator/cheater population on the global population growth. We patterned parallel lines of blue light (cooperator areas) separated by non-illuminated regions (cheater area) (**Figure 43A**). We chose to vary the pattern's wavelength (the width of one blue line and one dark line) while maintaining a constant light:dark area ratio of 25:75. To analyse the resulting population growth, we computed the mean density profile of the plates excluding any boarder effects (**Figure 43B**). These profiles were used to retrieve the final density of the centre of the illuminated area (1) and of the dark area (2), representing the cooperators and the cheaters subpopulations (**Figure 43C**). We also plotted the difference between these two values as it is a proxy for the cooperator benefit indicating how much cooperators grew compared to their surrounding cheaters. We observed an asymmetric bell-shaped curve for the cooperator benefit in function of the light-pattern wavelength (**Figure 43D**). Below a certain value ( $< 10$  mm), the smaller the wavelength is, the smaller the cooperator benefit will be: cheaters are closer to cooperators and will have more access to hexoses. For larger wavelengths ( $> 17$  mm), the cooperator benefit decreases with increasing wavelengths. The fact that increasing the cooperator area width led to a reduced final density for the centre of the line was already observed in the single line experiment presented previously (**Figure 42B**). Indeed, sucrose was quickly depleted, and its diffusion was not enough to reach cells at the centre of the cooperator line due to cooperator competition for sucrose.

We analysed these results using spatial filters terminology: the system behaves as a passband filter with the low cut-off wavelength (10mm) being due to cheater-cooperator competition for hexoses and high cut-off wavelength (17mm) due to cooperator competition for sucrose. Building on our model, we further investigated computationally the dependence of this transfer function (cooperator benefit) on one of the system parameters: the initial sucrose concentration (**Figure 43E**). The simulated maximal value of cooperator benefit (filter amplitude) increases with sucrose concentration. Low and high cut-off wavelengths decrease with increasing sucrose concentration, while the bandwidth also decreases. This additionally shows how a cooperative system's efficiency can depend on the nutrient availability.



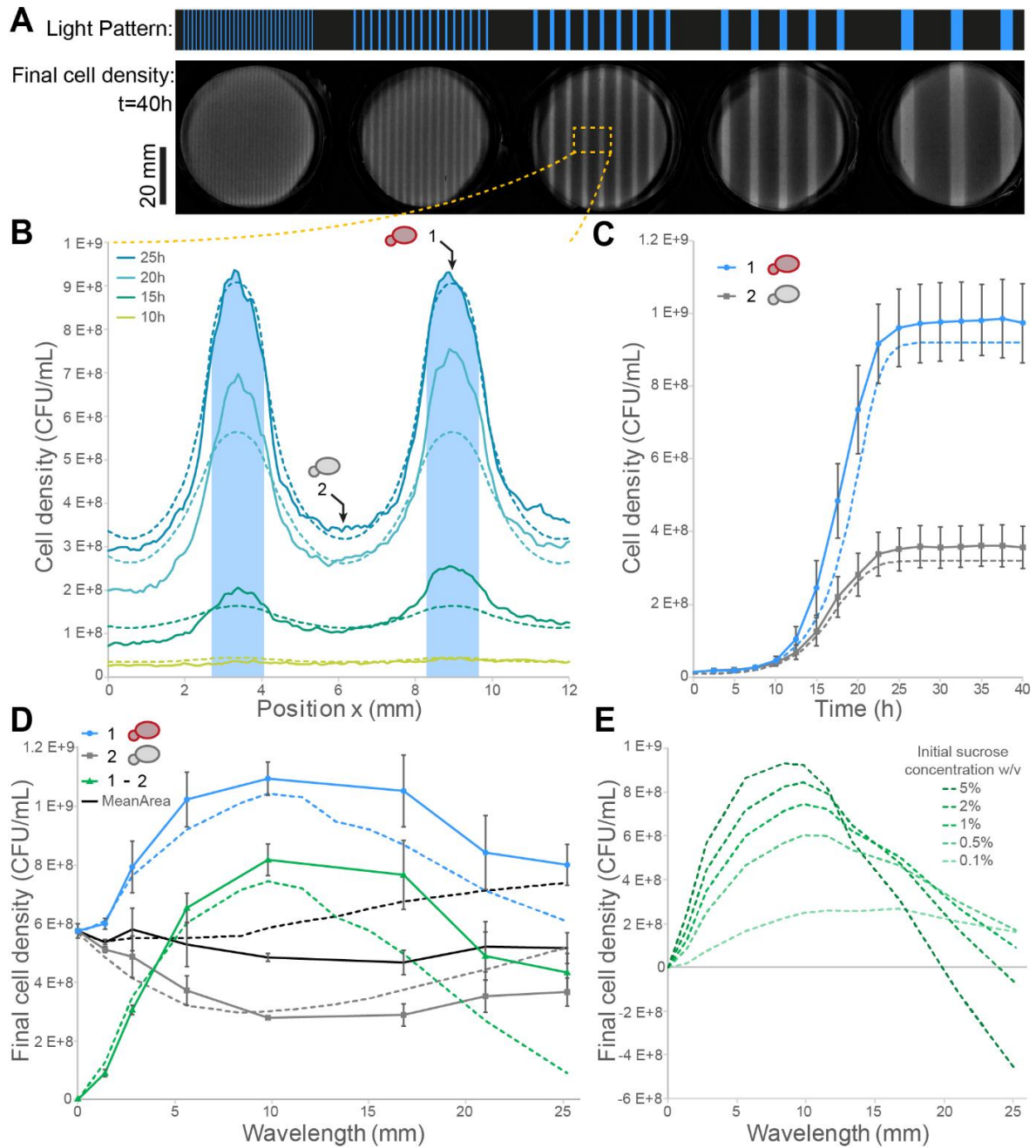


**Figure 43. Effect of the spatial wavelength of cooperator/cheater patterns on their growth.** We chose to investigate the effect of spatial organisation with a constant light:dark area ratio of 25:75. The spatial wavelength of the pattern corresponds to the width of a blue line and a dark line. (A) Projected light pattern and the corresponding scan of the plate after 40h of growth. Background subtraction was done using the first image in the timelapse. (B) Cell density profiles of a selected area (dashed orange rectangle) at different times for the wavelength of 5.6mm. (C) Corresponding growth curves for the blue lines centre (1) and dark lines centre (2). (D) Passband filter behaviours of the system. Dependence of the final cell density of (1), (2), as well as the cooperator benefit (1)-(2) and the mean final density over the selected area (MeanArea) on the spatial wavelength of the pattern (t=40h). Dashed lines represent the corresponding simulation results. (E) Simulated cooperator benefit (1)-(2) varying the pattern wavelength and sucrose concentrations. The maximal value of cooperator benefit (filter amplitude) increases with sucrose concentration. Low and high cut-off wavelengths decrease with increasing sucrose concentration, while the bandwidth also decreases. (Error bars represent  $\pm$  the standard deviation for 3 technical replicates)

These last results recapitulate well what are the spatial components of *S. cerevisiae* metabolism for sucrose in the context of cooperator/cheater consortia. Small distance (< 10mm) competition of cheaters on cooperators for public goods and long distance (> 17mm) cooperator intercompetition for sucrose were observed. The spatial filtering terminology is particularly useful to summarize the system's behaviours and, might be relevant for the analysis of other microbial community interactions which include spatial dependence. Obtaining such information helps better apprehend the behaviours of microbial systems in different spatial configurations. It can also improve the ability to predict the outcome of potential control strategies. To apply such filtering analysis, it is required to have the capacity to impose the spatial organisation of the microbial consortia to then analyse its influence on the system. The use of optogenetics is very convenient to generate spatial patterns of gene expression in engineered strains, but other strategies could be envisioned such as bioprinting or stamping of different strains with various geometries which have the advantage to be readily applicable to natural microbe isolates with no requirement for genetic modification.

Importantly, this work shows that microbial interactions can range up to the centimeter scale and that using the right growth culture recipient is important to recover all spatial dependencies.



## Chapter IV – Smart Microscopy, Cybersco.py: software for event-based, conditional microscopy

During my PhD, I have also worked on a project related to smart microscopy. The goal was to create an open-source software to control automated microscopes, such as MicroManager, but that would be more user-friendly for people uncomfortable with coding while still allowing great flexibility in acquisition protocol architectures. We also decided to code using a user-friendly language which is gaining in popularisation: Python. I have worked with two different research engineers successively, and we successfully released a first version of Cybersco.py. This version is working and quite stable, but I would mention that: (i) there are still occasional bugs, (ii) its responsivity is relatively low and can be limiting when recording rapid processes (timescale minimum ~1 second), (iii) it is currently only set-up for our specific equipment and (iv) some of its functionality remain only accessible with actual coding. More work on this project could resolve some of these drawbacks, for example participative contributions could help broaden the equipment brand compatibility.

My role in this project was to bring my expertise in fluorescent microscopy and as a biology experimentalist. This revealed to be quite important because our experimental constraints and needs can be difficult to anticipate (phototoxicity, photobleaching, sample preparation, ...). I helped designing the Graphical User Interface trying to keep it simple. I also designed and performed all the experiments used to test the software and to show its capabilities. This work has been summarized in the manuscript “CyberSco.Py an open-source software for event-based, conditional microscopy” published in Scientific Reports in July 2022 ([doi.org/10.1038/s41598-022-15207-5](https://doi.org/10.1038/s41598-022-15207-5)). The published main text is included below.



OPEN

## CyberSco.Py an open-source software for event-based, conditional microscopy

Lionel Chiron<sup>1,3</sup>, Matthias Le Bec<sup>1,3</sup>, Céline Cordier<sup>1</sup>, Sylvain Pouzet<sup>1</sup>, Dimitrije Milunov<sup>1</sup>, Alvaro Banderas<sup>1</sup>, Jean-Marc Di Meglio<sup>2</sup>, Benoit Sorre<sup>1</sup> & Pascal Hersen<sup>1</sup>✉

Timelapse fluorescence microscopy imaging is routinely used in quantitative cell biology. However, microscopes could become much more powerful investigation systems if they were endowed with simple unsupervised decision-making algorithms to transform them into fully responsive and automated measurement devices. Here, we report CyberSco.Py, Python software for advanced automated timelapse experiments. We provide proof-of-principle of a user-friendly framework that increases the tunability and flexibility when setting up and running fluorescence timelapse microscopy experiments. Importantly, CyberSco.Py combines real-time image analysis with automation capability, which allows users to create conditional, event-based experiments in which the imaging acquisition parameters and the status of various devices can be changed automatically based on the image analysis. We exemplify the relevance of CyberSco.Py to cell biology using several use case experiments with budding yeast. We anticipate that CyberSco.Py could be used to address the growing need for smart microscopy systems to implement more informative quantitative cell biology experiments.

Microscopy imaging is an invaluable tool in quantitative cell biology. Recent years have seen the emergence of increasingly sophisticated techniques to probe the dynamics of living systems at high spatio-temporal resolutions. These technological developments have mostly been obtained using novel optical methods that structure the illumination of biological samples in space and time, the rise of optogenetics that facilitates real-time interactions with living samples, and the development of deep learning algorithms to analyze images and segment cells. Many microscopes are now powerful semi-automated systems that can acquire pre-programmed timelapse sequences, usually via a process called Multi-Dimensional Acquisition (MDA), to observe and characterize the behaviors of single cells over extended periods of time. To define a MDA protocol, the user typically has to select several locations within the biological sample (X and Y coordinates) and focal planes (Z positions), as well as the illumination settings that will be applied to every position (wavelengths, intensities, exposure times) and then, choose how often images should be captured by the camera. Automation microscopy software is used to ensure synchronization of the devices attached to the microscope, by periodically looping through these dimensions (space, time, imaging parameters). MDA has become very popular and is used routinely in cell biology laboratories. While the value of this approach has been well-demonstrated for the study of time-varying phenomena at play in biological systems, MDA drastically limits the capacity of fluorescence timelapse microscopy to monitor complex, multiscale biological processes. Indeed, for every experiment, a balance must be found between the number of positions imaged, the spatial resolution (magnification of a given objective), the time resolution, and additional effects such as phototoxicity, the duration of the experiment, cell density, etc. The tradeoffs between these factors are not trivial to setup and are usually not known at the beginning of experiments. Moreover, a simple MDA cannot typically deal with all of these factors; for example, studies of fast, intermittent processes (e.g., mitotic events) require imaging at both a high framerate and over a long period of observation, which lead to either phototoxicity or improper sampling.

Such basic workflows have become outdated at the time when smart systems and artificial intelligence are being used to improve the functioning of many (scientific) devices. A key practical limitation of MDAs is the fact that the images are only analyzed at the end of the experiment, which sequentially separates the workflows of image acquisition and image analysis. The ability to employ real-time image analysis to inform and optimize

<sup>1</sup>Institut Curie, Université PSL, Sorbonne Université, CNRS UMR168, Laboratoire Physico Chimie Curie, 75005 Paris, France. <sup>2</sup>Laboratoire Matière et Systèmes Complexes, UMR 7057 CNRS, Université Paris Diderot, 10 rue Alice Domon et Léonie Duquet, 75013 Paris, France. <sup>3</sup>These authors contributed equally: Lionel Chiron and Matthias Le Bec. ✉email: pascal.hersen@curie.fr

or adjust the settings of ongoing image acquisition would be a game changer for studying complex, dynamic cellular processes. Although this strategy requires a deep dive into the software programming and automation of microscopy devices, transformation of a conventional timelapse automated microscope into a powerful unsupervised automaton that is able to acquire data from a live biological sample at the right place and at the right timing could empower researchers in the biomedical sciences.

Building on existing automation microscopy software, several groups have started to explore how smart microscopy automate can benefit the life sciences<sup>1–5</sup>. In 2011, MicroPilot<sup>5</sup> used LabVIEW (a proprietary systems engineering automation software) to interface  $\mu$ Manager<sup>6,7</sup> (the most popular open source and cross platform software used to pilot a large variety of microscopy devices) and other commercial vendor automation software with a machine learning algorithm to identify and only focus on cells in a specific phase of mitosis. This strategy increased the throughput and decreased the time required to screen the desired cells. Since then, the rise of machine learning and the popularization of simple automation strategies—using low cost prototyping microcontroller boards (Arduino<sup>8</sup>) or compact single-board computers (Raspberry Pi<sup>9</sup>) and Python programming—have made it easier to build simple open-source solutions to achieve the same goals. For example,  $\mu$ Magellan<sup>4</sup> and NanoJFluidics<sup>1</sup> were built directly on  $\mu$ Manager to achieve some level of feedback loop control and automation of image acquisition.  $\mu$ Magellan focuses on creating content-aware maps to adapt imaging modalities to a 3D biological sample. NanoJFluidics<sup>1</sup> homemade array of Arduino-controlled syringe pumps combined with  $\mu$ Manager can perform automated fixation, labeling and imaging of cells; notably, this system could be triggered by real-time detection of the rounding of mitotic cells through a basic image analysis algorithm. More recently, Pinkard et al.<sup>3</sup> established PycroManager, a Python library that can interact with  $\mu$ Manager to program a microscope in a very flexible way, though at the expense of a prerequisite for expert-level Python coding skills and the knowledge of additional software or programming language. Overall, these examples harness the capability of  $\mu$ Manager to pilot microscopy instruments and home-made image-analysis tool suites to trigger pre-programmed actions, and thus facilitate the development of complex or time-consuming microscopy experiments.

In addition, recent advances in the application of control theory to biology led to the development of external feedback loops, in which cells are analyzed and stimulated in real-time to force the cell state (e.g., expression of a gene<sup>10–17</sup>, activity of a signaling pathway<sup>18</sup>) to follow a user-defined (time varying) profile. Such feedback loops require the ability to perform real-time image analysis, in order to extract cellular features to feed an algorithm that decides how to stimulate the cells in live mode via microfluidics<sup>14,15</sup> and/or optogenetics<sup>10–13,16</sup>. This novel and active field of research, called *cybergenetics*, harnesses the possibility of creating interactions between cells and a numerical model in real-time, and thus opens novel areas of both applied and fundamental research. To demonstrate the power of cybergenetics, we and others have developed various software to implement feedback loop-controlled microscopy systems. These solutions combine  $\mu$ Manager and/or MATLAB with dedicated image analysis and control algorithms to close the feedback loop<sup>14,15</sup>. However, in practice, these solutions are difficult for non-experts to implement and cannot be easily transposed to a broad range of biological problems. More recently, several groups proposed Python and  $\mu$ Manager-based software to develop cybergenetic experiments<sup>19,20</sup>, though these approaches remain specific to the control of gene expression in cells over time and do not meet all of the varied needs of cell biologists.

Here, we present CyberSco.Py software, which is a follow-up to our contributions to piloting gene expression in real-time in yeast and bacteria<sup>14,15</sup>. CyberSco.Py is written in Python, has been designed with automated, real-time feedback loops in mind, and includes deep learning image analysis methods as an integral part of image acquisition. We focused on achieving a proof-of-concept software with a simple, robust, user-friendly interface that can be deployed as a web application. Importantly, CyberSco.Py natively includes the ability to control basic microfluidic devices through an Arduino board that drives electro-fluidic valves (see “Materials and methods”). CyberSco.Py is, by design, oriented towards advanced timelapse experiments that include triggered events and routed tree scenarios—rather than preprogrammed sequences of image acquisition. CyberSco.py is still a proof-of-concept and, here, our main goal is to demonstrate the potential of event-based, conditional microscopy to cell biologists. To this end, we first describe the principle of Cybersco.py, and then focus on several use case scenarios to exemplify how event-based microscopy can be applied to perform more informative experiments relevant to cell biology.

## Results

**CyberSco.py is an open-source web application for timelapse microscopy and microfluidics automation.** It is written in Python (Fig. 1) and employs real-time image analysis and decision-making algorithms to trigger changes in the imaging parameters in real-time during the experiment. At present, this proof-of-concept is operational on a fully automated Olympus microscope (IX81) equipped with brightfield and epifluorescence illumination and linked to an Arduino-based homemade microfluidic control device (Supplementary Figs. S1 and S2). A web interface allows the user to easily setup an experimental plan and/or to select pre-configured conditional experimental scenarios, together with the corresponding image analysis solutions. A local server receives these parameters and launches the experiment. During the experiment, the acquired images are constantly analyzed and used to trigger events according to the chosen scenario. In particular, the detected events can feedback on the microscopy settings and the microfluidic settings to adapt the experimental plan during the experiment (Fig. 1). Thus, CyberSco.Py transforms microscopes and their related devices into an advanced imaging automaton capable of performing unsupervised time-dependent tasks with the capacity to handle various user-defined triggers. More details of the CyberSco.Py source code and its documentation are available on the GitHub page of the project (Supplementary Information). Although the software has been developed for a given microscopy setup, it can be extended to any equipment providing there is a driver and/or

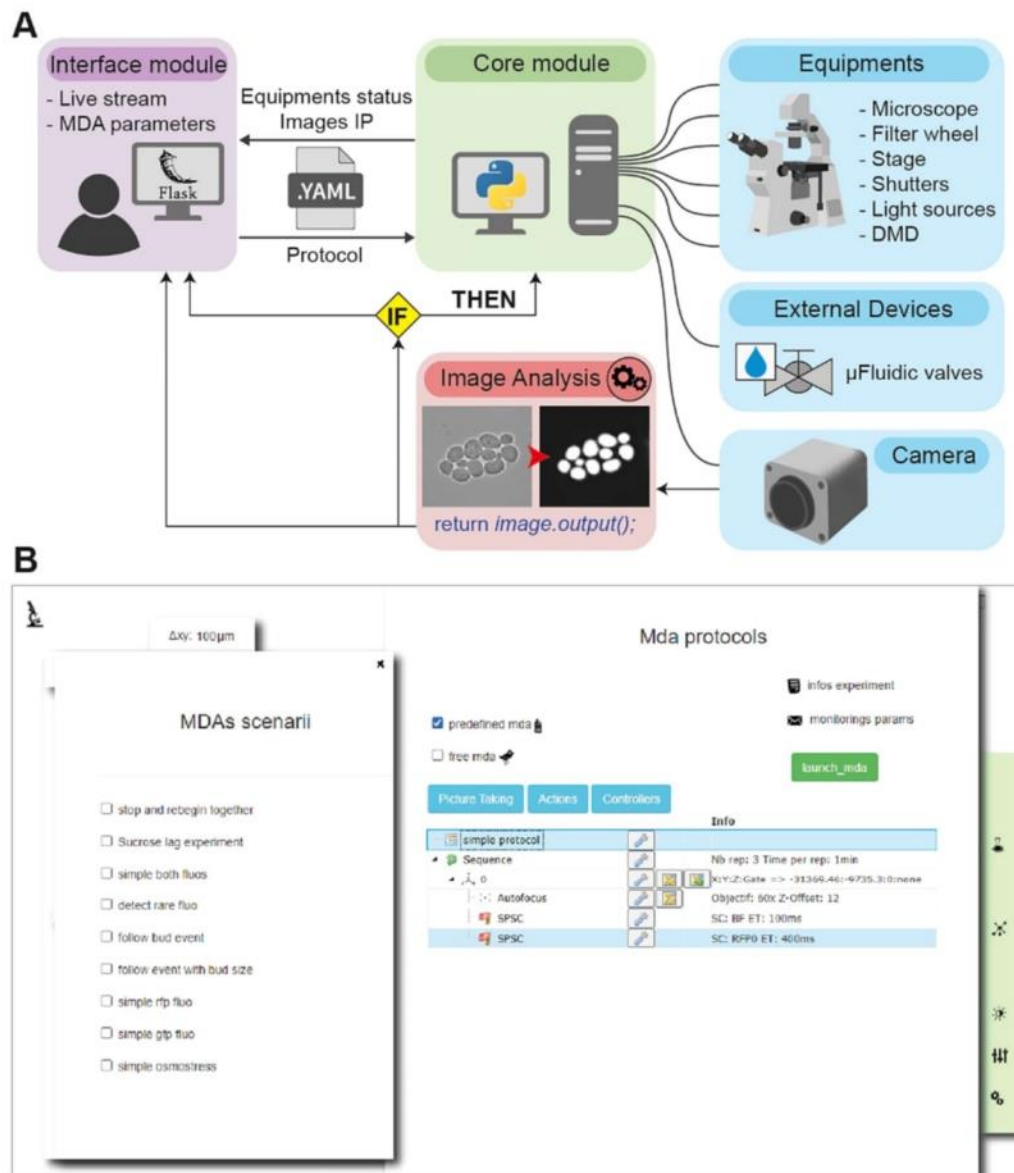


**Figure 1.** CyberSco.Py framework. **(A)** Architecture. CyberSco.Py is built in Python and uses the web application library Flask to create a web user interface. Microscopy protocols are written into a YAML (human readable data serialization language) file, which can be interpreted by the Python core module of CyberSco.Py, which drives the various components of a IX81 fully automated microscope. The core module also drives a set of fluidic valves that can be used to switch the media flowing into a microfluidic device. A class in Python is associated to each device. Images obtained from the camera are analyzed in real-time by a U-NET deep learning model to segment yeast cells and/or detect specific events, depending on the pre-trained model selected by the user. The result of the analysis is used by the core module to update the current state of any devices under its control (see “Materials and methods” for more information). **(B)** Snapshot of the current user interface. The user interface is very simple by design and allows the user to choose between several pre-programmed event-based scenarios, for which the user must define various relevant parameters and condition switches. The simple drag and drop interface can be used to modify a given Multi-Dimensional Acquisition protocol to give more flexibility and to create more advanced protocols. The same interface can be used in “live mode” to view what is currently being imaged and check that the live image analysis is performing correctly. Once the program is launched, the computer takes control of the microscope and will adjust the image acquisition parameters based on the event-based scenario that has been selected. It is possible to code a novel scenario directly in Python and/or to manually adjust the thresholds and parameters used to detect events (e.g., number of cells, size of cells, etc.). The structure of a scenario consists of a list of instructions for the microscope (“make the autofocus”, “take a picture”, etc.) to be serially executed at each iteration, a conditional block, and an initialization block. Each scenario corresponds to a unique Python file with the same consistent structure. The user can also enter information about the projected experiment, as well as selecting modalities for monitoring the experiment remotely via email (selecting where to send the emails and at which frequency) and/or through a discussion channel (e.g., Microsoft Teams or Slack).

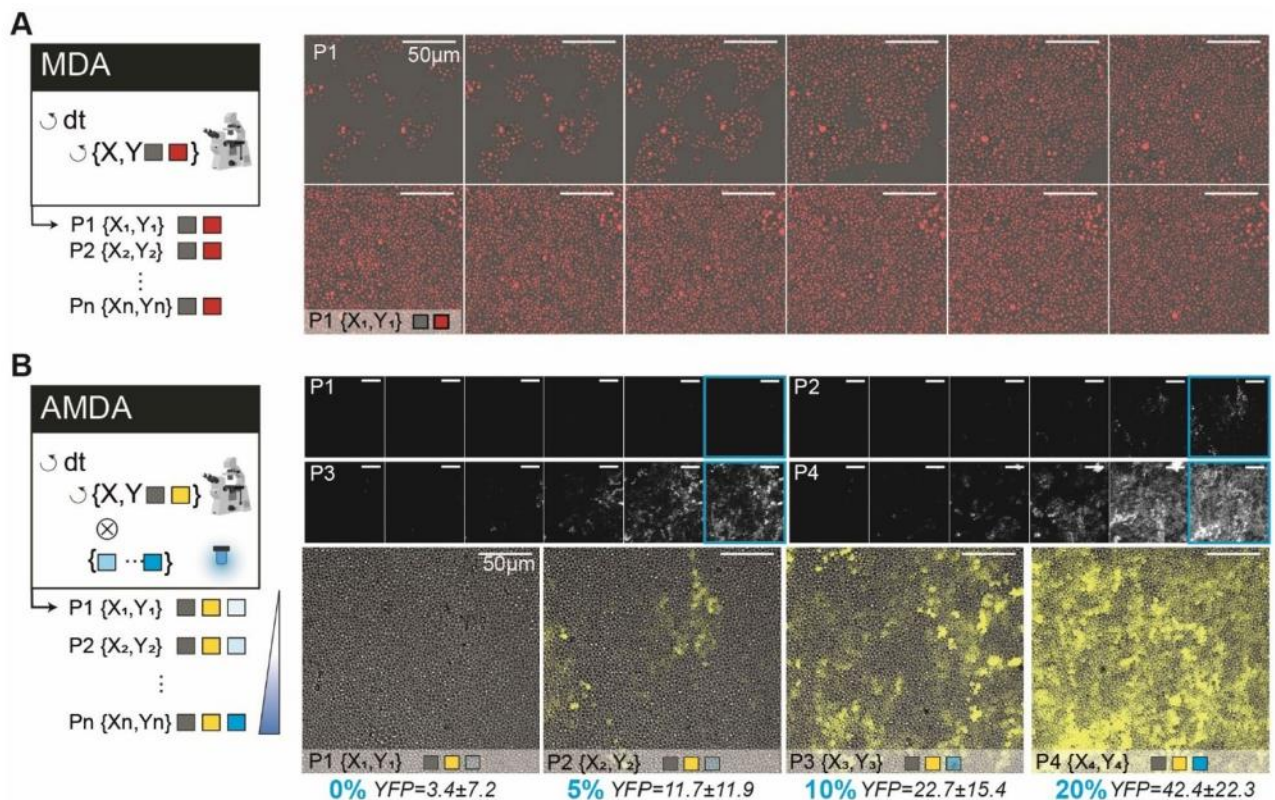


**Figure 2.** From simple to advanced MDA. **(A)** Example of a classic Multi-Dimensional Acquisition (MDA) protocol to observe yeast proliferation in a microfluidic chamber, with two imaging channels (brightfield and RFP) imaged every 6 min for several hours. The HTB2 protein of the yeast cells is tagged with a mCherry fluorescent reporter. A sketch of the program (nested loops) is shown on the left side: the imaging parameters are identical for every position and timepoint. **(B)** An advanced MDA, in which the user has defined several positions, but set different illumination settings in the blue channel (LED intensity: 0%, 5%, 10% and 20%). This programming was done without scripts, by just using the drag and drop interface (see Supplementary Materials). Yeast cells bearing an optogenetic gene expression system (pC120-venus) were imaged for 15 h. Each position is exposed to a different level of light stimulation, which alters the expression of a yellow fluorescent reporter both in terms of cell–cell variability, the maximum level of expression and dynamics. Thus, in one experiment, it was possible to quantitatively calibrate the pC120 optogenetic promoter using our settings without any requirement for coding (objective  $\times 20$ ). Fluorescence levels are averaged across the field of view and the error values are the standard deviation of pixel intensity.

a documented communication protocol (see Supplementary Information and the GitHub page of the project on how to proceed).

**CyberSco.Py allows to automate complex multidimensional acquisitions.** CyberSco.Py can obviously be used to build classic MDA experiments. A web interface enables the imaging acquisition settings to be easily defined through a drag and drop interface (Fig. 1 and Supplementary Information). The user can define X–Y positions and the corresponding focal planes and set the illumination parameters, as in conventional microscopy software. CyberSco.Py makes it easy to perform a classic MDA experiment that follows, for example, the proliferation of a population of yeast cells in a microfluidic device (Fig. 2A). Crucially, the user can define specific imaging settings for each position (Fig. 2B). This modification of how MDA is defined through the user interface is simple but powerful: by design, the user has full control over the acquisition settings without having to follow the classic MDA patterns of nested loops, which by default impose the same imaging acquisition parameters on all time points and positions. The ability to vary the imaging modalities per position imaged allows, for example, the user to conveniently and quickly optimize the imaging conditions by varying the exposure time for each position (to screen for phototoxicity or optimal illumination, for example). To demonstrate its usefulness, we used this feature to measure the light-dose response of a light-inducible promoter (Fig. 2B and Supplementary Fig. S3) with just one timelapse experiment. Setting up this experiment was quick and simple thanks to the minimal powerful user interface. More generally, any combination of imaging parameters can be assigned to a given position using the drag and drop tools within the user interface. For advanced users, the imaging parameters and positions can also be sent directly through a configuration file to create programmatically complex acquisition scenarios. More details of the user interface and scripting possibilities are available on the GitHub repository of the project (see also Supplementary Information). Notwithstanding such flexibility,



CyberSco.Py has been programmed to include several types of protocols relevant to quantitative cell biology. Such built-in capabilities include: (1) synchronization of the image acquisition framerate with the microfluidic valve switches that apply the environmental changes; (2) detection and tracking of a cell of interest in a microfluidic device over an extended period of time; (3) cell counting, and triggering of environmental changes when the cell population reaches a certain size in the field of view; and (4) prediction of the future occurrence of a cellular event and the corresponding changes in the illumination settings and framerate required to image this event at an appropriate time interval.

**External triggers and adaptative acquisition framerates enable the observation of cell signaling at the right pace.** Cells use a large set of signaling pathways and gene regulatory networks to process information from their surroundings. The signaling pathways in yeast are usually activated relatively quickly, within tens of seconds, while the transcriptional responses are slower (several minutes) and cell adaptation is even slower (tens of minutes). Therefore, it is difficult to image cell growth and signaling dynamics with fluorescence microscopy at the same time. Indeed, conventional MDA only allows image acquisition on one timescale. Fast periodic acquisition is possible, but leads to phototoxicity. Ideally, several acquisition frequencies need to be defined: a fast frequency to capture signaling events at the right pace, and slower frequencies, to image physiological adaptation and monitor cell growth. Moreover, the switch from a slow to fast acquisition framerate should be synchronized with the changes in the cellular environment through microfluidics. These technical requirements can be met by a simple scenario within Cybersco.py.

As an example, we studied nuclear import of the MAPK Hog1p following hyperosmotic stress<sup>21, 22</sup>. Yeast cells were grown inside a microfluidic device (see “Materials and methods”) to facilitate imaging and facilitate dynamic environmental changes. We observed that an acquisition rate faster than one fluorescent image every 5–6 min led to phototoxicity and cellular arrest if performed over extended periods of time. This acquisition rate is too slow to capture nuclear localization of the Hog1p protein, which peaks 1–2 min after cells are subjected to hyperosmotic stress. We programmed Cybersco.py to perform pulses of osmotic stress (by switching the state of an electrofluidic valve) every hour. Sending this command triggered modification of the acquisition framerate, which was increased from one frame every 5 min to one frame every 25 s (Fig. 3). No coding/ scripting was required for this modification: the user just needed to select this predefined scenario and set the desired framerates and illumination parameters. As shown in Fig. 3, we monitored several successive signaling events using this adaptative sampling rate without any user intervention. This example shows how the combination of external triggers and advanced MDA enables quantitative, time-resolved data on cellular responses and stress adaptation to be obtained without user supervision.

**Live cell segmentation enables the use of conditional events to dynamically change the modalities of image acquisition based on real time cellular features.** CyberSco.py also offers the possibility of operating the microscope and the attached devices in real-time based on events detected during unsupervised analysis of the cell sample. The central idea is to let the microscope focus on “interesting” events through adjustment of the imaging acquisition parameters without supervision. This task requires efficient image analysis to segment cells, measure their properties and detect cellular events of interest. Image analysis is conveniently achieved in Python using the U-NET convolutional neural network<sup>23</sup> (“Materials and methods” and Supplementary Information), which is trained on a set of images. Once the training is complete, CyberSco.Py can use the resulting model to segment cells, display the segmentation in the user interface, compute cellular features and trigger user-defined events. At present, CyberSco.Py comes with two U-NET-trained models for yeast segmentation at different magnifications that give the following outputs: (1) the number of cells in the field of view; (2) a segmentation map of the cells in the field of view, as well as (3) their size and (4) their fluorescence levels. These cellular features can then be used to define conditional statements and adapt the imaging acquisition parameters in real-time. The segmentation results can be instantly visualized in “live” mode as a quality control step before launching timelapse experiments (see Supplementary Material). Below, we describe three different use case scenarios to exemplify the potential of conditional microscopy.

**Cells of interest can be detected and tracked in real-time.** One interesting avenue of event-based microscopy is the ability to detect and focus on a particular cell of interest displaying a given phenotype at a given time. Instead of imaging many cells to find the cell of interest a posteriori, one can use real-time image analysis to identify cells with specific features and study their properties at an appropriate spatio-temporal resolution. There are two main challenges to overcome: defining the appropriate image analysis method to detect the cells of interest, and tracking those cells over time. Indeed, in an assembly of cells, growing cells push against their neighbors, often leading to large-scale displacement of the cells of interest, which may exit the field of view and be lost to subsequent imaging. Here, we demonstrate that it is possible to control the position of the X–Y stage to make sure that the cell of interest remains visible throughout the duration of the experiment. We studied a mixed population of yeast cells, in which a small fraction of the population (10%) express a fluorescent RFP histone tag. The program scans through the cells growing in a microfluidic device and once an RFP-expressing cell is detected, the scanning stops, the X–Y stage is moved to center the cell of interest and a timelapse is started to record RFP and brightfield images. The cell of interest is tracked throughout the timelapse, and the X–Y stage is moved so that this cell is always centered in the field of view. Figure 4 shows two such experiments, in different contexts, to demonstrate the efficiency of this detection and tracking scheme. Providing that the phenotype can be identified through image analysis (for example, a morphological feature or expression of a fluorescent reporter), this strategy could be employed to study rare phenotypes or, alternatively, to study long-term cellular

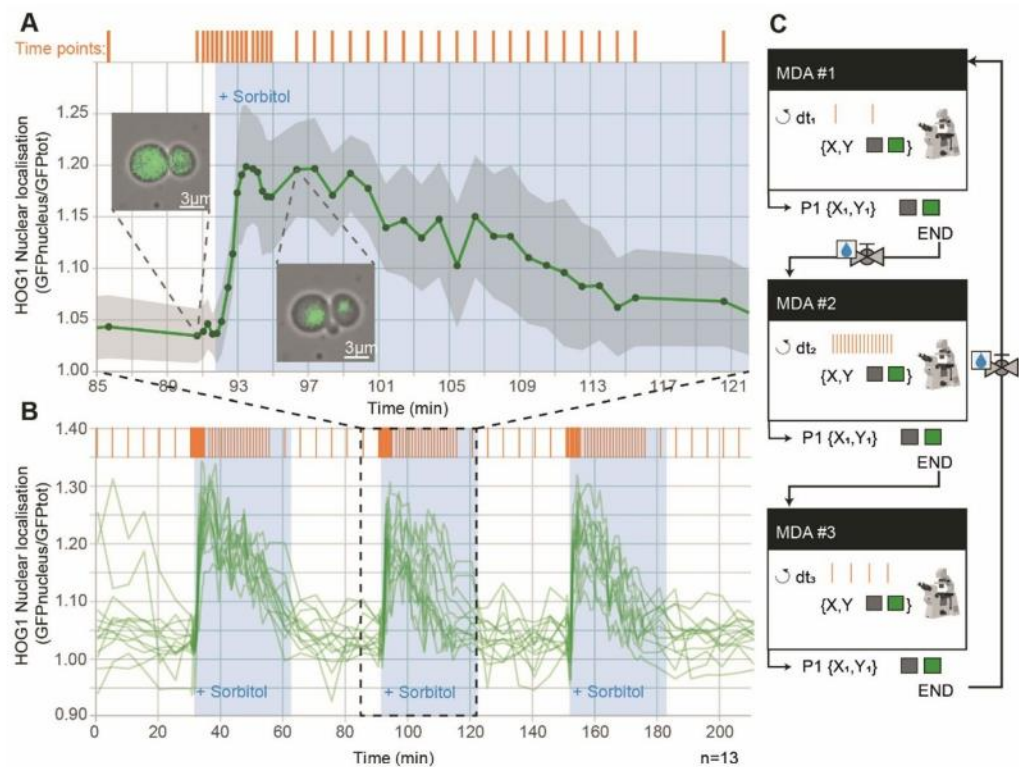


**Figure 3.** Synchronization of the acquisition framerate with dynamic perturbations to capture yeast cell signaling dynamics. **(A)** Time course of nuclear accumulation of Hog1p in yeast cells growing as a monolayer in a microfluidic chamber subjected to an osmotic stress (1 M sorbitol). The insets show localization of Hog1-GFP before and after the osmotic stress. The acquisition framerate (orange bars) is automatically adjusted from one frame every 5 min to one frame every 25 s (12 times faster) just before the cells are stressed osmotically. The autofocus was turned off during the first 4 min of rapid Hog1 nuclear import. Recovery of the cells was then monitored at one frame every minute for 20 min, and finally the framerate was set back to its initial value (one frame every 5 min) until the next stress. The grey area represents the  $\pm$  standard deviation of nuclear localization across 13 tracked cells from one microfluidic chamber. **(B)** The adaptive sampling rate used in **(A)** was repeated three times to demonstrate that cells exhibit reproducible dynamics in response to every stress. This experiment allowed the timescales of activation (fast) and deactivation (slow) of the HOG cascade to be measured in an unsupervised manner. **(C)** Sketch of the adaptive sampling MDA, which consists of three MDA experiments: one with a fast acquisition rate (nuclear import dynamics), one with a medium acquisition rate (nuclear export dynamics), and one with a slow acquisition rate (cell division after recovery). The switch from MDA#1 to MDA#2 is synchronized with the activation of an electrofluidic valve that delivers an osmotic stress of 30 min duration (repeated every 60 min). Nuclear localization is computed as the mean of GFP fluorescence in the nucleus normalized to the mean of GFP fluorescence in the entire cell.

behaviors (aging, cell-memory, habituation to repeated stress, etc.) within a large population of cells without user supervision. It is worth noting that this method can also compensate for spatial drift of the mechanical stage.

**Cybersco.Py can trigger a change in the microenvironment in function of a threshold in cell density through microfluidic automation.** Above, we showed how to control gene expression in cells based on real-time measurement of a fluorescent reporter. The same experimental strategy can be used to trigger a change in the cellular environment as a function of an observable feature in the field of view. This event-based strategy can be used to stimulate or perturb cells only when they have reached a given state. Alternative methods would require impractical, constant monitoring of the cells by the user. As a demonstration, we explored the impact of the number of yeast cells on the dynamics of recovery of cell division following a metabolic switch from glucose to sucrose. In response to glucose starvation, yeast cells produce and harbor the invertase Suc2p<sup>24</sup> in their cell wall, which hydrolyses sucrose into glucose and fructose in the extracellular environment. The yeast growth rate takes a certain amount of time to recover after a metabolic shift from glucose to sucrose. Since the benefit of Suc2p production is shared among the yeast population, we hypothesized that the size of the population of cells may impact the response time after a metabolic shift to sucrose<sup>24</sup>. To test this assumption, cells growing in a microfluidic chamber were counted in real-time and, as soon as the number of cells in the chamber reached a given value ( $N = 100, 500$  or  $2000$ ; Fig. 5), CyberSco.Py switched the perfusion from glucose to sucrose by triggering a microfluidic valve. Again, such experiments require an unsupervised, live method in order for the

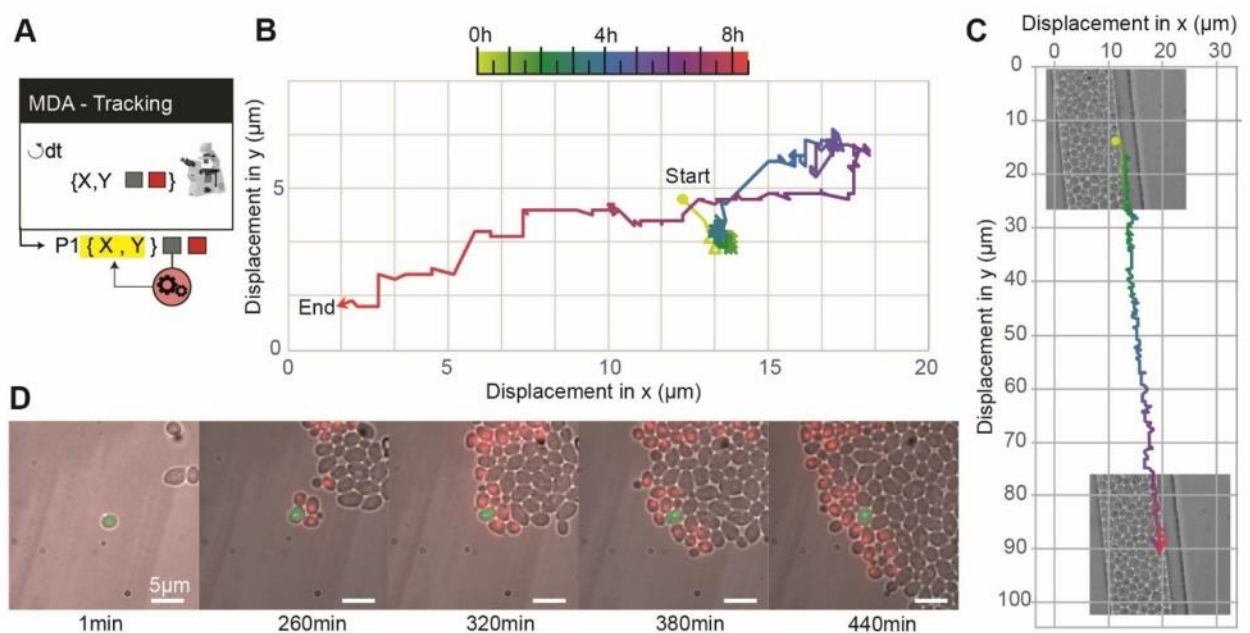


**Figure 4.** Detection and tracking of a cell of interest. **(A)** Sketch of the “detect and track scenario”. Once a cell of interest is found in the field of view, the field of view is centered on that cell and the stage is periodically moved to maintain this cell in the center of the field of view. **(B)** We mixed two populations of yeast cells in a microfluidic chamber, one of which express a HTB2-mCherry fluorescent reporter (1:10 cell ratio). The algorithm scans through several positions and when it detects cells with a signal in the RFP channel, picks one such cell randomly and centers it on the field of view. This cell is then tracked using brightfield segmentation, and the stage position is corrected through a feedback loop to compensate for cell displacement. **(C)** The cell of interest moves because it is pushed by the growth of neighboring cells, traveling approximately 20  $\mu\text{m}$  during the course of the experiment. The real-time stage compensation keeps the cell in the center of the field of view. The duration of the experiment (around 9 h) is long enough to observe the appearance of the progeny of the cell of interest. **(D)** Tracking a non-fluorescent yeast cell growing in a dead-end narrow microfluidic chamber, leading to global directed motion of all cells. The tracked cell remains in the field of view, even though it travels approximately 80  $\mu\text{m}$ ; in contrast, the field of view is only  $\sim 25 \times 25 \mu\text{m}$ .

switch to be made efficiently. We observed that the duration of the lag phase decreased as the size of the population in the microfluidic chamber at the time of the metabolic shift increased, indicating faster production and accumulation of the enzymatic products within larger yeast populations, and hence a better adaptability of large yeast populations to sucrose metabolic shifts. Moreover, this experiment demonstrates the capacity of CyberSco.Py to precisely control the sample size at the start of the experiment, and suggests that cell density is a biologically relevant parameter that should be considered to improve experimental reproducibility.

**Imaging of mitosis in yeast can be done at high temporal resolution by conditionally switching between two predefined MDAs.** As a final example, we used CyberSco.Py to precisely image mitotic events in a population of growing yeast cells (Fig. 6). We combined cell segmentation, cell tracking, and event-based modification of the imaging parameters to achieve imaging of mitotic events in yeast at a high temporal resolution in an unsupervised manner. Cells were observed and segmented at regular intervals (3 min). We assessed the increase in the size of buds over time to predict when mitosis will occur. We detected buds using U-NET segmentation and searched for yeast cells with buds that have grown to reach a threshold size and that have been increasing in size over the past three pictures (see “Materials and methods”). Both criteria were sufficient to detect mitotic events under our conditions and to eliminate segmentation artefacts. When all conditions are fulfilled, the first MDA is stopped and a second MDA with a faster acquisition framerate, along with fluorescence imaging for the HTB2-mCherry reporter, is initiated. In this manner, mitotic events can be imaged at a much faster rate than in a classic MDA experiment (Fig. 6) without the detrimental long term effect of phototoxicity. This kind of “search and zoom” scenario is presented for mitotic events as a proof-of-principle, but could be applied to any rare event that occurs within a population of cells.

## Discussion

The main goal of CyberSco.Py is to enable the design of augmented MDA experiments in which the imaging settings can be changed in real-time as a function of unsupervised image analysis conducted during the time course of the experiment. CyberSco.Py has been built as a modular web application; in addition to the modularity of the device management, both the image analysis and decision-making algorithm are separate modules that can be adjusted individually and plugged into the communication modules that drive the microscope and its

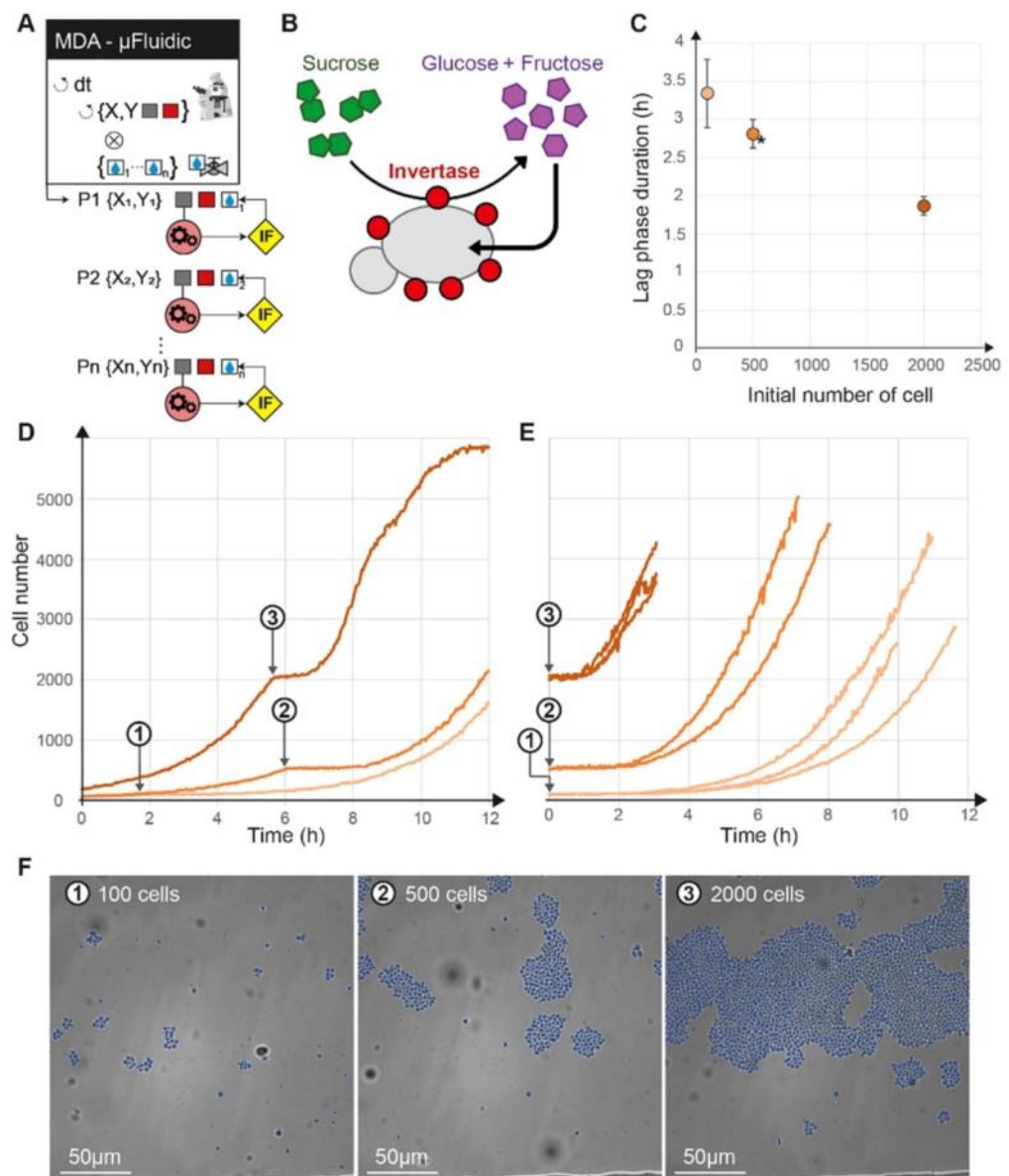


**Figure 5.** Conditional perturbation based on the number of cells. **(A)** Sketch of the protocol, showing that different positions have a different conditional statement ((IF)) on the number of cells to trigger the switch from glucose to sucrose independently of each other. **(B)** Sucrose conversion by yeast. The Suc2p invertase produced by cells is secreted extracellularly and can degrade extracellular sucrose into diffusible hexose. **(C)** Following a shift from glucose to sucrose, cells need some time to convert sucrose to glucose and restart division. We show here that this time depends on the initial cell density (the higher the number of cells, the shorter the lag phase). The duration of the lag phase was estimated as the time it took the population to reach 130% of its initial size after the switch from glucose to sucrose. Error bars represent  $\pm$  one standard deviation over three biological replicates (two replicates for the \*). **(D)** Temporal evolution of the number of cells for different initial densities: 100 (1), 500 (2) and 2000 (3) cells (grey arrows). **(E)** Population growth shifted temporally to the switch time (i.e., switch =  $t_0$ ), demonstrating that the lag time increases as the initial cell density decreases. **(F)** Cell counting is achieved by real-time segmentation, shown here as an overlay of the brightfield image with single cell masks (in blue) at the time of the valve switch.

associated components. In that respect, CyberSco.Py aims to push forward “low code” or “no code” strategies, which are becoming increasingly popular, and enable biologists without coding expertise to create complex, event-based routines and workflows using cloud-based web applications. Creation of automation protocols that contain simple logical, conditional statements such as “IF this THEN that” or “WHILE this DO that” are within the reach of CyberSco.Py and may have an impact for researchers in biology who do not want, nor have the time or expertise, to dive into programming. This goal could be reached progressively by building on the examples

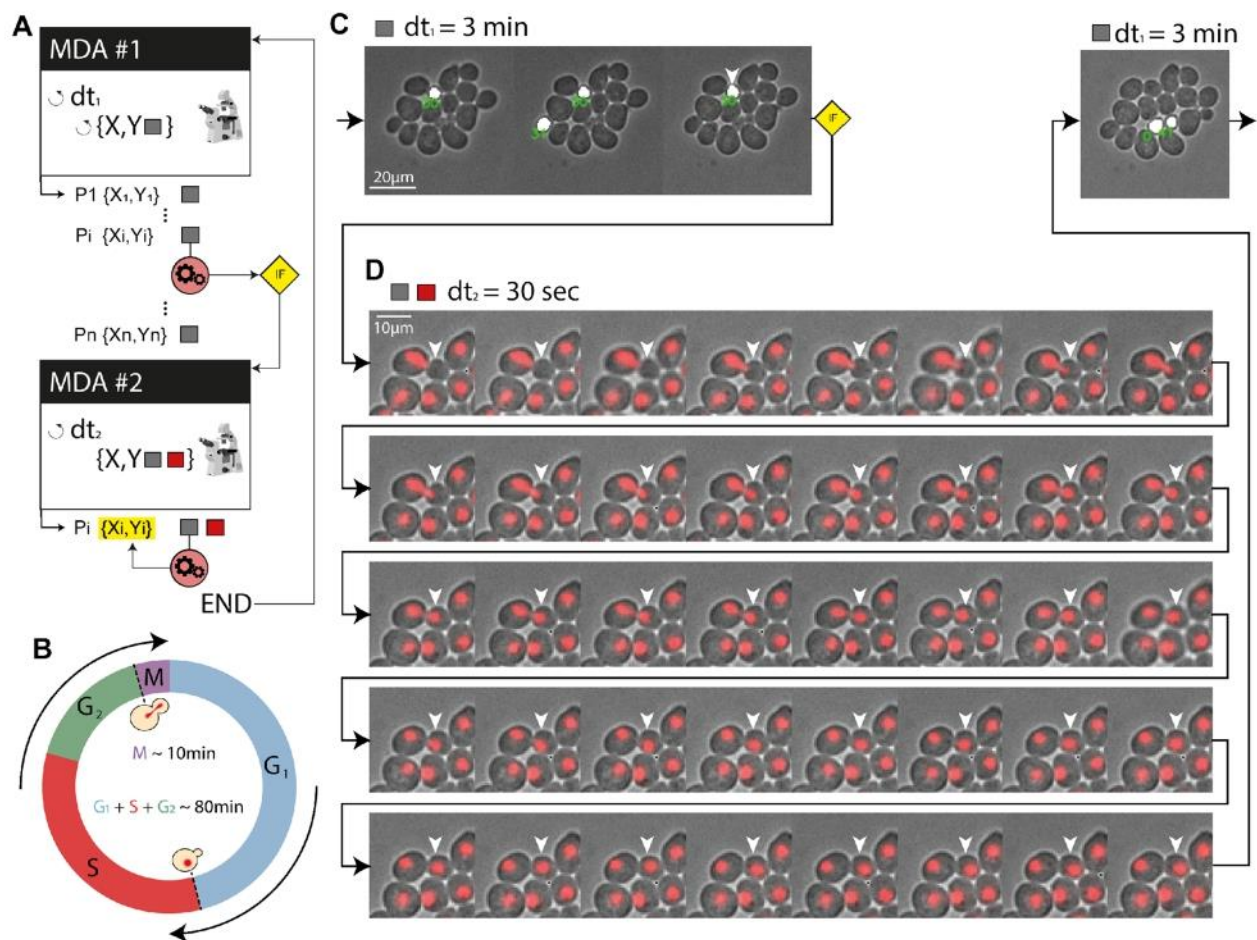


**Figure 6.** Bud detection and high-temporal-resolution imaging of mitosis. **(A)** Scenario used to detect and “zoom in” on a particular event (in this case, mitosis). Several positions are monitored and when a condition is fulfilled, image acquisition is performed on only this position at an adapted sampling framerate. **(B)** Cell cycle progression in yeast. The mitosis event to be captured represents a small-time fraction of the cell’s life cycle (~10%). **(C)** In practice, the acquisition of brightfield images of a population of budding yeast leads to a coarse timelapse with an acquisition framerate of 3 min to search for the next mitotic event. Cell segmentation is used to identify buds (size filtering), shown here as a white overlay. When a bud has reached a given size (and has been growing for at least three frames), we consider that a mitotic event is about to occur. **(D)** Then, the acquisition software “zooms in” on that cell by increasing the framerate to one frame every 30 s for 20 min and RFP imaging is added to image the nucleus (HTB2-mCherry reporter). As shown in panel **D**, this scenario allows the complete mitotic event and nuclear separation between the mother and daughter cells (around 10 min, as expected) to be captured at an appropriate framerate. Once this image acquisition sequence is complete, the program resumes its search at the lower framerate for another mitotic event.

proposed here and adding generic scenarios that are driven through the results of real-time image analysis. For example, the scenario developed in this work that acts on a microfluidic chip based on the number of cells could be directly reprogrammed by changing the trigger condition.

Image analysis remains the bottleneck of automation and will continue to require expertise in machine learning and coding. However, the pace at which deep learning is being adopted in laboratories and adapted into user-friendly software solutions and online tools<sup>25,26</sup> suggests that an increasing number of easy-to-use methods to create UNET-trained networks will be developed in the near future and could subsequently be incorporated into CyberSco.Py. While we modified several classic experiments to demonstrate the potential of event-based microscopy, rethinking automation software for microscopy and including complete management of triggers and event detection may provide other important benefits in quantitative cell biology.

To start with, we can use our conditional microscopy framework to better prepare experiments and obtain a level of quality control before starting an experiment. Indeed, we showed that the number of cells may be an important factor when exploring the dynamics of population growth after a metabolic shift. Other processes related to cell–cell communication, metabolic gradients and cell–cell contact inhibition are also likely to be dependent on cell density. To increase experimental reproducibility, it seems reasonable to add a condition (or a set of conditions) on cell density to start a timelapse experiment. Similarly, only starting experiments, even simple timelapse studies, when a steady state is reached or when a gene has been expressed at a given level could

improve experimental reproducibility. Only stimulating cells when the system is “ready” can also help avoiding phototoxicity and bleaching due to starting an experiment too early.

Timelapse experiments are usually long and prone to failures in both the microscopy system (e.g., loss of focus, improper control of temperature, drift in the stage) and the biological sample (e.g., contamination). However, in conventional timelapse microscopy, the user only realizes these issues at the end of the experiment, when it is too late. Our framework can be extended to regularly communicate the state of both the microscope and the experiment to the user. This could be in either a trigger mode, with the software sending a status report to the user through all sorts of classic communication channels (e.g., Slack, Teams, Email, SMS) when something goes wrong or the experiment reaches a given state, or—even better—the microscope could use the output of the image analysis to correct the problem automatically (e.g., by relaunching an autofocus step). Such simple automation workflows will certainly help to achieve high-quality data, reduce the time and cost of experiments, and improve experimental reproducibility.

Another important aspect is the huge amounts of data acquired in conventional, uninformed MDA. In many cases, this is due to the fact that image analysis is performed a posteriori, which requires as much data as possible to be acquired given the constraints of the imaging system and the biological sample. The ability to perform real-time analysis and conditional acquisition will make it possible to collect much sparser data, by focusing only on precisely what matters for a given study. This would speed up the analysis, facilitate data storage and sharing, and more generally improve the life cycle of imaging data.

We envision that advanced automation could be further used to perform online learning and automatically adjust the imaging parameters and stimulation of the biological system to obtain a model of the system under study. Such applications, which we are presently developing in the field of cancer research, may represent a game changer that increases the throughput of rare event detection and the quality of the resulting analysis by “zooming in” in time and space and/or sending drugs to perturb cells as soon as these rare events are detected among a large population of cells.

Our motivation to develop this proof-of-concept software with a simple user-friendly interface was to introduce conditional microscopy to a large audience. While this first step is relatively limited, the initial framework we propose here can be improved and developed further. Ideally, a global effort to develop application programming interfaces (APIs) for lab automation would facilitate the development of no-code workflows that are accessible to all researchers and integrate with commonly used collaborative online tools such as Slack and Teams. We believe that researchers could benefit from such advanced ways of conducting experiments, especially the ability to perform event-based automated imaging. CyberSco.Py is a first step to bring such concepts to the attention of biologists.

## Materials and methods

**Yeast strains and growth conditions.** All yeast strains used in this study are derived from the BY4741 background (EUROSCARF Y00000). The list of strains can be found in Supplementary Table 1. Yeast cells were picked from a colony in an agar plate, grown overnight in 2 mL YPD media, then the culture was diluted 1/100 in 5 mL of filtered synthetic complete media (SC; 6.7 g Yeast Nitrogen Base w/o amino acid [Difco 291940] and 0.8 g complete supplement mixture drop-out [Formedium DCS0019] to 1 L) supplemented with 2% glucose and cultured for 4–6 h at 30 °C with orbital shaking at 250 RPM (Innova 4230 incubator). The media used to perfuse the microfluidic chips during the experiments was SC supplemented with either 2% glucose or 1% sucrose. The microfluidic chips were made following a previously published protocol<sup>15</sup> (see Fig. S8). Liquid perfusion was performed using an Ismatec IPC (ISM932D) peristaltic pump at 50  $\mu$ L/min (or 120  $\mu$ L/min for the osmotic shock experiment). A homemade Arduino-based system was used to switch the state of an electrofluidic valve to change the media that perfuses the microfluidic chip. The microfluidic chip (Supplementary Fig. S2) allows yeast cells growing in a monolayer to be imaged and has been described in previous works<sup>27</sup>. Another microfluidic design<sup>28</sup> was used (in Fig. 4C) to constrain cell displacement in one direction.

**Microscopy imaging.** We used a fully automated Olympus IX81 inverted epifluorescence microscope equipped with a motorized stage (Prior Pro Scan III), Photometrix Evolve512 camera, and a pE-4000 CoolLed as a fluorescent light source. The objectives used in this study were either a 20 $\times$  UPlanSApo or 60 $\times$  PlanApo N. For the RFP channel, we used the 550 nm LED through a filter cube (EX) 545 nm/30; (EM) 620 nm/60 (U-N49005) with a 150 ms exposure time. For the GFP channel, we used the 460 nm LED through a filter cube (EX) 545 nm/30; (EM) 620 nm/60 (U-N49005) with a 150 ms exposure time. For the YFP channel, we used the 525 nm LED through a filter cube (EX) 514 nm/10; (EM) 545 nm/40 (49905-ET) with a 500 ms exposure time. Microscopy experiments were carried out in a thermostat chamber set to 30 °C.

**CyberSco.Py software.** CyberSco.Py is written in Python for the backend and HTML/CSS/ JS for the frontend, connected by a WebSocket channel. Communication to the different devices is made directly through serial communication and whenever necessary, the drivers provided by the vendors or a generic version from the  $\mu$ Manager community. CyberSco.Py is installed on computer software that must be equipped with a recent GPU to benefit from U-NET deep learning segmentation of cells. A server can interface several microscopes running CyberSco.Py and be extended with a user manager database and image database management program such as OMERO. The current open-source release of CyberSco.Py can be found on GitHub (<https://github.com/Lab513/CyberSco.Py>).

**Acquisition, segmentation and tracking.** Image acquisition is preceded by an autofocus algorithm that optimizes the quality of the segmentation, as well as the sharpness of the object under scrutiny. Cell segmenta-

tion is achieved via a machine-learning algorithm based on the U-NET architecture. Twenty images of cells at different positions and containing different numbers of cells were taken to produce the training set. This dataset was then augmented as it is classically done (see Supplementary Information). For the main model for yeast segmentation, the neural network was trained on five periods using a GPU NVIDIA GeForce GTX 1080; this training only took 5 min. Predictions with this model are obtained in around 0.2 s. Cell tracking is performed using both image correlation in real-time and using a simple proximity relationship between the predicted contours.

### Data availability

The datasets used and/or analysed during the current study are available from the corresponding author on reasonable request. The main datasets and code are available at the following address <https://github.com/Lab513/CyberSco.Py>.

Received: 18 March 2022; Accepted: 20 June 2022

Published online: 08 July 2022

### References

- Almada, P. *et al.* Automating multimodal microscopy with NanoJ-Fluidics. *Nat. Commun.* **10**, 1–9 (2019).
- Hossain, Z. *et al.* Interactive and scalable biology cloud experimentation for scientific inquiry and education. *Nat. Biotechnol.* **34**, 1293–1298 (2016).
- Pinkard, H., Stuurman, N. & Waller, L. Pycro-manager: Open-source software for integrated microscopy hardware control and image processing. *ArXiv200611330 Q-Bio* (2020).
- Pinkard, H., Stuurman, N., Corbin, K., Vale, R. & Krummel, M. F. Micro-Magellan: Open-source, sample-adaptive, acquisition software for optical microscopy. *Nat. Methods* **13**, 807–809 (2016).
- Conrad, C. *et al.* Micropilot: Automation of fluorescence microscopy-based imaging for systems biology. *Nat. Methods* **8**, 246–249 (2011).
- Edelstein, A., Amodaj, N., Hoover, K., Vale, R. & Stuurman, N. Computer control of microscopes using  $\mu$ Manager. *Curr. Protoc. Mol. Biol.* **92**, 14.20.1–14.20.17 (2010).
- Edelstein, A. D. *et al.* Advanced methods of microscope control using  $\mu$ Manager software. *J. Biol. Methods* **1**, e10 (2014).
- Kondaveeti, H. K., Kumaravelu, N. K., Vanambathina, S. D., Mathe, S. E. & Vappangi, S. A systematic literature review on prototyping with Arduino: Applications, challenges, advantages, and limitations. *Comput. Sci. Rev.* **40**, 100364 (2021).
- Jolles, J. W. Broad-scale applications of the Raspberry Pi: A review and guide for biologists. *Methods Ecol. Evol.* **12**, 1562–1579 (2021).
- Milias-Argeitis, A. *et al.* In silico feedback for in vivo regulation of a gene expression circuit. *Nat. Biotechnol.* **29**, 1114–1116 (2011).
- Milias-Argeitis, A., Rullan, M., Aoki, S. K., Buchmann, P. & Khammash, M. Automated optogenetic feedback control for precise and robust regulation of gene expression and cell growth. *Nat. Commun.* **7**, 12546 (2016).
- Rullan, M., Benzinger, D., Schmidt, G. W., Milias-Argeitis, A. & Khammash, M. An optogenetic platform for real-time, single-cell interrogation of stochastic transcriptional regulation. *Mol. Cell* **70**, 745–756.e6 (2018).
- Chait, R., Ruess, J., Bergmiller, T., Tkačik, G. & Guet, C. C. Shaping bacterial population behavior through computer-interfaced control of individual cells. *Nat. Commun.* **8**, 1535 (2017).
- Lugagne, J.-B. *et al.* Balancing a genetic toggle switch by real-time feedback control and periodic forcing. *Nat. Commun.* **8**, 1671 (2017).
- Uhlendorf, J. *et al.* Long-term model predictive control of gene expression at the population and single-cell levels. *Proc. Natl. Acad. Sci.* **109**, 14271–14276 (2012).
- Harrigan, P., Madhani, H. D. & El-Samad, H. Real-time genetic compensation defines the dynamic demands of feedback control. *Cell* **175**, 877–886.e10 (2018).
- Perkins, M. L., Benzinger, D., Arcak, M. & Khammash, M. Cell-in-the-loop pattern formation with optogenetically emulated cell-to-cell signaling. *Nat. Commun.* **11**, 1355 (2020).
- Toettcher, J. E., Gong, D., Lim, W. A. & Weiner, O. D. Light-based feedback for controlling intracellular signaling dynamics. *Nat. Methods* **8**, 837–839 (2011).
- Fox, Z. R. *et al.* MicroMator: Open and flexible software for reactive microscopy. *bioRxiv*. <https://doi.org/10.1101/2021.03.12.435206> (2021).
- Pedone, E. *et al.* Cheetah: A computational toolkit for cybergenetic control. *ACS Synth. Biol.* **10**, 979–989 (2021).
- Hersen, P., McClean, M. N., Mahadevan, L. & Ramanathan, S. Signal processing by the HOG MAP kinase pathway. *Proc. Natl. Acad. Sci.* **105**, 7165–7170 (2008).
- Muzzey, D., Gómez-Urbe, C. A., Mettetal, J. T. & van Oudenaarden, A. A systems-level analysis of perfect adaptation in yeast osmoregulation. *Cell* **138**, 160–171 (2009).
- Falk, T. *et al.* U-Net: Deep learning for cell counting, detection, and morphometry. *Nat. Methods* **16**, 67–70 (2019).
- Koschwanez, H., Foster, K. R. & Murray, A. W. Sucrose utilization in budding yeast as a model for the origin of undifferentiated multicellularity. *PLoS Biol.* **9**, e1001122 (2011).
- Ouyang, W., Mueller, F., Hjelmare, M., Lundberg, E. & Zimmer, C. ImJoy: An open-source computational platform for the deep learning era. *Nat. Methods* **16**, 1199–1200 (2019).
- Sullivan, D. P. & Lundberg, E. Seeing more: A future of augmented microscopy. *Cell* **173**, 546–548 (2018).
- Llamosi, A. *et al.* What population reveals about individual cell identity: Single-cell parameter estimation of models of gene expression in yeast. *PLoS Comput. Biol.* **12**, e1004706 (2016).
- Marinkovic, Z. S. *et al.* A microfluidic device for inferring metabolic landscapes in yeast monolayer colonies. *Elife* **8**, e47951 (2019).

### Acknowledgements

The authors would like to thank Pierre Louis Crescitz, Williams Brett and several colleagues and beta testers for their help and critical reading of this manuscript. This work was supported by the European Research Council grant SmartCells (724813) and received supports from grants ANR-11-LABX-0038 and ANR-10-IDEX-0001-02.

### Author contributions

Code implementation and automation troubleshooting were performed by L.C., M.L.B. designed, performed and analyzed all experiments. C.C., S.P. and D.M. participated in molecular biology and microfluidic efforts. J.-M.D.M., B.S. and P.H. conceived and designed the study. L.C., M.L.B., A.B., B.S. and P.H. wrote the manuscript.

### Competing interests

The authors declare no competing interests.

### Additional information

**Supplementary Information** The online version contains supplementary material available at <https://doi.org/10.1038/s41598-022-15207-5>.

**Correspondence** and requests for materials should be addressed to P.H.

**Reprints and permissions information** is available at [www.nature.com/reprints](http://www.nature.com/reprints).

**Publisher's note** Springer Nature remains neutral with regard to jurisdictional claims in published maps and institutional affiliations.



**Open Access** This article is licensed under a Creative Commons Attribution 4.0 International License, which permits use, sharing, adaptation, distribution and reproduction in any medium or format, as long as you give appropriate credit to the original author(s) and the source, provide a link to the Creative Commons licence, and indicate if changes were made. The images or other third party material in this article are included in the article's Creative Commons licence, unless indicated otherwise in a credit line to the material. If material is not included in the article's Creative Commons licence and your intended use is not permitted by statutory regulation or exceeds the permitted use, you will need to obtain permission directly from the copyright holder. To view a copy of this licence, visit <http://creativecommons.org/licenses/by/4.0/>.

© The Author(s) 2022





## Conclusions and perspectives

There is a growing interest in engineering microbial consortia<sup>7,8,66,81-86</sup>, where different types of cells cooperate to reach specific biological functions (bioproduction<sup>131,132,223-225</sup>, living materials<sup>226,227</sup> or live therapeutics<sup>110,228-230</sup>). It becomes thus essential to better grasp the physical limitations of such systems. Among them, chemical diffusion, consortia morphology and their interdependence matter greatly. The example of *Saccharomyces cerevisiae* sucrose utilisation is a simple system with such cooperative interaction, which produces diffusive public goods that shape the microbial growth in space. Using this system as a model for cooperator/cheater microbial consortia, we investigated its spatial properties by taking control over the cells' cooperative function.

Here, I designed a set of strains that can produce the sucrose invertase Suc2p upon light illumination. I carefully quantified how efficient those strains are at hydrolysing the sucrose and using the produced hexoses to grow in various illumination conditions. In contrast with another similar study based on the CRY2/CIB1 optogenetic system<sup>208</sup>, the EL222 system allows sufficient invertase production to recover the WT growth on sucrose. However, the known leakage of the pC120 promoter revealed to have a strong impact on sensitive systems like enzymatic hydrolysis, which combined with the uncontrolled sucrose hydrolysis in low pH environments resulted in background residual growth. Adding an mRNA degradation tag thanks to a hairpin sequence was critical to obtain a strain with reduced basal SUC2 activity and growth rate. I could thus study cooperation/competition spatial interplays with optogenetics. I explored the importance of long-range spatial metabolic interactions through the production of "public goods" locally. Metabolic interactions are occurring at a length scale which is set by multiple factors: the initial concentration of sucrose, the diffusion of sucrose and hexoses, the invertase production rate, and the density of cells that are setting the local invertase activity and hexose absorption. Given the diffusion coefficient of glucose in water ( $760 \mu\text{m}^2.\text{s}^{-1}$  at  $30^\circ\text{C}$ )<sup>231</sup> or in agar gel ( $573 \mu\text{m}^2.\text{s}^{-1}$  in 1.5% agarose at  $25^\circ\text{C}$ )<sup>232</sup>, we expected to observe a rapid effect of sucrose hydrolysis at short scale. But because yeast growth requires a certain minimal hexose concentration, it should be resumed only after some hexose accumulation. Indeed, under the microscope, when activating cells locally, I observed that once the invertase was produced, neighbouring cells started to grow with a delay (~2-4h). This suggests that competition/cooperation mechanisms also act at larger scales, at least when cells are grown in a rich environment. Our custom-built device called the *OptoCube* was used for larger scale observation, allowing to vary the spatial wavelength of an illumination pattern and revealing the impact of cooperation spatial organisation on the population growth. Sending parallel lines of light of various wavelengths led to modulate the fitness difference between the dark and illuminated surfaces of the agar gel. This effect can be identified as a spatial bandpass filter behaviour whose critical wavelengths are the trace of the typical

distance of metabolic interactions of the SUC2 yeast system: a low cut-off wavelength (~10mm) due to cheater-cooperator competition for hexoses and a high cut-off wavelength (~17mm) due to cooperator self-competition for sucrose. Importantly, these length scale values depend on experimental constraints (sucrose concentration, cooperation strength, initial cell density, light:dark ratio).

This work illustrates the power of optogenetic and light spatial patterning to decipher the metabolic interactions at play in spatially complex multicellular assemblies such as colonies, biofilms and engineered consortia. Indeed, it becomes possible to shape the chemical gradients that are set by cell absorption and metabolite diffusion. We anticipate that similar strategies using optogenetics to locally change the cellular metabolic capabilities can help understand microbial ecosystems' cooperation and competition mechanisms, and more generally how microbial interactions take place within spatially structured consortia. The use of light induction can also be applied to control complex synthetic microbial consortia. The tools, the methodology and the results of this study can guide synthetic biologists to appropriately dimension their Engineered Living Materials<sup>233-235</sup>, a crucial step to obtain precise functionalities and efficient external control. Such spatial constraints should also be considered when designing manipulation strategies to rectify imbalanced microbiomes (dysbiosis), which are linked with major problems in various fields such as methane emission by ruminant digestive fermentation<sup>123</sup>, human obesity and diabetes influenced by gut microbiome<sup>236,237</sup>, or unsustainable farm soil fertility with high need in nitrogen fertilization<sup>238-</sup>

<sup>240</sup>.

## Limitations

I will briefly give some of the limitations of this work, especially concerning the methods I used. This could help future work using similar technologies to better apprehend technical limitations they might also encounter.

### Optogenetics

Optogenetic control can suffer from various limitations. First, light spatial resolution suffers from scattering whenever the photon changes of propagation medium. Precise localized optogenetic activation can thus only be achieved on surfaces or small objects, whereas deeper tissue illumination would lose in precision or would require complex instruments (two-photons or light sheet microscope). In addition to scattering, light is absorbed by cells reducing its intensity along the tissue depth. This light penetration is for example a problem to apply optogenetics in existing bioproduction processes, which relies on ultra-dense cell suspension in large volumes. We can also mention that light intensity measurement is typically a problem, notably when comparing setups with different configurations. For example, focused light (DMD and microscope) will behave differently than unfocused light (OptoBox, or any LED use without optic parts).

Our particular case of optogenetic control of protein production with photosensitive transcription factors adds more limitations. The fact that we control a slow process such as transcription prevents harnessing the high temporal resolution of light. Only direct control of protein activity or localisation can allow fast dynamics and high responsiveness. Also, similarly to chemical induction systems, obtaining strong induced expression levels is not trivial. Low induction strength systems can be amplified by building a more complex gene regulation network<sup>241</sup>, although it can reduce its responsiveness. Optogenetics is however probably the most convenient method to spatially control biological systems.

### Microfluidic for microbiology

The use of microfluidic presents many advantages but using it to study collective microbial phenomena requires to consider certain constraints. First, most microfluidic devices are based on a continuous culture design, where the nutrients are constantly renewed. This type of culture presents the advantage to access pseudo steady state growth allowing to easily derive analytical solutions for the system, but this can be quite far from natural configurations. In contrast, studying non-steady state configuration might be more relevant to reproduce microbial niches, as nutrient depletion and secondary metabolite accumulation are common in microbial communities. Secondly, cell density dependent phenomena are highly important in these systems, and microscopic observation tends to limit the number of cells observed (~10 000 to 100 000 maximum). Millifluidics (or large microfluidic chambers) should thus be

preferably used to study large multicellular microbial assemblies. The corresponding acquiring can either be performed using a low magnification objective (typically 20x) for rapid sampling, or by tiling multiple fields of view with a high magnification to conserve single-cell resolution.

## Modelling

The model and the corresponding simulations presented in this manuscript allow to recover most of the observed microbial behaviours. It is however far from perfect. In particular, no transient phenomena are accounted for, such as metabolism reorganisation typically happening during the lag phase or diauxic shift. For example, the Monod equation is obtained by measuring the yeast growth rate at steady state with constant hexose concentrations (using a chemostat). In reality, yeast cells must produce different types of hexose transporters to optimize the hexose import for the current hexose concentration. The glucose consumption equation suffers from similar limitations, as it models the hexose input based on only two of the six possible hexose transporters.

## Perspectives

### Modelling

Modelling cell metabolism is quite challenging. Building on genomic and metabolomic experimental data, various modelling methods have been investigated to tackle the problem<sup>242</sup>, forming a consequent corpus which can be considered as an entire scientific field. Although quite complex, the goal of these models is to capture most of the cell metabolism diversity in one unifying model. In contrast, the model developed in the present work is a more heuristic approach, with the objective to obtain the minimal model to describe the sucrose metabolism in yeast. Importantly, the model connects the yeast growth to nutrient diffusion, to investigate sessile scenarios. Including diffusion constitute a large computational load on the simulation with the current numerical resolution methods and limit the number of solutes that can be modelled. Recent works<sup>243,244</sup> on using machine learning approaches to tackle the numerical resolution of the partial differential equations could drastically improve our capacity to include diffusion in biological models. Combining complex cell metabolism models with diffusion would then be within our computational reach. Such models could be used to investigate *in silico* various 3D configurations of multispecies communities exchanging metabolites that would be highly difficult to obtain and characterise experimentally.

### Control theory and Cybergenetics

In the context of the HERSEN team, I explored the potential of applying control theory to biological systems. Control Theory applies to any continuously operating dynamical system and aims to control at least one of its parameters in time. This framework is useful as it aims to mathematically formalise control strategies to determine their properties and behaviours. One of the main objects used and studied in control theory is feedback loop, as introducing such interaction between the controller and the parameter to control presents many advantages. Indeed, compared to an open loop (no feedback), it allows to improve reference tracking, to adapt for unexpected disturbance and to stabilize unstable configuration<sup>245</sup>, without requiring a precise model of the system. Recent efforts<sup>246-257</sup> have been made in adapting control theory principles to biological systems and their inherent properties, toward a better formalisation of such complex biological regulatory networks. This new scientific “discipline”, called Cybergenetic, is now gaining consideration in various types of biology branches, from embryology, microbiology, bioproduction, medicine or system biology.

Applying closed-loop feedback control strategies to the invertase production might seem to be an interesting addition to this work. It could for example allow to control the hexose concentrations in a bioreactor without any media exchange or to shape hexose gradients in space. This is however probably quite challenging for multiple reasons, the main

one being that the invertase stability prevents to reversibly control the rate of sucrose hydrolysis. In addition to this inertia, there is a consequent lag time between the light input and the actuation on the rate of sucrose hydrolysis due to the protein synthesis, maturation, and secretion. The combination of these two problems likely makes the system's dynamics difficult to control properly.

### Multi-species consortia

As *S. cerevisiae*, there are other microorganisms which cannot consume sucrose directly but can thrive on hexoses. The optogenetic yeast strain I developed could thus be included in multispecies consortia and be used as a "hexose accessibility" controller, in turn controlling the other species growth rate. Because of the ubiquity of the use of hexose as carbon source, our yeast strain could be used to control various types of organisms without requiring any genetic engineering. The use of yeast sucrose hydrolysis to control bacterial growth is typically encountered in Kombucha consortia<sup>227</sup>, although its function is unclear.

More generally, engineered microbial consortia are currently a topic of interest both in academia and industries. While the potential benefits to apply division of labour principles to microbial bioproduction are promising, engineering cooperative systems and tuning them to optimize the production of a chemical can be difficult. Importantly, bioproduction industries typically optimize a biomass/bioproduct trade-off: producing a large amount of a molecule is faster using a large number of cells, but this requires an initial biomass production phase which reduces the amount of nutrient available for subsequent chemical production. In this context, using a cooperative multi-species community instead of a clonal one would tend to increase the biomass production as more cells are required to perform the same chemical synthesis task. To compensate for this tendency, the bioproduct production rate of the consortium should thus be significantly higher than that of a single organism.

### Engineered Living Materials (ELM)

Other works on engineered microbial consortium have been directed toward the development of living biomaterials. Such Engineered Living Materials consist in a material hosting living organisms, which would perform novel functionalities such as stimuli responsivity. Using a top-down approach, researchers modified a Kombucha biofilm consortia to develop functional ELMs<sup>227</sup>. Kombucha is a fermented human beverage which is obtained thanks to a microbial consortium composed of at least one species of cellulose producing bacteria and one of yeast. When proliferating, this microbial community form a floating biofilm composed of the cellulose matrix embedding the living cells (**Figure 44A**). The interaction between the species is believed to be beneficial: bacteria share their biofilm matrix while yeasts release glucose from sucrose hydrolysis (**Figure 44B**). As in the previous example,

the authors first identified conditions in which the bacterium *K. rhaeticus* and the yeast *S. cerevisiae* can be efficiently co-cultured. Importantly, they choose to use *S. cerevisiae* as the engineering target because it has been extensively studied and that synthetic biology tools are already developed and optimized for this species. In addition, because of their eucaryotic nature, yeasts have a high capacity for secretion of recombinant proteins.

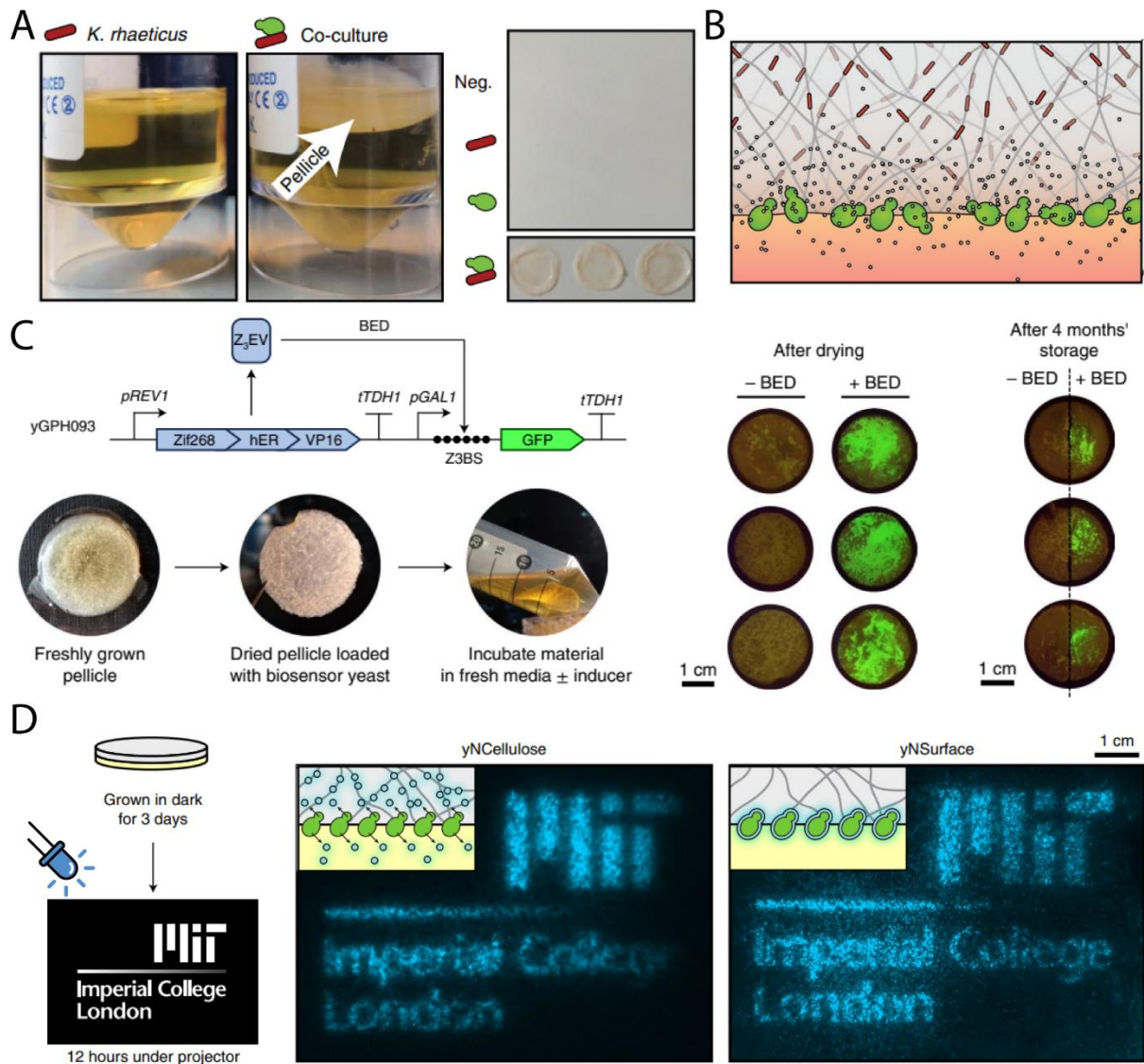


**Figure 44 – Kombucha-inspired living materials.** (A) Images of monocultures and co-cultures of *K. rhaeticus* and *S. cerevisiae* grown for 3 days. The harvested pellicles from three independent experiments are shown on the right panel. (B) Schematic view of the biofilm, yeast cells are depicted in green and bacteria are depicted in red. (C) Biosensor for  $\beta$ -oestradiol (BED). Scheme of the genetic circuits, picture of the drying and rehydration process and the corresponding sensing performances. (D) Light-sensitive yeast producing fluorescent proteins in the matrix or kept at their surfaces after a light pattern is applied. Figure extracted from<sup>227</sup>.



The resulting engineered biofilms were designed to perform various functions, which could be recovered after being dried, stored for prolonged periods of time, and rehydrated. Such practical aspects of ELMs might be crucial for most real-life applications. Using this engineerable microbial co-culture platform, they could produce biofilms functionalized with enzymes adsorbed on the cellulose fibres such as  $\beta$ -lactamase for antibiotic resistance, functionalized with a yeast biosensor strain responsive to the  $\beta$ -oestradiol hormone (BED) (Figure 44C), or functionalized with a light-sensitive yeast strain (Figure 44D).

Another example of engineered living material is based on filamentous fungi mycelial network. Building on the physical properties of such interconnected microscopic web, various structural composite materials have been developed as a sustainable alternative to styrofoam or wood composite (particle board). Typically, lignocellulosic feedstock is inoculated and colonised by *Ganoderma sp.* which produces a fast growing and strong mycelium. The resulting composite material is finally heat-treated to dry and kill the mycelium, to prevent unpredictable structural property changes due to biological activity. Instead, keeping the biomaterial alive has been investigated to obtain a functional and responsive biocomposite<sup>226</sup> (Figure 45A). One of the direct advantages of keeping the fungal cells alive is that they can regrow mycelium if the air humidity is relatively high. This allows to join multiple biocomposite bricks to build large structures such as arches (Figure 45B) or to heal a broken biocomposite piece and to recover its initial strength (Figure 45B). Importantly, such regrowth ability is observed for at least one year after inoculation, without maintenance intervention.

In addition to harness the potential of living mycelium, the authors investigate the microbiota of their biocomposites. Among the assessed bacterial communities, one  $\gamma$ -proteobacteria taxa belonging to the *Pantoea* genus, exhibited robust and reproducible blooms during the biomaterial growth. In addition, their bacterial domination remained stable for multiple generations and across different spatial locations of the biomaterial. Building on the natural occurrence and stability of this taxa in their biocomposite, the authors isolated, characterised and engineered a *Pantoea* chassis denominated *P. agglomerans*. They could thus inoculate an engineered bacterial strain in addition to the *Ganoderma sp.* to obtain a living material embedding synthetic biology genetic circuits. This is exemplified by a sender/receiver design, where one strain is constitutively producing AHL signalling molecules while the other strain can sense it and produce a fluorescent protein in response. Each strain is then inoculated in separate biomaterial blocks, so that the 'receiver block' respond only when in contact with a 'sender block' through AHL diffusion (Figure 45C). Such proof of concept is quite promising as an engineering platform for the future development of sustainable 'smart' materials, possibly qualified as both low and high-tech.

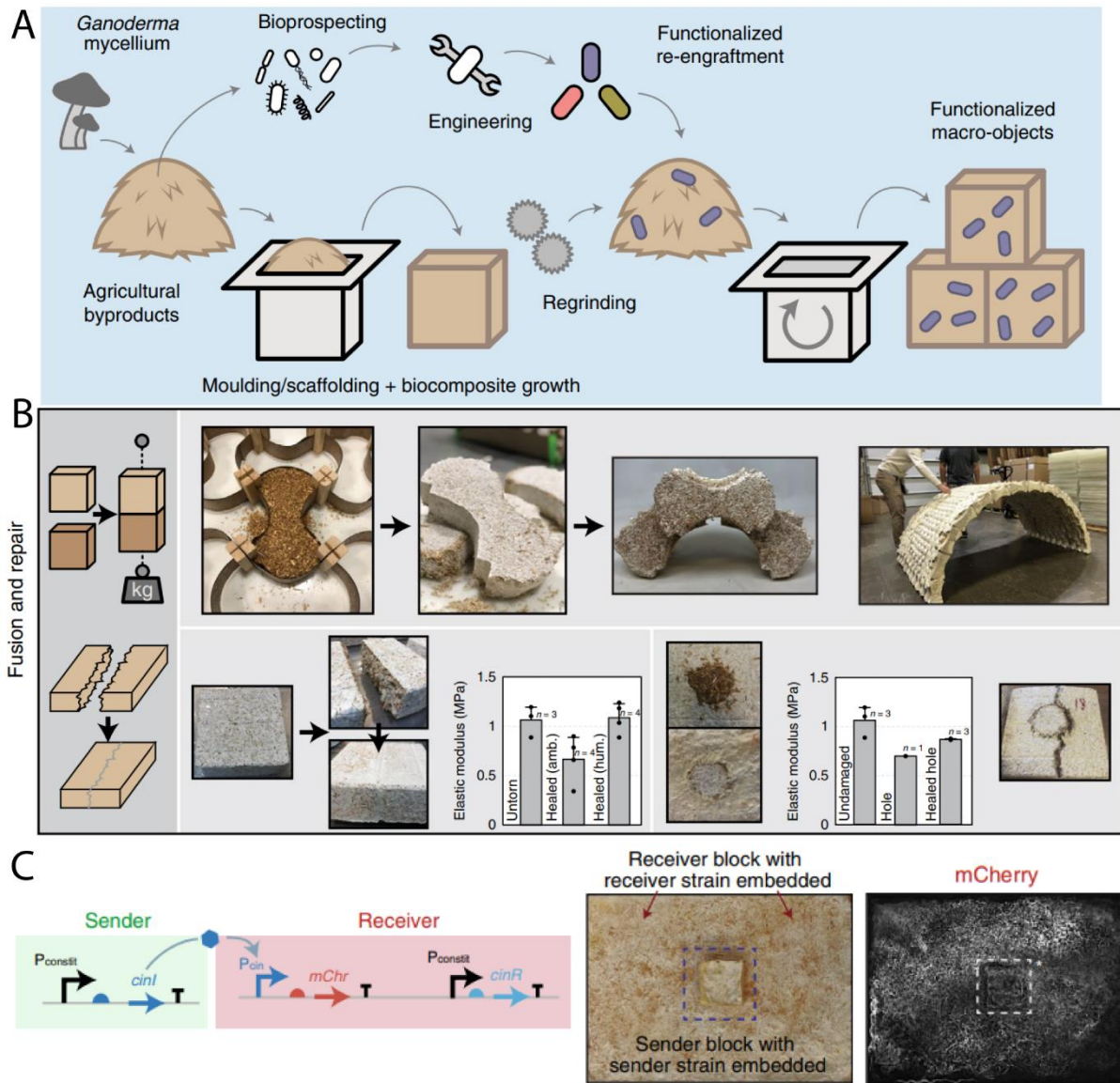


**Figure 45 – Engineered living fungal– bacterial biocomposite.** (A) A schematic outlining the design and functionalization of the fungal–bacterial biocomposites of the study. (B) The fungal mycelium of *Ganoderma sp.* is mixed with raw feedstock and placed in flat-pack slot-together moulds made from wax-coated cardboard to produce lightweight yet strong biocomposite blocks with curved geometries that can be assembled into larger structures by self-fusion such as arches. Broken blocks will self-repair over time when fragments are placed in physical contact. Healed material (grown in a controlled humidity of >60%) has similar physical characteristics to the original material. Similarly, backfilling of a punctured hole with fresh biomaterial enables robust wound repair with strong mechanical resistance to further fractures. (C) A *P. agglomerans* ‘sender’ strain is embedded in a sender block and produces a signalling molecule, AHL. When the sender block is placed in contact with a block containing a ‘receiver’ strain and rehydrated, the receiver block produces mCherry in response to the AHL signal. Figure extracted from<sup>226</sup>

But such engineered consortia can often be unstable, typically with one specie taking over the rest of the population. There is thus a need to control the consortia composition to ensure its proper activity. In addition, to obtain a functional and efficient synthetic division of labour, quantitative, robust and, possibly dynamic, control of the species interactions will be required.

One of the common constraints any Engineered Living Material will be subjected to is spatial heterogeneity. Indeed, depending on the ELM shape and size, embedded cells will experience various types and strengths of spatial variation in physico-chemical parameters. Typically, cells at the surface of an ELM will experience a different nutrient accessibility than the one embedded deep inside the material. In addition, rational shaping of spatial structures might be explored to obtain complex functions, for example patterning different species members of a consortium at different locations in the ELM. To properly design and control such materials, it is thus crucial to investigate the role of their geometry and diffusive capacity to obtain the targeted function. In particular, the length scale of microbial interactions such as competition and cooperation encountered in the system must be assessed. My work on characterising the cooperation/competition length scale in yeast and the tools I developed can help researchers to investigate the spatial properties of their systems. The use of optogenetics for spatial control of ELM might be a good strategy for their characterization and/or their functioning.





# Résumé de thèse en français

## Titre : Contrôle spatio-temporel de la coopération chez des communautés de levures

Cette thèse aborde le monde des communautés microbiennes avec une approche biophysique, se focalisant sur la structuration spatiale de tels systèmes multicellulaires. Les communautés microbiennes naturelles sont souvent structurées spatialement, avec différentes espèces qui interagissent et se développent de manière hétérogène. Même dans le cas des colonies clonales, le microenvironnement individuel des cellules est affecté par la consommation des nutriments, l'excrétion de molécules inhibitrices ou les communications chimiques, menant à la formation de gradients et à une différenciation phénotypique entre les cellules. Dans les domaines de l'écologie et de l'évolution microbienne, l'organisation spatiale joue un rôle déterminant dans le destin d'une population.

*L'objectif de cette thèse est de mieux comprendre le rôle de l'organisation spatiale dans les interactions des communautés microbiennes.*

Ce travail de recherche à été mené sur un organisme modèle couramment utilisé, la levure de boulanger *Saccharomyces cerevisiae*. Le système étudié est la coopération des communautés de levures pour la digestion du sucrose réalisé par une enzyme, l'invertase Suc2p. Cette protéine est sécrétée dans l'espace périplasmique, entre la membrane plasmique et le mur cellulaire, où elle sera retenue et hydrolysera les molécules de sucrose en glucose et fructose. Ces hexoses peuvent ensuite être internalisés dans le cytoplasme des levures grâce à des transporteurs transmembranaires, pour finalement alimenter le métabolisme de la cellule en source de carbone. Cependant, puisque la réaction d'hydrolyse se produit dans l'espace périplasmique, une partie des hexoses va diffuser au travers du mur cellulaire et échapper à la cellule. Les sucres ainsi relargués dans le milieu extracellulaire sont qualifiés de biens communs car ils sont accessibles à tous et non pas uniquement à l'individu qui a réalisé l'effort pour les produire, l'effort étant ici la production d'invertase. Dans les systèmes de biens communs, il est possible de tricher. Dans le cas du métabolisme du sucrose, des mutants tricheurs peuvent apparaître : ce sont des cellules qui ne produisent pas l'invertase mais qui consomment les hexoses produits par d'autres cellules, elles coopératrices car produisant l'invertase.

Pour étudier ce système de coopérateurs/tricheurs et ses dépendances spatiales, une stratégie de biologie synthétique et de contrôle spatial a été employée. À l'aide des derniers outils d'ingénierie génétique, des souches de levures *Saccharomyces cerevisiae* ont été construites pour contrôler optogénétiquement la production d'invertase SUC2. Le système optogénétique utilisé ici, EL222, permet d'induire l'expression du gène SUC2 par radiation lumineuse bleue (~460nm). L'utilisation de la lumière a été choisie car elle permet d'obtenir une excellente résolution spatiale de contrôle. Plusieurs itérations de constructions ont été nécessaires pour

obtenir une souche optimisée pour le contrôle de la croissance cellulaire des levures en sucrose. Il a fallu notamment résoudre un problème de fuite transcriptionnelle du promoteur optogénétique pC120, qui même en absence de lumière exprime le gène sous son contrôle. Un outil d'illumination pour plaque à puits décrit dans la littérature, le LPA, a été construit et utilisé pour caractériser le comportement de ces souches. La caractérisation de ces souches permet notamment de montrer que l'ajout d'une protéine de fusion sur Suc2p perturbe sa production, alors que l'utilisation d'une séquence séparatrice P2A précédant le reporteur fluorescent permet de meilleurs niveaux d'expression. La souche yPH\_536 possède le plus grand intervalle d'induction et sera donc utilisée pour induire la production locale de biens communs avec de la lumière bleue, donnant la possibilité de structurer dans l'espace une communauté de coopérateurs/tricheurs dans l'espace.

Pour étudier l'importance de l'espace dans cette communauté de coopérateurs/tricheurs pour la métabolisation du sucrose, une première exploration a été menée à l'échelle microscopique à l'aide des outils novateurs de la microfluidique. La puce microfluidique utilisée ici est composée de fines chambres de  $3.7 \times 400 \times 400 \mu\text{m}$  perfusées de part et d'autre par deux larges canaux où circule un flux de milieu de culture liquide. Les cellules de levures se retrouvent coincées dans la chambre, formant une mono-couche de cellule lors de la croissance de la population qui permet d'obtenir des informations cellule-unique. Pour quantifier la croissance cellulaire locale dans la chambre, une analyse d'image a été développée sur la base d'algorithmes de Particule Image Velocimetry et de la divergence du champ des vecteurs-vitesse ainsi obtenu. Pour contrôler l'illumination spatialement sous l'objectif du microscope, un DMD (Digital Micromirror Device) connecté à une source lumineuse a été utilisé pour projeter des patterns de lumière dans la chambre microfluidique. Lorsqu'une chambre occupée par quelques centaines de cellules de la souche yPH\_536 est illuminée avec de la lumière bleue localisée uniquement sur un des bords de la chambre, on observe que la croissance s'initie d'abord dans la région illuminée, et après quelques heures, se propage dans le reste de la chambre. Cela met bien en évidence que lorsque les cellules illuminées, les coopératrices, ont accumulé assez d'invertase dans leur espace periplasmique, il en résulte un relargage d'hexoses qui diffusent au-delà de la région coopératrice. Les cellules non-illuminées, les tricheuses, peuvent donc profiter de l'effort des coopératrices à au moins quelques dizaines de micromètre de distance.

Cette étude microscopique est une première tentative pour caractériser spatialement la communauté de coopérateur/tricheur, et permet de mesurer des variables cellulaires avec une bonne résolution spatiale, potentiellement jusqu'au niveau de la cellule unique. Cependant, notre capacité à contrôler spatialement le consortium de levure est fortement réduite due aux mouvements des cellules provoqués par leur croissance dans la chambre. Les cellules qui se trouvaient initialement dans la région illuminée vont ensuite être poussées et vont coloniser le reste de la chambre. Et puisque l'invertase est une protéine très stable, ces cellules vont

coopérer pour l'hydrolyse du sucrose hors de la zone illuminée ce qui n'est pas souhaité. De plus, la diffusion des hexoses dans ces expériences semble pouvoir atteindre des distances plus importantes que quelques centaines de micromètres, excédant les dimensions du dispositif microfluidique utilisé. Ces raisons ont motivé un changement d'échelle : étudier et quantifier les composantes spatiales des interactions microbiennes à l'échelle macroscopique, visible à l'œil nu.

Pour réaliser ce changement d'échelle, un appareil de mesure personnalisé a été mis au point. Nommé *l'OptoCube*, il est constitué d'un incubateur thermorégulé contenant un DMD pour la projection de patterns lumineux et un scanner à plat standard pour imager et quantifier la croissance microbienne sur gel d'agar en boîtes de pétri. L'ensemble est contrôlé par un microcontrôleur Arduino et un ordinateur. Cet outil est facile et peu cher à construire, et la documentation pour sa mise en place et son utilisation est libre d'accès et d'usage. Les boîtes de gel nutritif utilisé pour ces expériences ont été inoculées de manière à mieux contrôler l'organisation spatiale des coopérateurs et des tricheurs. Pour se faire, les levures sont mises en suspension dans une solution d'agarose non-gélifiée, qui est ensuite versée sur le gel nutritif, formant une fine pellicule de gel contenant les cellules et les maintenant dispersées. Celles-ci vont alors proliférer et croître en forme de micro-colonie sphérique, sans déplacement significatif des cellules dans l'espace. Une caractérisation des performances de ce dispositif est aussi détaillée.

Une première expérience de dose-réponse pour l'induction lumineuse de la souche yPH\_536, avec illumination homogène, montre qu'il est possible de contrôler quantitativement la vitesse de croissance des levures en sucrose. Elle montre aussi que ce changement de vitesse de croissance s'accompagne de changement de rendement métabolique. Les cellules fortement activées vont produire tellement d'invertase que les hexoses s'accumuleront rapidement, menant à un régime métabolique fermentatif qui a un faible rendement. Pour les cellules peu activées, les hexoses sont consommés aussi vite qu'ils sont produits, ce qui mène à un régime métabolique de respiration à haut rendement.

Ces observations et interprétations ont été confirmées par un modèle mathématique développé dans ce manuscrit. Ce modèle est composé d'un jeu d'équations différentielles partielles et utilise majoritairement des paramètres extraits de la littérature, excepté deux paramètres qui ont été ajustés sur des données expérimentales. Ce modèle est résolu numériquement pour simuler la croissance des levures en sucrose en prenant compte de la diffusion des sucres dans l'espace. Les différents résultats de simulation obtenus sont en relativement bonne adéquation avec les données expérimentales.

L'OptoCube a ensuite été utilisé pour imposer des organisations spatiales de coopérateur/tricheur définies. D'abord, une région de coopérateur de dimension variable, entourée de tricheur, est générée. Cette expérience permet de montrer qu'il existe une



compétition entre coopérateurs pour l'accès au sucrose. En effet, les régions de coopérateur qui sont grandes mènent à une déplétion de sucrose en leurs centres, résultant en une croissance majoritairement localisée à la frontière avec la région des tricheurs, qui elle contient encore beaucoup de sucrose.

Une autre expérience est réalisée cette fois en gardant le rapport de surface des régions coopérateur:tricheur constant à 25%:75%. Le motif projeté est constitué de bandes de lumière bleue répétées parallèlement et espacées de zones non-illuminées. Le paramètre spatial varié dans cette expérience est la longueur d'onde du pattern, qui correspond à la largeur d'une bande de coopérateur et d'une bande de tricheurs. En analysant la différence de croissance entre les coopérateurs et les tricheurs, considéré comme le bénéfice des coopérateurs, on peut utiliser la terminologie des filtres spatiaux. Ici, la croissance des levures sur sucrose se comporte comme un filtre passe bande avec des longueurs d'onde de coupure à 1cm et 1,7cm. Les motifs de coopérateurs/tricheurs de longueur d'onde inférieurs à 1cm sont atténués car les tricheurs rivalisent pour l'accès aux hexoses. Les motifs de longueur d'onde supérieurs à 1,7cm sont atténués due à la compétition des coopérateurs pour le sucrose. Ces valeurs de longueur d'onde de coupure sont dépendantes de nombreux paramètres expérimentaux, comme la concentration initiale de sucrose dont la dépendance est explorée par simulation numérique.

Le dernier chapitre est consacré à un logiciel libre qui a été développé en parallèle du projet principale de thèse. Publié sous le nom de Cybersco.py, ce logiciel de control de microscope se veut rendre l'utilisation de microscope moins « rigide », vers une microscopie intelligente qui s'adapte en temps réel à l'expérience en cours, déclenchant des actions conditionnées par de l'analyse d'image. Une version de l'article publié correspondant est incluse.

Les résultats présentés dans ce travail montrent l'importance de la structuration spatiotemporelle dans les systèmes coopératifs, due aux gradients de molécules diffusibles et à l'hétérogénéité phénotypique dans la population de cellules. Cela représente un pas vers une meilleure caractérisation des échelles spatiales des interactions microbiennes qui peut servir à approfondir notre compréhension des microbiomes naturels et à aider le design de microbiomes synthétiques. Le manuscrit se conclue par une brève exploration des perspectives et potentielles applications pour le futur des biotechnologies de « *matériaux vivants* ».





# References

1. Liu, J. *et al.* Metabolic co-dependence gives rise to collective oscillations within biofilms. *Nature* **523**, 550–554 (2015).
2. Rosenthal, A. Z. *et al.* Metabolic interactions between dynamic bacterial subpopulations. *eLife* **7**, e33099 (2018).
3. Hol, F. J. H., Galajda, P., Woolthuis, R. G., Dekker, C. & Keymer, J. E. The idiosyncrasy of spatial structure in bacterial competition. *BMC Res. Notes* **8**, 245 (2015).
4. Nadell, C. D., Drescher, K. & Foster, K. R. Spatial structure, cooperation and competition in biofilms. *Nat. Rev. Microbiol.* **14**, 589–600 (2016).
5. Cutler, N. A., Chaput, D. L., Oliver, A. E. & Viles, H. A. The spatial organization and microbial community structure of an epilithic biofilm. *FEMS Microbiol. Ecol.* **91**, fiu027 (2015).
6. Wang, C. *et al.* Microbial Platform for Terpenoid Production: *Escherichia coli* and Yeast. *Front. Microbiol.* **9**, (2018).
7. Roell, G. W. *et al.* Engineering microbial consortia by division of labor. *Microb. Cell Factories* **18**, 35 (2019).
8. Lindemann, S. R. *et al.* Engineering microbial consortia for controllable outputs. *ISME J.* **10**, 2077–2084 (2016).
9. Kylilis, N., Tuza, Z. A., Stan, G.-B. & Polizzi, K. M. Tools for engineering coordinated system behaviour in synthetic microbial consortia. *Nat. Commun.* **9**, 2677 (2018).
10. Okamura, K. Interdisciplinarity revisited: evidence for research impact and dynamism. *Palgrave Commun.* **5**, 1–9 (2019).
11. Weinbauer, M. G. Ecology of prokaryotic viruses. *FEMS Microbiol. Rev.* **28**, 127–181 (2004).
12. Moniruzzaman, M., Martinez-Gutierrez, C. A., Weinheimer, A. R. & Aylward, F. O. Dynamic genome evolution and complex virocell metabolism of globally-distributed giant viruses. *Nat. Commun.* **11**, 1710 (2020).
13. Ghuneim, L.-A. J., Jones, D. L., Golyshin, P. N. & Golyshina, O. V. Nano-Sized and Filterable Bacteria and Archaea: Biodiversity and Function. *Front. Microbiol.* **9**, (2018).
14. Ferguson, B. A., Dreisbach, T. A., Parks, C. G., Filip, G. M. & Schmitt, C. L. Coarse-scale population structure of pathogenic *Armillaria* species in a mixed-conifer forest in the Blue Mountains of northeast Oregon. *Can. J. For. Res.* **33** 612–623 (2003) doi:10.1139/x03-065.
15. Fujimura, R. *et al.* Analysis of Early Bacterial Communities on Volcanic Deposits on the Island of Miyake (Miyake-jima), Japan: a 6-year Study at a Fixed Site. *Microbes Environ.* **27**, 19–29 (2012).
16. Wang, J. L., Dragone, N. B., Avard, G. & Hynek, B. M. Microbial Survival in an Extreme Martian Analog Ecosystem: Poás Volcano, Costa Rica. *Front. Astron. Space Sci.* **9**, (2022).
17. Morono, Y. *et al.* Aerobic microbial life persists in oxic marine sediment as old as 101.5 million years. *Nat. Commun.* **11**, 3626 (2020).

18. Joung, Y. S., Ge, Z. & Buie, C. R. Bioaerosol generation by raindrops on soil. *Nat. Commun.* **8**, 14668 (2017).
19. Amato, P. *et al.* Active microorganisms thrive among extremely diverse communities in cloud water. *PLoS ONE* **12**, e0182869 (2017).
20. Agua, P. *Flickr - PARAMECIUM CAUDATUM, ENTRE LAS SOMBRAS DEL AGUA, SIERRA DE LA CULEBRA, MAHÍDE.* (2018).
21. User:NEON. *Wikimedia Commons - Chlorella vulgaris Beijerinck NIES-2170 / Olympus IX71+DP72.* (2014).
22. Näther, D. J., Rachel, R., Wanner, G. & Wirth, R. Flagella of *Pyrococcus furiosus*: Multifunctional Organelles, Made for Swimming, Adhesion to Various Surfaces, and Cell-Cell Contacts. *J. Bacteriol.* **188**, 6915–6923 (2006).
23. Dell'Arciprete, D. *et al.* A growing bacterial colony in two dimensions as an active nematic. *Nat. Commun.* **9**, 4190 (2018).
24. cyanobacteria, blue-green algae. <http://www.dr-ralf-wagner.de/Blaualgen-englisch.html>.
25. Shunmugam, A. P., Subramanian, G. & Fernandez, J. G. Measurements of the swimming speeds of motile microorganisms using object tracking and their correlation with water pollution and rheology levels. *Sci. Rep.* **11**, 11821 (2021).
26. Herzog, B. & Wirth, R. Swimming Behavior of Selected Species of Archaea. *Appl. Environ. Microbiol.* **78**, 1670–1674 (2012).
27. Dhakshinamoorthy, R. & Singh, S. P. Evolution of Reproductive Division of Labor – Lessons Learned From the Social Amoeba *Dictyostelium discoideum* During Its Multicellular Development. *Front. Cell Dev. Biol.* **9**, (2021).
28. Splivallo, R., Ottonello, S., Mello, A. & Karlovsky, P. Truffle volatiles: From chemical ecology to aroma biosynthesis. *New Phytol.* **189**, 688–99 (2011).
29. Mazzetto, F. *et al.* Olfactory attraction of *Drosophila suzukii* by symbiotic acetic acid bacteria. *J. Pest Sci.* **89**, (2016).
30. Schaeffer, R. N., Rering, C. C., Maalouf, I., Beck, J. J. & Vannette, R. L. Microbial metabolites elicit distinct olfactory and gustatory preferences in bumblebees. *Biol. Lett.* **15**, 20190132 (2019).
31. Atis, S., Weinstein, B. T., Murray, A. W. & Nelson, D. R. Microbial Range Expansions on Liquid Substrates. *Phys. Rev. X* **9**, 021058 (2019).
32. Benzi, R., Nelson, D. R., Shankar, S., Toschi, F. & Zhu, X. Spatial population genetics with fluid flow. *Rep. Prog. Phys.* **85**, 096601 (2022).
33. Kamath, R. S. & Bungay, H. R. Y. 1988. Growth of Yeast Colonies on Solid Media. *Microbiology* **134**, 3061–3069.
34. Fujikawa, H. & Morozumi, S. Modeling Surface Growth of *Escherichia coli* on Agar Plates. *Appl. Environ. Microbiol.* **71**, 7920–7926 (2005).

35. Hallatschek, O., Hersen, P., Ramanathan, S. & Nelson, D. R. Genetic drift at expanding frontiers promotes gene segregation. *Proc. Natl. Acad. Sci.* **104**, 19926–19930 (2007).
36. Müller, M. J. I., Neugeboren, B. I., Nelson, D. R. & Murray, A. W. Genetic drift opposes mutualism during spatial population expansion. *Proc. Natl. Acad. Sci.* **111**, 1037–1042 (2014).
37. Tronolone, H. *et al.* Diffusion-Limited Growth of Microbial Colonies. *Sci. Rep.* **8**, 5992 (2018).
38. Mimura, M., Sakaguchi, H. & Matsushita, M. Reaction–diffusion modelling of bacterial colony patterns. *Phys. Stat. Mech. Its Appl.* **282**, 283–303 (2000).
39. Granek, J. A. & Magwene, P. M. Environmental and Genetic Determinants of Colony Morphology in Yeast. *PLOS Genet.* **6**, e1000823 (2010).
40. Bourke, A. F. G. *Principles of Social Evolution*. (OUP Oxford, 2011).
41. West, S. A., Griffin, A. S. & Gardner, A. Evolutionary Explanations for Cooperation. *Curr. Biol.* **17**, R661–R672 (2007).
42. Hamilton, W. D. The genetical evolution of social behaviour. I. *J. Theor. Biol.* **7**, 1–16 (1964).
43. Hamilton, W. D. The genetical evolution of social behaviour. II. *J. Theor. Biol.* **7**, 17–52 (1964).
44. Krebs, Dennis and Crawford, Charles B and Smith, Martin S. *Sociobiology and psychology: Ideas, issues, and applications*. (L. Erlbaum Associates, 1987).
45. Dawkins, R. Twelve Misunderstandings of Kin Selection. *Z. Für Tierpsychol.* **51**, 184–200 (1979).
46. Queller, D. C. Kin Selection and Its Discontents. *Philos. Sci.* **83**, 861–872 (2016).
47. Park, J. H. Persistent Misunderstandings of Inclusive Fitness and Kin Selection: Their Ubiquitous Appearance in Social Psychology Textbooks. *Evol. Psychol.* **5**, 147470490700500400 (2007).
48. Bshary, R. & Grutter, A. S. Asymmetric cheating opportunities and partner control in a cleaner fish mutualism. *Anim. Behav.* **63**, 547–555 (2002).
49. Bshary, R. & Grutter, A. S. Punishment and partner switching cause cooperative behaviour in a cleaning mutualism. *Biol. Lett.* **1**, 396–399 (2005).
50. Wall, D. Kin recognition in bacteria. *Annu. Rev. Microbiol.* **70**, 143–160 (2016).
51. Dawkins, R. & Davis, N. *The Selfish Gene*. (Macat Library, 2017). doi:10.4324/9781912281251.
52. Smukalla, S. *et al.* FLO1 Is a Variable Green Beard Gene that Drives Biofilm-like Cooperation in Budding Yeast. *Cell* **135**, 726–737 (2008).
53. Rankin, D. J., Rocha, E. P. C. & Brown, S. P. What traits are carried on mobile genetic elements, and why? *Heredity* **106**, 1–10 (2011).
54. West, S. A., Griffin, A. S., Gardner, A. & Diggle, S. P. Social evolution theory for microorganisms. *Nat. Rev. Microbiol.* **4**, 597–607 (2006).
55. Federle, M. J. & Bassler, B. L. Interspecies communication in bacteria. *J. Clin. Invest.* **112**, 1291–1299 (2003).

56. Taga, M. E. & Bassler, B. L. Chemical communication among bacteria. *Proc. Natl. Acad. Sci.* **100**, 14549–14554 (2003).
57. Redfield, R. J. Is quorum sensing a side effect of diffusion sensing? *Trends Microbiol.* **10**, 365–370 (2002).
58. Mukherjee, S. & Bassler, B. L. Bacterial quorum sensing in complex and dynamically changing environments. *Nat. Rev. Microbiol.* **17**, 371–382 (2019).
59. Hense, B. A. *et al.* Does efficiency sensing unify diffusion and quorum sensing? *Nat. Rev. Microbiol.* **5**, 230–239 (2007).
60. Miller, M. B., Skorupski, K., Lenz, D. H., Taylor, R. K. & Bassler, B. L. Parallel Quorum Sensing Systems Converge to Regulate Virulence in *Vibrio cholerae*. *Cell* **110**, 303–314 (2002).
61. Hammer, B. K. & Bassler, B. L. Quorum sensing controls biofilm formation in *Vibrio cholerae*. *Mol. Microbiol.* **50**, 101–104 (2003).
62. Hawver, L. A., Giulietti, J. M., Baleja, J. D. & Ng, W.-L. Quorum Sensing Coordinates Cooperative Expression of Pyruvate Metabolism Genes To Maintain a Sustainable Environment for Population Stability. *mBio* **7**, e01863-16 (2016).
63. Watve, S. *et al.* Parallel quorum-sensing system in *Vibrio cholerae* prevents signal interference inside the host. *PLOS Pathog.* **16**, e1008313 (2020).
64. Venturi, V. Regulation of quorum sensing in *Pseudomonas*. *FEMS Microbiol. Rev.* **30**, 274–291 (2006).
65. Miller, E. L. *et al.* Eavesdropping and crosstalk between secreted quorum sensing peptide signals that regulate bacteriocin production in *Streptococcus pneumoniae*. *ISME J.* **12**, 2363–2375 (2018).
66. Gregorio-Godoy, P., Pulgar, G. P. del, Rodríguez-Regueira, M. & Rodríguez-Patón, A. Deriving general conditions and mechanisms for division of labor using the cell-based simulator gro. 363093 Preprint at <https://doi.org/10.1101/363093> (2018).
67. Banderas, A., Le Bec, M., Cordier, C. & Hersen, P. Autonomous and Assisted Control for Synthetic Microbiology. *Int. J. Mol. Sci.* **21**, 9223 (2020).
68. Gore, J., Youk, H. & van Oudenaarden, A. Snowdrift game dynamics and facultative cheating in yeast. *Nature* **459**, 253–256 (2009).
69. Smith, P. & Schuster, M. Public goods and cheating in microbes. *Curr. Biol.* **29**, R442–R447 (2019).
70. Meyer, J.-M. *et al.* Use of Siderophores to Type *Pseudomonads*: The Three *Pseudomonas Aeruginosa* Pyoverdine Systems. *Microbiology* **143**, 35–43.
71. Sharma, J., Sundar, D. & Srivastava, P. Biosurfactants: Potential Agents for Controlling Cellular Communication, Motility, and Antagonism. *Front. Mol. Biosci.* **8**, (2021).
72. Giri, S., Waschina, S., Kaleta, C. & Kost, C. Defining Division of Labor in Microbial Communities. *J. Mol. Biol.* (2019) doi:10.1016/j.jmb.2019.06.023.
73. Kumar, K., Mella-Herrera, R. A. & Golden, J. W. Cyanobacterial Heterocysts. *Cold Spring Harb. Perspect. Biol.* **2**, a000315 (2010).

74. Herrero, A., Stavans, J. & Flores, E. The multicellular nature of filamentous heterocyst-forming cyanobacteria. *FEMS Microbiol. Rev.* **40**, 831–854 (2016).
75. Beeckman, F., Motte, H. & Beeckman, T. Nitrification in agricultural soils: impact, actors and mitigation. *Curr. Opin. Biotechnol.* **50**, 166–173 (2018).
76. Norton, J. & Ouyang, Y. Controls and Adaptive Management of Nitrification in Agricultural Soils. *Front. Microbiol.* **10**, (2019).
77. Gordillo, M., Evans, T. & Gouon-Evans, V. Orchestrating liver development. *Development* **142**, 2094–2108 (2015).
78. Ober, E. A. & Lemaigre, F. P. Development of the liver: Insights into organ and tissue morphogenesis. *J. Hepatol.* **68**, 1049–1062 (2018).
79. Bruno, S. *et al.* Human Liver Stem Cells: A Liver-Derived Mesenchymal Stromal Cell-Like Population With Pro-regenerative Properties. *Front. Cell Dev. Biol.* **9**, (2021).
80. Stapornwongkul, K. S. & Vincent, J.-P. Generation of extracellular morphogen gradients: the case for diffusion. *Nat. Rev. Genet.* **22**, 393–411 (2021).
81. Grandel, N. E., Gamas, K. R. & Bennett, M. R. Control of synthetic microbial consortia in time, space, and composition. *Trends Microbiol.* **29**, 1095–1105 (2021).
82. Giri, S., Shitut, S. & Kost, C. Harnessing ecological and evolutionary principles to guide the design of microbial production consortia. *Curr. Opin. Biotechnol.* **62**, 228–238 (2020).
83. Stephens, K. & Bentley, W. E. Synthetic Biology for Manipulating Quorum Sensing in Microbial Consortia. *Trends Microbiol.* **28**, 633–643 (2020).
84. Tsoi, R. *et al.* Metabolic division of labor in microbial systems. *Proc. Natl. Acad. Sci.* **115**, 2526–2531 (2018).
85. Estrela, S. *et al.* Metabolic rules of microbial community assembly. 2020.03.09.984278 Preprint at <https://doi.org/10.1101/2020.03.09.984278> (2020).
86. Cavaliere, M., Feng, S., Soyer, O. S. & Jiménez, J. I. Cooperation in microbial communities and their biotechnological applications. *Environ. Microbiol.* **19**, 2949–2963 (2017).
87. Chaudhary, D. K., Khulan, A. & Kim, J. Development of a novel cultivation technique for uncultured soil bacteria. *Sci. Rep.* **9**, 6666 (2019).
88. Nagy, K., Abraham, Á., Keymer, J. E. & Galajda, P. Application of Microfluidics in Experimental Ecology: The Importance of Being Spatial. *Front. Microbiol.* **9**, (2018).
89. van Vliet, S. *et al.* Spatially Correlated Gene Expression in Bacterial Groups: The Role of Lineage History, Spatial Gradients, and Cell-Cell Interactions. *Cell Syst.* **6**, 496-507.e6 (2018).
90. Marinkovic, Z. S. *et al.* A microfluidic device for inferring metabolic landscapes in yeast monolayer colonies. *eLife* **8**, e47951 (2019).
91. Gupta, S. *et al.* Investigating the dynamics of microbial consortia in spatially structured environments. *Nat. Commun.* **11**, 2418 (2020).



92. Goodrich, J. K. *et al.* Human Genetics Shape the Gut Microbiome. *Cell* **159**, 789–799 (2014).
93. Rothschild, D. *et al.* Environment dominates over host genetics in shaping human gut microbiota. *Nature* **555**, 210–215 (2018).
94. Valdes, A. M., Walter, J., Segal, E. & Spector, T. D. Role of the gut microbiota in nutrition and health. *BMJ* **361**, k2179 (2018).
95. Turnbaugh, P. J. *et al.* A core gut microbiome in obese and lean twins. *Nature* **457**, 480–484 (2009).
96. de Goffau, M. C. *et al.* Fecal Microbiota Composition Differs Between Children With  $\beta$ -Cell Autoimmunity and Those Without. *Diabetes* **62**, 1238–1244 (2013).
97. Lambeth, S. M. *et al.* Composition, Diversity and Abundance of Gut Microbiome in Prediabetes and Type 2 Diabetes. *J. Diabetes Obes.* **2**, 1 (2015).
98. Wong, S. H. & Yu, J. Gut microbiota in colorectal cancer: mechanisms of action and clinical applications. *Nat. Rev. Gastroenterol. Hepatol.* **16**, 690–704 (2019).
99. Manichanh, C. *et al.* Reduced diversity of faecal microbiota in Crohn's disease revealed by a metagenomic approach. *Gut* **55**, 205–211 (2006).
100. Schippa, S. *et al.* A distinctive 'microbial signature' in celiac pediatric patients. *BMC Microbiol.* **10**, 175 (2010).
101. Menni, C. *et al.* Gut microbial diversity is associated with lower arterial stiffness in women. *Eur. Heart J.* **39**, 2390 (2018).
102. Scher, J. U. *et al.* Decreased Bacterial Diversity Characterizes the Altered Gut Microbiota in Patients With Psoriatic Arthritis, Resembling Dysbiosis in Inflammatory Bowel Disease. *Arthritis Rheumatol.* **67**, 128–139 (2015).
103. Zhang, F., Luo, W., Shi, Y., Fan, Z. & Ji, G. Should We Standardize the 1,700-Year-Old Fecal Microbiota Transplantation? *Off. J. Am. Coll. Gastroenterol. ACG* **107**, 1755 (2012).
104. Jia, N. A Misleading Reference for Fecal Microbiota Transplant. *Off. J. Am. Coll. Gastroenterol. ACG* **110**, 1731 (2015).
105. van Nood, E. *et al.* Duodenal Infusion of Donor Feces for Recurrent *Clostridium difficile*. *N. Engl. J. Med.* **368**, 407–415 (2013).
106. Schneider, K. M. *et al.* Successful Fecal Microbiota Transplantation in a Patient with Severe Complicated *Clostridium difficile* Infection after Liver Transplantation. *Case Rep. Gastroenterol.* **12**, 76–84 (2018).
107. Suez, J. *et al.* Post-Antibiotic Gut Mucosal Microbiome Reconstitution Is Impaired by Probiotics and Improved by Autologous FMT. *Cell* **174**, 1406–1423.e16 (2018).
108. Huff, B. A. Caveat emptor. 'Probiotics' might not be what they seem. *Can. Fam. Physician* **50**, 583–587 (2004).
109. Bafeta, A., Koh, M., Riveros, C. & Ravaud, P. Harms Reporting in Randomized Controlled Trials of Interventions Aimed at Modifying Microbiota. *Ann. Intern. Med.* (2018).

110. Khoruts, A. Targeting the microbiome: from probiotics to fecal microbiota transplantation. *Genome Med.* **10**, 80 (2018).
111. Byrd, A. L., Belkaid, Y. & Segre, J. A. The human skin microbiome. *Nat. Rev. Microbiol.* **16**, 143–155 (2018).
112. Webster, G. F., Ruggieri, M. R. & McGinley, K. J. Correlation of Propionibacterium acnes Populations with the Presence of Triglycerides on Nonhuman Skin. *Appl. Environ. Microbiol.* **41**, 1269–1270 (1981).
113. Begum, N. *et al.* Role of Arbuscular Mycorrhizal Fungi in Plant Growth Regulation: Implications in Abiotic Stress Tolerance. *Front. Plant Sci.* **10**, (2019).
114. Mitter, E. K., Tosi, M., Obregón, D., Dunfield, K. E. & Germida, J. J. Rethinking Crop Nutrition in Times of Modern Microbiology: Innovative Biofertilizer Technologies. *Front. Sustain. Food Syst.* **5**, (2021).
115. Chaudhry, V. *et al.* Shaping the leaf microbiota: plant–microbe–microbe interactions. *J. Exp. Bot.* **72**, 36–56 (2021).
116. Ma, A., Lv, D., Zhuang, X. & Zhuang, G. Quorum Quenching in Culturable Phyllosphere Bacteria from Tobacco. *Int. J. Mol. Sci.* **14**, 14607–14619 (2013).
117. Chen, T. *et al.* A plant genetic network for preventing dysbiosis in the phyllosphere. *Nature* **580**, 653–657 (2020).
118. Vergnes, S. *et al.* Phyllosphere Colonization by a Soil Streptomyces sp. Promotes Plant Defense Responses Against Fungal Infection. *Mol. Plant-Microbe Interactions®* **33**, 223–234 (2020).
119. Li, F. *et al.* Host genetics influence the rumen microbiota and heritable rumen microbial features associate with feed efficiency in cattle. *Microbiome* **7**, 92 (2019).
120. Wallace, R. J. *et al.* A heritable subset of the core rumen microbiome dictates dairy cow productivity and emissions. *Sci. Adv.* **5**, eaav8391 (2019).
121. Martínez-Álvaro, M. *et al.* Identification of Complex Rumen Microbiome Interaction Within Diverse Functional Niches as Mechanisms Affecting the Variation of Methane Emissions in Bovine. *Front. Microbiol.* **11**, (2020).
122. Liu, K. *et al.* Ruminal microbiota–host interaction and its effect on nutrient metabolism. *Anim. Nutr.* **7**, 49–55 (2021).
123. Mizrahi, I., Wallace, R. J. & Morais, S. The rumen microbiome: balancing food security and environmental impacts. *Nat. Rev. Microbiol.* **19**, 553–566 (2021).
124. Guo, M. *et al.* Dynamics of Gut Microbiome in Giant Panda Cubs Reveal Transitional Microbes and Pathways in Early Life. *Front. Microbiol.* **9**, (2018).
125. FAOSTAT. <https://www.fao.org/faostat/en/#data/GE/visualize>.
126. Creevey, C. J., Kelly, W. J., Henderson, G. & Leahy, S. C. Determining the culturability of the rumen bacterial microbiome. *Microb. Biotechnol.* **7**, 467–479 (2014).
127. Zehavi, T., Probst, M. & Mizrahi, I. Insights Into Culturomics of the Rumen Microbiome. *Front. Microbiol.* **9**, (2018).

128. Rahman, M. S. *et al.* Microbiome signature and diversity regulates the level of energy production under anaerobic condition. *Sci. Rep.* **11**, 19777 (2021).
129. De Vrieze, J. The next frontier of the anaerobic digestion microbiome: From ecology to process control. *Environ. Sci. Ecotechnology* **3**, 100032 (2020).
130. Sposob, M., Wahid, R. & Fischer, K. Ex-situ biological CO<sub>2</sub> methanation using trickle bed reactor: review and recent advances. *Rev. Environ. Sci. Biotechnol.* **20**, 1087–1102 (2021).
131. Jiang, Y. *et al.* Consolidated bioprocessing performance of a two-species microbial consortium for butanol production from lignocellulosic biomass. *Biotechnol. Bioeng.* **n/a**.
132. Li, T. *et al.* Mimicking lichens: incorporation of yeast strains together with sucrose-secreting cyanobacteria improves survival, growth, ROS removal, and lipid production in a stable mutualistic co-culture production platform. *Biotechnol. Biofuels* **10**, 55 (2017).
133. Pronk, J. T. Auxotrophic yeast strains in fundamental and applied research. *Appl. Environ. Microbiol.* **68**, 2095–2100 (2002).
134. Liu, H., Styles, C. A. & Fink, G. R. *Saccharomyces cerevisiae* S288C Has a Mutation in FL08, a Gene Required for Filamentous Growth. *Genetics* **144**, 967–978 (1996).
135. Soares, E. V. Flocculation in *Saccharomyces cerevisiae*: a review. *J. Appl. Microbiol.* **110**, 1–18 (2011).
136. Baker Brachmann, C. *et al.* Designer deletion strains derived from *Saccharomyces cerevisiae* S288C: A useful set of strains and plasmids for PCR-mediated gene disruption and other applications. *Yeast* **14**, 115–132 (1998).
137. Verduyn, C., Zomerdijk, T. P. L., van Dijken, J. P. & Scheffers, W. A. Continuous measurement of ethanol production by aerobic yeast suspensions with an enzyme electrode. *Appl. Microbiol. Biotechnol.* **19**, 181–185 (1984).
138. Pfeiffer, T. & Morley, A. An evolutionary perspective on the Crabtree effect. *Front. Mol. Biosci.* **1**, (2014).
139. Pfeiffer, T., Schuster, S. & Bonhoeffer, S. Cooperation and Competition in the Evolution of ATP-Producing Pathways. *Science* **292**, 504–507 (2001).
140. Berthels, N. J., Cordero Otero, R. R., Bauer, F. F., Thevelein, J. M. & Pretorius, I. S. Discrepancy in glucose and fructose utilisation during fermentation by *Saccharomyces cerevisiae* wine yeast strains. *FEMS Yeast Res.* **4**, 683–689 (2004).
141. Stein, O. & Granot, D. An Overview of Sucrose Synthases in Plants. *Front. Plant Sci.* **10**, 95 (2019).
142. Hijaz, F. & Killiny, N. Collection and Chemical Composition of Phloem Sap from *Citrus sinensis* L. Osbeck (Sweet Orange). *PLoS ONE* **9**, e101830 (2014).
143. Baker, H. G., Baker, I. & Hodges, S. A. Sugar Composition of Nectars and Fruits Consumed by Birds and Bats in the Tropics and Subtropics<sup>1</sup>. *Biotropica* **30**, 559–586 (1998).
144. Stefanini, I. *et al.* Role of social wasps in *Saccharomyces cerevisiae* ecology and evolution. *Proc. Natl. Acad. Sci.* **109**, 13398–13403 (2012).

145. Meriggi, N., Di Paola, M., Cavalieri, D. & Stefanini, I. Saccharomyces cerevisiae – Insects Association: Impacts, Biogeography, and Extent. *Front. Microbiol.* **11**, 1629 (2020).
146. H. Koschwanez, J., R. Foster, K. & W. Murray, A. Sucrose Utilization in Budding Yeast as a Model for the Origin of Undifferentiated Multicellularity. *PLoS Biol.* **9**, (2011).
147. Sutton, D. D. & Lampen, J. O. Localization of sucrose and maltose fermenting systems in Saccharomyces cerevisiae. *Biochim. Biophys. Acta* **56**, 303–312 (1962).
148. Carlson, M. & Botstein, D. Two differentially regulated mRNAs with different 5' ends encode secreted and intracellular forms of yeast invertase. *Cell* **28**, 145–154 (1982).
149. Berthelot, M. Sur la fermentation glucosique du sucre de canne. *Comptes Rendus Académie Sci.* **50**, 983–984 (1860).
150. Brown, A. J. Enzyme action. *J. Chem. Soc. Trans.* **81**, 373–388 (1902).
151. Michaelis, L. & Menten, M. Die Kinetik der Invertinwirkung. *Biochem Z* 1913 49 33369.
152. Johnson, K. A. & Goody, R. S. The Original Michaelis Constant: Translation of the 1913 Michaelis–Menten Paper. *Biochemistry* **50**, 8264–8269 (2011).
153. Naumova, E. S., Sadykova, A. Zh., Martynenko, N. N. & Naumov, G. I. Molecular polymorphism of  $\beta$ -fructosidase SUC genes in the Saccharomyces yeasts. *Mol. Biol.* **48**, 573–582 (2014).
154. Carlson, M. & Botstein, D. Organization of the SUC gene family in Saccharomyces. *Mol. Cell. Biol.* **3**, 351–359 (1983).
155. Naumova, E. S., Naumov, G. I., Masneuf-Pomarède, I., Aigle, M. & Dubourdieu, D. Molecular genetic study of introgression between Saccharomyces bayanus and S. cerevisiae. *Yeast* **22**, 1099–1115 (2005).
156. Bozdag, G. O. & Greig, D. The genetics of a putative social trait in natural populations of yeast. *Mol. Ecol.* **23**, 5061–5071 (2014).
157. Koschwanez, J. H., Foster, K. R. & Murray, A. W. Improved use of a public good selects for the evolution of undifferentiated multicellularity. *eLife* **2**, e00367 (2013).
158. Trumbly, R. J. Glucose repression in the yeast Saccharomyces cerevisiae. *Mol. Microbiol.* **6**, 15–21 (1992).
159. Belinchón, M. M. & Gancedo, J. M. Different signalling pathways mediate glucose induction of SUC2, HXT1 and pyruvate decarboxylase in yeast. *FEMS Yeast Res.* **7**, 40–47 (2007).
160. Özcan, S., Vallier, L. G., Flick, J. S., Carlson, M. & Johnston, M. Expression of the SUC2 Gene of Saccharomyces cerevisiae is Induced by Low Levels of Glucose. *Yeast* **13**, 127–137 (1997).
161. Geng, F. & Laurent, B. C. Roles of SWI/SNF and HATs throughout the dynamic transcription of a yeast glucose-repressible gene. *EMBO J.* **23**, 127–137 (2004).
162. Meijer, M. M., Boonstra, J., Verkleij, A. J. & Verrips, C. T. Glucose repression in Saccharomyces cerevisiae is related to the glucose concentration rather than the glucose flux. *J. Biol. Chem.* **273**, 24102–24107 (1998).
163. Marques, W. L., Raghavendran, V., Stambuk, B. U. & Gombert, A. K. Sucrose and Saccharomyces cerevisiae: a relationship most sweet. *FEMS Yeast Res.* **16**, (2016).

164. Tester, R. F. & Karkalas, J. CARBOHYDRATES | Classification and Properties. in *Encyclopedia of Food Sciences and Nutrition (Second Edition)* (ed. Caballero, B.) 862–875 (Academic Press, 2003). doi:10.1016/B0-12-227055-X/00166-8.
165. Sainz-Polo, M. A. *et al.* Three-dimensional Structure of Saccharomyces Invertase ROLE OF A NON-CATALYTIC DOMAIN IN OLIGOMERIZATION AND SUBSTRATE SPECIFICITY. *J. Biol. Chem.* **288**, 9755–9766 (2013).
166. Kaur, N., Kaur, M., Gupta, A. K. & Singh, R. Properties of  $\beta$ -fructosidases (invertases and inulinases) of *Fusarium oxysporum* grown on an aqueous extract of *Cichorium intybus* roots. *J. Chem. Technol. Biotechnol.* **53**, 279–284 (1992).
167. Zeng, C. & Biemann, K. Determination of N-linked glycosylation of yeast external invertase by matrix-assisted laser desorption/ionization time-of-flight mass spectrometry. *J. Mass Spectrom. JMS* **34**, 311–329 (1999).
168. Kern, G., Schülke, N., Schmid, F. X. & Jaenicke, R. Stability, quaternary structure, and folding of internal, external, and core-glycosylated invertase from yeast. *Protein Sci. Publ. Protein Soc.* **1**, 120–131 (1992).
169. Chu, F. K. & Maley, F. The effect of glucose on the synthesis and glycosylation of the polypeptide moiety of yeast external invertase. *J. Biol. Chem.* **255**, 6392–6397 (1980).
170. Chu, F. K., Watorek, W. & Maley, F. Factors affecting the oligomeric structure of yeast external invertase. *Arch. Biochem. Biophys.* **223**, 543–555 (1983).
171. Tammi, M., Ballou, L., Taylor, A. & Ballou, C. E. Effect of glycosylation on yeast invertase oligomer stability. *J. Biol. Chem.* **262**, 4395–4401 (1987).
172. Nobel, J. G. D. & Barnett, J. A. Passage of molecules through yeast cell walls: A brief essay-review. *Yeast* **7**, 313–323 (1991).
173. Mwene-Mbeja, T. M. & Vaneckhaute, C. Conference Paper: Green Industry Adapted to Recycling Needs of Lubumbashi City and Surrounding Areas in Democratic Republic of the Congo. *Green Sustain. Chem.* **9**, 11–25 (2019).
174. Weusthuis, R. A., Adams, H., Scheffers, W. A. & van Dijken, J. P. Energetics and kinetics of maltose transport in *Saccharomyces cerevisiae*: a continuous culture study. *Appl. Environ. Microbiol.* **59**, 3102–3109 (1993).
175. Basso, T. O. *et al.* Engineering topology and kinetics of sucrose metabolism in *Saccharomyces cerevisiae* for improved ethanol yield. *Metab. Eng.* **13**, 694–703 (2011).
176. Badotti, F. *et al.* Switching the mode of sucrose utilization by *Saccharomyces cerevisiae*. *Microb. Cell Factories* **7**, 4 (2008).
177. Charron, M. J., Read, E., Haut, S. R. & Michels, C. A. Molecular Evolution of the Telomere-Associated Mal Loci of *Saccharomyces*. *Genetics* **122**, 307–316 (1989).
178. Marques, W. L. *et al.* Elimination of sucrose transport and hydrolysis in *Saccharomyces cerevisiae*: a platform strain for engineering sucrose metabolism. *FEMS Yeast Res.* **17**, (2017).
179. Zelman, B. V., Lee, G. A., Ng, M. & Miesenböck, G. Selective Photostimulation of Genetically ChARGed Neurons. *Neuron* **33**, 15–22 (2002).

180. Zemelman, B. V., Nesnas, N., Lee, G. A. & Miesenböck, G. Photochemical gating of heterologous ion channels: Remote control over genetically designated populations of neurons. *Proc. Natl. Acad. Sci. U. S. A.* **100**, 1352–1357 (2003).
181. Nagel, G. *et al.* Channelrhodopsin-1: A Light-Gated Proton Channel in Green Algae. *Science* **296**, 2395–2398 (2002).
182. Nagel, G. *et al.* Channelrhodopsin-2, a directly light-gated cation-selective membrane channel. *Proc. Natl. Acad. Sci. U. S. A.* **100**, 13940–13945 (2003).
183. Dwijayanti, A., Zhang, C., Poh, C. L. & Lautier, T. Toward Multiplexed Optogenetic Circuits. *Front. Bioeng. Biotechnol.* **9**, (2022).
184. Fernandez-Rodriguez, J., Moser, F., Song, M. & Voigt, C. A. Engineering RGB color vision into *Escherichia coli*. *Nat. Chem. Biol.* **13**, 706–708 (2017).
185. Lan, T.-H., He, L., Huang, Y. & Zhou, Y. Optogenetics for transcriptional programming and genetic engineering. *Trends Genet.* (2022) doi:10.1016/j.tig.2022.05.014.
186. Qin, X. *et al.* Cell-matrix adhesion and cell-cell adhesion differentially control basal myosin oscillation and *Drosophila* egg chamber elongation. *Nat. Commun.* **8**, 14708 (2017).
187. de Mena, L., Rizk, P. & Rincon-Limas, D. E. Bringing Light to Transcription: The Optogenetics Repertoire. *Front. Genet.* **9**, (2018).
188. Taslimi, A. *et al.* Optimized second generation CRY2/CIB dimerizers and photoactivatable Cre recombinase. *Nat. Chem. Biol.* **12**, 425–430 (2016).
189. Valon, L. *et al.* Predictive Spatiotemporal Manipulation of Signaling Perturbations Using Optogenetics. *Biophys. J.* **109**, 1785–1797 (2015).
190. de Beco, S. *et al.* Optogenetic dissection of Rac1 and Cdc42 gradient shaping. *Nat. Commun.* **9**, 4816 (2018).
191. Zoltowski, B. D., Motta-Mena, L. B. & Gardner, K. H. Blue Light-Induced Dimerization of a Bacterial LOV–HTH DNA-Binding Protein. *Biochemistry* **52**, 6653–6661 (2013).
192. Motta-Mena, L. B. *et al.* An optogenetic gene expression system with rapid activation and deactivation kinetics. *Nat. Chem. Biol.* **10**, 196–202 (2014).
193. Stockley, J. H. *et al.* Surpassing light-induced cell damage in vitro with novel cell culture media. *Sci. Rep.* **7**, 849 (2017).
194. Wäldchen, S., Lehmann, J., Klein, T., van de Linde, S. & Sauer, M. Light-induced cell damage in live-cell super-resolution microscopy. *Sci. Rep.* **5**, 15348 (2015).
195. Gerhardt, K. P. *et al.* An open-hardware platform for optogenetics and photobiology. *Sci. Rep.* **6**, 35363 (2016).
196. Wong, B. G., Mancuso, C. P., Kiriakov, S., Bashor, C. J. & Khalil, A. S. Precise, automated control of conditions for high-throughput growth of yeast and bacteria with eVOLVER. *Nat. Biotechnol.* **36**, 614–623 (2018).

197. Lee, M. E., DeLoache, W. C., Cervantes, B. & Dueber, J. E. A Highly Characterized Yeast Toolkit for Modular, Multipart Assembly. <https://pubs.acs.org/doi/full/10.1021/sb500366v> (2015) doi:10.1021/sb500366v.
198. A synthetic library of RNA control modules for predictable tuning of gene expression in yeast. *Mol. Syst. Biol.* **7**, 471 (2011).
199. Ryan, M. D., King, A. M. Q. & Thomas, G. P. Cleavage of foot-and-mouth disease virus polypeptide is mediated by residues located within a 19 amino acid sequence. *J. Gen. Virol.* **72**, 2727–2732 (1991).
200. Rothwell, D. G. *et al.* Functional Expression of Secreted Proteins from a Bicistronic Retroviral Cassette Based on Foot-and-Mouth Disease Virus 2A Can Be Position Dependent. *Hum. Gene Ther.* **21**, 1631–1637 (2010).
201. Delic, M. *et al.* The secretory pathway: exploring yeast diversity. *FEMS Microbiol. Rev.* **37**, 872–914 (2013).
202. Marques, W. L. *et al.* Elimination of sucrose transport and hydrolysis in *Saccharomyces cerevisiae*: a platform strain for engineering sucrose metabolism. *FEMS Yeast Res.* **17**, (2017).
203. Shimanouchi, T. *et al.* Kinetic pH Titration to Predict the Acid and Hydrothermal Conditions for the Hydrolysis of Disaccharides: Use of a Microcapillary System. *J. Chem.* **2019**, e3985915 (2019).
204. Benzinger, D. & Khammash, M. Pulsatile inputs achieve tunable attenuation of gene expression variability and graded multi-gene regulation. *Nat. Commun.* **9**, (2018).
205. Bassetti, F. J., Bergamasco, R., Moraes, F. F. & Zanin, G. M. Thermal stability and deactivation energy of free and immobilized invertase. *Braz. J. Chem. Eng.* **17**, 867–872 (2000).
206. Margetić, A. & Vujčić, Z. Comparative study of stability of soluble and cell wall invertase from *Saccharomyces cerevisiae*. *Prep. Biochem. Biotechnol.* **47**, 305–311 (2017).
207. Schülke, N. & Schmid, F. X. The stability of yeast invertase is not significantly influenced by glycosylation. *J. Biol. Chem.* **263**, 8827–8831 (1988).
208. Moreno Morales, N., Patel, M. T., Stewart, C. J., Sweeney, K. & McClean, M. N. Optogenetic Tools for Control of Public Goods in *Saccharomyces cerevisiae*. *mSphere* **6**, e00581-21.
209. Torres, A. P., Oliveira, F. a. r., Silva, C. l. m. & Fortuna, S. p. THE INFLUENCE of pH ON the KINETICS of ACID HYDROLYSIS of SUCROSE. *J. Food Process Eng.* **17**, 191–208 (1994).
210. Yamabe, S., Guan, W. & Sakaki, S. Three Competitive Transition States at the Glycosidic Bond of Sucrose in Its Acid-Catalyzed Hydrolysis. *J. Org. Chem.* **78**, 2527–2533 (2013).
211. Bhaumik, P. & Dhepe, P. L. Chapter 1 Conversion of Biomass into Sugars. 1–53 (2015) doi:10.1039/9781782622079-00001.
212. Wilhelm, L. Ueber das Gesetz, nach welchem die Einwirkung der Säuren auf den Rohrzucker stattfindet (The Law By Which the Action of Acids on Cane Sugar Occurs). *Ann. Phys.* **81**, 413–433 (1850).
213. Arrhenius, S. Über die Reaktionsgeschwindigkeit bei der Inversion von Rohrzucker durch Säuren (About the rate of reaction in the inversion of cane sugar by acids). *Z. Für Phys. Chem.* **4U**, 226–248 (1889).

214. Mega, T. L. & Van Etten, R. L. The oxygen-18 isotope shift in carbon-13 nuclear magnetic resonance spectroscopy. 12. Position of bond cleavage in the acid-catalyzed hydrolysis of sucrose. *J. Am. Chem. Soc.* **110**, 6372–6376 (1988).
215. Prins, R. C. & Billerbeck, S. A buffered media system for yeast batch culture growth. *BMC Microbiol.* **21**, 127 (2021).
216. Llamosi, A. *et al.* What Population Reveals about Individual Cell Identity: Single-Cell Parameter Estimation of Models of Gene Expression in Yeast. *PLoS Comput. Biol.* **12**, e1004706 (2016).
217. Chiron, L. *et al.* CyberSco.Py an open-source software for event-based, conditional microscopy. *Sci. Rep.* **12**, 11579 (2022).
218. Tinevez, J.-Y. *et al.* TrackMate: An open and extensible platform for single-particle tracking. *Methods* **115**, 80–90 (2017).
219. Gray, B. F. & Kirwan, N. A. Growth rates of yeast colonies on solid media. *Biophys. Chem.* **1**, 204–213 (1974).
220. Pirt, S. J. Y. 1967. A Kinetic Study of the Mode of Growth of Surface Colonies of Bacteria and Fungi. *Microbiology* **47**, 181–197.
221. Váchová, L. *et al.* Architecture of developing multicellular yeast colony: spatio-temporal expression of Ato1p ammonium exporter. *Environ. Microbiol.* **11**, 1866–1877 (2009).
222. Čáp, M., Štěpánek, L., Harant, K., Váchová, L. & Palková, Z. Cell Differentiation within a Yeast Colony: Metabolic and Regulatory Parallels with a Tumor-Affected Organism. *Mol. Cell* **46**, 436–448 (2012).
223. Chen, L. *et al.* Consolidated bioprocessing for cellulosic ethanol conversion by cellulase–xylanase cell-surfaced yeast consortium. *Prep. Biochem. Biotechnol.* **48**, 653–661 (2018).
224. Mauri, M., Gouzé, J.-L., Jong, H. de & Cinquemani, E. Enhanced production of heterologous proteins by a synthetic microbial community: Conditions and trade-offs. *bioRxiv* 2020.02.19.955815 (2020) doi:10.1101/2020.02.19.955815.
225. Li, X. *et al.* Design of stable and self-regulated microbial consortia for chemical synthesis. *Nat. Commun.* **13**, 1554 (2022).
226. McBee, R. M. *et al.* Engineering living and regenerative fungal–bacterial biocomposite structures. *Nat. Mater.* 1–8 (2021) doi:10.1038/s41563-021-01123-y.
227. Gilbert, C. *et al.* Living materials with programmable functionalities grown from engineered microbial co-cultures. *Nat. Mater.* **20**, 691–700 (2021).
228. Michael, D. r. *et al.* In vitro neuroprotective activities of two distinct probiotic consortia. *Benef. Microbes* **10**, 437–447 (2019).
229. Stein, R. R. *et al.* Computer-guided design of optimal microbial consortia for immune system modulation. *eLife* **7**, e30916 (2018).
230. van der Lelie, D. *et al.* Rationally designed bacterial consortia to treat chronic immune-mediated colitis and restore intestinal homeostasis. *Nat. Commun.* **12**, 3105 (2021).



231. Ribeiro, A. C. F. *et al.* Binary Mutual Diffusion Coefficients of Aqueous Solutions of Sucrose, Lactose, Glucose, and Fructose in the Temperature Range from (298.15 to 328.15) K. *J. Chem. Eng. Data* **51**, 1836–1840 (2006).
232. Weng, L., Liang, S., Zhang, L., Zhang, X. & Xu, J. Transport of Glucose and Poly(ethylene glycol)s in Agarose Gels Studied by the Refractive Index Method. *Macromolecules* **38**, 5236–5242 (2005).
233. Reshetnikov, V. V., Smolskaya, S. V., Feoktistova, S. G. & Verkhusha, V. V. Optogenetic approaches in biotechnology and biomaterials. *Trends Biotechnol.* **40**, 858–874 (2022).
234. Molinari, S., Tesoriero, R. F. & Ajo-Franklin, C. M. Bottom-up approaches to engineered living materials: Challenges and future directions. *Matter* **4**, 3095–3120 (2021).
235. Rodrigo-Navarro, A., Sankaran, S., Dalby, M. J., del Campo, A. & Salmeron-Sanchez, M. Engineered living biomaterials. *Nat. Rev. Mater.* **6**, 1175–1190 (2021).
236. Everard, A. & Cani, P. D. Diabetes, obesity and gut microbiota. *Best Pract. Res. Clin. Gastroenterol.* **27**, 73–83 (2013).
237. Zaky, A., Glastras, S. J., Wong, M. Y. W., Pollock, C. A. & Saad, S. The Role of the Gut Microbiome in Diabetes and Obesity-Related Kidney Disease. *Int. J. Mol. Sci.* **22**, 9641 (2021).
238. Cardinale, M. *et al.* The Response of the Soil Microbiota to Long-Term Mineral and Organic Nitrogen Fertilization is Stronger in the Bulk Soil than in the Rhizosphere. *Genes* **11**, 456 (2020).
239. Ren, N. *et al.* Effects of Continuous Nitrogen Fertilizer Application on the Diversity and Composition of Rhizosphere Soil Bacteria. *Front. Microbiol.* **11**, (2020).
240. Villamil, M. B. *et al.* Microbial Signatures in Fertile Soils Under Long-Term N Management. *Front. Soil Sci.* **1**, (2021).
241. Zhao, E. M. *et al.* Optogenetic Amplification Circuits for Light-Induced Metabolic Control. *ACS Synth. Biol.* **10**, 1143–1154 (2021).
242. Yasemi, M. & Jolicoeur, M. Modelling Cell Metabolism: A Review on Constraint-Based Steady-State and Kinetic Approaches. *Processes* **9**, 322 (2021).
243. Toledo-Marín, J. Q., Fox, G., Sluka, J. P. & Glazier, J. A. Deep Learning Approaches to Surrogates for Solving the Diffusion Equation for Mechanistic Real-World Simulations. *Front. Physiol.* **12**, (2021).
244. Zobeiry, N. & Humfeld, K. D. A physics-informed machine learning approach for solving heat transfer equation in advanced manufacturing and engineering applications. *Eng. Appl. Artif. Intell.* **101**, 104232 (2021).
245. Lugagne, J.-B. *et al.* Balancing a genetic toggle switch by real-time feedback control and periodic forcing. *Nat. Commun.* **8**, 1671 (2017).
246. Lugagne, J.-B. & Dunlop, M. J. Cell-machine interfaces for characterizing gene regulatory network dynamics. *Curr. Opin. Syst. Biol.* **14**, 1–8 (2019).
247. Thomas, P. J. *et al.* Control theory in biology and medicine. *Biol. Cybern.* **113**, 1–6 (2019).
248. *Control Theory and Systems Biology.* (MIT Press, 2009).

249. Baetica, A.-A., Westbrook, A. & El-Samad, H. Control theoretical concepts for synthetic and systems biology. *Curr. Opin. Syst. Biol.* **14**, 50–57 (2019).
250. Scott, T. D., Sweeney, K. & McClean, M. N. Biological signal generators: integrating synthetic biology tools and in silico control. *Curr. Opin. Syst. Biol.* **14**, 58–65 (2019).
251. Khammash, M. H. Cybergenetics: Theory and Applications of Genetic Control Systems. *Proc. IEEE* **110**, 631–658 (2022).
252. Del Vecchio, D., Dy, A. J. & Qian, Y. Control theory meets synthetic biology. *J. R. Soc. Interface* **13**, 20160380 (2016).
253. Shin, Y.-J. & Bleris, L. Linear Control Theory for Gene Network Modeling. *PLOS ONE* **5**, e12785 (2010).
254. Baldissera, F. L., Cury, J. E. R. & Raisch, J. A Supervisory Control Theory Approach to Control Gene Regulatory Networks. *IEEE Trans. Autom. Control* **61**, 18–33 (2016).
255. Shin, Y.-J. Digital Signal Processing and Control for the Study of Gene Networks. *Sci. Rep.* **6**, 24733 (2016).
256. Harris, A. W. K., Dolan, J. A., Kelly, C. L., Anderson, J. & Papachristodoulou, A. Designing Genetic Feedback Controllers. *IEEE Trans. Biomed. Circuits Syst.* **9**, 475–484 (2015).
257. Steel, H., Lillacci, G., Khammash, M. & Papachristodoulou, A. Challenges at the interface of control engineering and synthetic biology. in *2017 IEEE 56th Annual Conference on Decision and Control (CDC)* 1014–1023 (2017). doi:10.1109/CDC.2017.8263791.



# Appendixes

# Appendixes

## Appendixes summary

1. Scientific productions
  - 1.1. Reviews
    - 1.1.1. Autonomous and assisted control for synthetic microbiology
    - 1.1.2. The promise of optogenetics for bioproduction: dynamic control strategies and scale-up instruments
  - 1.2. Posters
    - 1.2.1. First year poster
    - 1.2.2. Third year poster
2. Protocols
  - 2.1. Molecular biology
    - 2.1.1. Culture media for yeast
    - 2.1.2. LiAc transformation in *S. cerevisiae*
    - 2.1.3. CRISPR/Cas9 for *S. cerevisiae*
    - 2.1.4. *S. cerevisiae* transformation for CRISPR
    - 2.1.5. Plasmid transformation in competent *E. Coli*
    - 2.1.6. Modular Cloning (MoClo) for yeast
    - 2.1.7. Construction of the strains used
  - 2.2. Tools and devices
    - 2.2.1. OptoCube – Spatially resolved light stimulation
    - 2.2.2. Make microfluidic moulds (wafers)
    - 2.2.3. Make microfluidic chips
    - 2.2.4. Scikit FiniteDiff - PDE solver (Python)
    - 2.2.5. OptoBox (or Light-Plate Apparatus)
3. Data
  - 3.1. Molecular biology
    - 3.1.1. Strain list
    - 3.1.2. Plasmid list
    - 3.1.3. Primer list
  - 3.2. Modelling script

# 1. Scientific productions

## 1.1. Reviews



Review

# Autonomous and Assisted Control for Synthetic Microbiology

Alvaro Banderas <sup>1,2,\*</sup>, Matthias Le Bec <sup>1,2</sup> , Céline Cordier <sup>1,2</sup> and Pascal Hersen <sup>1,2,\*</sup>

<sup>1</sup> Institut Curie, Université PSL, CNRS UMR168, Sorbonne Université, Laboratoire Physico Chimie Curie, 75005 Paris, France; matthias.lebec@curie.fr (M.L.B.); celine.cordier@curie.fr (C.C.)

<sup>2</sup> Laboratoire MSC, UMR7057, Université de Paris—CNRS, 75013 Paris, France

\* Correspondence: alvaro.banderas@curie.fr (A.B.); pascal.hersen@curie.fr (P.H.)

Received: 6 October 2020; Accepted: 25 November 2020; Published: 3 December 2020



**Abstract:** The control of microbes and microbial consortia to achieve specific functions requires synthetic circuits that can reliably cope with internal and external perturbations. Circuits that naturally evolved to regulate biological functions are frequently robust to alterations in their parameters. As the complexity of synthetic circuits increases, synthetic biologists need to implement such robust control “by design”. This is especially true for intercellular signaling circuits for synthetic consortia, where robustness is highly desirable, but its mechanisms remain unclear. Cybergenetics, the interface between synthetic biology and control theory, offers two approaches to this challenge: external (computer-aided) and internal (autonomous) control. Here, we review natural and synthetic microbial systems with robustness, and outline experimental approaches to implement such robust control in microbial consortia through population-level cybergenetics. We propose that harnessing natural intercellular circuit topologies with robust evolved functions can help to achieve similar robust control in synthetic intercellular circuits. A “hybrid biology” approach, where robust synthetic microbes interact with natural consortia and—additionally—with external computers, could become a useful tool for health and environmental applications.

**Keywords:** robustness; cybergenetics; relative sensing; microbial consortia; synthetic biology; control

## 1. Introduction

Homeostasis is the ability to maintain physiological parameters at steady levels, for example, body temperature or blood salt concentration in an organism and turgor pressure or macromolecular crowding in cells [1,2]. The robustness of the underlying molecular networks is a crucial component of cellular homeostasis. Robustness can be generally defined as the property that allows a system to maintain its functions, at least partially, in the presence of internal and external perturbations [3]. Robustness has been observed in a variety of molecular systems, including the pathways that control gene expression, metabolism and cellular signaling [4], with negative feedback being at the core of the operation of such circuits. Advances towards a quantitative definition of biological robustness have emerged from the similarity between negative feedback in electronic circuits and negative autoregulation in genetic circuits [5]. Electronic and biological circuits can both be seen as information processing flows and share conceptual similarities regarding the description of their dynamics and sensitivity to external perturbations. For both, one can define the robustness of a circuit based on the ratio of the relative change in steady-state output to the relative change in each parameter value.

Synthetic biology aims to construct genetic circuits from the bottom-up for both applied and fundamental research. However, the predictability and scalability of synthetic circuits remain poor overall [6], making implementation of robust (and therefore reliable) circuitry desirable. Synthetic biologists have already proposed theoretically and produced experimentally such robust genetic

circuits. These advances pave the way towards the construction of more complex cellular networks with predictable and useful functions, which could enable desired complex cellular behaviors to be engineered from the bottom-up.

Systematic, quantitative characterization of the wide range of uncertainties that affect synthetic circuits, as well as the variety of access points to spatiotemporally and orthogonally control natural circuits, has been reviewed elsewhere [6,7]. Here, we focus on how nature-inspired circuitry can provide design schemes and components to accomplish robust control over both synthetic and natural complex cellular ecologies. First, we introduce robust control in natural intra- and intercellular circuits, focusing on examples with well-described derived biological functions. Second, we establish the challenges involved in applying such knowledge to the problem of controlling synthetic ecologies. Third, we introduce cybergenetics as a multifaceted solution, and divide the approach into external (computer-aided) and internal (autonomous) interventions. Finally, we explore how such interventions may help to achieve robust control of natural populations for biomedical applications.

## 2. Natural Robust Control

### 2.1. Perfect Adaptation and Relative Sensing of Stimuli

Robust perfect adaptation—where large external perturbations are attenuated back to a baseline—is a feature that can be useful to maintain outputs at desired levels in synthetic systems. Furthermore, it could help to generate biologically and ecologically relevant input–output response patterns for synthetic microbes, as it does in their natural counterparts. Bacterial chemotaxis is a prototypical example of natural robust control leading to a relevant biological function. Robust perfect adaptation is achieved in *Escherichia coli* via an integral negative feedback strategy [8–10], where the output is integrated over a period of time before being fed back to the input. When an *E. coli* cell senses an increase in the nutrient concentration as it explores the environment, its chemoreceptors become less sensitive, allowing cells to sense nutrients across a wide range of concentrations without saturating their response, while also reducing variability (noise) among responding cells. This mechanism results in response magnitudes that follow the Weber–Fechner law for sensory systems (or logarithmic sensing) [11–13], where the perceived magnitude (a pathway output in the case of cells) is proportional to the logarithm of the input magnitude. In practice, chemotactic responses of *E. coli* are then proportional to the fractional gradient (gradient normalized to the chemoattractant concentration) of nutrients—rather than the absolute gradient [14–16], allowing *E. coli* to climb up exponential gradients with constant drift velocity. Similar relative sensing strategies have been observed in a variety of cellular and biochemical systems with different underlying mechanisms, notably the incoherent feed-forward loop (IFFL) [11,17–20], showing that sensing relative stimuli is of primary importance to a cell's performance in its native environment, and that mechanisms other than integral feedback can bring about perfectly adapting relative stimulus sensing.

Natural control topologies, such as the one in *E. coli* chemotaxis, can provide inspiration for the design of circuits with complex behavior. Implementing similar capabilities in synthetic microbes might therefore be useful for achieving improved performance in complex ecosystems.

### 2.2. Sensing Relative Population Composition

Another form of relative sensing—in this case pertaining to the population level—is ratiometric sensing, for which a handful of examples have been described (Figure 1). Ratio sensing is the ability of cells to produce an output proportional to the composition of the cell population, with the output remaining robust to variations in total cell density (Figure 1A). One example is the mating-pheromone pathway of *Saccharomyces cerevisiae* [21] (Figure 1B). During mating, two mating types communicate via extracellular pheromone signals to activate mating responses such as cell–cell agglutination and cell-cycle arrest. Mating-type *MAT* $\alpha$  produces the  $\alpha$ -factor pheromone, which activates *MAT* $\alpha$  cells in proportion to the concentration of *MAT* $\alpha$ . However, *MAT* $\alpha$  also produces the extracellular protease



Bar1, which degrades  $\alpha$ -factor at a rate proportional to the concentration of MATa. This system enables MATa cells to remain sensitive to ratio changes and be less sensitive to the total population density. Another example is the PhrA-RapA-Spo0F signaling pathway in *Bacillus subtilis* (Figure 1C). When part of the population “cheats” by not producing an extracellular signal that benefits the population [22], the ratio of producers to “cheaters” can specifically be sensed by cells. This happens because of a population-wide signal internalization or “pumping in” through a signal-specific permease and subsequent signal degradation. Again, equal increases in both cell densities increase production, but also increase the depletion rate—making the concentration of available signal proportional to the cell ratio. Similar ratio sensitivity can be found in plasmid conjugation in Gram-positive *Enterococcus faecalis* (Figure 1D), where two antagonistic signals—each produced specifically by plasmid-carrying or plasmid-free cells—provide the necessary balance to maintain responses that are roughly insensitive to the total cell density [23,24]. Functionally, the yeast and *E. faecalis* systems regulate costly mating induction. As the ratio is a proxy for the likelihood of a successful random encounter with a mating partner, measuring it and acting accordingly avoids unproductive activation when mating chances are low. In a more distant example, the mammalian bone morphogenetic protein (BMP) signaling pathway can specifically compute the ratio of two particular BMP ligands (Figure 1E). This capacity directly arises from competitive receptor–ligand interactions [25]. The signals could potentially be produced by two specific cell types, and the circuit’s output could therefore report their ratio. Finally, a synthetic intercellular toggle-switch system can also function as a ratiometric sensing circuit [26] (Figure 1F). The system is designed to switch on or off depending on which cell type is in the majority. The output is effectively linearly dependent on the cell fraction for defined periods of time, making this system a potentially useful ratio sensor.

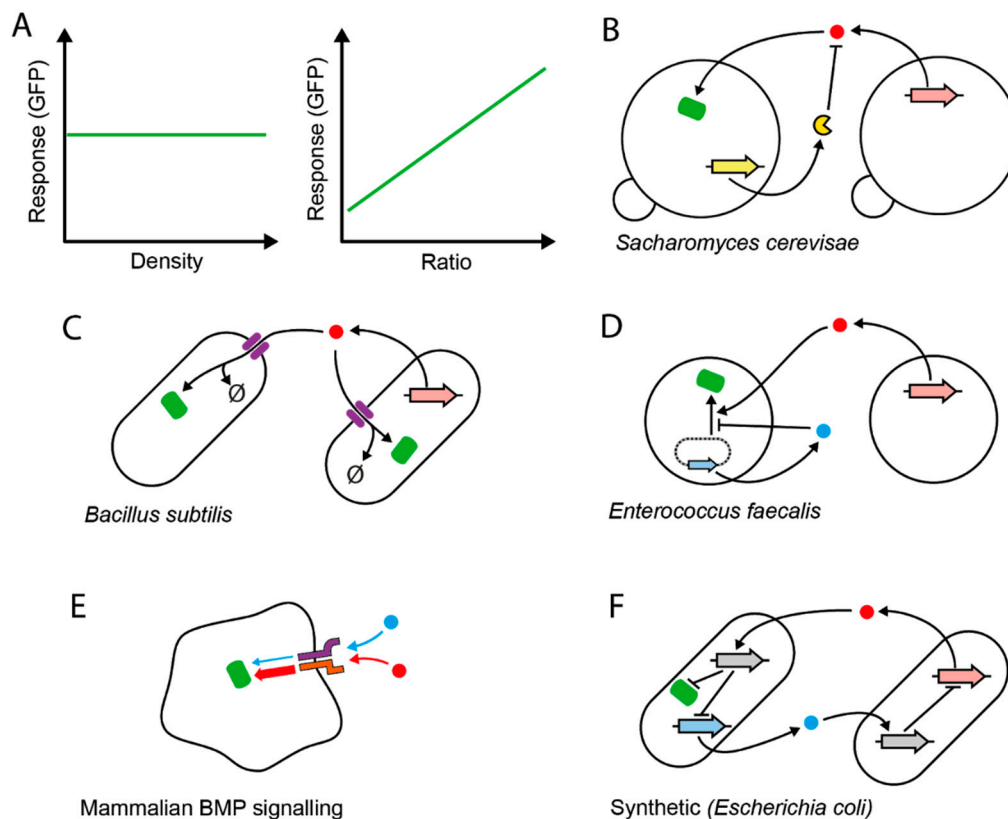


**Figure 1.** Relative sensing of population parameters. (A) Theoretical perfect ratio sensing. The mean gene expression output of a reporter population (Response) is insensitive to changes in the total density

of the co-culture, but sensitive to the relative abundance of the individual populations. (B–D) Natural microbial intercellular signaling networks composed of distinct cell populations that perform ratio sensing. A stimulatory signal (red circle) accumulates in the media in proportion to the density of the signal emitter and stimulates green fluorescent protein (GFP) production (green). The concentration of the signal also depends on antagonistic activity, which balances out activation. For this, *S. cerevisiae* (B) uses an extracellular protease (yellow), which directly degrades the signal produced by partner cells. *B. subtilis* (C) depletes the signal by internalizing it through active pumps (purple) and degrading it ( $\emptyset$  symbol) internally. In *Enterococcus faecalis* (D), cells carrying a conjugative plasmid (dotted line) produce an inhibitory signal (blue circle) from a plasmidial gene (blue arrow), which antagonizes the interaction between the signal produced by plasmid-free cells (red) and its cognate transcription factor (not shown). The thick arrows correspond to the genes encoding the corresponding products. (E) Ratiometric sensing of distinct extracellular signals in mammalian cells. One of the two signals (blue) forms receptor–signal complexes with low activity, while the other (red) forms high-activity complexes, such that one signal (blue) competitively inhibits activation by the other stronger ligand (red). Receptors are represented by the purple and orange symbols. Thick and thin arrows pointing to GFP (green) represent high and low activity of the receptor complexes, respectively. (F) Synthetic intercellular toggle switch. Signals (blue and red) produced by each cell from their respective genes (thick blue and red arrows, respectively) inhibit the production of signals by the other cell in a co-repressive circuit, via signal-specific expression of a transcriptional repressor (its coding gene is shown in grey). In this case, the per-cell output level is directly proportional to the ratio of the blue signal-producing strain to the red signal-producing strain (“majority wins”). The opposite pattern (“minority wins”) can be obtained by changing the circuit such that GFP is directly inducible by the red signal instead of repressed by the induced transcription factor (grey).

These systems share the general need for opposing activities, and do not necessarily require feedback motifs in their circuitry for their basic operation. Importantly for synthetic biology, these circuit topologies can potentially allow a two-cell population to inform a downstream process about which cell type is in the majority, and with varying degrees of precision, the current fraction of cells. Conversely, if linked to expression of growth-determining genes, this system could enable control of the ratio itself, with applications in microbial consortia with precise cellular-stoichiometry needs.

### 3. Synthetic Population Control

Natural microbial consortia exemplify how multi-organismic communities achieve robustness to environmental fluctuations by augmenting metabolic capacity through division of labor, and have inspired recent research to rationally design synthetic microbial consortia [27]. Similarly, synthetic consortia can be engineered to distribute the cost of heterologous expression of metabolic pathways, compartmentalize competing cross-inhibiting yet complementary pathways, and expand their metabolic capabilities compared to monocultures [28]. One potential application for synthetic sensors of relative population composition is to help create synthetic microbial consortia with a stable cellular composition. This is important for any process where the stoichiometry of the different activities performed by corresponding cells is determinant for optimal performance of the whole. However, current approaches generally suffer from long-term instability, as competition for resources and exponential growth drive the composition out of balance [29]. Recent attempts using cell lysis to control binary populations demonstrated higher stability [30]—yet can result in undesired proteins and other components in the spent cultures, which crucially limits the purity of the end-products for bioproduction applications. Moreover, this approach only works with highly biased initial cell ratios, as one population quickly overtakes the other when added at equal initial densities. Furthermore, much biomass (and therefore energy) is sacrificed for the benefit of population stability.

We argue that a microbial consortium with autonomous, robust control of cellular stoichiometry—a *ratiostat*—could be constructed, at least in its simplest form (two-cell population), by with two different strategies. First, synthetic circuits inspired by the ratiometers (Figure 1) could be constructed. This is increasingly possible thanks to the availability of several orthogonal (non-crosstalking) communication

channels for synthetic biology, where up to six separate orthogonal channels have been implemented at one in bacteria [31–34]. Since the ratiometer's readout ignores fluctuations in total cell density and provides precise composition measures for downstream processes, linking such output to cellular growth actuators provides an opportunity to attain stable compositions because responsive cells could induce growth according to current ratio measurements, e.g., if their fraction drops below a certain value. Second, there is also the possibility to build *ratiostats* through external control, by delocalizing the circuit complexity within a computer/algorithm and directly control cell growth. The advantage of computers is the possibility to control the composition of communities with several members more easily, as a single input to directly control growth in each population is needed. Both these strategies can be implemented using the cybergenetics framework, which brings useful tools from control theory to guide the design of the synthetic circuits.

#### 4. Cybergenetic Control

Cybergenetics, the interface between synthetic biology and control theory, enables different types of control strategies, including external and internal control of biological circuits [35–37]. External control aims to regulate cell cultures, single cells, or complex cell assemblies through computer-assisted feedback. Specifically, information collected on a particular cellular state or states (e.g., a fluorescent protein that reports a signaling pathway output) is used to compute an appropriate intervention through chemical or physical inputs that change the cell to a new desired state in real-time. The computer measures these outputs dynamically and makes decisions on the timing and intensity of subsequent inputs; these decisions are dictated by a control algorithm that can vary in complexity. On the other hand, internal control uses DNA-encoded small regulatory networks containing feedback structures for a similar purpose. Although cybergenetics has not been explored extensively as a means of control and design intercellular circuits, its current use to control intracellular circuits can serve as guidance for such purpose. Thus, here we show some available examples. Cybergenetics has increasingly been used as a strategy to apply automated dynamic control for bioproduction [38,39], in this section however, we rather focus on the fundamental aspects of control; namely, how cybergenetics provides insight into natural biological behaviors and the initial steps required to control complex functions in synthetic systems.

##### 4.1. External (Computer-Aided) Control

Computer-assisted feedback control (Figure 2A) provides an experimental platform to interrogate biological systems in unprecedented ways. Dynamic compensation represents one example of the cybergenetic approach to this issue [40] (Figure 2B). To understand the role of feedback regulatory elements in biological signal transduction, biologists have traditionally relied on gene-knockouts and genetic complementation. Dynamic compensation allows such complementation to be dynamically modulated in real-time. This approach was used to explore the roles of the various negative feedbacks that act on upstream elements of a prototypical MAPK signaling pathway in *S. cerevisiae*. By optogenetically inducing various elements via a real-time control loop, the authors revealed the dynamic requirements that such feedback processes must possess to preserve wild-type function. These requirements varied depending on the element studied; for example, the phosphatase Msg5 had to be provided in pulses to recover wild-type function, whereas the negative regulator of G protein signaling Sst2 did not have any dynamic requirements, and a constant step input sufficed. Similar approaches have yielded insight into transcriptional dynamics using spatiotemporal delivery of inputs [41], spatiotemporal control of gene expression in multiple single cells [42] and virtual pattern formation [43].

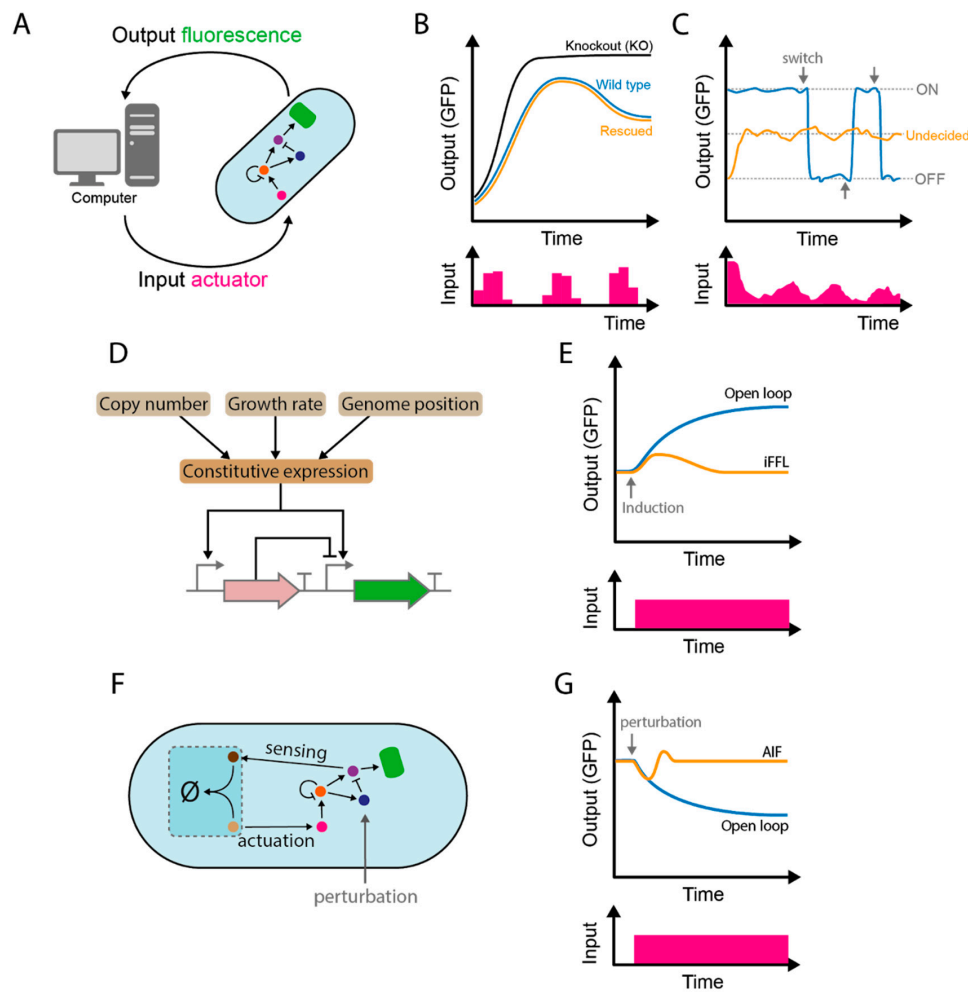


**Figure 2.** Internal and external control strategies from cybergenetics. **(A)** Computer-aided control. A network of interacting molecular components (circles) with a fluorescent protein output (green) interacts with a computer, which measures and acts on the output by delivering network inputs. **(B)** Dynamic compensation. Native (blue) and negative-feedback knockout (black) outputs for a signaling pathway, compared to computer-controlled negative feedback expression (orange). In this case, regular input pulses (bottom) restored wild-type behavior. **(C)** Application of external control to maintain a bistable system—in this case, a synthetic toggle switch circuit—close to its unstable equilibrium point. The circuit is switched on or off (blue) using two specific chemicals (arrows). By maintaining one input at roughly constant levels (not shown) and adding the other periodically (bottom), the system is maintained at its unstable point and remains undecided (orange). **(D)** Incoherent feed-forward loop (IFFL) based robust constitutive expression. Constitutive expression machinery activates the target gene (green, GFP) and its repressor gene (pink, transcription-activator-like effector (TALE) protein); the repressor gene is encoded upstream in the cassette and binds non-cooperatively to the target gene. Promoters and terminators are represented by right-angled and T-shaped lines, respectively. Sources of perturbations in the capacity for constitutive expression are shown in the upper three boxes. **(E)** Adaptation of output levels to an induced step increase (bottom) in the copy number of the incoherent feed-forward loop cassette (IFFL, orange) and a regular non-feedback system (blue). **(F)** A biomolecular (embedded) antithetic integral feedback controller based on inactivation ( $\emptyset$ ) by molecular titration (darker blue square, see text) controls the network, which reports a fluorescent output (as in A). The setpoint is determined by the ratio of the titrated elements (brown and beige circles). **(G)** Robust perfect adaptation of the antithetic integral feedback controller (AIF). Normally, a perturbation (a step function that activates degradation of circuit component; bottom) brings the system to a new steady state (blue). Using the control loop, the system is brought back to its set point (orange).

External control has also enabled the exploration of states normally not maintained by cells for long; for example, maintaining a bistable molecular circuit in its unstable transition state. Lugagne et al. [44] used a synthetic toggle switch in *E. coli* to demonstrate the feasibility of this approach (Figure 2C). The system has two stable equilibrium points that can be switched by the addition of specific chemical signals, and one unstable equilibrium point corresponding to an “undecided” state. Using these inputs and by following the behavior of single cells in a microfluidic device, the system could be periodically forced to maintain the undecided state. This approach provided a proof-of-principle that could allow, for example, the study of transient cellular states such as cell differentiation or malignant transformation at high sample sizes for quantitative analyses. Further theoretical developments in this area include an improved robust version of periodic forcing through integral feedback [45] and ratio control [46], where rather than keeping a toggle switch undecided, computer feedback controls the proportions of cells in each of the two states.

#### 4.2. Internal Cybergenetic Control

Internal control relies on the addition of control structures to synthetic circuits. Implementation of robust perfect adaptation (Section 2.1) is one way to increase the performance of synthetic circuits through internal control. For example, IFFLs [47,48] have been used to ensure constant levels of chromosome-inserted circuit components that are otherwise highly susceptible to variation in the genetic context or variation in genetic dosages due to multiple insertions (Figure 2D,E). In one example [49], the authors used an IFFL strategy based on compensatory non-cooperative transcriptional inhibition provided by transcription-activator-like effectors (TALEs). Similarly, synthetic circuits that combine an IFFL with negative feedback in mammalian cells enable robust gene expression against gene dosage variations [49].

Antithetic integral feedback [50,51] is another circuit that allows perfect adaptation (Figure 2D). The antithetic integral feedback circuit is a synthetic biological implementation (in *E. coli*) of a generalized model born from control theory, but nevertheless present in natural signaling pathways [8]. Rigorous mathematical treatment of robust perfect adaptation mediated by antithetic integral feedback shows that, if the technical challenges of implementation can be overcome, this strategy can eventually keep any cellular output of choice at steady levels. The feedback can be embedded in any arbitrary intracellular network with noisy dynamics, and the user-defined setpoint for the output will remain robust to a broad range of biochemical parameter values. Implementation of the antithetic control strategy crucially relies on proteins that stoichiometrically inactivate each other, such as those already proven useful in synthetic circuits [52,53]. In the antithetic controller, such molecular titration is achieved using the SigW/RsiW  $\sigma$ -factor/anti- $\sigma$ -factor system from *Bacillus subtilis* [54,55]. The  $\sigma$ -factor SigW, which determines the output of the circuit (a fluorescent protein), is inactivated by the anti- $\sigma$ -factor RsiW. The levels of SigW are determined by chemical activation of its constitutively expressed transcription factor. On the other hand, the inactivating counterpart is expressed in proportion to the levels of its own specific transcription factor, which can also be chemically activated. As both transcriptional regulators can be independently tuned, and output levels rely on the stoichiometry of the titrated partners (available free SigW), a setpoint for the output can be determined externally.

Proposed extensions of the antithetic integral feedback controller include a biomolecular proportional-integral-derivative controller, also inspired by control theory [56], and a cellular (rather than embedded) antithetic feedback controller composed of two cell types controlling the state of a third cell type [57]. Interestingly, an integral feedback controller has also been constructed in vitro, opening yet another avenue of cell-free regulation in synthetic biology [58]. Moreover, antithetic control was shown to ensure optimal biofuel production without knowledge of the system's parameters [59].

## 5. Interactions between Controllers and Natural Populations

The robustness strategies outlined above could be implemented in both intra and intercellular circuits for the improved robustness (and performance) of synthetic microbes used to directly intervene

natural ecosystems (Figure 3A). For example, therapeutic microbes promise to provide innovative means for diagnosing or treating infection, cancer and other diseases using cells reprogrammed to perform specific functions. Important advances have been made in this field; for example, detection of cancer in mice using orally consumed reporter bacteria that produce an easy-to-read colorimetric output in urine [60] or several systems for drug delivery using bacterial lysis, e.g., to release nanobodies in the tumor microenvironment—inducing tumor regression in mice [61]—to synchronize cyclic delivery of drugs [62], and to kill a human pathogen using a species-specific antibiotic [63]. These microbes must sense and respond to dynamically changing environments and noisy signals, and therefore could benefit from robust circuit design. One way of improving the performance of microbes with engineered behaviors is to use external computer control to monitor and aid their stability and action, namely, by detecting properties of target cells, synthetic microbes provide externally measurable outputs that in turn guide external intervention, e.g., adding more sensors or a specific drug (Figure 3B). Here we rather focus on engineering microbes capable of performing tasks autonomously, i.e., of displaying specific engineered behaviors by robust intra- and intercellular circuit design only.

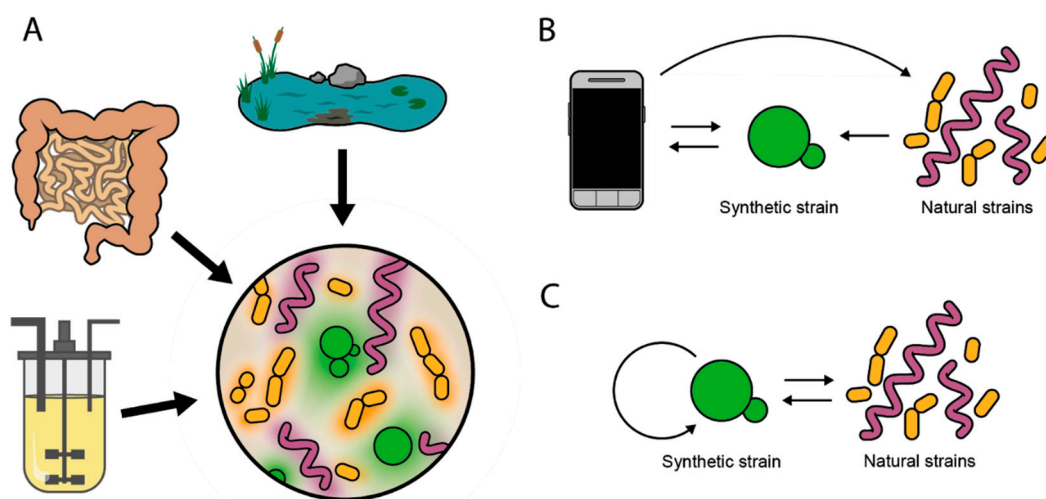


**Figure 3.** Ecosystem intervention. (A) Various ecosystems such as a natural water source, the human gut, or a bioreactor are susceptible to interventions using engineered cell populations to enable, e.g., remediation, therapy, or optimization processes, respectively. The engineered cells (green) coexist and interact with the natural microbiota (purple and yellow) via secreted molecules (corresponding colored halos around cells). (B) External control. Synthetic cells (center) can detect and report specific properties of the natural population (right). Data collection and computer-aided analysis (left) can be used to modify the detector itself (e.g., replenish the detector strain to avoid its extinction) or the natural population (e.g., add a specific dose of a species-specific toxin). (C) Internal control. The synthetic cell interacts bidirectionally with the natural microbiota. Using the information collected, the synthetic cell can both control itself (e.g., maintain its relative abundance) and the natural system (e.g., secrete killing agents).

Synthetic pathogen-seekers are an interesting case of intracellular circuit susceptible to improvements by robust design. In one example [64], bacteria effectively followed gradients via a cleverly intervened chemotaxis system, where inputs enter the network transcriptionally—by inducing expression of the key phosphatase CheZ—rather than interacting with specific receptors, as natural chemoattractants do. Interestingly, this shows that an arbitrary signaling pathway with a transcriptional output could enable a sensed extracellular molecule to function as a chemoattractant, widening the spectrum of possibilities for engineering chemotaxis towards unnatural substrates, beyond the use of chemotaxis receptor engineering. Although promising, the narrow range of concentrations in which the protein CheZ must operate in the synthetic system [64] limits its performance. This provides an opportunity for robust control strategies to ensure its expression remains constant at the desired basal

levels by, for example, ensuring perfect adaptation of CheZ levels through co-induced (as the case in Figure 2D,E)—rather than constitutive (as in the cited work)—antagonistic action (CheZ degradation). This could eventually bring engineered chemotaxis closer to wild type performance.

Intercellular robust circuits in the context of therapeutic microbes are a more exploratory idea. For example, engineered robustness could improve “controller cells” that interact with native populations in their ecosystem. Controller cells could potentially sense chemical cues produced naturally by microbial communities—which has become increasingly possible through engineered metabolite sensing [65]—and respond to achieve or restore specific states in the target population (e.g., specific pathogen killing) (Figure 3C). For such purpose, controller cells must first prevent their own extinction, ensure that their action only happens when in the majority (e.g., for effective killing) and activate suicide (e.g., for clearance). A controller-cell population—adapted to its target environment (as in [66])—equipped with ratiometric capacities (Section 2.2) could help to achieve the three tasks, by preventing its extinction by activating fast growth when in the minority, and activating lysis to release a specific toxin when in the majority.

## 6. Conclusions

Natural biochemical robust signaling networks keep constancy in the levels of specific outputs, with such levels being naturally selected in their native operating environments. Molecular sensory pathways integrate the information provided by signals that transiently alter those levels, to generate biologically meaningful responses. Therefore, the construction of synthetic cells that interact with complex ecosystems might benefit from the implementation of similar robust computational capabilities. With the limited amount of adequate signals that synthetic microbes can be engineered to sense in such scenario, the specific computation made is crucial, as signals can inform various relevant parameters of the physical and “social” environment [67,68]. In this sense, the relative sensing strategies presented, provide useful inspiration for designing circuits for effective interactions between synthetic cells and natural ecosystems. Making such interactions functional and safe in natural scenarios is however a difficult task. The advances presented here suggest that a way forward is to, starting from a niche-adapted chassis and robust circuit design, place computer algorithms in the control loop and force the microbe’s correct performance. By understanding the computer feedbacks necessary for such semi-autonomous display, we might in turn understand what is needed for synthetic circuits to improve both the cell’s autonomous behavior and capacity to die when necessary.

**Author Contributions:** Writing—original draft preparation, A.B., M.L.B., C.C. and P.H.; writing—review and editing, A.B., P.H. All authors read and agreed to the published version of the manuscript.

**Funding:** This research was funded by the European Research Council grant SmartCells (724813), the European FET OPEN grant Cosybio (766840), and the following grants from the French National Research Agency: ANR-16-CE33-0018, ANR-11-LABX-0038 and ANR-10-IDEX-0001-02.

**Acknowledgments:** We thank Ariel Lindner and Sylvain Pouzet for helpful discussions.

**Conflicts of Interest:** The authors declare no conflict of interest. The funders had no role in the design of the study; in the collection, analyses, or interpretation of data; in the writing of the manuscript, or in the decision to publish the results.

## References

1. Wood, J.M. Bacterial osmoregulation: A paradigm for the study of cellular homeostasis. *Annu. Rev. Microbiol.* **2011**, *65*, 215–238. [[CrossRef](#)] [[PubMed](#)]
2. van den Berg, J.; Boersma, A.J.; Poolman, B. Microorganisms maintain crowding homeostasis. *Nat. Rev. Microbiol.* **2017**, *15*, 309–318. [[CrossRef](#)] [[PubMed](#)]
3. Kitano, H. Towards a theory of biological robustness. *Mol. Syst. Biol.* **2007**, *3*, 137. [[CrossRef](#)]
4. Masei, J.; Siegal, M.L. Robustness: Mechanisms and consequences. *Trends Genet.* **2009**, *25*, 395–403. [[CrossRef](#)]
5. Khammash, M. An engineering viewpoint on biological robustness. *BMC Biol.* **2016**, *14*, 22. [[CrossRef](#)]

6. Arkin, A.P. A wise consistency: Engineering biology for conformity, reliability, predictability. *Curr. Opin. Chem. Biol.* **2013**, *17*, 893–901. [[CrossRef](#)]
7. Xie, M.; Fussenegger, M. Designing cell function: Assembly of synthetic gene circuits for cell biology applications. *Nat. Rev. Mol. Cell Biol.* **2018**, *19*, 507–525. [[CrossRef](#)]
8. Yi, T.M.; Huang, Y.; Simon, M.I.; Doyle, J. Robust perfect adaptation in bacterial chemotaxis through integral feedback control. *Proc. Natl. Acad. Sci. USA* **2000**, *97*, 4649–4653. [[CrossRef](#)]
9. Barkai, N.; Leibler, S. Robustness in simple biochemical networks. *Nature* **1997**, *387*, 913–917. [[CrossRef](#)] [[PubMed](#)]
10. Alon, U.; Surette, M.G.; Barkai, N.; Leibler, S. Robustness in bacterial chemotaxis. *Nature* **1999**, *397*, 168–171. [[CrossRef](#)]
11. Adler, M.; Mayo, A.; Alon, U. Logarithmic and power law input-output relations in sensory systems with fold-change detection. *PLoS Comput. Biol.* **2014**, *10*, e1003781. [[CrossRef](#)] [[PubMed](#)]
12. Ferrell, J.E. Signaling Motifs and Weber's Law. *Mol. Cell* **2009**, *36*, 724–727. [[CrossRef](#)] [[PubMed](#)]
13. Daniel, R.; Rubens, J.R.; Sarpeshkar, R.; Lu, T.K. Synthetic analog computation in living cells. *Nature* **2013**, *497*, 619–623. [[CrossRef](#)] [[PubMed](#)]
14. Colin, R.; Sourjik, V. Emergent properties of bacterial chemotaxis pathway. *Curr. Opin. Microbiol.* **2017**, *39*, 24–33. [[CrossRef](#)]
15. Kalinin, Y.V.; Jiang, L.; Tu, Y.; Wu, M. Logarithmic sensing in Escherichia coli bacterial chemotaxis. *Biophys. J.* **2009**, *96*, 2439–2448. [[CrossRef](#)]
16. Sourjik, V.; Wingreen, N.S. Responding to chemical gradients: Bacterial chemotaxis. *Curr. Opin. Cell Biol.* **2012**, *24*, 262–268. [[CrossRef](#)]
17. Shoval, O.; Goentoro, L.; Hart, Y.; Mayo, A.; Sontag, E.; Alon, U. Fold-change detection and scalar symmetry of sensory input fields. *Proc. Natl. Acad. Sci. USA* **2010**, *107*, 15995–16000. [[CrossRef](#)]
18. Goentoro, L.; Shoval, O.; Kirschner, M.W.; Alon, U. The incoherent feedforward loop can provide fold-change detection in gene regulation. *Mol. Cell* **2009**, *36*, 894–899. [[CrossRef](#)]
19. Adler, M.; Alon, U. Fold-change detection in biological systems. *Curr. Opin. Syst. Biol.* **2018**, *8*, 81–89. [[CrossRef](#)]
20. Kim, J.; Khetarpal, I.; Sen, S.; Murray, R.M. Synthetic circuit for exact adaptation and fold-change detection. *Nucleic Acids Res.* **2014**, *42*, 6078–6089. [[CrossRef](#)]
21. Banderas, A.; Koltai, M.; Anders, A.; Sourjik, V. Sensory input attenuation allows predictive sexual response in yeast. *Nat. Commun.* **2016**, *7*, 12590. [[CrossRef](#)] [[PubMed](#)]
22. Babel, H.; Naranjo-Meneses, P.; Trauth, S.; Schulmeister, S.; Malengo, G.; Sourjik, V.; Bischofs, I.B. Ratiometric population sensing by a pump-probe signaling system in *Bacillus subtilis*. *Nat. Commun.* **2020**, *11*, 1176. [[CrossRef](#)] [[PubMed](#)]
23. Banderas, A.; Carcano, A.; Sia, E.; Li, S.; Lindner, A.B. Ratiometric quorum sensing governs the trade-off between bacterial vertical and horizontal antibiotic resistance propagation. *PLoS Biol.* **2020**, *18*, e3000814. [[CrossRef](#)] [[PubMed](#)]
24. Chatterjee, A.; Cook, L.C.C.; Shu, C.-C.; Chen, Y.; Manias, D.A.; Ramkrishna, D.; Dunny, G.M.; Hu, W.-S. Antagonistic self-sensing and mate-sensing signaling controls antibiotic-resistance transfer. *Proc. Natl. Acad. Sci. USA* **2013**, *110*, 7086–7090. [[CrossRef](#)] [[PubMed](#)]
25. Antebi, Y.E.; Linton, J.M.; Klumpe, H.; Bintu, B.; Gong, M.; Su, C.; McCardell, R.; Elowitz, M.B. Combinatorial Signal Perception in the BMP Pathway. *Cell* **2017**, *170*, 1184–1196. [[CrossRef](#)] [[PubMed](#)]
26. Alnahhas, R.N.; Sadeghpour, M.; Chen, Y.; Frey, A.A.; Ott, W.; Josić, K.; Bennett, M.R. Majority sensing in synthetic microbial consortia. *Nat. Commun.* **2020**, *11*, 3659. [[CrossRef](#)]
27. Giri, S.; Shitut, S.; Kost, C. Harnessing ecological and evolutionary principles to guide the design of microbial production consortia. *Curr. Opin. Biotechnol.* **2020**, *62*, 228–238. [[CrossRef](#)]
28. McCarty, N.S.; Ledesma-Amaro, R. Synthetic Biology Tools to Engineer Microbial Communities for Biotechnology. *Trends Biotechnol.* **2019**, *37*, 181–197. [[CrossRef](#)]
29. Mee, M.T.; Collins, J.J.; Church, G.M.; Wang, H.H. Syntrophic exchange in synthetic microbial communities. *Proc. Natl. Acad. Sci. USA* **2014**, *111*, E2149–E2156. [[CrossRef](#)]
30. Scott, S.R.; Din, M.O.; Bittihn, P.; Xiong, L.; Tsimring, L.S.; Hasty, J. A stabilized microbial ecosystem of self-limiting bacteria using synthetic quorum-regulated lysis. *Nat. Microbiol.* **2017**, *2*, 17083. [[CrossRef](#)]



31. Du, P.; Zhao, H.; Zhang, H.; Wang, R.; Huang, J.; Tian, Y.; Luo, X.; Luo, X.; Wang, M.; Xiang, Y.; et al. De novo design of an intercellular signaling toolbox for multi-channel cell-cell communication and biological computation. *Nat. Commun.* **2020**, *11*, 4226. [[CrossRef](#)] [[PubMed](#)]
32. Jiang, W.; He, X.; Luo, Y.; Mu, Y.; Gu, F.; Liang, Q.; Qi, Q. Two Completely Orthogonal Quorum Sensing Systems with Self-Produced Autoinducers Enable Automatic Delayed Cascade Control. *ACS Synth. Biol.* **2020**, *9*, 2588–2599. [[CrossRef](#)] [[PubMed](#)]
33. Miano, A.; Liao, M.J.; Hasty, J. Inducible cell-to-cell signaling for tunable dynamics in microbial communities. *Nat. Commun.* **2020**, *11*, 1193. [[CrossRef](#)] [[PubMed](#)]
34. Kyllilis, N.; Tuza, Z.A.; Stan, G.-B.; Polizzi, K.M. Tools for engineering coordinated system behaviour in synthetic microbial consortia. *Nat. Commun.* **2018**, *9*, 2677. [[CrossRef](#)]
35. Khammash, M.; Di Bernardo, M.; Di Bernardo, D. Cybergenetics: Theory and Methods for Genetic Control System. In Proceedings of the 2019 IEEE 58th Conference on Decision and Control (CDC), Nice, France, 11–13 December 2019; pp. 916–926.
36. Lugagne, J.-B.; Dunlop, M.J. Cell-machine interfaces for characterizing gene regulatory network dynamics. *Curr. Opin. Syst. Biol.* **2019**, *14*, 1–8. [[CrossRef](#)]
37. Baetica, A.-A.; Westbrook, A.; El-Samad, H. Control theoretical concepts for synthetic and systems biology. *Curr. Opin. Syst. Biol.* **2019**, *14*, 50–57. [[CrossRef](#)]
38. Carrasco-López, C.; García-Echauri, S.A.; Kichuk, T.; Avalos, J.L. Optogenetics and biosensors set the stage for metabolic cybergenetics. *Curr. Opin. Biotechnol.* **2020**, *65*, 296–309. [[CrossRef](#)]
39. Lalwani, M.A.; Zhao, E.M.; Avalos, J.L. Current and future modalities of dynamic control in metabolic engineering. *Curr. Opin. Biotechnol.* **2018**, *52*, 56–65. [[CrossRef](#)]
40. Harrigan, P.; Madhani, H.D.; El-Samad, H. Real-Time Genetic Compensation Defines the Dynamic Demands of Feedback Control. *Cell* **2018**, *175*, 877–886. [[CrossRef](#)]
41. Rullan, M.; Benzinger, D.; Schmidt, G.W.; Miliias-Argeitis, A.; Khammash, M. An Optogenetic Platform for Real-Time, Single-Cell Interrogation of Stochastic Transcriptional Regulation. *Mol. Cell* **2018**, *70*, 745–756. [[CrossRef](#)]
42. Chait, R.; Ruess, J.; Bergmiller, T.; Tkačik, G.; Guet, C.C. Shaping bacterial population behavior through computer-interfaced control of individual cells. *Nat. Commun.* **2017**, *8*, 1535. [[CrossRef](#)] [[PubMed](#)]
43. Perkins, M.L.; Benzinger, D.; Arcak, M.; Khammash, M. Cell-in-the-loop pattern formation with optogenetically emulated cell-to-cell signaling. *Nat. Commun.* **2020**, *11*, 1355. [[CrossRef](#)]
44. Lugagne, J.-B.; Sosa Carrillo, S.; Kirch, M.; Köhler, A.; Batt, G.; Hersen, P. Balancing a genetic toggle switch by real-time feedback control and periodic forcing. *Nat. Commun.* **2017**, *8*, 1671. [[CrossRef](#)] [[PubMed](#)]
45. Guarino, A.; Fiore, D.; Salzano, D.; di Bernardo, M. Balancing Cell Populations Endowed with a Synthetic Toggle Switch via Adaptive Pulsatile Feedback Control. *ACS Synth. Biol.* **2020**, *9*, 793–803. [[CrossRef](#)] [[PubMed](#)]
46. Salzano, D.; Fiore, D.; di Bernardo, M. Ratiometric control for differentiation of cell populations endowed with synthetic toggle switches. In Proceedings of the 2019 IEEE 58th Conference on Decision and Control (CDC), Nice, France, 11–13 December 2019.
47. Mangan, S.; Alon, U. Structure and function of the feed-forward loop network motif. *Proc. Natl. Acad. Sci. USA* **2003**, *100*, 11980–11985. [[CrossRef](#)]
48. Segall-Shapiro, T.H.; Sontag, E.D.; Voigt, C.A. Engineered promoters enable constant gene expression at any copy number in bacteria. *Nat. Biotechnol.* **2018**, *36*, 352–358. [[CrossRef](#)]
49. Lillacci, G.; Benenson, Y.; Khammash, M. Synthetic control systems for high performance gene expression in mammalian cells. *Nucleic Acids Res.* **2018**, *46*, 9855–9863. [[CrossRef](#)]
50. Briat, C.; Gupta, A.; Khammash, M. Antithetic Integral Feedback Ensures Robust Perfect Adaptation in Noisy Biomolecular Networks. *Cell Syst.* **2016**, *2*, 15–26. [[CrossRef](#)]
51. Aoki, S.K.; Lillacci, G.; Gupta, A.; Baumschlager, A.; Schweingruber, D.; Khammash, M. A universal biomolecular integral feedback controller for robust perfect adaptation. *Nature* **2019**, *570*, 533–537. [[CrossRef](#)]
52. Hsiao, V.; de los Santos, E.L.C.; Whitaker, W.R.; Dueber, J.E.; Murray, R.M. Design and implementation of a biomolecular concentration tracker. *ACS Synth. Biol.* **2015**, *4*, 150–161. [[CrossRef](#)]
53. Chen, D.; Arkin, A.P. Sequestration-based bistability enables tuning of the switching boundaries and design of a latch. *Mol. Syst. Biol.* **2012**, *8*, 620. [[CrossRef](#)] [[PubMed](#)]

54. Devkota, S.R.; Kwon, E.; Ha, S.C.; Chang, H.W.; Kim, D.Y. Structural insights into the regulation of *Bacillus subtilis* SigW activity by anti-sigma RsiW. *PLoS ONE* **2017**, *12*, e0174284. [[CrossRef](#)] [[PubMed](#)]
55. Schöbel, S.; Zellmeier, S.; Schumann, W.; Wiegert, T. The *Bacillus subtilis* sigmaW anti-sigma factor RsiW is degraded by intramembrane proteolysis through YluC. *Mol. Microbiol.* **2004**, *52*, 1091–1105. [[CrossRef](#)] [[PubMed](#)]
56. Chevalier, M.; Gómez-Schiavon, M.; Ng, A.H.; El-Samad, H. Design and Analysis of a Proportional-Integral-Derivative Controller with Biological Molecules. *Cell Syst.* **2019**, *9*, 338–353. [[CrossRef](#)]
57. Fiore, D.; Salzano, D.; Cristòbal-Cóppulo, E.; Olm, J.M.; di Bernardo, M. Multicellular Feedback Control of a Genetic Toggle-Switch in Microbial Consortia. *IEEE Control Syst. Lett.* **2020**, *5*, 151–156. [[CrossRef](#)]
58. Agrawal, D.K.; Marshall, R.; Noireaux, V.; Sontag, E.D. In vitro implementation of robust gene regulation in a synthetic biomolecular integral controller. *Nat. Commun.* **2019**, *10*, 5760. [[CrossRef](#)]
59. Briat, C.; Khammash, M. Perfect Adaptation and Optimal Equilibrium Productivity in a Simple Microbial Biofuel Metabolic Pathway Using Dynamic Integral Control. *ACS Synth. Biol.* **2018**, *7*, 419–431. [[CrossRef](#)]
60. Danino, T.; Prindle, A.; Kwong, G.A.; Skalak, M.; Li, H.; Allen, K.; Hasty, J.; Bhatia, S.N. Programmable probiotics for detection of cancer in urine. *Sci. Transl. Med.* **2015**, *7*, 289ra84. [[CrossRef](#)]
61. Chowdhury, S.; Castro, S.; Coker, C.; Hinchliffe, T.E.; Arpaia, N.; Danino, T. Programmable bacteria induce durable tumor regression and systemic antitumor immunity. *Nat. Med.* **2019**, *25*, 1057–1063. [[CrossRef](#)]
62. Din, M.O.; Danino, T.; Prindle, A.; Skalak, M.; Selimkhanov, J.; Allen, K.; Julio, E.; Atolia, E.; Tsimring, L.S.; Bhatia, S.N.; et al. Synchronized cycles of bacterial lysis for in vivo delivery. *Nature* **2016**, *536*, 81–85. [[CrossRef](#)]
63. Saeidi, N.; Wong, C.K.; Lo, T.-M.; Nguyen, H.X.; Ling, H.; Leong, S.S.J.; Poh, C.L.; Chang, M.W. Engineering microbes to sense and eradicate *Pseudomonas aeruginosa*, a human pathogen. *Mol. Syst. Biol.* **2011**, *7*, 521. [[CrossRef](#)] [[PubMed](#)]
64. Hwang, I.Y.; Tan, M.H.; Koh, E.; Ho, C.L.; Poh, C.L.; Chang, M.W. Reprogramming microbes to be pathogen-seeking killers. *ACS Synth. Biol.* **2014**, *3*, 228–237. [[CrossRef](#)] [[PubMed](#)]
65. Pandi, A.; Koch, M.; Voyvodic, P.L.; Soudier, P.; Bonnet, J.; Kushwaha, M.; Faulon, J.-L. Metabolic perceptrons for neural computing in biological systems. *Nat. Commun.* **2019**, *10*, 3880. [[CrossRef](#)] [[PubMed](#)]
66. Mimee, M.; Tucker, A.C.; Voigt, C.A.; Lu, T.K. Programming a Human Commensal Bacterium, to Sense and Respond to Stimuli in the Murine Gut Microbiota. *Cell Syst.* **2015**, *1*, 62–71. [[CrossRef](#)]
67. Platt, T.G.; Fuqua, C. What's in a name? The semantics of quorum sensing. *Trends Microbiol.* **2010**, *18*, 383–387. [[CrossRef](#)]
68. Youk, H.; Lim, W.A. Secreting and sensing the same molecule allows cells to achieve versatile social behaviors. *Science* **2014**, *343*, 1242782. [[CrossRef](#)]



**Publisher's Note:** MDPI stays neutral with regard to jurisdictional claims in published maps and institutional affiliations.



© 2020 by the authors. Licensee MDPI, Basel, Switzerland. This article is an open access article distributed under the terms and conditions of the Creative Commons Attribution (CC BY) license (<http://creativecommons.org/licenses/by/4.0/>).

Review

# The Promise of Optogenetics for Bioproduction: Dynamic Control Strategies and Scale-Up Instruments

Sylvain Pouzet <sup>1,2,3,\*</sup>, Alvaro Banderas <sup>1,2,3</sup>, Matthias Le Bec <sup>1,2,3</sup> , Thomas Lautier <sup>4,5</sup>, Gilles Truan <sup>4</sup>  and Pascal Hersen <sup>1,2,3,\*</sup>

<sup>1</sup> Laboratoire Physico Chimie Curie, Institut Curie, PSL Research University, CNRS UMR168, 26 rue d'Ulm, 75005 Paris, France; alvaro.banderas@curie.fr (A.B.); matthias.lebec@curie.fr (M.L.B.)

<sup>2</sup> Sorbonne Université, 75005 Paris, France

<sup>3</sup> Laboratoire MSC, UMR7057, Université Paris Diderot-CNRS, 75013 Paris, France

<sup>4</sup> Toulouse Biotechnology Institute, Université de Toulouse, CNRS, INRAE, INSA, 31400 Toulouse, France; thomas.lautier@insa-toulouse.fr (T.L.); gilles.truan@insa-toulouse.fr (G.T.)

<sup>5</sup> Singapore Institute of Food and Biotechnology Innovation, Agency for Science Technology and Research, Singapore 138673, Singapore

\* Correspondence: sylvain.pouzet@curie.fr (S.P.); pascal.hersen@curie.fr (P.H.)

Received: 13 October 2020; Accepted: 19 November 2020; Published: 24 November 2020



**Abstract:** Progress in metabolic engineering and synthetic and systems biology has made bioproduction an increasingly attractive and competitive strategy for synthesizing biomolecules, recombinant proteins and biofuels from renewable feedstocks. Yet, due to poor productivity, it remains difficult to make a bioproduction process economically viable at large scale. Achieving dynamic control of cellular processes could lead to even better yields by balancing the two characteristic phases of bioproduction, namely, growth *versus* production, which lie at the heart of a trade-off that substantially impacts productivity. The versatility and controllability offered by light will be a key element in attaining the level of control desired. The popularity of light-mediated control is increasing, with an expanding repertoire of optogenetic systems for novel applications, and many optogenetic devices have been designed to test optogenetic strains at various culture scales for bioproduction objectives. In this review, we aim to highlight the most important advances in this direction. We discuss how optogenetics is currently applied to control metabolism in the context of bioproduction, describe the optogenetic instruments and devices used at the laboratory scale for strain development, and explore how current industrial-scale bioproduction processes could be adapted for optogenetics or could benefit from existing photobioreactor designs. We then draw attention to the steps that must be undertaken to further optimize the control of biological systems in order to take full advantage of the potential offered by microbial factories.

**Keywords:** bioproduction; biomanufacturing; optogenetics; cybergenetics; dynamic regulation; bioprocess; biotechnology; photobioreactors

## 1. Merging Optogenetics and Bioproduction

### 1.1. Introduction to Bioproduction

Human societies have employed bioproduction since the ancient Egyptians first fermented grapes to produce ethanol for wine. Since then, bioproduction has been employed to address numerous global issues, such as the production of acetone using *Clostridium acetobutylicum* by Chaim Weizmann during World War One, the discovery of penicillin by Alexander Fleming in 1928 and the production of insulin by conventional *Saccharomyces cerevisiae* in the early 1980s [1]. Biomanufactured products have become

ubiquitous components of our daily lives, including therapeutics (antibiotics, hormones [2], vaccines [3]), enzymes (stabilizers and cocktails [4]) and chemicals (amino acids, dyes [5], biodiesel [6]). The rise of systems biology (*omics* tools and databases, bioinformatics, metabolic engineering) and synthetic biology (cloning, metabolic and protein engineering, CRISPR, DNA synthesis) has expanded the possibilities for bioengineering, and sophisticated pathways have been successfully implemented into various cellular chassis; for example, the production of artemisinin [7], cannabinoids [8], and tropane alkaloids such as scopolamine [9]. Similarly to chemistry in the 19th century, biology is now shifting from a descriptive field to a constructive field, and bioproduction holds the potential to play a significant role by enabling the biomanufacturing of affordable medicines, and the sustainable production of high value-added chemicals and biofuels from renewable feedstock.

Despite these advances, biomanufacturing a new product remains challenging in many ways. Advances in systems and synthetic biology, as well as automation using high-throughput robotics, have reduced the time required to successfully produce a molecule or enzyme using a specific chassis. Nonetheless, achieving an economically viable and market-competitive production process using such whole-cell applications can be tricky, due to difficulties with scaling-up, the long duration of process development and the expensive, specific downstream processing steps. Therefore, extensive efforts have been made to optimize bioprocesses for existing engineered strains. The accumulation of the maximal number of producing cells is the first step towards maximizing production yield. However, the production of a molecule of interest will consume cellular resources and may generate toxic intermediaries or by-products. Thus, production often creates a stress or a burden that impairs cells' ability to grow. Such burden can give rise to microbial heterogeneity and evolutionary escape, and lead to poor yields. Two-phase fermentation strategies are frequently implemented in bioreactors to minimize this burden. In the first phase, growth is favored; the production system is "silent" and cells actively divide without producing any heterologous component, allowing biomass to accumulate. In the second phase, production is "unleashed", for example by inducing the expression of the recombinant enzyme or activating a synthetic pathway that leads to the production of the molecule of interest. During this second phase, the total content of metabolic precursors is divided between the cells' endogenous needs and the synthetic pathway. Thus, the decoupling of growth from production—often irreversibly—has become standard in bioproduction, and this strategy is employed at every production scale. The switch from growth to the production phase can be mediated by various inducible promoters that respond to specific cues; for example, a triggered change in temperature [10] or pH [11], or the presence of a specific molecule such as IPTG (in *E. coli*), galactose (in *S. cerevisiae*) or methanol (in *Pichia pastoris*), or other changes in the environment (nutrient depletion, high cell density). Strong, non-reversible inductions are frequently employed; however, more comprehensive and subtle induction patterns are now increasingly preferred. In this context, the use of light as an inducer has attracted interest, given its ability to be finely tuned in space, time and intensity.

Optogenetics, i.e., using light to control cellular processes, is a versatile tool to induce production in industrial microorganisms. Light is a straight-forward output for computer control systems, as it is tunable down to the millisecond scale, reversible, and offers a range of different and compatible signals of various wavelengths. Moreover, light is more easily delivered and removed from bioreactors compared to the extensive media changes that would be required for chemical inducers, it is considered to be rather non-invasive to cells, and it is cheaper than chemical inducers. Only a small number of studies have applied this emerging strategy to bioproduction. However, researchers increasingly acknowledge optogenetics as a promising tool to achieve fine (and even real-time) control of complex biological systems. In this review, we aim to highlight recent advances and explore the limitations of merging optogenetics with bioproduction in the context of simple and more sophisticated bioproduction control strategies. We also discuss recent optogenetic instruments that will help to develop, characterize and control newly built strains, and the potential issues and opportunities that may be encountered during the scale-up of light-controlled bioproduction processes to the industrial scale.

## 1.2. Optogenetics

Light is widely used by biological systems, not only as an energy source, but also as a signal to which they respond in a variety of ways. Bacteria can express different types of photoreceptors to regulate, for example, the synthesis of protective pigments. Bacterial photoreceptors (opsins, LOV domains—blue light; CcaS/CcaR—red and green light) and plant cryptochromes (CRY2-CIB1—blue light), phytochromes (Phy-PIF—red/far-red light), or UV response systems (UVR8-COP1—UV light), form the basis of most optogenetic systems developed to date [12]. Although optogenetics was first used in neurosciences to excite or inhibit specific neurons via light-gated ion channels [13], the technique has recently been extended to other mammalian cell types to study developmental timing and coordination [14], regulatory cascades' responses to dynamic signals [15], and cellular biophysical processes [16]. With respect to microbial systems, numerous optogenetic systems have been developed and used to investigate the protein control of biofilm formation, metabolic flux control (reviewed in [17]) and dynamic regulation of gene expression to dissect pathway dynamics [18]. In non-neural studies, light is used to control protein interactions, which can give rise to various molecular functions (dimerization, relocalization, anchoring, phosphorylation/activation, oligomerization). In the context of bioproduction, it is the transcriptional control resulting from such optogenetic interactions that is mostly employed.

Some optogenetic systems are particularly efficient and versatile. In the pDusk system [19], the histidine kinase YF1 phosphorylates the transcription factor FixJ in the dark, which activates transcription from the *FixK2* promoter. This process is reversed by blue light stimulation. In contrast, to achieve induction upon blue light stimulation, the pDawn system [19] (Figure 1a) was built by adding another regulation step: by placing the lambda phage repressor cI under the control of the *FixK2* promoter, the repressor cI is repressed by light, which enables the activation of the target promoter *pR*. In the PhyB-PIF system [20], the PhyB and PIF proteins dimerize upon red light stimulation (Figure 1b) and dissociate when exposed to far red light. The two photosensitive domains PhyB and PIF are usually fused separately to effector protein domains, typically a DNA-binding domain and a trans-activation domain, to regulate transcription. This interaction requires the presence of the cofactor phycocyanobilin (PCB), which is naturally present in plants, but must be externally added or engineered in microbial systems. In the single-component EL222 system [21] (Figure 1c,f), the engineered EL222 protein (composed of a caged DNA-binding domain, LOV domain and VP16 transactivation domain) homodimerizes upon blue light stimulation, which promotes DNA binding and transcription from the C120 promoter. When the CcaS/CcaR system is stimulated by green light [22] (Figure 1d) in the presence of the cofactor PCB, membrane-bound CcaS phosphorylates the transcription factor CcaR, which activates transcription from the *Cpcg2* promoter. This process is reversed by red light, which therefore prevents transcription. Finally, similar to the PhyB-PIF system, the Cry2 and Cib1 proteins of the CRY2-CIB1 system [23] dimerize upon blue light stimulation (which is reversed in the dark) due to the interaction between photons and the (naturally present) protein cofactor flavin adenine dinucleotide (FAD). Cry2 has also been engineered to self-multimerize upon light stimulation [24], as illustrated in Figure 1e. For more details on these and other optogenetic systems, we recommend consulting [optobase.org](http://optobase.org) [25].

## 1.3. Adapting Induction Systems for Optogenetics

In an effort to adapt current genetic induction systems for bioproduction, several systems have been designed to facilitate the transition of existing industrial organisms from chemical to optogenetic induction without the need for full reconstruction or redesign.

Optogenetic regulation has been achieved in *E. coli* by combining optogenetics with classical IPTG, arabinose or T7 regulation systems. IPTG, the gold standard inducer in *E. coli*, binds the LacI repressor and thus induces the expression of genes containing a *lac* operator in their promoter by preventing LacI from shielding DNA from RNA polymerase. Lalwani et al. [26] (Figure 1a) placed *LacI* under the control of the pDawn system, so that blue light induces *LacI* expression and therefore represses

the genes of interest. In contrast, the absence of light represses *LacI* expression and therefore activates the various IPTG-inducible promoters. This system was optimized to reduce leakiness, and although the expression dynamics are slower than those of IPTG induction systems (2 h delay), the final induction levels are higher and production exceeds that of the IPTG induction systems. Thus, the pDawn system is a successful alternative to IPTG induction, and has already been tested and applied to bioproduction and scaled-up to 2 L [26]. The pDusk and pDawn systems also highlight the possibility of activating or repressing a system by illumination or darkness, depending on how the optogenetic system is connected to the bioproduction system. Similarly, Romano et al. [27] substituted arabinose with light to control the BAD promoter by switching the endogenous dimerization domain of the AraC transcription factor with the VVD blue light optogenetic domains, which dimerize upon blue light stimulation. Thus, this system is compatible with pBAD-based vectors or strains, which are frequently used in smaller-scale studies. Finally, expression control using the T7 promoter is another standard in *E. coli* and is also used in *S. cerevisiae*. Raghavan et al. [28] used a split version of the T7 RNA polymerase (T7RNAP), with each part of split-T7RNAP fused to the N- or C-terminus domain of an intein, and also to either the Phy or PIF component of *Arabidopsis thaliana* phytochrome (see Figure 1b). The red light illumination of the PCB cofactor triggers the Phy-PIF interaction, which allows the intein domains to interact; trans-splicing occurs to deliver a functional T7RNAP that promotes the expression of genes under the control of the T7 promoter. Raghavan et al. successfully used this system to control the production of lycopene in *E. coli*. However, this system relies on the PCB cofactor and is not reversible, since T7RNAP is stabilized once trans-spliced. A similar strategy was used to increase the controllability and simplicity of T7RNAP. Baumschlager et al. [29] created a split version of T7RNAP that heterodimerizes upon blue light illumination due to the presence of engineered VVD domains fused to each T7RNAP termini (“Magnet” domains [30]), to create an Opto-T7RNAP system that exhibits rapid, reversible dynamics. Another version, paT7P-1, was developed by Han et al. [31].

Zhao et al. [32] connected the well-studied galactose regulation system used in the yeast *Saccharomyces cerevisiae* to the EL222 optogenetic system (Figure 1c). The authors first built the simple OPTO-EXP system, in which the protein EL222 induces the transcription of genes controlled by the C120 promoter (more subtle versions of this promoter have since been made and evaluated [33]). Then, to reverse the system and achieve activation in the dark (OPTO-INVRT), Zhao et al. placed *GAL80* under the control of the C120 promoter. In the presence of the (non-naturally) constitutively expressed GAL4 transcription factor, genes under the control of the GAL promoter are expressed in the dark. Upon blue light illumination, GAL80 is expressed and inhibits the activity of GAL4, therefore repressing genes under the control of the GAL promoter. Using both the OPTO-EXP and OPTO-INVRT systems, genes can be actively induced or repressed in a mutually exclusive way given the presence or absence of light, making this bidirectional system particularly versatile. Zhao et al. used this system to achieve dynamic control of isobutanol production up to the 2 L scale at high cell density.

It is worth noting that optogenetic systems have also been implemented in non-conventional microorganisms, such as *Pseudomonas putida* [34], and other chassis already used in industry, such as *Bacillus subtilis* [35]. The widely used yeast *Pichia pastoris* has not, to date, been adapted to optogenetic control, but we expect this to be achieved within a few years. Moreover, widely used synthetic biology systems have also been adapted for optogenetics: photo-inducible CRE recombinases [36] and photosensitive degrons [37] could be used to complement the current optogenetic systems used for bioproduction.

## 2. Control Strategies

### 2.1. Simple Switch for Flux Rewiring

Flux control lies at the heart of bioproduction strategies. To prevent production from impairing the accumulation of biomass, production is inhibited and induced after a growth phase; only then is metabolic flux redirected towards the product of interest. Chemicals or auto-induction systems

have been extensively used to achieve flux control, and optogenetics has the potential to perform at least as well as other methods of induction, while also improving controllability. Using the CcaS/CcaR optogenetic system, Senoo et al. [38] (Figure 1d) and Tandar et al. [39] controlled the expression of the *tpiA* and *pgi* genes, respectively, two important genes that channel metabolite flux towards glycolysis in *E. coli*. Both studies demonstrated enrichment in their respective competing pathways, as expected. To obtain more insight into induction timing, Raghavan et al. [28] used the PhyB-PIF system (Figure 1b) and Lalwani et al. [26] used FixJ (Figure 1a) to explore light induction at different optical densities during growth. Raghavan et al. found that the illumination pulse was most efficient during the late exponential phase of growth, and Lalwani et al. found that constant illumination at an OD of about 1 was optimal. Thus, similarly to chemical inducers, the timing of illumination must be considered in the context of the growth state; the optimal timing may essentially depend on the induction time delay of the optogenetic system, as well as the amount of burden that the cells will experience.

Compartmentalization is another strategy that can be controlled using optogenetics to redirect flux towards a specific metabolite, by using higher-order structures that bring enzymes close to each other to create reversible metabolons inside the cell. Thus, intermediate metabolites are channeled to the next enzymes in the pathway, located in close proximity, which increases the final product yield. Zhao et al. [40] built two systems for this purpose: OptoClusters (Figure 1e) is based on the engineered Cry2olig domain [24], which oligomerizes upon blue light stimulation, fused to the intrinsically disordered region (IDR) FUSN to create a phase-separated synthetic organelle. On the other hand, the PixELLS system (based on PixE/PixD from *Synechocystis* sp. fused to FUSN) loses its phase-separated structure upon blue light stimulation. These two systems form or dissociate droplets within seconds upon light stimulation. After optimization, Zhao et al. demonstrated flux redirection control using the VioC and VioE enzymes fused to the optogenetic components to control deoxyviolacein formation (Figure 1e).

Although light can be used as a simple switch-like inducer, it is its reversibility and high-controllability that makes it a singular tool facilitating the fine-tuning of cell-processes in a dynamic way.

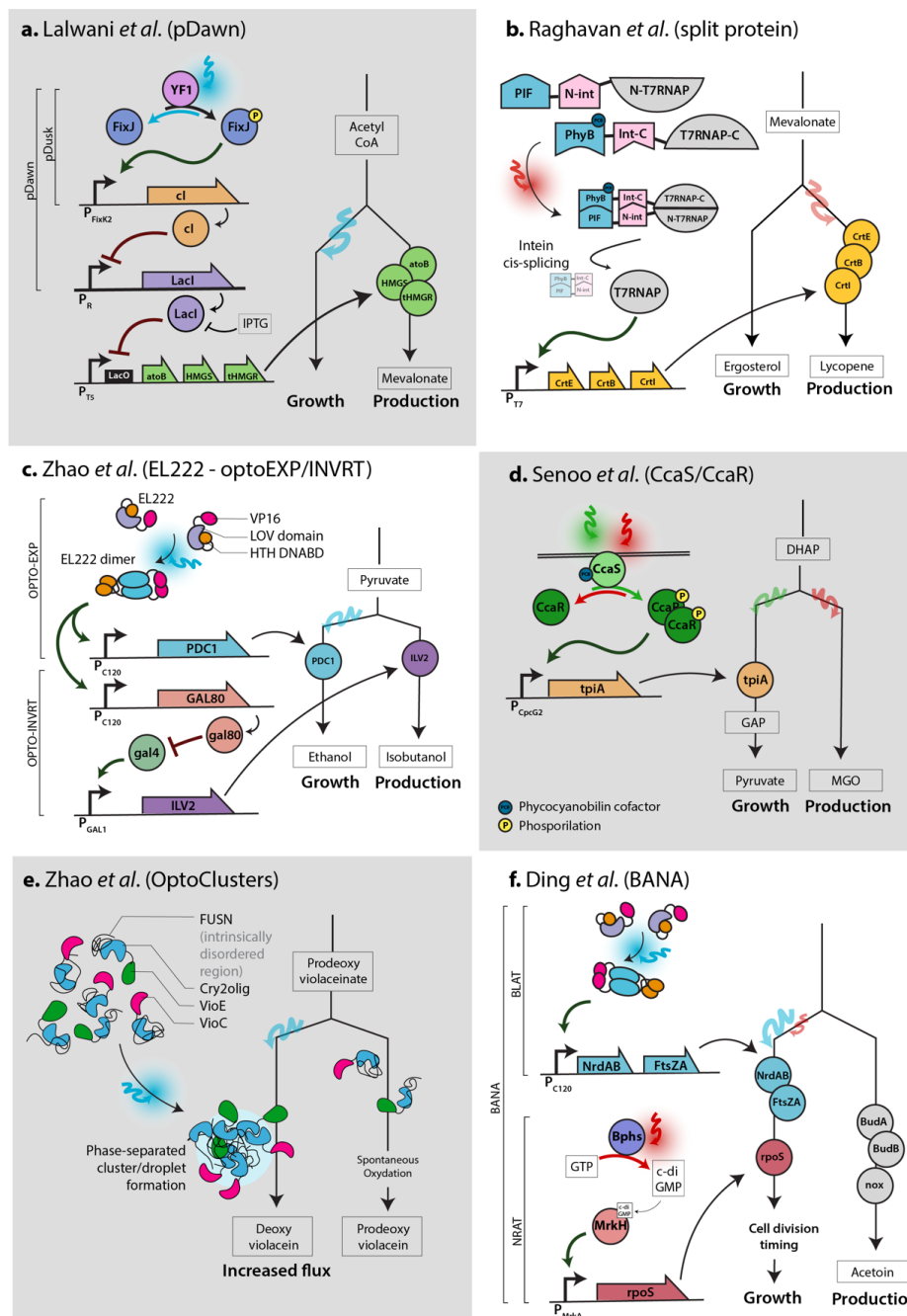


**Figure 1.** Different optogenetic systems can be used to achieve flux control in various ways. Sketch of circuits adapted from each paper. (a). Lalwani et al. [26] controlled mevalonate production using the pDawn system. (b). Raghavan et al. [28] used a light-responsive split T7 RNA polymerase (T7RNAP) to control lycopene production. (c). Zhao et al. [32] used EL222—composed of the VP16 trans-activation domain, light-voltage photosensitive domain (LOV) and helix-turn-helix DNA-binding domain (HTH DNABD)—to dynamically regulate isobutanol production. Blue light stimulation activates gene expression in the OPTO-EXP system, and gene expression in the optoINVRT system is activated in the dark via the GAL regulatory pathway (GAL4 is constitutively expressed in this system). (d). Senoo et al. [38] used the CcaS/CcaR system to regulate glycolysis flux. (e). Zhao et al. [40] developed a light-induced phase-separated cluster formation. Sequential enzymatic reactions are favored in this conformation. (f). Ding et al. [41] used the EL222 and Bphs systems to regulate division timing in *E. coli* to restore the growth rate and improve acetoin production.



## 2.2. Dynamic Switch

Many recent papers mention the possibility of using optogenetic systems to achieve dynamic control over bioproduction. During the production phase, cells may still undergo some growth (or simply maintenance) and experience a burden. However, this trade-off between growth and production can be more closely controlled (Figure 2). This idea was confirmed by studies that used stress-related promoters to modulate the induction of bioproduction systems [42] and lead to increased production. This “host aware” [43] or “burden-driven” strategy shows that dynamic control must be considered, based on the cellular state of the producing cell, in order to improve yields.

Given the ease with which such strategies can be implemented using optogenetics, dynamic control is starting to appear in bioproduction studies. For instance, Lalwani et al. [26] tested the ability of illumination duty cycles to control protein expression levels over a period of about 17 min. They managed to recapitulate a full range of induction strengths (similarly to [33]), which can be very difficult to obtain using chemical inducers (such as IPTG) that induce high expression levels regardless of their concentration, i.e., in a more switch-like manner. Controllability is significant, since strong and sudden induction is not necessarily the best strategy to maximize yield. Indeed, an overload of toxic intermediates and overexpression of a recombinant protein may impair folding and create stress [44], and therefore directly limit production.

Dynamic induction could enable repeated and reversible switching between the growth and production phases, which would let cells produce, then “recover” from production, and then produce again later. Current chemical induction systems may allow such dynamic control to an extent, but auto-induced systems (based on nutrient limitation or cell density) are frequently irreversible. Indeed, using chemical inducers such as IPTG would require complex media changes, and inducers such as galactose or methanol are metabolized by the cells, and thus hard to control. Temperature-sensitive promoters could act as reversible systems, but provide low reactivity. In addition, temperature changes involve hard-to-handle bioprocesses and certain temperatures will not necessarily fit the thermal optima of the enzymes required for endogenous and synthetic pathways. Using optogenetics to control the production of isobutanol in *S. cerevisiae*, Zhao et al. [32] applied bidirectional control using the OPTO-EXP and OPTO-INVRT systems to express *PDC1* (essential for fermentation and growth) only upon light stimulation, and express isobutanol-related genes in the dark. This way, using light, they not only favored the channeling of metabolic flux towards production, but also blocked the competing route; instead of just opening a single valve, they opened one and closed another to specifically control growth and production. Using this system as a simple switch, Zhao et al. realized that the cells were unable to consume all of the glucose in the medium by the end of the production phase, probably due to metabolic arrest related to  $\text{NAD}^+$  depletion. However, using periodic 30 min light pulses to activate *PDC1* every 10 h, the  $\text{NAD}^+$  pool could be restored; this method tripled the amount of isobutanol produced. Most importantly, the authors demonstrated that dynamically controlling growth and production—not simply just separating them—has substantial potential in improving yield (Figure 2b).

In light of these advances, the next logical step is to best adjust the induction pattern based on the cell’s state or content of specific metabolite pools, and automatize this dynamic control in real-time. Such control could be achieved using a cybergenetics approach.

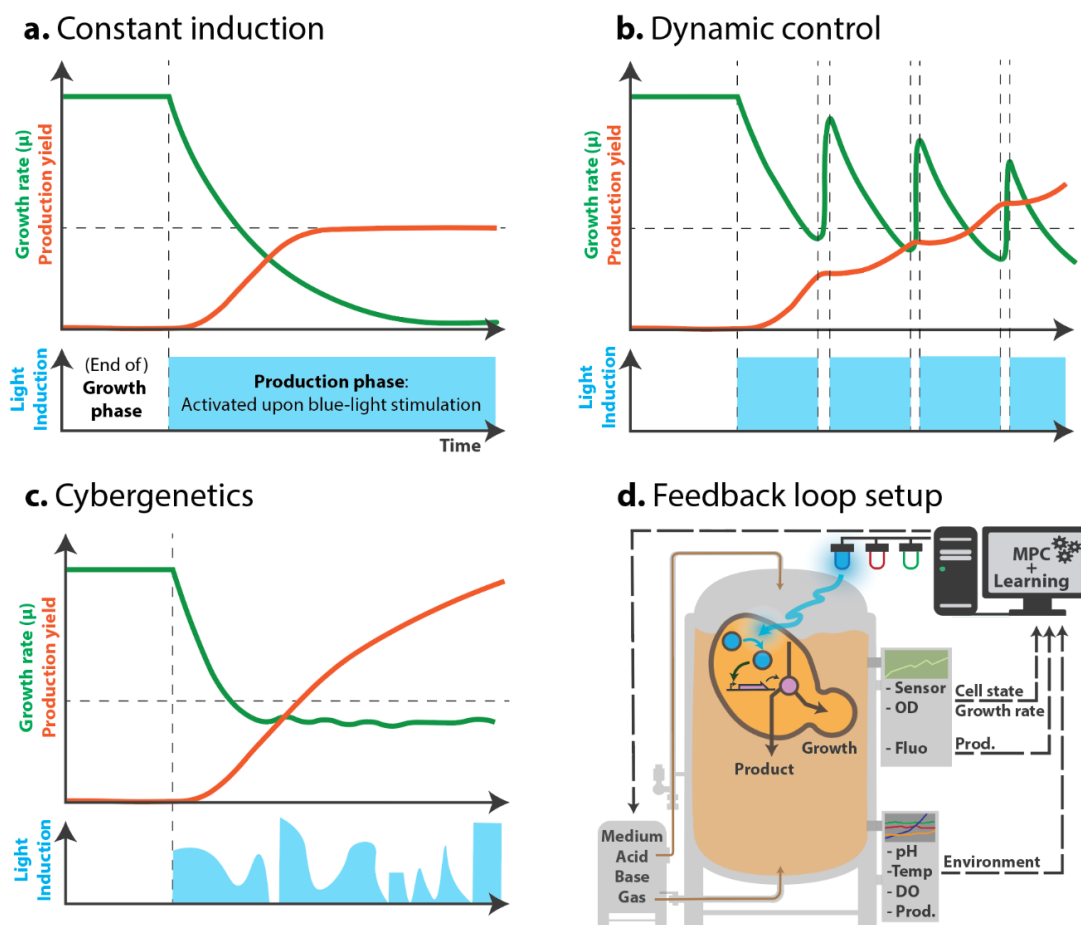


**Figure 2.** Sketch of different putative light-induction patterns to balance growth and production. (a–c). Green curve: growth rate; orange curve: production yield. In blue: light induction pattern that activates bioproduction. (a). With a constant and irreversible induction, production yield increases and plateaus as growth plummets and stalls due to bioproduction-induced stress. (b). Dynamic control of induction: alternating growth and production phases allows cells to “recover” from the production phase and resume growth, before starting to produce again. This strategy was successfully implemented in Zhao et al. [32]. (c). Cybergenetic control would allow for balancing, in real-time, growth and production, by inducing production given the cell’s state. In this sketch, keeping cell growth at a certain rate could ensure a low stress level that would result in a sustained productivity. (d). To implement the feedback loop, besides regular bioproduction parameters control (medium composition, pH, temperature, etc.), the optogenetic actuator (induction upon blue light in this example) is regulated given an output from the system (a cue from the environment, a measure of the growth, or cell fluorescence indicating production level, stress or metabolite pool status) that is interpreted by an algorithm (Model predictive control - MPC) to predict and act upon the behavior of the cell and balance the bioproduction process.

### 2.3. Cybergenetics

Cybergenetics seeks to combine control engineering with synthetic biology as a mean to control biological processes in real-time from outside the cell. Cybergenetics requires three elements: an actuator (for example, an optogenetic system), a biosensor (a reporter of the metabolic state, via a fluorescent protein level or growth rate) and a computer algorithm to control the actuator (via light) based on the biosensor output (subtly reviewed by Carrasco-Lopez et al. [45]). While simple dynamic induction is considered open-loop control (Figure 2b), cybergenetics aims to close this loop to achieve automation via real-time feedback loop control (Figure 2c,d). Such closed-loop control is especially important when experiments yield poor reproducibility, as closed-loop control can adapt and stabilize noisy systems.

Cells naturally use internal control mechanisms to adapt to changes in their environment, cope with fluctuations in internal metabolite pools and respond to stress. In the context of bioproduction, this natural ability has already been exploited to balance growth and production. Taking advantage of the innate regulatory networks of *E. coli*, Ceroni et al. [42] used the stress-responsive pHtpG1 promoter to control the expression of a guide RNA to repress—via a constitutively expressed dead Cas9—the expression of a heterologous gene used to produce the fusion protein VioB-mCherry. Using this “burden-responsive biomolecular feedback controller”, they managed to improve production using a continuous production strategy, but did not compare the results to the two-phase strategy. Such a host-aware approach has not yet been implemented using optogenetics, though this step appears feasible and promising. Another strategy to monitor burden in the cell employs metabolite-responsive transcription factors (MRTFs; see [46]) to report the level of a key metabolite pool required for the production of the final product, or the final product itself, to prevent stress.

Automated control of protein expression levels is also of particular interest. Indeed, as mentioned before, excessive expression can decrease production. Given the potential changes in the environment and cell density, closed-loop control is required to maintain constant per-cell expression throughout the production phase. Using fluorescent proteins as biosensors, such real-time control was demonstrated using chemicals as inducers [47–49] and using optogenetics with the Phy-PIF [50] and CcaS/CcaR systems [51].

In addition to controlling the intracellular concentration of a protein, Miliadis-Argeitis et al. [51] showed that the growth rate of *E. coli* could be regulated via optogenetics using the CcaS/CcaR system to control the *metE* gene, which is responsible for the last step of methionine biosynthesis. Controlling the growth rate in bioproduction is important, since productivity can be either proportional or inversely proportional to growth, or only be optimal at a certain growth rate [52]. In this context, by tuning the intensity and time of both blue and near-IR illumination, Ding et al. [41] finely controlled the division timing of *E. coli* by connecting their custom optogenetic systems to control the expression of the ribonucleotide reductases *NrdAB* or *NrdA* and division proteins *ftsZA* or *Sula*, which influence dNTP biosynthesis and cell division (Figure 1f). This system enhanced the yields of acetoin and poly(lactate-co-3-hydroxybutyrate) by shortening and prolonging cell division, respectively (which restored a reduced growth rate in both cases), in two different strains, up to the 5 L scale. Although closed-loop feedback control was not employed, this method demonstrates the potential of growth control for bioproduction and the possibility of combining several optogenetic systems responding to different wavelengths. Both aspects could very well be applied in the context of cybergenetics (Figure 2d).

### 3. Scale-Up Instruments

#### 3.1. Milliliter Scale

Optogenetic experiments with microbial cultures require dedicated equipment to screen for and characterize strains, and to initiate the scale-up work. This is why, at present, most labs either develop new devices in-house or adapt previously published systems, mostly in a highly flexible Do-It-Yourself (DIY) spirit. Therefore, basic knowledge of electronics, a 3D printer, a laser cutter and some device programming, i.e., the presence of a typical fablab, are usually required. The resulting device should be robust, not too expensive, and rather simple to build and calibrate.

The Light-Plate Apparatus devised by Gerhardt et al. [53] (Figure 3a) was one of the first platforms able to accommodate 24-well plates and apply two wavelengths per well. It only requires printed circuit boards (PCB) that can be easily ordered from specialized companies, some LEDs, LED sockets, 3D-printed parts for assembly, a soldering iron, a chip burner and a few screws. With this system, once the illumination power of the LEDs has been calibrated, the programming is very simple thanks to the graphical user interface (GUI) provided and experiments can be designed fairly quickly, enabling various illumination intensities and patterns to be independently delivered to any well, providing a good

throughput of strain testing. Similar systems have been reported for microwell plates (up to 96-wells or more) [27,54] or larger volumes (up to 10 mL [55,56]). These types of systems are great for small-scale experiments, such as strain characterization and screening various illumination patterns or media compositions. However, reading an output (a fluorescence level, a growth rate, etc.) from each well can be hard to automate and labor-intensive, especially if time-course profiles have to be achieved manually. For this type of study, and at such scale, plate-readers may be of value, particularly if the plate-reader can illuminate various wells independently while simultaneously measuring fluorescence or the optical density. Such sophistication is already available in state-of-the-art plate-readers. Yet, such instruments remain much more expensive and harder to handle than DIY devices.

### 3.2. Mini-Bioreactor Scale and Feedback Implementation

Once a producing optogenetic strain has passed screening and milliliter small scale characterization, it can be time to monitor its growth and production dynamics at larger scale and test illumination patterns accordingly. DIY mini-bioreactor systems have recently been developed by different labs to enable such real-time measurements and, most importantly, contain illumination setups. These systems include the eVOLVER [57] (Figure 3b) and Chi.Bio [58] systems, both of which work with at least 30 mL culture volumes, are customizable, and allow fluidic inputs and illumination at various wavelengths, as well as optical density measurements, and stirring and temperature control. Both devices are open-source projects, freely providing all details regarding the construction steps and components used. Both of the authors also offer commercial versions of their devices with appropriate GUIs for designing experiments and extracting output data. Usually, a set of these small bioreactors (typically 16 mini-bioreactors) are used to screen various media compositions, illumination patterns, temperatures, stirring speeds, etc. Moreover, compared to previously discussed well plates-based optogenetic instruments, eVOLVER and Chi.Bio enable the manipulation of larger culture volumes, an important intermediate step towards scaling-up to industrial conditions. Therefore, these systems combine the advantages of a small, versatile screening tool, while actually more closely mimicking larger-scale settings in terms of control and monitoring. Note, however, that pH and dissolved oxygen levels are two important factors that are not considered in those devices—although they could be implemented in the future. The embedded optogenetic hardware (mainly LEDs) can be easily tuned, and Chi.Bio especially allows for the measurement of at least two fluorescence outputs thanks to its seven-color LED and small spectrophotometer. To better control the production given the cell's state, the devices' measurement capacities will come to be crucial if fluorescent biosensors are to be used to establish automatized real-time control.

Since these devices are quite small and emit relatively powerful light, there are only a few concerns related to poor light penetration or distribution in the medium. However, it will be crucial to address this issue when scaling-up to industrial settings. Although the small size of those instruments comes as an advantage in the lab, variations in growth and production caused by the effects of larger culture volumes cannot be assessed using these devices, such that they will not replace pilot-scale testing. Nonetheless, they will be essential to start balancing growth and production and fine tune computer control models.

### 3.3. Industrial Settings and Photobioreactors

Even in the absence of optogenetics, scaling-up to the industrial scale (from 10 to 10,000 L) represents a challenge for any potential industrial strain. At such scales, the raw materials used for fermentation will change given the costs and quantities of chemicals required to piece together the culture medium. Moreover, mixing and oxygenation become more demanding due to the energy needed to move dense culture volumes; the inoculum volume may become critical, and pressure and shear stress may be unevenly distributed. All of these changes might impact the performance of the strain at the larger scale [59], which may prompt researchers to another round of refinement of the initial strain design. One of the main concerns regarding optogenetics at larger scales is

the penetration of light in the medium. Indeed, high-density cell cultures can become very opaque, which would prevent light from reaching a maximum number of cells (light-shading effect), or make it hard to sufficiently activate the biological process (due to dilution of the signal). Simply adding light panels around a standard bioreactor (Figure 3(c1,c4)) can overcome these issues at relatively small scales (2 to 250 L), but poses serious issues for scaling-up. Indeed, the low surface to volume ratio of larger bioreactors is a crucial factor that must be considered in the context of light exposure [60].

Light penetration is a crucial issue for the cultivation of micro-algae and cyanobacteria. As these organisms are also a valuable chassis for bioproduction (mostly for biofuels), this issue has actually been addressed in various ways, along with how to deal with pH, dissolved oxygen (DO), temperature and mixing. Different types of photobioreactors are commercially available and used to produce various biomasses or specific compounds [60]. Closed-type algal photobioreactors, such as airlift or bubble columns (Figure 3(c4)), stacked tubular (Figure 3(c3)), flat-plate and multilayered photobioreactors [61], are illuminated from the outside. These designs aim to increase the surface area of the culture in contact with, mostly, ambient light or custom light sources, and counteract the shading effect caused by high culture density or large volumes. In bioproduction, yeast cultures can result in an extremely dense, very opaque, paste-like textured medium, so that the number of cells is maximized to reach higher titers. The compatibility of algal photobioreactors with such high-density yeast cultures remains to be tested; and although light penetration is the main advantage of such photobioreactors, large-scale algal photobioreactors may not be adaptable to heavy and dense cultures (harder to pump, harder to cool down, less diffusion in the medium). Besides, algal photobioreactors often rely on continuous cultures, which generates a significant risk of evolutionary escape in burdened yeast cultures. We suggest that lower-density yeast cultures may potentially benefit light penetration and controllability. Owing to a refined dynamic control strategy, the reduction in the final biomass could be compensated for by increased production per cell; the trade-off between these aspects will need to be balanced.

Another solution to the light penetration issue could be the use of “inverted” optogenetic systems, where genes for the production phase are activated in the dark, when light becomes scarce, i.e., when a certain cell density is reached [26]; however, this would hardly allow for dynamic control.

Finally, it may be possible to redesign or tune existing large-scale bioreactors. Most standard large-scale bioreactors are made of metal, which limits the use of light; however, internal illumination may overcome this issue (Figure 3(c2)). Internal illumination is usually achieved using optical fibers or light wells that reach inside the culture medium and transmit light collected outside into the bioreactor, or by using fluorescent lamps. LEDs are increasingly being used, as they offer the advantages of being able control the exact wavelength used in the medium [60] and even possibly deliver several wavelengths to control combinations of multiple optogenetic systems. However, such modifications may also conflict with other aspects of the bioreactor, such as the stirring mechanism (Figure 3(c2)). As an alternative to modifying the original design, one could also take advantage of existing plug devices—such as probes or external loops—which may be used to easily implement optogenetic control into existing bioreactors. For instance, during the synthesis of organic chemicals, photochemical reactors sometimes use external illumination chambers (flat panels or coils around a light source; see Figure 3(c5,c6)). Illumination chambers could enable the regulation of the optogenetic system based on the regulated flow of cells across the illuminated chamber, therefore tuning the amount of light received per cell per time. Such an approach may minimize the redesign of the bioreactors and thus may be a more feasible and economically advantageous first step to combine optogenetics and bioproduction at a large scale.

Finally, it is worth noting that modeling light distribution given bioreactor design [62], together with the optogenetic system, metabolic pathways and the bioprocess, will be key to optimizing bioproduction [63,64].

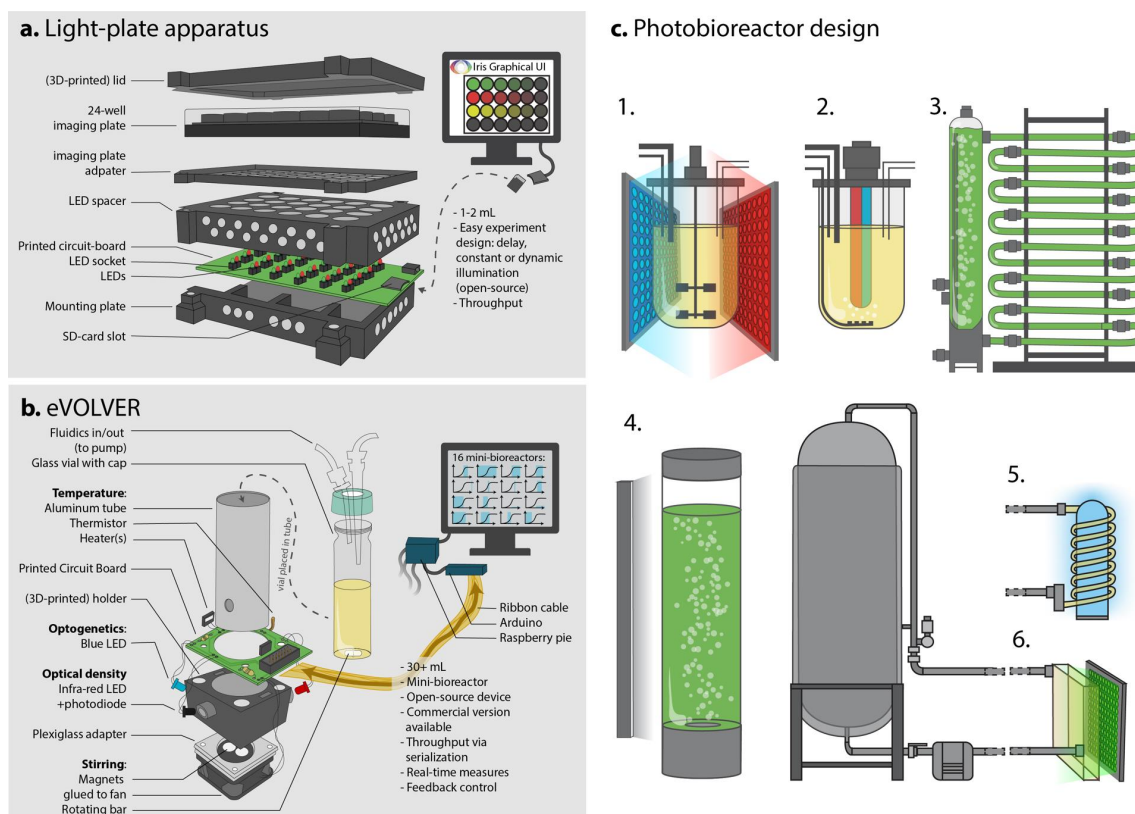


**Figure 3.** Instrumentation for optogenetic control and scale-up of bioproduction. (a). The light-plate apparatus [53] allows screening and simple experiments using small culture volumes in imaging plates and easily-programmable well-independent experiments. (b). The eVOLVER system [57] used as mini-bioreactors allows larger scale (30 mL) cultures and dynamic real-time control, as well as culture and illumination conditions screening thanks to its 16-unit array. (c). Bioreactor design to improve light penetration is crucial to successfully implement optogenetics as an induction method at the industrial scale. (1). Externally illuminated 10 L fermenter-type bioreactor using LED panels. Such systems offer the best control over every process parameter. (2). Internally illuminated 10 L bioreactor, which would allow better light penetration in a dense culture medium. Note the subsequent change in the gas-exchange strategy. (3). Stacked tubular photobioreactor, typically used for algal culture, increases the surface to volume ratio of large culture volumes to maximize light exposure. Up to thousands of liters of cultures can be handled, but temperature may be difficult to control and O<sub>2</sub> and CO<sub>2</sub> levels may fluctuate [61]. (4). Standard 250 L bubble column algal photobioreactor (illumination pane on the left) is considered an intermediate volume for algal cultivation. It is easy and cheap to set up and can be scaled-up, but has a relatively low surface to volume ratio. (6). Connection of an illumination chamber to a 1000 L bioreactor could allow illumination of flowing cells and reduce the need for large fermenter-type bioreactor redesign. Similarly, in (5), a loop passing out of the fermenter coils around a light source to enhance exposure to light.

#### 4. Discussion and Conclusions

As metabolic engineering increasingly relies on the fine tuning of intricate endogenous and synthetic pathways, light is becoming the inducer of choice for bioproduction—as evidenced by the fact that many standard induction systems have already been connected to optogenetic systems. Light can be used to regulate metabolic valves in a similar manner to existing inducers used in bioproduction: by unleashing bioproduction after a growth phase. However, light can also be used to control cellular growth itself by regulating endogenous essential genes, or even used to actively and dynamically balance both bioproduction and growth using bidirectional optogenetic systems. Optogenetics enables increasingly simpler and more precise dynamic control over these processes,

and holds the promise of maximizing yields from industrial organisms engineered for complex pathways that frequently require multilevel regulation. The automation of this dynamic control via a cybergenetics approach seems the natural next step: under industrial conditions, every aspect of the culture is rigorously monitored and controlled, including temperature, pressure, pH, medium composition, dissolved oxygen and optical density. In addition to controlling these external cellular cues, cybergenetics aims to control the intricate internal behavior of cells based on a designated output (Figure 2d). This output can be the level of the final product detected using a biosensor, the cellular concentration of an enzyme or component of the pathway, or the burden that production represents—which can be detected using metabolite pool biosensors, stress-related promoters or directly monitoring the growth rate. Cybergenetic control could be achieved using various optogenetic systems, i.e., actuators, and biosensors that currently exist (with many others in development) [65]. The last element needed for cybergenetics is an appropriate control algorithm that takes into account and predicts the behavior of the cell, as well as how the culture density affects the diffusion of light—to better control the bioproduction *versus* growth trade-off. Various algorithms have been tested for the control of rather simple behaviors, such as the expression level of a fluorescent protein, and some of these already use optogenetic systems. Building models to represent burden will require extensive experimental fitting, and this may be facilitated by implementing machine learning strategies that can train from concrete experimental data [66]. Such models can easily be tested on smaller scales in the lab before being adapted to large culture volumes.

Many optogenetic devices have been developed in recent years to tackle every step of strain development; the real challenge now is to prove that optogenetics can truly be used in the context of bioproduction at the industrial scale in an economically sustainable manner. Thanks to their generally well-developed graphical user interfaces, small-scale devices that allow illumination of imaging plates will be convenient for the throughput testing of various media compositions, genetic designs and, most importantly, light illumination intensities or basic illumination patterns. Mini-bioreactors will enable the testing of larger volumes and fluidics inputs and outputs. They offer the capacity to control temperature and stirring and, crucially, to monitor growth and production in real-time—as well as implement feedback loop control based on such outputs. Mini-bioreactors that enable the use of optogenetics without critical light penetration issues will allow users to start to tune the dynamic control of the strain to optimize bioproduction. However, due to the opacity of high-density yeast cultures, light penetration becomes one major issue when shifting dynamic control from the small scale to the industrial scale. Although light panels or internal illumination strategies may be suitable solutions for bioreactors up to about 250 L, larger scale bioreactors will require further modeling, redesign or tuning, though existing algal photobioreactors or photochemistry may provide inspiration.

The use of light as an inducer can facilitate real-time dynamic control strategies. The first applications of light to bioproduction—as well as the optogenetic instruments presented here—show that although challenges remain to be solved, the application of optogenetics to bioproduction holds the promise of maximizing yields in bioproduction; promise that can be expected to be fulfilled in the years to come.

**Author Contributions:** Writing—original draft preparation, S.P., A.B., M.L.B., T.L., G.T. and P.H.; writing—review and editing, S.P., P.H. All authors have read and agreed to the published version of the manuscript.

**Funding:** This research was funded by the European research council grant ERC-SmartCells (724813), the H2020 FET-OPEN grant COSYBIO (766840) and from the grants ANR-16-CE12-0025-01, ANR-11-LABX-0038 and ANR-10-IDEX-0001-02 of the French national research agency (ANR).

**Conflicts of Interest:** The authors have no conflict of interest to declare.

## References

1. Pham, J.V.; Yilma, M.A.; Feliz, A.; Majid, M.T.; Maffetone, N.; Walker, J.R.; Kim, E.; Cho, H.J.; Reynolds, J.M.; Song, M.C.; et al. A review of the microbial production of bioactive natural products and biologics. *Front. Microbiol.* **2019**, *10*, 1–27. [[CrossRef](#)]
2. Germann, S.M.; Baallal Jacobsen, S.A.; Schneider, K.; Harrison, S.J.; Jensen, N.B.; Chen, X.; Stahlhut, S.G.; Borodina, I.; Luo, H.; Zhu, J.; et al. Glucose-based microbial production of the hormone melatonin in yeast *Saccharomyces cerevisiae*. *Biotechnol. J.* **2016**, *11*, 717–724. [[CrossRef](#)] [[PubMed](#)]
3. Gerngross, T.U. Advances in the production of human therapeutic proteins in yeasts and filamentous fungi. *Nat. Biotechnol.* **2004**, *22*, 1409–1414. [[CrossRef](#)] [[PubMed](#)]
4. van Dijk, J.M.; Hecker, M. *Bacillus subtilis*: From soil bacterium to super-secreting cell factory. *Microb. Cell Fact.* **2013**, *12*, 3. [[CrossRef](#)] [[PubMed](#)]
5. Grewal, P.S.; Modavi, C.; Russ, Z.N.; Harris, N.C.; Dueber, J.E. Bioproduction of a betalain color palette in *Saccharomyces cerevisiae*. *Metab. Eng.* **2018**, *45*, 180–188. [[CrossRef](#)] [[PubMed](#)]
6. Buijs, N.A.; Siewers, V.; Nielsen, J. Advanced biofuel production by the yeast *saccharomyces cerevisiae*. *Curr. Opin. Chem. Biol.* **2013**, *17*, 480–488. [[CrossRef](#)]
7. Paddon, C.J.; Westfall, P.J.; Pitera, D.J.; Benjamin, K.; Fisher, K.; McPhee, D.; Leavell, M.D.; Tai, A.; Main, A.; Eng, D.; et al. High-level semi-synthetic production of the potent antimalarial artemisinin. *Nature* **2013**, *496*, 528–532. [[CrossRef](#)]
8. Luo, X.; Reiter, M.A.; d’Espaux, L.; Wong, J.; Denby, C.M.; Lechner, A.; Zhang, Y.; Grzybowski, A.T.; Harth, S.; Lin, W.; et al. Complete biosynthesis of cannabinoids and their unnatural analogues in yeast. *Nature* **2019**, *567*, 123–126. [[CrossRef](#)]
9. Srinivasan, P.; Smolke, C.D. Biosynthesis of medicinal tropane alkaloids in yeast. *Nature* **2020**, *585*, 614–619. [[CrossRef](#)]
10. Menart, V.; Jevševar, S.; Vilar, M.; Trobiš, A.; Pavko, A. Constitutive versus thermoinducible expression of heterologous proteins in *Escherichia coli* based on strong PR,PL promoters from phage lambda. *Biotechnol. Bioeng.* **2003**, *83*, 181–190. [[CrossRef](#)]
11. Chou, C.-H.; Aristidou, A.A.; Meng, S.-Y.; Bennett, G.N.; San, K.-Y. Characterization of a pH-inducible promoter system for high-level expression of recombinant proteins in *Escherichia coli*. *Biotechnol. Bioeng.* **1995**, *47*, 186–192. [[CrossRef](#)] [[PubMed](#)]
12. Pudasaini, A.; El-Arab, K.K.; Zoltowski, B.D. LOV-based optogenetic devices: Light-driven modules to impart photoregulated control of cellular signaling. *Front. Mol. Biosci.* **2015**, *2*, 1–15. [[CrossRef](#)] [[PubMed](#)]
13. Yizhar, O.; Fenno, L.E.; Davidson, T.J.; Mogri, M.; Deisseroth, K. Optogenetics in Neural Systems. *Neuron* **2011**, *71*, 9–34. [[CrossRef](#)] [[PubMed](#)]
14. Izquierdo, E.; Quinkler, T.; De Renzis, S. Guided morphogenesis through optogenetic activation of Rho signalling during early *Drosophila* embryogenesis. *Nat. Commun.* **2018**, *9*, 1–13. [[CrossRef](#)] [[PubMed](#)]
15. Johnson, H.E.; Toettcher, J.E. Signaling Dynamics Control Cell Fate in the Early *Drosophila* Embryo. *Dev. Cell* **2019**, *48*, 361–370. [[CrossRef](#)]
16. Valon, L.; Etoc, F.; Remorino, A.; Di Pietro, F.; Morin, X.; Dahan, M.; Coppey, M. Predictive Spatiotemporal Manipulation of Signaling Perturbations Using Optogenetics. *Biophys. J.* **2015**, *109*, 1785–1797. [[CrossRef](#)]
17. Liu, Z.; Zhang, J.; Jin, J.; Geng, Z.; Qi, Q.; Liang, Q. Programming bacteria with light-sensors and applications in synthetic biology. *Front. Microbiol.* **2018**, *9*, 2692. [[CrossRef](#)]
18. Harrigan, P.; Madhani, H.D.; El-Samad, H. Real-Time Genetic Compensation Defines the Dynamic Demands of Feedback Control. *Cell* **2018**, *175*, 877–886. [[CrossRef](#)]
19. Ohlendorf, R.; Vidavski, R.R.; Eldar, A.; Moffat, K.; Möglich, A. From dusk till dawn: One-plasmid systems for light-regulated gene expression. *J. Mol. Biol.* **2012**, *416*, 534–542. [[CrossRef](#)]
20. Shimizu-Sato, S.; Huq, E.; Tepperman, J.M.; Quail, P.H. A light-switchable gene promoter system. *Nat. Biotechnol.* **2002**, *20*, 1041–1044. [[CrossRef](#)]
21. Motta-Mena, L.B.; Reade, A.; Mallory, M.J.; Glantz, S.; Weiner, O.D.; Lynch, K.W.; Gardner, K.H. An optogenetic gene expression system with rapid activation and deactivation kinetics. *Nat. Chem. Biol.* **2014**, *10*, 196–202. [[CrossRef](#)] [[PubMed](#)]



22. Tabor, J.J.; Levskaya, A.; Voigt, C.A. Multichromatic control of gene expression in escherichia coli. *J. Mol. Biol.* **2011**, *405*, 315–324. [[CrossRef](#)] [[PubMed](#)]
23. Kennedy, M.J.; Hughes, R.M.; Peteya, L.A.; Schwartz, J.W.; Ehlers, M.D.; Tucker, C.L. Rapid blue-light-mediated induction of protein interactions in living cells. *Nat. Methods* **2010**, *7*, 973–975. [[CrossRef](#)] [[PubMed](#)]
24. Taslimi, A.; Vrana, J.D.; Chen, D.; Borinskaya, S.; Mayer, B.J.; Kennedy, M.J.; Tucker, C.L. An optimized optogenetic clustering tool for probing protein interaction and function. *Nat. Commun.* **2014**, *5*, 1–9. [[CrossRef](#)]
25. Kolar, K.; Knobloch, C.; Stork, H.; Žnidarič, M.; Weber, W. OptoBase: A Web Platform for Molecular Optogenetics. *ACS Synth. Biol.* **2018**, *7*, 1825–1828. [[CrossRef](#)]
26. Lalwani, M.A.; Ip, S.S.; Carrasco-López, C.; Day, C.; Zhao, E.M.; Kawabe, H.; Avalos, J.L. Optogenetic control of the lac operon for bacterial chemical and protein production. *Nat. Chem. Biol.* **2020**, 1–9. [[CrossRef](#)]
27. Romano, E.; Baumschlager, A.; Akmeriç, E.B.; Palanisamy, N.; Houmani, M.; Schmidt, G.; Öztürk, M.A.; Ernst, L.; Khammash, M.; Di Ventura, B. An inducible AraC that responds to blue light instead of arabinose. *bioRxiv* **2020**. [[CrossRef](#)]
28. Raghavan, A.R.; Salim, K.; Yadav, V.G. Optogenetic control of heterologous metabolism in *E. coli*. *ACS Synth. Biol.* **2020**, *9*, 2291–2300. [[CrossRef](#)]
29. Baumschlager, A.; Aoki, S.K.; Khammash, M. Dynamic Blue Light-Inducible T7 RNA Polymerases (Opto-T7RNAPs) for Precise Spatiotemporal Gene Expression Control. *ACS Synth. Biol.* **2017**, *6*, 2157–2167. [[CrossRef](#)]
30. Kawano, F.; Suzuki, H.; Furuya, A.; Sato, M. Engineered pairs of distinct photoswitches for optogenetic control of cellular proteins. *Nat. Commun.* **2015**, *6*, 1–8. [[CrossRef](#)]
31. Han, T.; Chen, Q.; Liu, H. Engineered Photoactivatable Genetic Switches Based on the Bacterium Phage T7 RNA Polymerase. *ACS Synth. Biol.* **2017**, *6*, 357–366. [[CrossRef](#)] [[PubMed](#)]
32. Zhao, E.M.; Zhang, Y.; Mehl, J.; Park, H.; Lalwani, M.A.; Toettcher, J.E.; Avalos, J.L. Optogenetic regulation of engineered cellular metabolism for microbial chemical production. *Nature* **2018**, *555*, 683–687. [[CrossRef](#)] [[PubMed](#)]
33. Benzinger, D.; Khammash, M. Pulsatile inputs achieve tunable attenuation of gene expression variability and graded multi-gene regulation. *Nat. Commun.* **2018**, *9*, 1–10. [[CrossRef](#)] [[PubMed](#)]
34. Hueso-Gil, A.; Nyerges, Á.; Pál, C.; Calles, B.; De Lorenzo, V. Multiple-Site Diversification of Regulatory Sequences Enables Interspecies Operability of Genetic Devices. *ACS Synth. Biol.* **2020**, *9*, 104–114. [[CrossRef](#)] [[PubMed](#)]
35. Castillo-Hair, S.M.; Baerman, E.A.; Fujita, M.; Igoshin, O.A.; Tabor, J.J. Optogenetic control of *Bacillus subtilis* gene expression. *Nat. Commun.* **2019**, *10*, 1–11. [[CrossRef](#)] [[PubMed](#)]
36. Duplus-Bottin, H.; Spichty, M.; Triqueneaux, G.; Place, C.; Mangeot, P.E.; Ohlmann, T.; Vittoz, F.; Yvert, G. A monogenic and fast-responding Light-Inducible Cre recombinase as a novel optogenetic switch. *bioRxiv* **2020**. [[CrossRef](#)]
37. Hasenjäger, S.; Trauth, J.; Hepp, S.; Goenrich, J.; Essen, L.-O.; Taxis, C. Optogenetic Downregulation of Protein Levels with an Ultrasensitive Switch. *ACS Synth. Biol.* **2019**, *8*, 1026–1036. [[CrossRef](#)]
38. Senoo, S.; Tandar, S.T.; Kitamura, S.; Toya, Y.; Shimizu, H. Light-inducible flux control of triosephosphate isomerase on glycolysis in *Escherichia coli*. *Biotechnol. Bioeng.* **2019**, *116*, 3292–3300. [[CrossRef](#)]
39. Tandar, S.T.; Senoo, S.; Toya, Y.; Shimizu, H. Optogenetic switch for controlling the central metabolic flux of *Escherichia coli*. *Metab. Eng.* **2019**, *55*, 68–75. [[CrossRef](#)]
40. Zhao, E.M.; Suek, N.; Wilson, M.Z.; Dine, E.; Pannucci, N.L.; Gitai, Z.; Avalos, J.L.; Toettcher, J.E. Light-based control of metabolic flux through assembly of synthetic organelles. *Nat. Chem. Biol.* **2019**, *15*, 589–597. [[CrossRef](#)]
41. Ding, Q.; Ma, D.; Liu, G.Q.; Li, Y.; Guo, L.; Gao, C.; Hu, G.; Ye, C.; Liu, J.; Liu, L.; et al. Light-powered *Escherichia coli* cell division for chemical production. *Nat. Commun.* **2020**, *11*, 1–14. [[CrossRef](#)] [[PubMed](#)]
42. Ceroni, F.; Boo, A.; Furini, S.; Gorochoowski, T.E.; Borkowski, O.; Ladak, Y.N.; Awan, A.R.; Gilbert, C.; Stan, G.B.; Ellis, T. Burden-driven feedback control of gene expression. *Nat. Methods* **2018**, *15*, 387–393. [[CrossRef](#)] [[PubMed](#)]

43. Boo, A.; Ellis, T.; Stan, G.B. Host-aware synthetic biology. *Curr. Opin. Syst. Biol.* **2019**, *14*, 66–72. [[CrossRef](#)]
44. Gasser, B.; Saloheimo, M.; Rinas, U.; Dragosits, M.; Rodríguez-Carmona, E.; Baumann, K.; Giuliani, M.; Parrilli, E.; Branduardi, P.; Lang, C.; et al. Protein folding and conformational stress in microbial cells producing recombinant proteins: A host comparative overview. *Microb. Cell Fact.* **2008**, *7*, 11. [[CrossRef](#)] [[PubMed](#)]
45. Carrasco-López, C.; García-Echauri, S.A.; Kichuk, T.; Avalos, J.L. Optogenetics and biosensors set the stage for metabolic cybergenetics. *Curr. Opin. Biotechnol.* **2020**, *65*, 296–309. [[CrossRef](#)] [[PubMed](#)]
46. Xu, P. Production of chemicals using dynamic control of metabolic fluxes. *Curr. Opin. Biotechnol.* **2018**, *53*, 12–19. [[CrossRef](#)] [[PubMed](#)]
47. Fiore, G.; Perrino, G.; Di Bernardo, M.; Di Bernardo, D. In Vivo Real-Time Control of Gene Expression: A Comparative Analysis of Feedback Control Strategies in Yeast. *ACS Synth. Biol.* **2016**, *5*, 154–162. [[CrossRef](#)]
48. Lugagne, J.B.; Sosa Carrillo, S.; Kirch, M.; Köhler, A.; Batt, G.; Hersen, P. Balancing a genetic toggle switch by real-time feedback control and periodic forcing. *Nat. Commun.* **2017**, *8*, 1671. [[CrossRef](#)]
49. Uhlenendorf, J.; Miermont, A.; Delaveau, T.; Charvin, G.; Fages, F.; Bottani, S.; Batta, G.; Hersen, P. Long-term model predictive control of gene expression at the population and single-cell levels. *Proc. Natl. Acad. Sci. USA* **2012**, *109*, 14271–14276. [[CrossRef](#)]
50. Miliás-Argeitis, A.; Summers, S.; Stewart-Ornstein, J.; Zuleta, I.; Pincus, D.; El-Samad, H.; Khammash, M.; Lygeros, J. In silico feedback for in vivo regulation of a gene expression circuit. *Nat. Biotechnol.* **2011**, *29*, 1114–1116. [[CrossRef](#)]
51. Miliás-Argeitis, A.; Rullan, M.; Aoki, S.K.; Buchmann, P.; Khammash, M. Automated optogenetic feedback control for precise and robust regulation of gene expression and cell growth. *Nat. Commun.* **2016**, *7*, 1–11. [[CrossRef](#)]
52. Looser, V.; Bruhlmann, B.; Bumbak, F.; Stenger, C.; Costa, M.; Camattari, A.; Fotiadis, D.; Kovar, K. Cultivation strategies to enhance productivity of *Pichia pastoris*: A review. *Biotechnol. Adv.* **2014**, *33*, 1177–1193. [[CrossRef](#)] [[PubMed](#)]
53. Gerhardt, K.P.; Olson, E.J.; Castillo-Hair, S.M.; Hartsough, L.A.; Landry, B.P.; Ekness, F.; Yokoo, R.; Gomez, E.J.; Ramakrishnan, P.; Suh, J.; et al. An open-hardware platform for optogenetics and photobiology. *Sci. Rep.* **2016**, *6*, 1–13. [[CrossRef](#)] [[PubMed](#)]
54. Bugaj, L.J.; Lim, W.A. High-throughput multicolor optogenetics in microwell plates. *Nat. Protoc.* **2019**, *14*, 2205–2228. [[CrossRef](#)] [[PubMed](#)]
55. Wang, H.; Yang, Y.T. Mini Photobioreactors for in Vivo Real-Time Characterization and Evolutionary Tuning of Bacterial Optogenetic Circuit. *ACS Synth. Biol.* **2017**, *6*, 1793–1796. [[CrossRef](#)] [[PubMed](#)]
56. Olson, E.J.; Hartsough, L.A.; Landry, B.P.; Shroff, R.; Tabor, J.J. Characterizing bacterial gene circuit dynamics with optically programmed gene expression signals. *Nat. Methods* **2014**, *11*, 449–455. [[CrossRef](#)]
57. Wong, B.G.; Mancuso, C.P.; Kiriakov, S.; Bashor, C.J.; Khalil, A.S. Precise, automated control of conditions for high-throughput growth of yeast and bacteria with eVOLVER. *Nat. Publ. Gr.* **2018**, *36*, 614–623. [[CrossRef](#)]
58. Steel, H.; Habgood, R.; Kelly, C.; Papachristodoulou, A. In situ characterisation and manipulation of biological systems with Chi.Bio. *PLoS Biol.* **2020**, 1–12. [[CrossRef](#)]
59. Crater, J.S.; Lievens, J.C. Scale-up of industrial microbial processes. *FEMS Microbiol. Lett.* **2018**, *365*, 1–5. [[CrossRef](#)]
60. Chang, J.-S.; Show, P.-L.; Ling, T.-C.; Chen, C.-Y.; Ho, S.-H.; Tan, C.-H.; Nagarajan, D.; Phong, W.-N. Photobioreactors. In *Current Developments in Biotechnology and Bioengineering: Bioprocesses, Bioreactors and Controls*; Elsevier: Amsterdam, The Netherlands, 2017; pp. 313–352.
61. Płaczek, M.; Patyna, A.; Witzak, S. Technical evaluation of photobioreactors for microalgae cultivation. In Proceedings of the E3S Web of Conferences, Szczyrk, Poland, 25–27 October 2017; Volume 19.
62. Gernigon, V.; Chekroun, M.A.; Cockx, A.; Guiraud, P.; Morchain, J. How Mixing and Light Heterogeneity Impact the Overall Growth Rate in Photobioreactors. *Chem. Eng. Technol.* **2019**, *42*, 1663–1669. [[CrossRef](#)]
63. Xu, L.; Weathers, P.J.; Xiong, X.R.; Liu, C.Z. Microalgal bioreactors: Challenges and opportunities. *Eng. Life Sci.* **2009**, *9*, 178–189. [[CrossRef](#)]
64. Posten, C. Design principles of photo-bioreactors for cultivation of microalgae. *Eng. Life Sci.* **2009**, *9*, 165–177. [[CrossRef](#)]

65. Rogers, J.K.; Church, G.M. Genetically encoded sensors enable real-time observation of metabolite production. *Proc. Natl. Acad. Sci. USA* **2016**, *113*, 2388–2393. [[CrossRef](#)] [[PubMed](#)]
66. Zhang, J.; Petersen, S.D.; Radivojevic, T.; Ramirez, A.; Pérez-Manríquez, A.; Abeliuk, E.; Sánchez, B.J.; Costello, Z.; Chen, Y.; Fero, M.J.; et al. Combining mechanistic and machine learning models for predictive engineering and optimization of tryptophan metabolism. *Nat. Commun.* **2020**, *11*, 4880. [[CrossRef](#)]

**Publisher’s Note:** MDPI stays neutral with regard to jurisdictional claims in published maps and institutional affiliations.



© 2020 by the authors. Licensee MDPI, Basel, Switzerland. This article is an open access article distributed under the terms and conditions of the Creative Commons Attribution (CC BY) license (<http://creativecommons.org/licenses/by/4.0/>).

## 1.2 Posters

# Spatio-temporal control of labor division in yeast communities

Matthias Le Bec, Pascal Hersen

Laboratoire Physico-Chimie Curie, UMR168, Institut Curie, Paris, FR

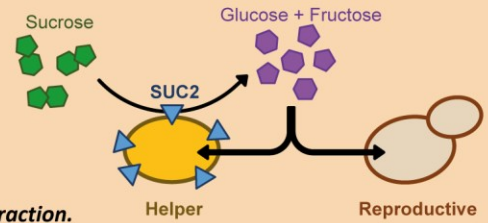
Laboratoire Matière et Systèmes Complexes, CNRS - Université Paris Diderot, Paris, FR

## Introduction

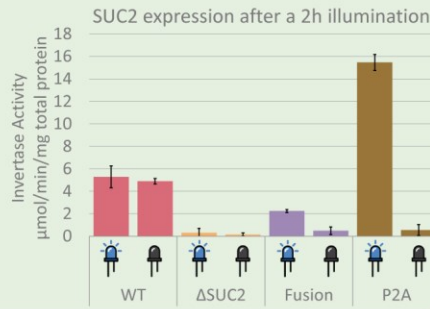
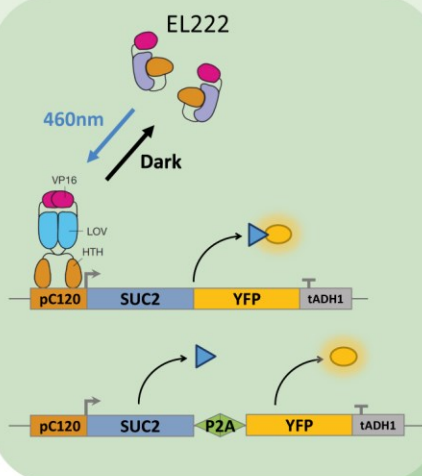
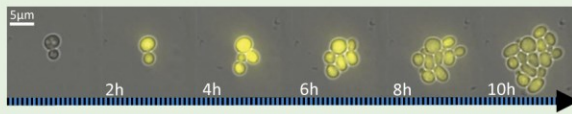
- Micro-organisms **transform** their **micro-environment** while growing: they absorb, transform and produce molecules - they multiply, move and reproduce.
- Most of microbe's **interactions** are transmitted through **spatial structuration**.<sup>1,2,3</sup>
- Scientific research usually favors **homogenous culture** conditions to study microbial processes.
- Division of labor** is found in many level of biology: it allows cells to be **specialized** in simple tasks avoiding excessive **metabolic burden**.<sup>4</sup>

We choose to study the **SUC2** expression in yeast as a model for gradient-driven microbial interaction.

## Division of labor

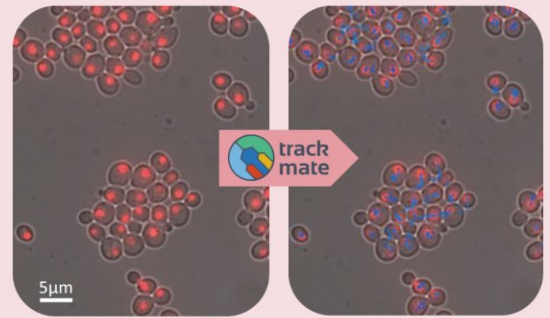
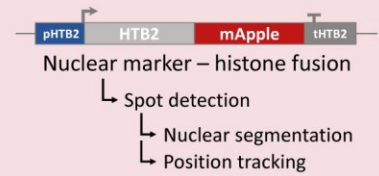


## Optogenetics



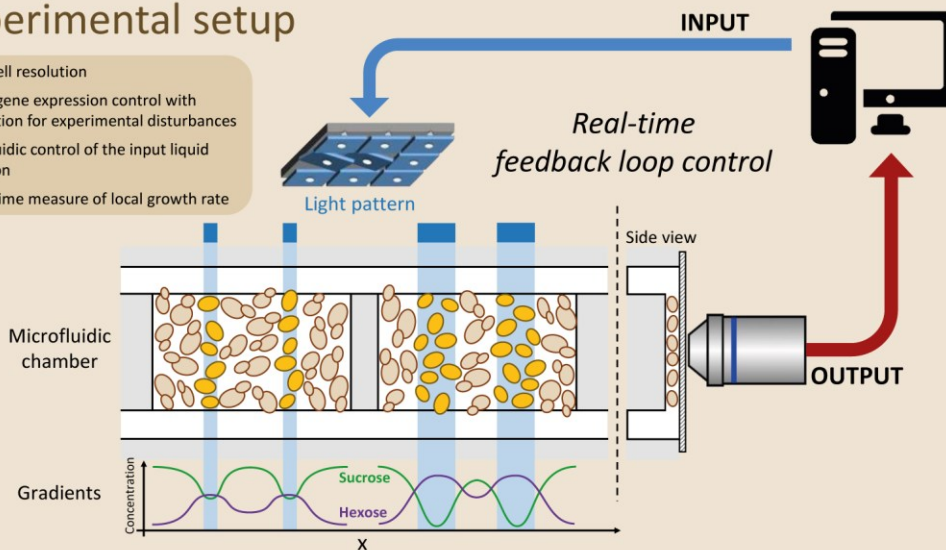
- SUC2 expression induction with high spatio-temporal resolution
- Fluorescence co-expression to monitor the resulting protein production
- P2A self-cleaving peptides to avoid secretion pathway interferences

## Image analysis

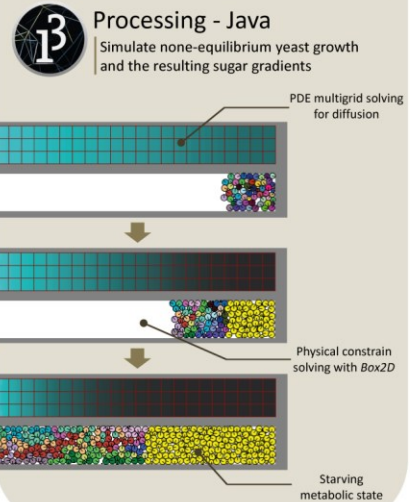


## Experimental setup

- Single cell resolution
- Robust gene expression control with compensation for experimental disturbances
- Microfluidic control of the input liquid composition
- In real-time measure of local growth rate



## Agent-based modeling



## Literature

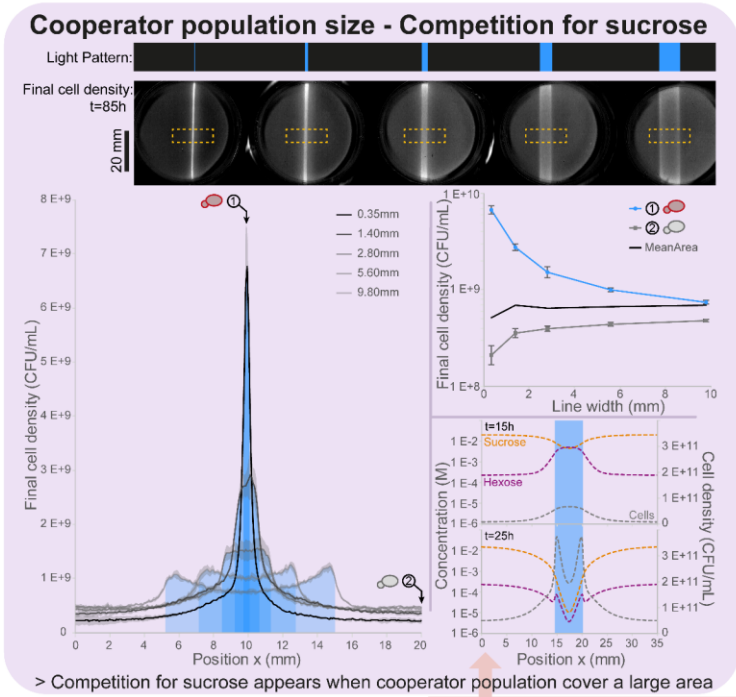
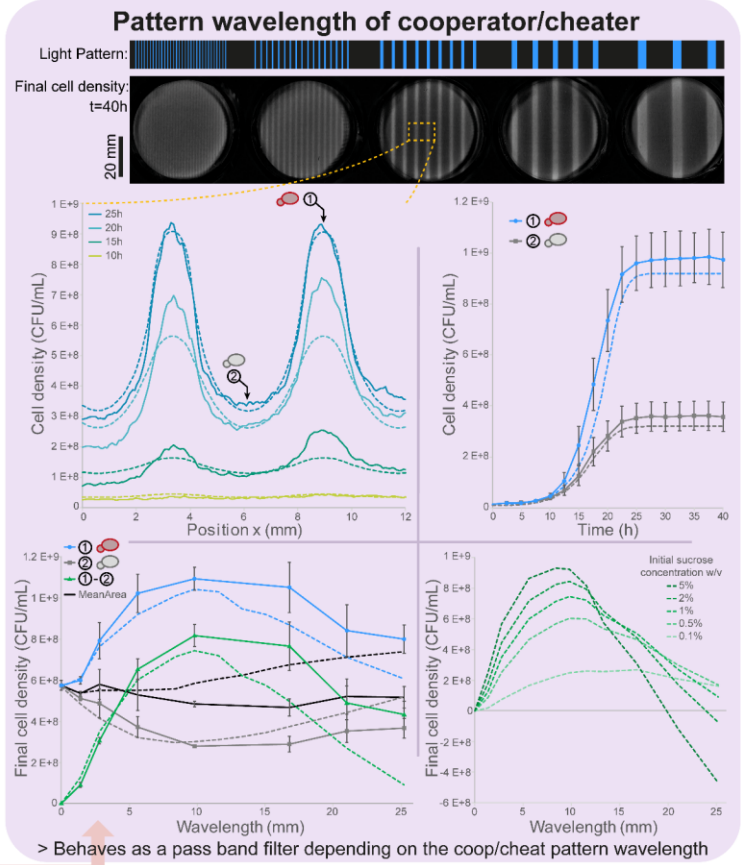
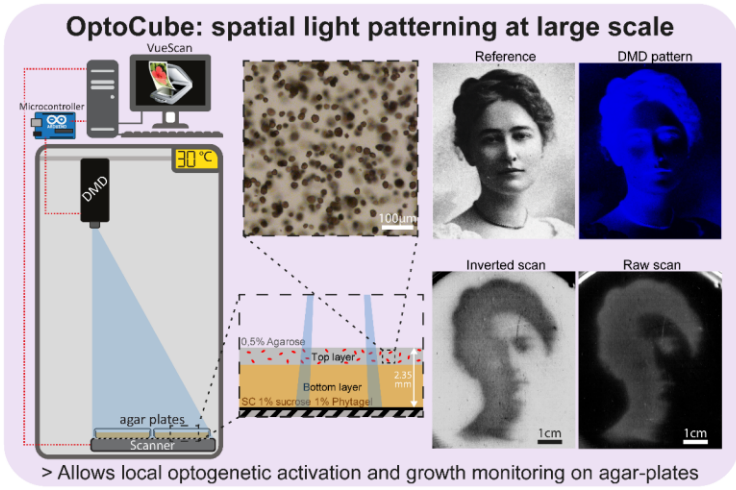
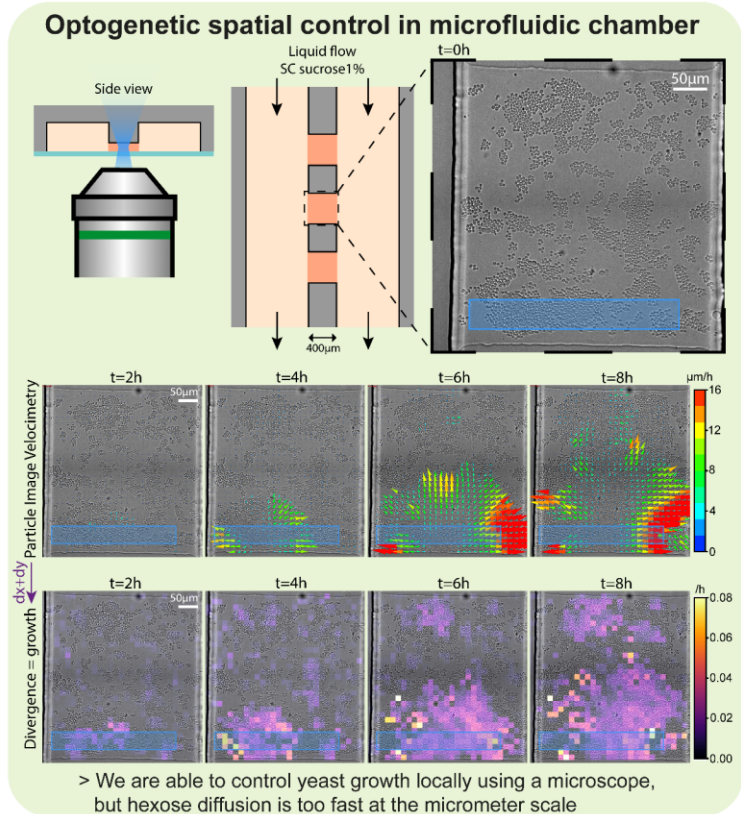
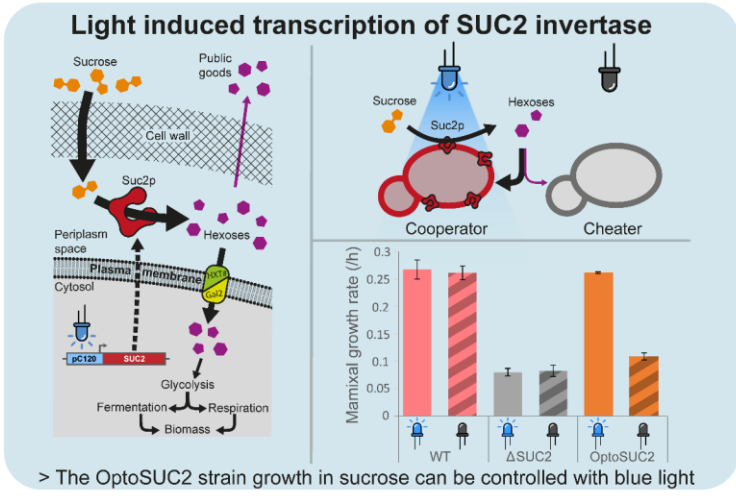
- Liu, J. et al. Metabolic co-dependence gives rise to collective oscillations within biofilms. *Nature* 523, 550–554 (2015).
- Koschwanez, J. H., Foster, K. R. & Murray, A. W. Improved use of a public good selects for the evolution of undifferentiated multicellularity. *eLife* 2, e00367 (2013).
- Momeni, B., Waite, A. J. & Shou, W. Spatial self-organization favors heterotypic cooperation over cheating. *eLife* 2, e00960 (2013).
- Roell, G. W. et al. Engineering microbial consortia by division of labor. *Microb. Cell Factories* 18, 35 (2019).

## Perspectives

- Developing a setup for **real-time control** of microbial communities.
- Understand more on how **spatial structure** can affect **population fates**.
- Investigate how **division of labor** could be applied in **bioproduction**.

Matthias Le Bec, Sylvain Pouzet, Céline Cordier, Simon Barral, Benoit Sorre, Alvaro Banderas, Pascal Hersen

Institut Curie, Université PSL, Sorbonne Université, CNRS UMR168, Laboratoire Physico Chimie Curie, 75005 Paris, France



### Model for simulation

Partial Differential Equations Solver

Sucrose concentration:  $\frac{dS}{dt}(x) = D_S \frac{d^2S}{dx^2} - I(x)$

Hexose concentration:  $\frac{dM}{dt}(x) = D_M \frac{d^2M}{dx^2} + 2I(x) - Q(x)$

Invertase activity:  $I(x) = E(x) K_{cat} \frac{S}{K_M + S}$

Hexose consumption:  $Q(x) = \left( V_{max}^1 \frac{M}{K_M^1 + M} + V_{max}^2 \frac{M}{K_M^2 + M} \right) d_{cell}(x)$

Invertase concentration:  $\frac{dE}{dt}(x) = \alpha \frac{M}{K_M + M} d_{cell}(x)$

Cell density:  $\frac{d(d_{cell})}{dt}(x) = \mu_{max} \frac{M}{K_S + M} d_{cell}(x) - \gamma d_{cell}(x)$

### Conclusions:

- We are able to control yeast growth in sucrose through light inducible SUC2 production
- Microfluidic chips and the OptoCube allow to investigate different spatial scales
- The *Saccharomyces cerevisiae* catabolism for sucrose act as a pass-band filter:
  - > low cut-off wavelength (~10mm) due to cheater competition for glucose
  - > high cut-off wavelength (~17mm) due to cooperator competition for sucrose

## 2. Protocols

### 2.1. Molecular biology

# 2.1.1.Culture Media for yeast

Authors: Céline Cordier, Sylvain Pouzet

## CSM

CSM (Complete Supplement Mixture) is one of the most used culture media for *S. cerevisiae*. It is especially useful if you want to select for auxotrophic markers (i.e. remove one or more amino acid).

### List of Reagents

Aa Ingredient	# for 1L (gr)	Σ for 200mL (gr)	≡ ref
<u>Yeast Nitrogen Base w/o AA</u>	6.7	1.34	BD ref: 291940
<u>Glucose (Dextrose)</u>	20	4	euromedex ref: UG3050
<u>CSM (Dropout mix)</u>	0.8	0.16	MP Biomedicals™ ref: 114500022 or ForMedium DCS0029
<u>For 2% Agar Plates only : Bacto Agar</u>	20	4	BD Biosciences ref: 214010

## Protocol

1. Prepare first a 10x glucose stock solution (200g/L). This can be prepared by dissolving 40g of glucose into 100mL of distilled H2O, and then complete with distilled water up to 200mL. Autoclave this and keep it sterile (program 4, add tape, unscrew cap).
2. Mix Yeast Nitrogen Base (w/o Amino Acid), CSM dropout mix and if needed agar in a 500mL bottle.
3. Add 180 mL of water (to prepare a 200mL final solution).
4. Autoclave

 [Autoclave](#)

5. Add 20mL of your glucose stock solution working in a sterile environment (under the PSM or near a flame on your bench).

For Auxotrophic marker selection, use a CSM without the desired AA, e.g. CSM-URA. We have several of them in the lab.

## Notes

how to autoclave something?

 [Autoclave](#)

It is important to autoclave glucose separately so that the CSM medium remains relatively clear and is not too much autofluorescent for microscopy experiments.



For microfluidics experiments, it is better to mix all the components (glucose powder included), shake until complete dissolution, and filter sterilise the medium to remove dust (that would be a problem in your device during experiments).

## CSM 4X for microfluidics

### List of Reagents

Aa Ingredient	# for 500 mL (gr)	≡ Ref
---------------	-------------------	-------



Aa Ingredient	# for 500 mL (gr)	≡ Ref
<u>Yeast Nitrogen Base w/o AA</u>	13.4	BD ref: 291940
<u>Glucose (Dextrose)</u>	40	euromedex ref: UG3050
<u>CSM (Dropout mix)</u>	1.6	MP Biomedicals™ ref: 114500022

## Protocol

Mix the three components in a beaker containing 300 mL of distilled water. Wait for total dissolution under shaking for 30-60 min. Measure the exact volume and adjust to 500 mL with distilled water. Filter sterilise (0.2 um), do not autoclave.

## YPD

YPD is a cheap, rich growing media, mainly used for agar petri dishes or for growing to high OD in Li-Ac transformations or before freezing strains.

For agar plates: YPD Agar plate media already prepared (Ref 4001-232 MP Bio) — 67g for 1L — Autoclave and pour

For YPD liquid: YPD powder media already prepared (Ref 4001-032 MP Bio) — 50g for 1L — Autoclave and use

### List of Reagents

Aa Ingredient	≡ for 1L	≡ for 200mL	≡ ref
<u>Difco Yeast extract</u>	10g	2g	
<u>Glucose (Dextrose)</u>	20g	4g	
<u>Bacto Peptone</u>	20g	4g	
<u>For 2% Agar Plates only : Bacto Agar</u>	20g	4g	

## YPG - Agar plates

YPG means with glycerol as carbon source: eliminates the *petite* phenotype.

### List of Reagents

Aa Ingredient	≡ for 1L	≡ for 500mL	≡ ref
<u>Yeast extract</u>	10g	5g	Bacto/BD ref: 212750
<u>Glycerol</u>	50mL	25mL	Sigma Aldrich ref: G2025-1L
<u>Peptone</u>	20g	10g	Bacto/BD ref: 211677
<u>For 2% Agar Plates only : Bacto Agar</u>	20g	10g	Bacto/BD ref 214010

## Protocol

For 500mL:

Get the ingredients ready (to be found in chemical shelf)

- 1L/500mL cylinder (glass shelf)
- Spatulas (near the sink)
- 1L Bottle

1. 300 mL of distilled water in the bottle
2. Weigh yeast extract, peptone and agar: put it in the bottle (those take ~30mL volume)
3. Add the Glycerol using the pipetboy and a disposable 25mL pipet
4. Stir using magnetic bar on stirring plate (won't fully dissolve - agar need more heat).

5. Pour in cylinder and top up to 500mL with distilled water
6. Put back in bottle and stir some more
- ▼ 7. Autoclave (stirring bar can stay in)

 Autoclave

8. Stir while cooling down on stirring plate ~1hour
- ▼ 9. Display in petri dishes (about 13)
  - Prepare petri dishes with appropriate color code
  - Pour medium, close petri dish
  - Leave at RT O/N
  - Flip around and leave at RT for 2 days
  - Keep at 4°C.

## SC + 5-FOA plates

5-FOA medium is used to counter-select the URA3 gene.

### List of Reagents

Aa Ingredient	≡ for 1L (gr)	≡ for 700mL (gr)	≡ ref
<u>Yeast Nitrogen Base w/o AA</u>	6.7g	4.69g	BD ref: 291940
<u>Glucose (Dextrose)</u>	20g	14g	euromedex ref: UG3050
<u>CSM-URA (Dropout mix)</u>	0.8 g	0,56	MP Bio ref: 4511-212
<u>For 2% Agar Plates only : Bacto Agar</u>	20g	14g	BD Biosciences ref: 214010
<u>Uracil (1g/L in H2O), filtered</u>	50 mL	35 mL	
<u>5-FOA (at the end after autoclave)</u>	0.8 g	0.56 g	Fisher ref: 10619920

## Protocol

1. For 700 mL (adjust the volume according to your needs, 5FOA is expensive and plates expires quickly): prepare a bottle filled with 665 mL H2O + 35 mL Uracile solution at 1g/L and add powders (YNB, Glucose, CSM-ura and bacto agar).
2. Autoclave. The bottle should not be filled more than 700mL in 1L bottle. Do not forget to add special autoclave tape and to unscrew the bottle cap.

 Autoclave

3. Cool-down the medium after autoclave. After ~30 min (T=55°C, you can hold the bottle bare hand) add the 5-FOA. Let the solution stir for 5 min.  
Warning: Wear a mask + goggles while weighing 5-FOA
4. Poor in plate

## 2.1.2.LiAc transformation in *S. cerevisiae*

**Authors: Sylvain Pouzet, Céline Cordier, Matthias Le Bec**

This protocol describe how to put a piece of DNA (plasmid or linear) in yeast cells. At the end you want to be able to select for the yeast colonies that successfully "absorbed" the DNA, so you have to always has a selection marker in your piece of DNA.

### Materials & Equipment

- ▼ PEG 3350 50% (Sigma Aldrich/ref: 20244-250G)
  - 25g for 50mL
  - 25g + 20 mL distilled water in beaker w/ magnetic bar
  - put on heating plate (50C) for around 45min under agitation
  - measure volume w/ pipet and add water up to 50mL
  - Filter using 0.45um filter (too viscous for 0.2um)
- ▼ LiAc 1M (Sigma Aldrich/ref: L4158-250G)
  - 5.1g in 50mL dH<sub>2</sub>O
  - filter 0.2 um
- ▼ LiAc 0.1M
  - 5mL of 1M solution + 45mL dH<sub>2</sub>O
- ▼ Salmon Sperm DNA at 2 mg/mL (Sigma Aldrich/ref: D9156-5ML)
  - aliquots stored at -20°C
  - YPD medium (liquid) (MP Biomedicals™ 114001032)
  - sterile distilled water
  - plasmid to be transformed
  - (repair strand)
- Water bath 42C
- Incubator 30C

### Protocol

- **grow strain o/n** at 30C in at least 2mL YPD
- **grow for 4 hours** in the morning: 100-200µL of cells in 5mL YPD: (until  $\sim 1 \cdot 10^7$  cells/mL; OD<sub>660</sub>spectro= 1.0)
  - Check water bath at 42C
  - Check Salmon Sperm DNA was boiled (10min at 99C in PCR machine)
  - Check all solutions are at Room Temperature (including water)
  - Check plasmid volume for transformation
- ▼ **Clean cells:** water, water, LiAc0.1M
  - Big centrifuge in the lab at the entrance for tubes:
    - 3 000 rpm x 7min at RT**
    - Empty supernatant
    - Add **950uL dH<sub>2</sub>O** (yeasts are strong, they can sustain that)

- resuspend w/ ups and downs w/ the pipette
- transfer in an **eppendorf tube**
- centrifuge 11 000 rpm x 1min (smaller centri)
  - remove supernatent w/ pipet
  - wash again with **950uL dH2O** (resuspend)
- centrifuge 11 000 rpm x 1min
  - remove sup
  - wash with **950uL LiAc 0.1M**
- centrifuge 11 000 rpm x 1min
  - remove sup

**Add to clean pellet** (watch out for the order:)

- 240 uL PEG 50% (slowly pipet)
- 36 uL LiAc 1M
- 50 uL boiled Salmon Sperm (2mg/mL)
- 34 uL plasmid (miniprep total 0.5 - 1 µg) or PCR fragment (total ? µg)

▼ **Note : no more than 6min for all those steps**

otherwise PEG is going to damage the cells.

- Set pipets to rights amounts before

**VORTEX** the tubes

▼ Incubate at **30C** x 30min

in the classic big incubator

▼ Incubate at **42C** x 30min

in the water bath that was preheated at least one hour before, or in the heating tube holder

▼ **Clean** with dH2O, resuspend in 110µL dH2O

to remove transformation reactants.

- centrifuge 11 000 rpm x 1min
- discard supernatant **with P1000**
- resuspend pellet with 1mL dH2O: gently pipet up and down, this resuspension will be a bit longer than before (you can do it in 2 steps).
- centrifuge again 11 000 rpm x 1min
- discard supernatent
- resuspend in 110 uL dH2O

## Plating: depend of your selection marker

### URA3 (or other auxotrophic marker)

▼ Plate on SC-URA petri dishes and grow for > 2 days

2 petri dishes per transformation :

- 100 uL on the first one
- transfer 10 uL in 90yL dH2O to dilute the cells and plate on the second one.
- Streak a few colonies on a new SC-URA, grow for > 2 days

### **Kanamycin G418 (plates at 350µg/mL, G418 stock is at 200mg/mL)**

NO SC media or plate, it interact with the Kanamycine !!!

Preferably resuspend in 200µL H2O. Then divide in 2 different "plating techniques":

**A.** Plate half on YPD petri dishes and grow at 30°C for 14-16h. Replica plate from YPD to YPD+G418 plates using velvets, grow for > 2 days

**B.** Add 1mL YPD to the other half, grow at 30°C for 2h, centrifuge, discard, resuspend in 100µL H2O, plate on YPD+G418, grow for > 2 days

- Streak a few colonies on a new YPD+G418, grow for > 2 days

## 2.1.3. CRISPR/Cas9 for *S. cerevisiae*

Authors: Fabien Duveau, Sylvain Pouzet, Erwan Eriau

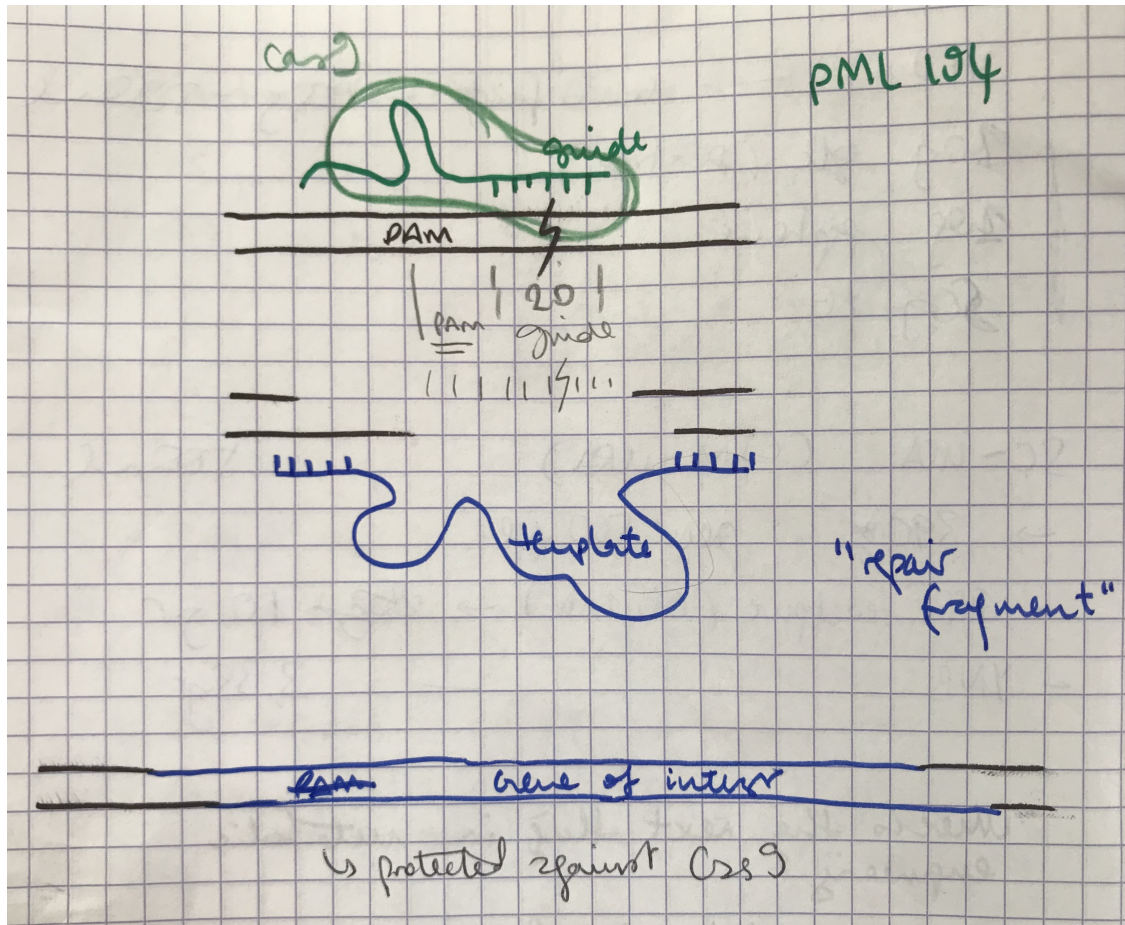
GOAL : Insert a piece of DNA in yeast and co.

Based on [Laughery et al. 2015](#).

▼ More details

Explain the basic principles/functioning of CRISPR things...

▼ Drawing:



### 1. *In silico* design

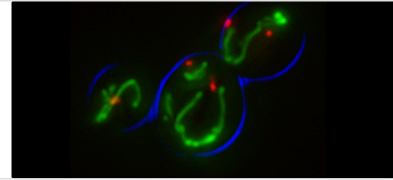
#### 1.0 Get things ready

- Get onto [Geneious](#)
- ▼ Get initial genomic state of the region of interest and annotate it.
  - can be raw from yeast database:

## Saccharomyces Genome Database | SGD

The Saccharomyces Genome Database (SGD) provides comprehensive integrated biological information for the budding yeast *Saccharomyces cerevisiae*.

<https://www.yeastgenome.org/>



Find gene/area and generally download "Genomic DNA +/- 1kb".

- can be from previous construction according to the strain and loci.

## 1.1 CRISPR design

### ▼ Decide where to CUT

- On geneious, use the "Find CRISPR Sites" in the "Cloning" toggle at the TOP of the window.
- Choose the best one (best "Doench activity score")
- Annotate the PAM sequence and the CRISPR site
- Name the file "myregion\_CRISPR"

### ▼ Design Oligos to produce the guideRNA

- Get to:

#### CRISPR Toolset

Click here to identify guide RNA target sites in a user specified yeast gene

<http://wyrickbioinfo2.smb.wsu.edu/crispr.html>

```
mutator target
          4
Rim1 protein:..T T I E L D N L A A E T C A Y M T..
gDNA: 5'...aca aca atc gaa cta gac aac tta ggc cct gaa aca tgc cct tat atg act...3'
                                     PAM + guide target
                                     (on opposite strand)
mri1 D57N protein:..T T I E L N L A A E T C A Y M T..
Template: 5'...aca aca atc gaa ctaaac aac tta ggc cct gaa aca tgc cct tat atg act...3'

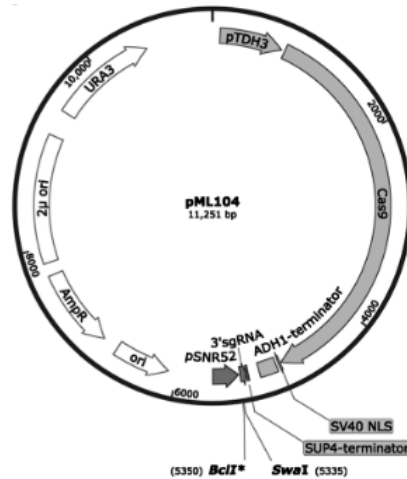
Mutations in Blue

Mutant Oligonucleotide Template:
OH108
```

- Chose to design user-designed guide RNA sequences (3rd choice)
- Enter guide RNA sequences INCLUDING PAM and submit
- /!\ If your guide is reverse, still **always give a Forward** sequence to the website : use the revert complement, that is, always give a sequence ending with the NGG PAM.
- You now have the two oligos to build the guideRNA and insert the sequence into the pML104 plasmid. Oligo lengths are 37 and 33 (for oligo 1 and 2 respectively)

### ▼ More details

- The oligos are built in a way such that they overlap to create a double-stranded DNA strand that will insert in the BclI and SwaI restriction sites upon digestion/ligation etc. into the plasmid below that also contains the Cas9 protein.



## 1.2 Final sequence

Draw the final sequence expected in the genome.

- Copy the previous "\_CRISPR" file and copy/cut/paste various DNA sequences!

### ▼ Get rid of the CRISPR PAM site ! (avoiding Cas9 cut in your final construct)

Either:

- Delete the whole sequence
- Turn NGG into NCG or other (if in coding sequence, find a synonym mutation with similar frequency: <https://www.kazusa.or.jp/codon/cgi-bin/showcodon.cgi?species=4932>)

### ▼ Add linker for fusion protein if needed

- remove previous stop codon
- remove subsequent start codon

### ▼ More details

These modifications will be introduced in the repair strand

## 1.3 Repair strand design

From another plasmid or genomic DNA sequence, oligos need to be designed in such a way that primers overhangs will correspond to genomic regions for homologous recombination (~70bp) while ~20bp correspond to the region to amplify from a plasmid containing the part to insert into the genome (à revoir).

- Copy the \_Final file and create the \_Repair file

### ▼ Design the 90bp oligos

- Start with G for better hybridization
- Make sure the forward and reverse seqs make sense because geneious revcom options can be a bit tricky if not careful.

## 1.4 Primers for further verification

After transformation etc. we will check if the inserted sequence is correct:

### ▼ Design 20bp primers

- 150bp away from what we really want
- Expect 800nt sequenced for 1 primer



- Start with G for better hybridization
- Make sure the forward and reverse seqs make sense because geneious revcom options can be a bit tricky if not careful
- Check 9 to 14 CGs out of the 20bp

## 1.5 Order oligos

- ▼ Get onto [IDTDNA](#)

### Integrated DNA Technologies - Home

Integrated DNA Technologies, Inc. (IDT) is your Advocate for the Genomics Age, providing innovative tools and solutions for genomics applications

 <https://www.idtdna.com/pages>



- paste the info in the table format using an excel sheet as intermediary

## 2. At the bench

### 2.0 Get things ready

- ▼ Prepare oligos

- Generally received 2 days after ordering
- Get ultrapure distilled water stock (15mL)

- ▼ Dilute to 100uM

#### [Resuspension of Oligonucleotides](#)

- Spin down (coz some lyophilized DNA might be on the lid)
- Add the right amount of water:
  - If written 29.5 nmol on the tube: add 295  $\mu$ L.
  - If written 65 nmol on the tube: add 650  $\mu$ L.
- Shake shake shake it up
- Spin down
- Write number on lid
- Stock in the -20 in common oligonucleotides database (red boxes)
- Can make your own 10uM fyawanna

### 2.1 Build guide-containing plasmid


- ▼ pML104 Maxiprep - *if needed*

- Grow pML104 (glycerol stock bPH\_140) O/N

Note: pML104 must be grown in a dam- cell type for the subsequent steps to work.

- ▼ pML104 Digestion - *if needed*

Warning: it is recommended to do a big pool of digested pML104 for the common stock. Typically, do 16 individual 1 $\mu$ g in 50  $\mu$ L reactions in PCR microtubes (2 strips of 8 PCR tubes) and combine them together before PCR cleanup step. Prepare a master mix with 16  $\mu$ g of pML104 in 800  $\mu$ L reaction volume and then do 50  $\mu$ L aliquots in microtubes.

- For a 50  $\mu$ L reaction volume:
  - 1  $\mu$ g pML104
  - 1  $\mu$ L BclI
  - 1  $\mu$ L SwaI
  - 5  $\mu$ L Buffer 3.1 (NEB)
  - Top up with dH<sub>2</sub>O
- Digest at 25C for ~6 hours and then 50C for ~6 hours.
- Add 1  $\mu$ L rSAP and incubate at 37C for 1 hour.
- ▼ Use  [PCR clean-up \(Nucleospin\)](#)

pool 4 digestion tubes together and put each 200  $\mu$ L on a purification column. In total: 4 columns with 200  $\mu$ L/column. For each column, resuspend DNA after purification in 50  $\mu$ L ultrapure water (expected concentration after elution = 30-60 ng/ $\mu$ L)
- Use Nanodrop to get concentration (optional: check to digestion on a gel, with non digested plasmid as a control)
- !\ Might be already digested plasmid stock somewhere!
- ▼ **gRNA hybridization**
  - Better start at ~3pm for O/N ligation
  - Get the 33 and 37bp oligos designed online (*100 $\mu$ M stock fridge-20 drawer n°2 or make stock from powder*)
  - **For a 10 $\mu$ L reaction volume in PCR tubes:**
    - 6.5  $\mu$ L dH<sub>2</sub>O (*commercial*)
    - 1.0  $\mu$ L first oligo (*100 $\mu$ M stock*)
    - 1.0  $\mu$ L second oligo (*100 $\mu$ M stock*)
    - 1.0  $\mu$ L 10X (NEB) T4 **Ligase** Buffer (*fridge-20 drawer n°3*)
    - 0.5  $\mu$ L T4 **PNK** (*fridge-20 drawer n°3*)
  - Yes this is: Ligase buffer and PNK, this has been optimized
  - T4 PNK adds a 5' phosphate to the oligos
- ▼ Incubate at 37C for 30 minutes, 95C for 5 minutes, then decrease 1C every minute to 25C (~1h45). ("**HYBRIDIZ**" program on PCR machine)
  - Use the programme HYBRIDIZ in Fabien's saved programs
  - On the PCR machine, make sure 4 empty tubes are at the corners for homogeneous balance thing, with the same caps as your tubes.
- ▼ **Ligation**

Here the guide is inserted into the plasmid:


  - **For a 25  $\mu$ L reaction volume in PCR tubes:**
    - 100 **ng** of digested pML104 vector (*possible stock in fridge-20*)
    - 2.0  $\mu$ L of 1/20 diluted hybridized gRNA (add 190 $\mu$ L H<sub>2</sub>O in previous PCR tubes)
    - 2.5  $\mu$ L 10X T4 ligase Buffer (NEB) (*fridge-20 drawer n°3*)
    - 1.0  $\mu$ L T4 ligase (Invitrogen) (*fridge-20 drawer n°3*)
    - Top up with dH<sub>2</sub>O (*commercial*)
  - Incubate overnight at 16C followed by a 10 minutes at 65C. ("**LIGAT-CRISPR**" program on PCR machine ~16h)
- ▼ **Transformation in Bacteria**
  - First thing in the mornin', - and + controls plz.
  - ▼ Get a 50  $\mu$ L DH5alpha stock (*fridge -80C*) - keep on ice
    - + control: 500pg plasmid pUC (*standard plasmid with high transformation yield, fridge -20C drawer n°3*)
    - - control: no plasmid


- THEREFORE GET 3 TUBES (if you do more, you can take 5 DH5alpha tubes for 6 transformations because they contain a bit more than 50µL)
- Gently mix cells with pipette tip and aliquot 50µL in 1,7mL tubes **on ice**
- Add 2-10 µL of ligation product - do not pipet up&down but mix with the pipette
- Keep on ice 30 min
- Heat Shock: 20 seconds at 42°C (*bain-marie or hot tube holder*)
- Place back on ice for 2 min
- Under PSM or burner:
- Add 250 µL of SOC (*fridge 4°C*), incubate for 1 hour at 37°C (225 RPM, maybe more ?) - *prepare two LB plate per transformation (at RT)*
- Plate 150 µL on LB+Amp using glass balls
- ▼ Grow O/N at 37°C
 

Parafilm your plate and put them in the incubator upside down
- The next day: put them in the fridge 4°C
- ▼ Expected results
  - Relatively few transformants (about 10) but no false positives.
  - The negative control is helpful to checking that the Amp plates are still effective. If all is well, there should be ZERO colonies on the negative control.
  - The positive control should produce thousands of transformants if all is well. If fewer than thousands of colonies appear on the pUC plate, the cells may have poor viability.
- ▼ PCR screen insert - *if needed*

**In order to eliminate any transformed uncut WT plasmid from being used.**

  - Colony PCR: Take only part of colony so that there is more to glycerol stock later (and note which colony you have chosen).
  - Screen 2-8 colonies per transformation using primer oPH\_0032 (in the backbone of the plasmid) and one of the gRNA primers (check to make sure it's the correct direction, should be the primer with the overhang, total of 37 bp in length). It is an important negative control to also perform a PCR on pML104 (other gRNAs are not adequate controls because all have the primer sequence in common).
- ▼ Miniprep good colonies
  - Grow 2-4 positive colonies for 12-16 hours in 5 ml LB + 5 ul 100mg/ml Ampicillin.

Use  [Miniprep \(NucleoSpin\)](#) kit (elute in ~30 ul).

  - ▼ Use  [NANODROP](#) to get concentration.
 

Should be in the range of ~250 ng/ul. Anything below ~100 ng/ul is likely to fail
- ▼ Check Plasmid
  - Sequence miniprep using primer oPH\_0032 to confirm correct gRNA insertion
  - After sequences are back confirming correct insertion, prepare a glycerol stock.

## 2.2 Prepare Repair fragment

- ▼ PCR protocol
 

PCR mix (per 50 µL reaction): **on ice**

  - 25 µL Phusion 2x Master Mix (*fridge -20°C drawer n°3*) - *contains the taq etc.*


- 1  $\mu\text{L}$  Primer Fwd 10  $\mu\text{M}$  (*dilute the stock solution by 1/10, you can keep the diluted solution at  $-20^{\circ}\text{C}$* )
- 1  $\mu\text{L}$  Primer Rev 10  $\mu\text{M}$  (*dilute the stock solution by 1/10, you can keep the diluted solution at  $-20^{\circ}\text{C}$* )
- 1.5  $\mu\text{L}$  DMSO (*fridge  $-20^{\circ}\text{C}$  drawer n°3*)
- 16.5  $\mu\text{L}$  dH<sub>2</sub>O (*commercial*)
- 5  $\mu\text{L}$  DNA template (20 ng/ $\mu\text{L}$  plasmid or just water if primers are the template)

Thermocycler protocol:

1.  $98^{\circ}\text{C}$  for 2 min
2.  $98^{\circ}\text{C}$  for 20 sec
3.  $55^{\circ}\text{C}$  for 20 sec
4.  $72^{\circ}\text{C}$  for 30 sec (adapt this time depending on your oligo length)
5. Repeat 2-4 34 times
6.  $72^{\circ}\text{C}$  for 10 min
7.  $10^{\circ}\text{C}$  forever


After PCR, run 5  $\mu\text{L}$  of each sample on 1% Agarose gel with SybrSafe and take a picture under UV lamp.

## 2.3 Transformation in Yeast


 [Yeast Transformation CRISPR](#)

You will end up with ~8 yeast patches per transformation.

## 2.4 Verify colonies by sequencing


 [Yeast colony PCR screening](#)

Purify 2-3 successful PCR sample per transformation, send them to sequencing

 [How to sequence DNA samples](#)

## 2.5 Remove pML104

Patch the good clones onto 5FOA plates.  $30^{\circ}\text{C}$  for 2 days.

 If you intend to keep your clones for more than 1 week, patch them back to YPD (or YPG).

## 2.5 Add glycerol stock to yeast collection

# 2.1.4.S. *cerevisiae* transformation for CRIPSR

Authors: Sylvain Pouzet, Céline Cordier

## Materials & Equipment

- ▼ PEG 3350 50% (Sigma Aldrich/ref: 20244-250G)
  - 25g for 50mL
    - 25g + 20 mL distilled water in beaker w/ magnetic bar
    - put on heating plate (50C) for around 45min under agitation
    - measure volume w/ pipet and add water up to 50mL
    - Filter using 0.45um filter (too viscous for 0.2um)
- ▼ LiAc 1M (Sigma Aldrich/ref: L4158-250G)
  - 5.1g in 50mL dH2O
  - filter 0.2 um
- ▼ LiAc 0.1M
  - 5mL of 1M solution + 45mL dH2O
- ▼ Salmon Sperm DNA at 2 mg/mL (Sigma Aldrich/ref: D9156-5ML)
  - aliquots stored at -20°C
  - YPD medium (liquid) (MP Biomedicals™ 114001032)
  - sterile distilled water
  - plasmid to be transformed
  - (repair strand)
- Water bath 42C
- Incubator 30C

## Protocol

- **grow strain o/n** at 30C in at least 2mL YPD
- **grow for 4 hours** in the morning: 100-200uL of cells in 5mL YPD: (to get  $\sim 10^7$  cells/mL)
  - Check water bath at 42C
  - Check Salmon Sperm DNA was boiled (10min at 99C in PCR machine)
  - Check all solutions are at Room Temperature (including water)
  - Check plasmid volume for transformation (for 500ng to 1  $\mu$ g)
- ▼ **Clean cells:** water, water, LiAc0.1M
  - Big centrifuge in the lab at the entrance for culture tubes:
    - 3 000 rpm x 7min at RT**
    - Empty supernatant
    - Add **950uL dH2O** (yeasts are strong, they can sustain that)
    - resuspend w/ ups and downs w/ the pipette
    - transfer in an **ependorf tube**
  - centrifuge 11 000 rpm x 1min (smaller centri)
    - remove supernatent w/ pipet

- wash again with **950uL dH2O** (resuspend)
- centrifuge 11 000 rpm x 1min
  - remove sup
  - wash with **950uL LiAC 0.1M**
- centrifuge 11 000 rpm x 1min
  - remove sup

**Add to clean pellet** (watch out for the order:)

- 240 uL PEG 50% (slowly pipet)
- 36 uL LiAc 1M
- 50 uL boiled Salmon Sperm DNA (2mg/mL)
- 32 uL repair fragment
- 2 uL plasmid at ~ 300-500 ng/uL
- ▼ **Note : no more than 6min for all those steps**  
otherwise PEG is going to damage the cells.
  - Set pipets to rights volumes before

**VORTEX** the tubes

- ▼ Incubate at **30C** x 30min  
in the classic big incubator
- ▼ Incubate at **42C** x 30min  
in the water bath that was preheated at least one hour before)
- ▼ **Clean** with dH2O, resuspend in 110uL dH2O  
to remove transformation reactants.
  - centrifuge 11 000 rpm x 1min
  - discard supernatant **with P1000**
  - resuspend pellet with 1mL dH2O: gently pipet up and down, this resuspension will be a bit longer than before (you can do it in 2 steps).
  - centrifuge again 11 000 rpm x 1min
  - discard supernatent
  - resuspend in 110 uL dH2O
- ▼ Plate on SC-URA petri dishes and grow for > 2 days  
2 petri dishes per transformation :
  - 100 uL on the first one
  - transfer 10 uL in 90uL dH2O to dilute the cells and plate on the second one.
- ▼ Streak colonies on new SC-URA plates (**18 streaks per transformation**), grow for > 2 days  
After the transfo, big colonies are typically the good ones to select for streaking
- Under PSM or burner: Patch on YPG (**8 patches per transformation**), grow for > 2 days
- ▼ PCR and sequence 2-4 clones

check 🍷 [How to sequence DNA samples](#)

Remove pML104:

- Replicate YPG patch on 5-FOA
- Freeze positive strains

## 2.1.5. Plasmid transformation in home-made competent E.coli

**Authors: Jean-Baptiste Lugagne, Carine Vias, Céline Cordier, Gabriel Thon**

Transformation is the process by which foreign DNA is introduced into a cell. Transformation of bacteria with plasmids is important not only for studies in bacteria but also because bacteria are used as the means for both storing and replicating plasmids. Because of this, nearly all plasmids, even those designed for use in mammalian cells, carry both a bacterial origin of replication and an antibiotic resistance gene for use as a selectable marker in bacteria.

### Materials & Equipment

▼ Home-made NEB 10-beta competent E. coli (originally from NEB/ref: C3019I) from -80°C freezer. Thaw on ice. These cells are streptomycin resistant.

as many as you have plasmids to transform

- LB + antibiotic plates (as many as you have different plasmids to transform). Pre-heat them in the 37°C incubator to avoid heat shocks when you streak them.
- liquid LB medium (made from Sigma-Aldrich/ref: L3022-1KG)
- Plasmids you want to transform
  
- Water bath at 42°C
- Shaking incubator at 37°C
- Stationary incubator at 37°C
- sterile glass beads or Pasteur pipettes to spread cells on plates

### Protocol

#### First step (T = 0)

Let the cells melt 10 minutes on ice.

▼ Add between 10 pg to 100 ng (usually 50 ng works well) of your plasmids DNA into the tube. Do not leave them out of the ice for too long or touch the bottom of the tube with your fingers in order to avoid heat shocks. Put the cells back on the ice for about 20 minutes.

If it's for doing a transformation after a ligation, use 5 µL of your ligation. And if it's for a complex construction, make 2 transformations : one with 5 µL ligation and a second with 15 µL ligation.

Although it may be counter-intuitive, you will often get higher transformation efficiencies with less DNA, especially when using highly competent cells. If you used 100-1000 ng of total DNA in a ligation you will often get more colonies if you use 1 µL of a 1:5 or 1:10 dilution rather than 1 µL directly.

Put the tubes into the water bath at 42°C for 45 seconds (= heat shock).

Put tubes back on ice for 2 minutes to reduce damage to the E.coli cells.

Feed cells with 250-1000 µL sterile LB (with no antibiotic added).

▼ Incubate tubes for 1 hour at 37°C under agitation.

This outgrowth step allows the bacteria time to generate the antibiotic resistance proteins encoded in the plasmid backbone so that they will be able to grow once plated on the antibiotic containing agar plate.





This incubation step is not critical for Ampicillin resistance, because it takes a lot more time for ampicillin to take effect in the cell in comparison to other antibiotics. Before the ampicillin takes effect, the cells have plenty of time to express the resistance, and therefore do not need a recovering before being streaked on a plate.

## Second step (T +/- 1h)

Because after one hour of incubation you are not sure how concentrated your cells will be in the LB, you will have to streak two different concentrations on your plates to ensure that you get single colonies:

Drop 25-150  $\mu$ l of cells on a first plate (1X plate) and spread on the whole plate.

Centrifuge the rest of the cells 30s at 13000rpm. Remove supernatant, and re-suspend in the remaining LB. (After you quickly got rid of the supernatant, about 25-50 $\mu$ l of LB should remain in the eppendorf tube)

Drop 25 - 150  $\mu$ l of concentrated cells on another plate (10X plate) and spread on the whole plate.

▼ Incubate at 37°C for 12 to 15 hours

once you see colonies, do not leave them for too long at 37°C to avoid the development of satellite colonies

also possible to leave them between 10~20°C for a few days if some time is necessary. Some kind of plasmid can take until 20h to grow at 37°C.

## Third step (T +/- 12-15h)

Once your cells have grown into single colonies, you can pick them and grow them in 5 mL LB. Put 5mL LB + 5 $\mu$ L antibiotic in a 14mL round-bottom tube. Pick one isolated colony with the tip of your pipette cone and drop the cone in the tube (Do not forget to rinse the tip of your pipette with EtOH beforehand). Put them in the shaker at 37°C for ~12hrs.

## Fourth step (T +/- 8-15h)

Once the cells have grown in the tubes, you can start your miniprep.



A Golden Gate reaction mixture was prepared as follows: **0.5 µL** of each **DNA insert or plasmid**, **1 µL T4 DNA Ligase buffer** (NEB), **0.5 µL T4 DNA Ligase** (NEB), **0.5 µL** restriction enzyme, and water to bring the final volume to 10 µL. The restriction enzymes used were either **BsaI** (=BsaI-HFV2) or **BsmBI** (both 10 000 U/mL from NEB). The amount of DNA inserts can optionally be **normalized to equimolar concentrations** (~20 fmol each) to improve assembly efficiencies (not necessary **but highly recommended**!).

Reaction mixtures were incubated in a thermocycler according to the following program: 25 cycles of digestion and ligation (42 °C for 2 min, 16 °C for 5 min) followed by a final digestion step (60 °C for 10 min), and a heat inactivation step (80 °C for 10 min).

You can use **NEB online tool** to design your parts, and they can automatically find you smart overhang to get **scarless junction**:

<https://goldengate.neb.com/>

## Different modules and levels:

⚠ NEVER use a MoClo plasmid l0 as template for a PCR that will be used for another l0. The problem is that you will have residual template plasmids during your transformation instead of the new construct. Instead you can use a l1 for template as it require another antibiotic selection! ⚠

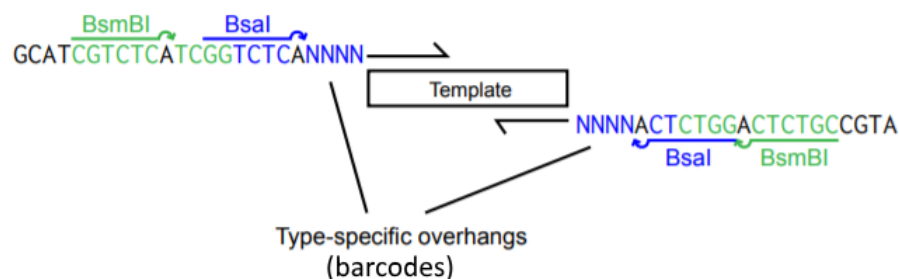
- ▼ Add a new sequence to the MoClo: Construction of "Part Plasmids" (or "level 0")

The goal is to insert your sequence+overhangs into the "Part Plasmid Entry Vector" (pYTK001)

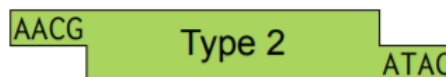
**Check if there is BsmBI (CGTCTC) or BsaI (GGTCTC) site in your SOI (see below)**

1. Design the primers

- ▼ You have to add overhang to your Sequence Of Interest (SOI or template). The overhang should contain: BsmBI site, BsaI site, a barcode and **possibly** start/stop codon or CC linker.



The barcode should correspond to the "Type" of your SOI. For exemple if your SOI is a promoter, you should add AACG and ATAC.



- ▼ If your SOI is a coding sequence, you should do type 3, 3a, 3b and 4a !!!

Your SOI should not have neither a Start codon nor a Stop codon; and you should add CC just before the barcode (link for fusion proteins)

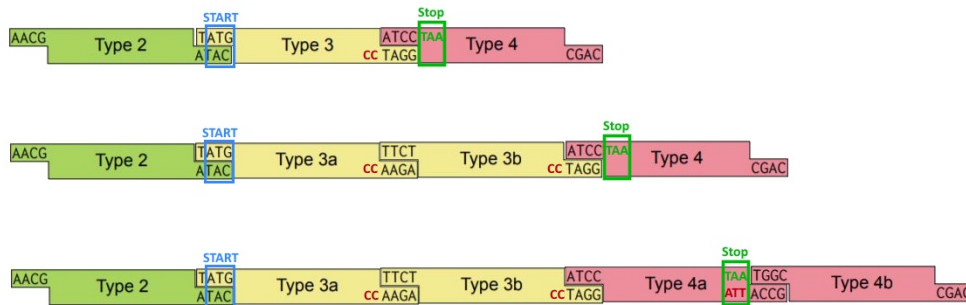
Except for the 4a: you have to add a Stop codon at the end: ATT-ACCG

- ▼ If your SOI is a terminator, you should do type 4 and 4b !!!

4: You have to add a Stop codon at the beginning: ATCC-TAA

4b: Don't add a stop codon

⚠ You have to be careful to add or remove start/stop codon and GG linkers for some of them ⚠



2. Do PCR to amplify your fragment (Phusion Master Mix). (don't use template lv0 !)  
Check out PCR protocol "repair fragment" in [CRISPR for Yeast](#)
3. Purify PCR product with Wizard kit (not sure if necessary but very probable that it is)  
If you are worried that you will have not enough DNA, recover in 30µL H2O instead of 50µL
4. Insert your sequence+overhangs into the "Part Plasmid Entry Vector"  
Perform a BsmBI Golden Gate reaction with the entry vector and your PCR product (sequence+overhangs)
5. Transformation - amplification  
This step select only good plasmid and produce a good amount of your "Part Plasmids"  
Transform the "Part Plasmid" in bacteria (DH5 or home-made ones works), you can then select for **chloramphenicol** antibiotic and/or **anti-green** expression. Typically I transform 10µL of plasmid (see [Yeast Transformation CRISPR](#))
6. [Miniprep \(NucleoSpin\)](#) & sequencing (oPH\_331 and oPH\_332)

To pick anti-green colonies: use blue led + green filter paper

▼ Create an assembly (typically one gene) (or "level 1")

**IMPORTANT: there are two ways to get lv1: either you use a pre-built vector (eg.pYKT110 or you can make your own with the lv0 pYTK47) and you will select for anti-GFP; either you build your lv1 plasmid using only lv0 plasmid and will select for anti-RFP.**

The goal is to assemble all the part you need to get the synthetic gene.

Typically you will assemble in order: promoter, coding sequence, terminator.

If you have done correctly the first step (Construction of "Part Plasmids"), each "part plasmid" will have the correct barcode.

If you want to use this individual cassette in a multi-gene assembly(lv2), you as to design first the all multi-gene assembly to choose the right connectors. If not just take **ConLS and ConR1**.

Perform a **Bsal Golden Gate** assembly with the following "part plasmids":

- An assembly connector Left (ConL)
- A promoter
- A coding sequence
- A terminator

- An assembly connector Right (ConR)
- Part type 6 (by default let's say LEU)
- Part type 7 (pYTK082)
- Part type 8 for Bacteria selection (let's say Amp as default: pYTK083 or pYTK089)

Transform the GoldenGate product in bacteria (DH5 or home-made ones works), you can then select for **Ampicilin** antibiotic and/or **anti-red** expression. Typically I transform 10µL of plasmid (see 📄 [Yeast Transformation CRISPR](#) )  
Miniprep&sequencing with oPH\_335 and oPH\_336

To pick anti-rfp colonies: use green led + red filter paper

▼ Create a multi-gene assemble (or "level 2")

You should have all your "level 1" assembly, with a good succession of connectors. (The first cassette must contain the ConLS part, and the last cassette must contain the ConRE part)

▼ Remove a BsmBI (CGTCTC) or BsaI (GGTCTC) site in your SOI

You can remove the restriction site at the same time as inserting your SOI in the lv10 plasmid. To do so, you need to do two different PCR of your SOI, one before the restriction site and one after. The 2 primers used close to the restriction site should be design with only a BsmBI site, with a user-defined barcode which will replace the restriction site to remove (mutate one nucleotide with a silent mutation), so that the two PCR will assemble during the GoldenGate reaction .

## Genome integration:

▼ Using PCR (best and easiest method for CRISPR)

- For CRISPR:

Use your plasmid to PCR the fragment of interest + overhangs with homology to the locus to target.

Typically you can use oPH524&525 to PCR anything between **ConLS** and **ConR1** for HO loci integration

In this case, use pML104 plasmide expressing the gRNA targeting HO = pPH\_162

- For Selection marker (homologous recombination)

Use your plasmid to PCR the fragment of interest (including the Type 6 selection marker) + overhangs with homology to the locus to target.

If this PCR is too long or fail (notably for lv12), use the restriction enzyme NotI below

▼ Using restriction enzyme NotI (not convenient because one plasmid only target one locus)

[If you have a NotI restriction site in your construct, you have to do a PCR as repair fragment](#), otherwise:

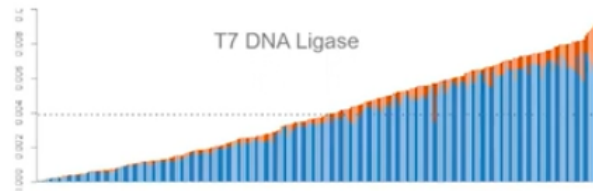
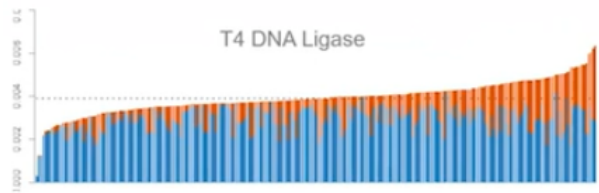
You just have to choose 2 part for locus homology, ex:

-7 URA3 3' Homology (pYTK086)

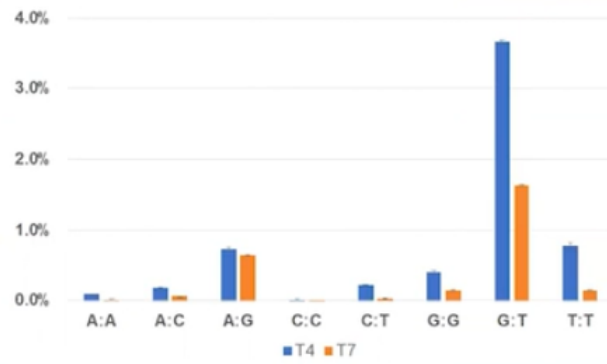
-8b URA3 5' Homology (pYTK092)

Between them : 8a AmpR-CoIE1 (pYTK089). This will be use as selection in bacteria AND to cut your plasmide (NotI restriction site) before transformation in yeast





All possible combinations of overhang



## Construction of the strains used

All yeast strains used in this study are derived from the BY4741 yeast background (EUROSCARF Y00000) and are listed in Table S1. All genetic parts have been integrated in the genomic DNA of the yeast to ensure construct stability, and all transformations have been performed using a classical Lithium-Acetate protocol. For better comparisons between the strains, all strains possess a nuclear marker mApple-HTB2 and an EL222 expression cassette. They have been integrated at the HTB2 or HIS3 locus using Kanamycin G418 resistance or HIS selection marker respectively (using a PCR product from pPH\_330 and digested pPH\_297 respectively). The rest of the genetic modifications were undertaken using the CRISPR/Cas9 system<sup>1</sup>. Guide RNA sequences (gRNA) were obtained from oligo synthesis (IDT) and integrated in the plasmid pML104 which already possesses a Cas9 expression cassette and a URA3 marker used for auxotrophic selection. The repair strands were obtained from either oligo hybridisation for deletion, or PCR product from plasmid for integration.

1. Laughery, M. F. *et al.* New Vectors for Simple and Streamlined CRISPR-Cas9 Genome Editing in *Saccharomyces cerevisiae*. *Yeast Chichester Engl.* **32**, 711–720 (2015).



## 2.2. Tools and devices

## 2.2.1. OptoCube - Spatially resolved light stimulation

Author: Matthias Le Bec

### Build the OptoCube

Building an OptoCube is cheap and easy to do, the main expense been the commercial incubator. One could also build a DIY incubator with thermal regulation, but it might induce heterogeneous temperature around the sample which tend to favour condensation on the petri dish lid. The DMD could also be replaced by a cheap video projector but it might be less performant for its intensity range and its leaking. The flatbed scanner model can also be change as many models are supported by the VueScan software. For the model Canon LIDE400, we had to open the glass cover and apply black tape on some part of the bottom which are reflecting surfaces (this prevent undesired optogenetic activation reflection artefacts). Other Arduino-like microcontrollers could be used instead of the classical Arduino UNO.

The DMD is facing down, mounted on an incubator rack using OpenBeam construction kits. The scanner is placed below, facing up, on an incubator rack. The distance between the scanner glass and the DMD lens was 39cm.

The DMD is powered with a 12V 4.16A power supply and connected to the Arduino at the pins J11.4 and J11.5 using a molex 51021-0600 connector. The scanner is connected to the computer with a USB cable. The Arduino UNO is also connected to the computer with a USB cable to allow serial communication, and is controlling the DMD using its pin number to apply 3.3V at the J11.5 pin trough a voltage divider (2.2kOhm and 3.3kOhm). The Arduino 3.3V pin is connected to the J11.4 pin. The voltage divider was done using a prototyping breadboard.

### Script for Arduino and Jupyter

The scripts can be found on the following github repository: <https://github.com/Lab513>

#### ▼ Jupyter script

```
import serial
import time
from time import sleep
import os

ser = serial.Serial('COM3', 9600, timeout=1) #Connect the Arduino

ser.write(b'H') # Send the command "LED HIGH" to the Arduino
ser.write(b'L') # Send the command "LED LOW" to the Arduino

dirInput = "C:/Users/public/Desktop/OptoCube/Timelapse/CUB01/"
deltat=60*30 # framerate of the timelapse in VueScan in sec
pulselen=30 # Length of light pulse in sec
pulseperiod=60 # Length of pulses period in sec (light + dark)

ListImage=[f for f in os.listdir(dirInput) if os.path.isfile(os.path.join(dirInput, f))] #import all file in the directory dirInput without subfolder
nfile=len(ListImage)
endpictime=int(time.time()) #initialise with the time of script run
lastpulse=int(time.time()) #initialise with the time of script run
imaging=0

### Launch a timelapse:
print("Loop start at", time.strftime('%Y/%m/%d %H:%M:%S', time.gmtime()))
print("Condition Initial: nfile=",nfile, " EndPicTime=",endpictime," lastpulse=",lastpulse)
while (1>0):
    nfilenow=len([f for f in os.listdir(dirInput) if os.path.isfile(os.path.join(dirInput, f))])
    nowtime=int(time.time())

    if (nfile!=nfilenow): #Detect the end of the scan process to synchronize the next scanning
        nfile=nfilenow
        imaging=0
        print("NewImageDone at", time.strftime('%H:%M:%S', time.gmtime()))
        print("nfile=",nfile)
        endpictime=nowtime
        print("End Pic Time=",endpictime)
        sleep(0.5)

    if (nowtime==endpictime+deltat): #Turn OFF the DMD during scanning
        print("NewImage at", time.strftime('%H:%M:%S', time.gmtime()))
        print("nfile=",nfile)
        ser.write(b'L')
        imaging=1
        nowtime=int(time.time())
        sleep(0.5)

    if (nowtime>=lastpulse+pulseperiod)and(imaging==0): #Turn ON the DMD if pulseperiod is "done"
        lastpulse=nowtime
        print("NewPulse at", time.strftime('%H:%M:%S', time.gmtime()))
        ser.write(b'H')
        print("DMD ON")
        sleep(0.5)

    if (nowtime==lastpulse+pulselen): #Turn OFF the DMD if pulselenght is "done"
        ser.write(b'L')
        print("DMD OFF")
        print("EndPulse at", time.strftime('%H:%M:%S', time.gmtime()))
        sleep(0.5)

    sleep(0.5) #refresh every 0.5sec
```

#### ▼ Arduino script

```
const int pinDMD=2;

void setup() {
  Serial.begin(9600);
  pinMode(pinDMD, OUTPUT);
}

void loop() {
  while(Serial.available()>0){
    int received_value = Serial.read();
    //Serial.println(received_value);
    if (received_value=='H'){
      Serial.println("HIGH");
      digitalWrite(pinDMD,HIGH);
    }
    if (received_value=='L'){
      Serial.println("LOW");
      digitalWrite(pinDMD,LOW);
    }
  }
}
```

To run the Jupyter script, you need to install the following package: serial, time and os

You can alternatively directly download an anaconda environment containing all required packages with the following link:

<https://anaconda.org/matthias.lebec/optocube>

## VueScan parameters

Media: "Black&White"

Media size: A4

Output file: 16 bit greyscale .tiff (no reduction nor compression)

Make Grey from: Auto

Scan resolution: 600 dpi

Number of passes: 1

Color balance: "None"

## Plate requirement

Plates should be:

- Highly transparent gel to avoid light scattering
- Thin gel to allow the yeast layer to be in the focal plan of the scanner
- The lid should be coated with a surfactant solution to reduce droplet formation due to condensation. Eg: solution of Triton 100X 0.05% (v/v) (Eth 20%)

## How to control the DMD

The DLP® LightCrafter™ 4500 TI is a Digital Micromirror Device composed of 912 × 1140 micromirror that can switch ON or OFF to reflect the light coming from integrated LEDs (Red, Green and Blue). The projected pixel intensity is controlled by Pulse Width Modulation. An important technical limitation is that even when the mirrors are completely OFF, there is a significant amount of light leaking out of the DMD onto the projected surface.

The DMD offer two main modes of projection: video mode or sequence mode. The video mode is performed through classical HDMI communication with a computer, allowing for straightforward and dynamic patterning. However, the range of light intensity in video mode is quite reduce, with a strong leaking. We thus used the sequence mode which give better intensities range (from 0.0014 mW/cm<sup>2</sup> to 1.13mW/cm<sup>2</sup> for the blue LED). The main drawback of this mode is the rigidity to change the mask to pattern. Indeed, masks has to be loaded in the DMD before the experiment using the DLPLCR software, and the maximum number of 8-bits masks that can be stored is 6.

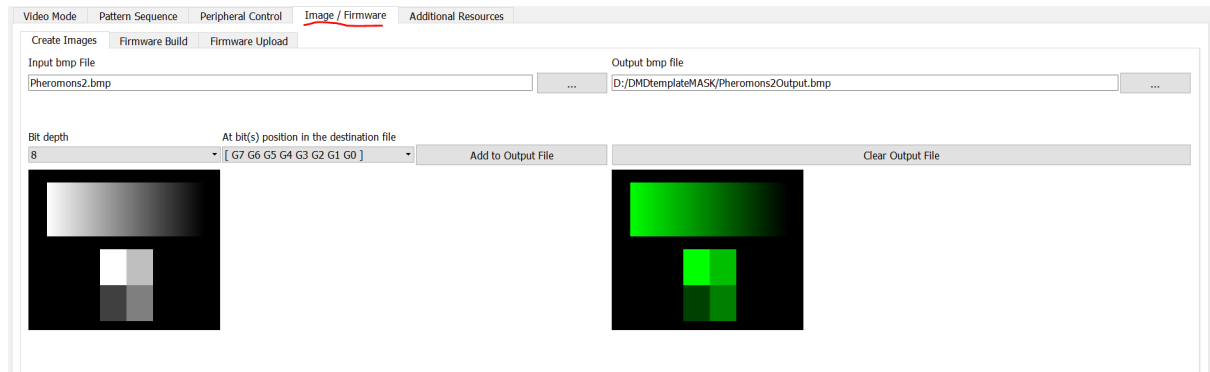
We use the DLPLCR software to create and load the masks, and to design the pattern sequence. More information on the procedure can be found in the DMD user guide. Briefly the workflow is the following:

1. Create a 8 bits image in the BMP format, of dimension 912x1140 (Width x Height). The pattern has to be drawn with a 200% deformation in the vertical axe (due to the diamond shaped of the mirrors)
2. This image is transformed by the DLPLCR software to a 24 bits BMP image.
3. In the DLPLCR software we load the 24 bits images to add to the Firmware. The firmware is then built.
4. Connect the Computer to the DMD using a USB cable and power the DMD. (This is not mandatory for the previous step)
5. Load the firmware in the DMD.
6. Edit the pattern sequence and save it in the DMD. You can then unplug the computer to the DMD.

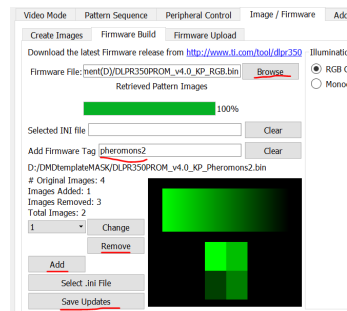
## "DLP Light Crafter" Software

### Create a mask compatible with the DMD, and save them in the firmware

1. create Bitmap image (8-bit) in illustrator or imageJ with a specific pixel size (Careful you need to actually double the verticale scale (weird property of the DMD...), so it give 912x1140) [For illustrator, display the pixel grid, be careful that the pixel your draw are align with this pixel grid. Export as bitmap, grey level, resolution "screen" 72pp, smoothing : "text optimized". Be careful the color of the document is RGB for grayscale values]
2. load it in the tab Image/firmware



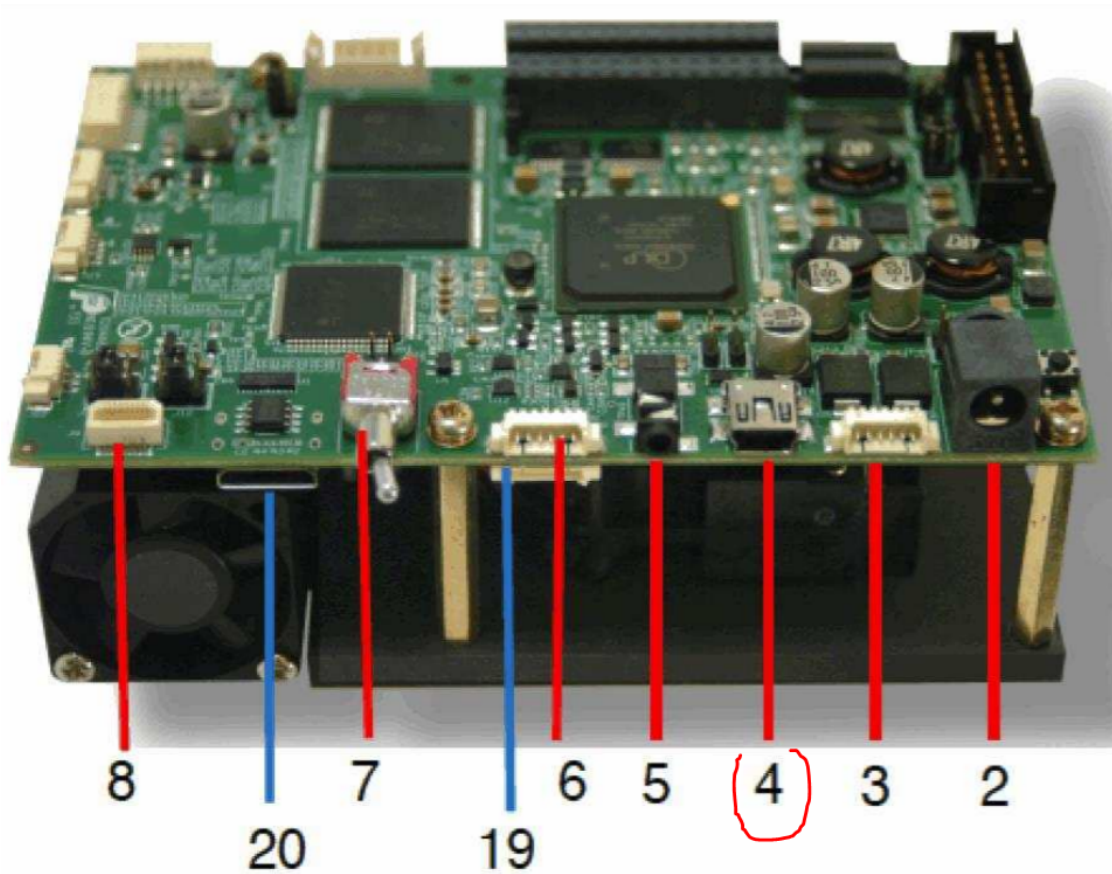
3. transform it into output image. Select 8bit
4. Firmware build: browse and locate the latest firmware



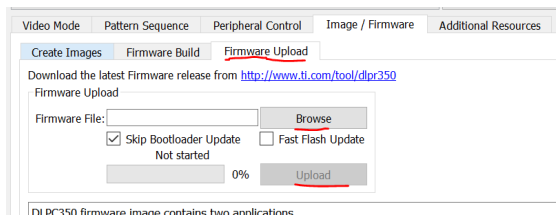
5. Delete all unwanted masks and add... your output image
6. Save updates

### Load the firmware in the DMD memory

- ▼ Connect the DMD to the computer with the USB cable  
Here it's the "4"



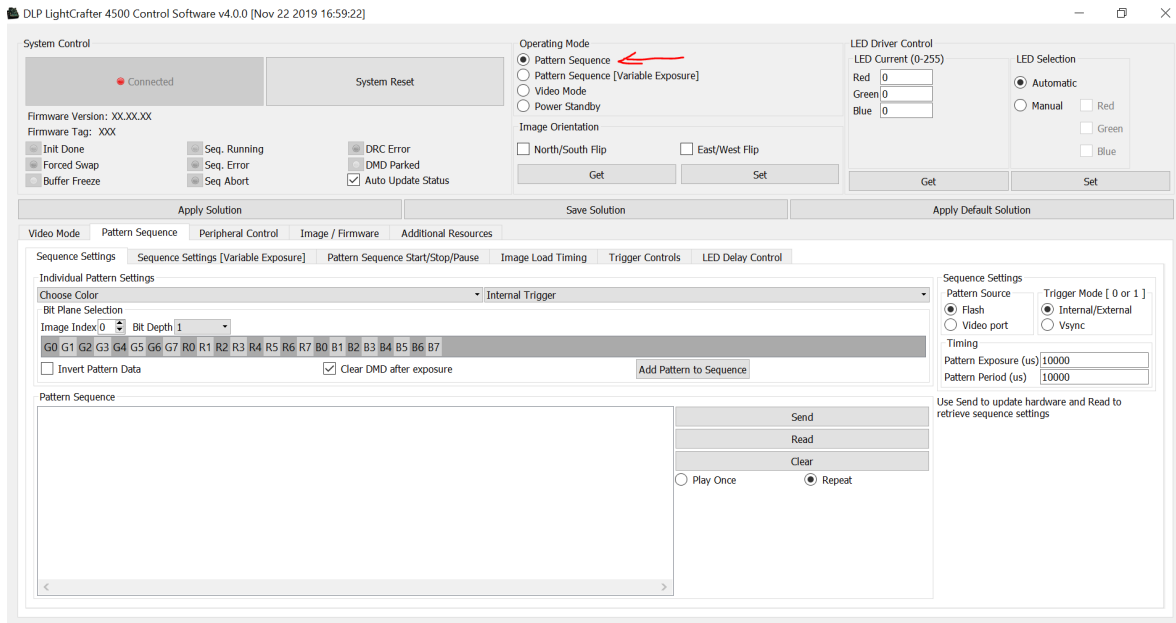
Upload the firmware in the DMD:



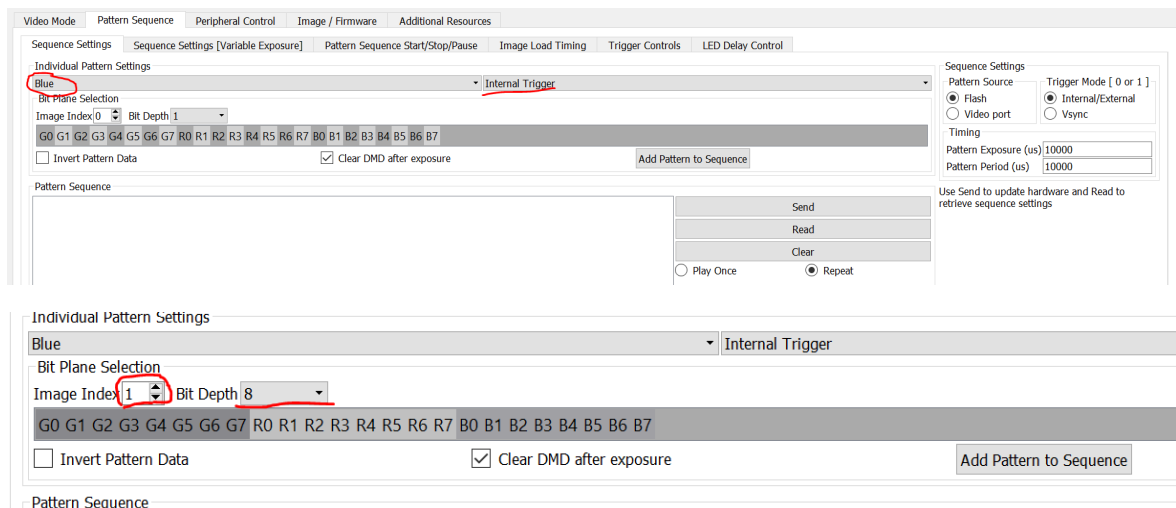
(You can save the firmware for later use)

### Load a pattern sequence in the DMD memory

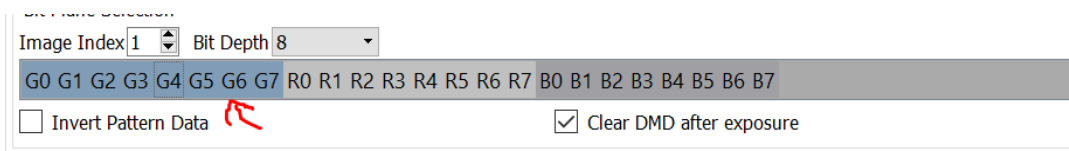
1. Go in pattern setting



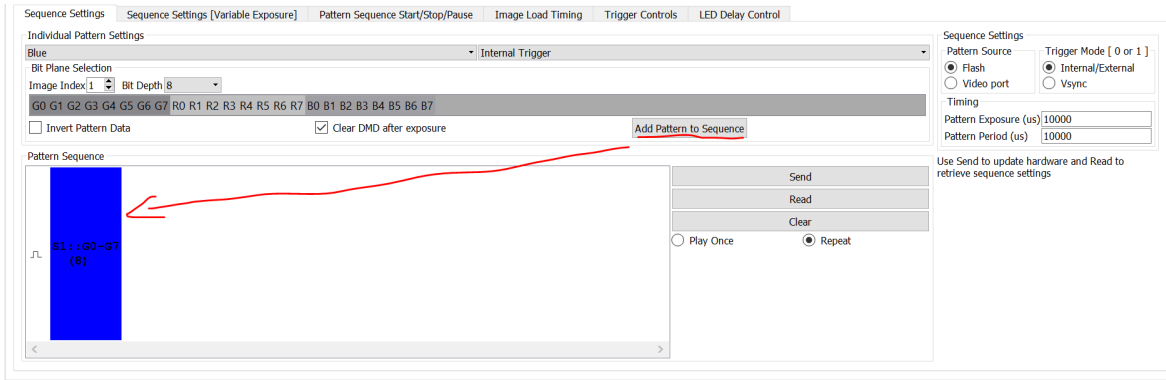
2. go in sequence setting
3. choose blue led; internal trigger (also triggered by pin J11.5/11.6)
4. Choose the number of the mask already saved in the DMD (image index) and 8 bits



5. Select the first 8 bits "G0 G1 G2 ... G7"



6. Add the pattern to sequence



7. "Send"

8. "Validate"

9. "Play once" This should turn the DMD ON with your mask

10. Stop

You can then unplug the microUSB cable connection between the DMD and the computer.

Careful: if you unplug the DMD power cable, any pattern sequence will be erase from the DMD memory

You can remove a pattern using a right click on the pattern > remove

## 2.2.2. Make microfluidic moulds (wafers)

**Authors: Sylvain Pouzet, Matthias Le Bec**

To build the mould for the microfluidic chip, we use the commonly used soft photolithography. It consists in polymerize successively multiple layers of resin onto a wafer, a flat silicon disk. This is achieved using a photopolymerizing resin and exposing it to a 2D light pattern. First, the wafer is covered with a homogeneous layer of resin using spin-coating. This is actually a crucial step as it defines the height of the layer which can be very important for the proper functioning of the chip. Then, the mask printed in step (1) is placed above the uncured resin layer using an alignment microscope, which will apply UV light through the mask for a defined duration to cure the resin. Finally, the wafer with the cured and uncured resin is washed in a solvent to remove all the uncured resin. These steps can be repeated to add more layer to the wafer. In practice, the most important aspect of these procedure was to obtain the specific layer height during the spin-coating. To achieve a targeted height, one can play with the resin viscosity and the spinning speed. While there are calibration curves that should allow to predictably obtain a certain height with a given commercial resin and a given spinning speed, this strategy did not function for us. Instead, we used a trial-and-error process, by measuring the layer height obtain on the cured resin and tuning the viscosity of the resin by varying the solvent/resin ratio, until the desired height was achieved.

A copy of the wafer mould can be made in epoxy so that multiple chips can be poured simultaneously, and to have replacement copy if the original mould is damaged.

Silanisation of the mould surface can help the proper un moulding of the chip. Such mould can be used a huge number of times with no visible changes.

Example of the mask we used:

### Prepare the machines and materials:

#### Chambers: smaller part

- EVAPORATE H<sub>2</sub>O : place the wafer on a heat plate for **5min at 120°C**
- ▼ Place in spincoater
  - Place little white board, make it turn till it fits, push and it's in
  - place the wafer at the center
  - turn on vacuum
- Add a mix of Resist 2005 and SU8 thinner (dilution ratio X or not)  
**This step has to be tune to get the right thickness ( for exemple 8mL SU8-2005 + 4mL thinner give ~3µm)**  
**Using a pipet, cover the all wafer with your mix before spinning (the coating is more uniform when the wafer is wet)**
- Calibrate and launch spin cycles: 500rpm-9-10sec ; 6000rpm-9-10sec
- **SOFT BAKE:** 2 min 95°C
- ▼ **UV exposure - 2min (or more, 2min30 seems to make cleaner results)**
  - Ask to turn on the microscope if not done
  - Place the round iron support part in the microscope
  - Place the mask on the glass filter using blue tape,
  - Place the glass filter on the metal support, plug the vacuum tube, place in the microscope
  - Place the wafer
  - Push the lever, pchhh
  - Click on WEC Settings (calibrate the contact pressure)
  - Turn ↻ till bip (increases pressure) ~16



- Turn ☞ till ok menu
  - Settings - Soft contact + align ; 2min
  - Launch exposure
  - Pull the lever
- **BAKE:** 3 min 95°C
  - develop in SU8 1min
  - Neutralize in Isopropanol 1min
  - Dry it with nitrogen gun
  - Check under the microscope: if there are cracks, but it 1-3 min onto 120°C
  - Note where the crosses are on the wafer!

## Check big channels thickness with the Dektak

Should be 3.7µm

- Turn on the dektak FIRST
- Turn on the cpu
- Place the wafer
- ▼ Window > Scan routine :
  - Length: 1000 um
  - time: 30 sec
  - meas range: 65um (otherwise risk of saturation)
  - Choose Hills and Valleys
- Check where the tip is on the wafer and change it somehow?
- On the graph, select in X where to check for the difference in height
- Close the software.

## Big channels

### ▼ Trick to avoid the stickiness of developing the crosses

Best trick so far (from Zoran, edited by Artemis): after the first layer is done, and before spreading thicker resist, protect alignment crosses with blue tape. Attention, this does not mean you simply put tape on them because unsticking it will probably remove the cross! What you need to do is for each cross, to cut two squares of blue tape, one at the size of the cross, and the other a bit larger. Then stick both (sticky part to sticky part) so you in the end obtain a piece of tape a bit larger than your cross which is sticky on the borders (to adhere to the wafer) and NON sticky over the cross (not to damage it). Remove carefully this protection after spincoating the larger resist and before other steps.

- Change the mask: **WATCH OUT** for:
  - Which motif to use
  - which face do you use
- SOFT BAKE: **3min at 65° → 6min 95°C**
- After this step the resin is supposed to not be sticky anymore

- **If you didn't use the trick:** Reveal crosses with SU8 on cotton-tige (Avoid revealing too much of the surrounding of the cross close to the design). This make the resin sticky... (maybe bake it a bit...)

▼ Alignment and UV: 4 min

This si a pain, especially when the resin is sticky. In theory:

- Turn on the transmission light (on the left next to the red button)
- push the lever, and pull the knob "cont" to "gap"
- Choose the view you want (left or right or both objectives)
- align the 2 crosses using x, y and angle knob.
- push the knob to "cont"
- Expose

In practice it's really a pain because the "gap" doesn't work if your resin is sticky, so you can play with the lever by holding it while aligning...

- **BAKE: 1min30 65°C → 6min30 95°**
- place in **SU8 developer : 6min**
- Stop in **Isopropanol : 1min**
- Blow
- Check under the microscope: if there are cracks, but it 1-3 min onto 120°C

### Check thickness with the Dektak.

Should be 50µm; use measure range ~650µm

## 2.2.3. Make microfluidics chips

**Authors: Sylvain Pouzet, Matthias Le Bec**

This step is preferably done freshly before the chip must be used, as the PDMS seems to suffer physical properties changes when stored for few days.

Dust should be avoided at all steps, and especially for the last step of irreversible adhesion with the cover slip as it can be quite sensitive to airborne particles. Typically, a particle can prevent the adhesion of the PDMS and the glass on an area, leading to undesired connection between channels and/or with the atmosphere, making the chip useless. Just before using the plasma chamber, removing dust can be done with a gas duster for the cover slip and generic scotch for the PDMS surface.

### Moulding

#### ▼ Get the moulds

- Clean them with compressed air thing

The molds are made in the white chamber - training to be taken

#### ▼ Prepare PDMS: 10 g/mould + 1/10 (1 g/mould) of durcissant: mix'em

Use the little cups just underneath the PDMS bench

- stir vigorously till it becomes whitish (like 1 minute)

#### ▼ Pour liquid PDMS/durcissant in the mould

just enough to cover the chip area + border (not too much)

#### ▼ Put under vacuum for 1 hour (removes the bubbles)

- Put mold in the bowl
- close it
- Plug tube for small vacuum pump
- launch pump
- let for one hour
- !\ TO REMOVE IT:
- stop the pump
- close the white little tap on the bowl
- take the tube out of the tap  
Be careful to hold the tap against the bowl so that it doesnt come with the tube
- Gently open tap: air gets inside
- Open the bowl

#### ▼ Let solidify: 4 hours (or O/N) at 65°C

- in the incubator just under the table on the left

### Extraction

- Let cool down at RT

#### ▼ Cut the chip out of the mould

- Gloves on
- Go to the PDMS bench, use the microfluidics pencil case
- Use scalpel, cut around on the edges of the mold

- Use the spatula to help get it out
- Pierce through using sharp home-made needle, remove the PDMS stuck inside the needle with wire, each time
- Transport in an empty petri dish

## Mounting

Has to be done for the chips, one by one.

- ▼ Get these specific 24 mm x 60 mm slides and the chip: briefly clean with compressed air



- ▼ Use tape to further clean the chip
  - Slide your fingers on the tape to make sure to capture all dust
- Place chip + slide in the plasma cleaner - the side facing upward will be the one to be stuck to mount the chip (chip up side is the one that contains the circuit).
- ▼ Use plasma cleaner / activate surfaces for sticking
  - Put slide and chip in (surfaces to be stuck together facing upwards)
  - Close the door (make sure to close it well)
  - Turn ON vacuum pump
  - Screw door
  - Prepare time for 1min10sec
  - Turn to HI on control knob
  - Turn Power ON the plasma cleaner
  - When **purple** light inside, start timer for 1min10sec.
  - Reverse order to get slide + chip out:
    - Turn Power OFF
    - Control knob back to OFF
    - Unscrew door
    - Turn OFF vacuum pump
    - Let pchhht and open the door
  - Get the stuff out
- Stick both upward surfaces together - very gently push (preferentially on the sides) to make it stick
- Let stick for 10min at 65C.
- Get out, let cool down at RT for few minutes
- Ready to use

## 2.2.4.Scikit FiniteDiff - PDE solver (Python)

**Author: Matthias Le Bec**

scikit-fdiff use Sympy

It uses *finite difference method* to discretize the spatial derivative, based on *\*method of lines\** where all the dimension of the PDE but the last (the time) is discretized. That turns the PDE in a high-dimension ODE that can be solved with standard numerical integration of ODEs.

The discretization is done in a symbolic way using `sympy`, and the exact Jacobian matrix associated with the resulting ODE is also obtained via symbolic derivation.

It should be able to deal with almost every model you will provide, but never in an optimal way.

<https://scikit-fdiff.readthedocs.io/en/latest/>

### Installation

Open an anaconda cmd and **Activate your environment**

(not mandatory)Set the python version:

```
conda install python=3.7.0
```

Install in anaconda environment:

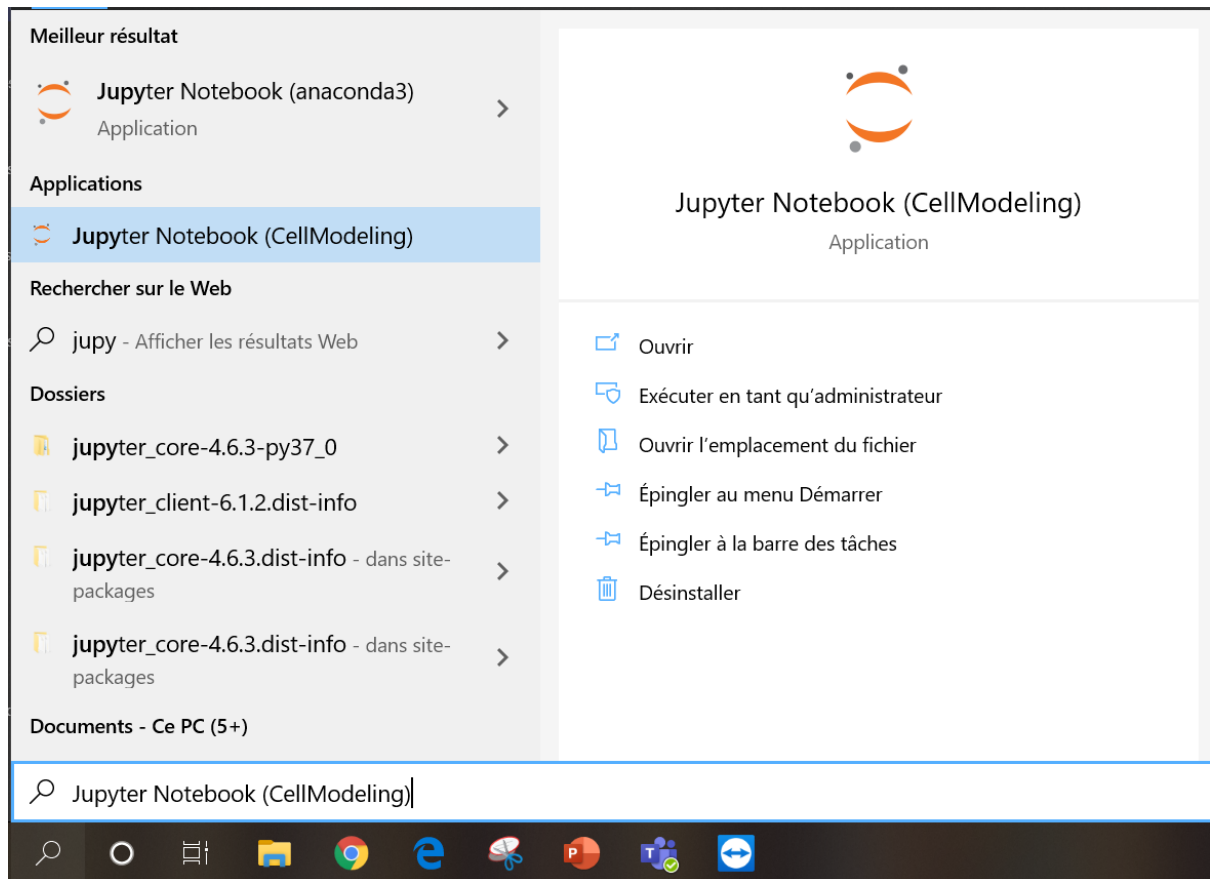
Maybe holoview need to be install as <conda install -c pyviz holoviews bokeh>

```
pip install skfdiff
pip install skfdiff --upgrade
conda install matplotlib
conda install holoviews
conda install scipy
conda install -c conda-forge ipywidgets
```

Install Numba (not mandatory but don't ask too many question):

```
conda install Numba
```

Jupyter: (in the right environment)



## Codes

### How to use it

#### Model

One variable system:

```
model = Model("k * (dxxT)-c", "T(x)", parameters=["k", "c"], boundary_conditions=bc)
```

Two variables system:

```
model = Model(["dxx(v) * dxx(u) + dyy(v) * dyy(u)",
              "dxx(v) + dxx(u) + dyy(v) + dyy(u)"],
              ["u(x, y)", "v(x, y)"],
              boundary_conditions="periodic")
```

#### Boundary conditions

- Source/sink → "dirichlet" or "T - 3" (don't know what the 3 is for)
- Reflective wall → "noflux"
- Loop → "periodic"
- Neuman (flux) → "dxT + 5" (sign + or - do opposite between left and right, 5 is the flux per dt)
- Robin (useless) → "dxT - (T - 3)"

#### What scheme ?

- Default is : "RODASPR"

Carefull because this method gives weird diffusion pattern if deltat is to big.

But adaptive time stepping is computation-free

- Euler/Crank-Nicolson ("Theta"):

Adaptive time stepping is **not** computation-free

```
simulation = model.init_simulation(initial_fields, dt=.25, tmax=1,
                                  scheme="Theta", # using a theta scheme
                                  theta=0.5) # use theta=0.5 for Crank-Nicolson.
```

## Hook - acces to parameter/variable from simul in real time

Allow to force a variable to be positive !

And allow to had non-linear term in your equation (for exemple heterogeneous degradation).

```
degmap=np.zeros(x.size)
degmap[20]=consoceLL/deltat

def degrad_hook(t, fields):
    fields["deg"] = "x", degmap
    fields["T"] = "x", np.where(fields.T <= 0, 0, fields.T) #This prevent T to go negative
    return fields
```

This will be computed every **internal time step** (refer to time stepping). If this is not mandatory to do the simulation (for exemple calculation for plotting), you can do it with a **post\_process** which only compute on the **external time step** (thus saving computation time).

(Maybe this is a way to simulate to model with two different time step: put non-linear term calculation in the post\_process instead of the hook)

## Initialisation of the simulation

### Time step

**dt** is an **external time step** (what you want in output), but the calculation are done on an **"internal time step"**.

The temporal schemes will take the user **dt** as internal time step, or use an error estimation to adapt/compute the internal time-step (which is the default behaviour, and strongly recommended)

- Adaptative internal time-step: **(not possible with Theta schemes)**

```
simulation = Simulation(model, initial_fields, dt=deltat,
                        tmax=tmax, hook=hook, time_stepping=True, tol=1e8)
```

The time step will adapt to ensure that the maximum relative error on **all fields** stay under that value.

The lower **tol** is, the slower your simulation will compute:

Start with a high value for **tol**, then decrease until the simulation doesn't want to even start

This mean that you're simulation can slow down drastically if one of your field is getting wrong, for example if you have a number of cell growing exponentially, the approximation error is also exponential (not totally sure but it's the idea).

Choose your **deltat** so that it's the biggest time step you want. This will define the maximal speed of your simulation

- Fixed internal time-step: time\_stepping=False

### Pixel value (Space step)

Mainly you need to verify this type of conditions ("the diffusion can't be faster than your timestep")

$$\Delta t < \tau \sim \frac{\Delta x^2}{D}$$

## Run simulation

```
for t, fields in simulation:
    print("time:",t/3600,"hour, S mean:" ,float(fields["S"].mean()))
```

## Data container and plot

The data (fields) of each time-steps of the simulation are concatenate in the `Container.data` that return the underlying `xarray.Dataset` .

```
container = simulation.attach_container()
hv.Dataset(container.data.C)
```

- Using holoview in Jupyter

### ▼ script

```
hmap = hv.Dataset(container.data.C).to(hv.Image, ["x", "y"])
hmap
```

- Using holoview in spyder to save result in HTML:

<https://github.com/holoviz/holoviews/issues/2885>

### ▼ script

```
import holoviews as hv
simulation = Simulation(model, initial_fields, dt=.1, tmax=1)
container = simulation.attach_container()
tmax, final_fields = simulation.run()
#container.data.T is used to acces T in the data
#hmap = hv.Dataset(container.data.T).to(hv.Curve, ["x"]) #To plot curves across time
hmap = hv.Dataset(container.data.T).to(hv.Image, ["x", "y"]) #To plot 2D maps across time
hv.renderer('bokeh').save(hmap, 'result', fmt='scrubber')
```

## Simple examples

### Example 1 - Diffusion 1D

- ▼ script A - diffusion of a drop of liquide in the middle

```
# -*- coding: utf-8 -*-
"""
Created on Wed Apr  8 14:06:49 2020

@author: matth
"""
import pylab as pl
import numpy as np
from skfdiff import Model, Simulation

bc = {"T", "x": ("dirichlet", "dirichlet")}

model = Model("k * (dxxT)", "T(x)", parameters="k", boundary_conditions=bc)

valuepixelX=1

nbrpixelX=40
```



```

x = np.linspace(0, valuepixelX*nbrpixelX, nbrpixelX) #Initialize the size of the window
T = [ 0 for i in range(nbrpixelX) ] #Initialise the field with 0
T[int(nbrpixelX/2)]=1 #Initialise the middle point of the field

initial_fields = model.Fields(x=x, T=T, k=10) #Initialise the field
#initial_fields["T"].plot()
simulation = Simulation(model, initial_fields, dt=1, tmax=10)
for t, fields in simulation:
    print("time: %g, T mean value: %g" %(t, fields["T"].mean()))
    fig = pl.figure()
    fields["T"].plot()

fig = pl.figure()
fields["T"].plot()
#last_fields["T"].plot()

```

#### ▼ script B - diffusion from source to sink

```

# -*- coding: utf-8 -*-
"""
Created on Wed Apr  8 14:06:49 2020

@author: matth
"""
import pylab as pl
import numpy as np
from skfdiff import Model, Simulation
import holoviews as hv

bc = {"T", "x": ("dirichlet", "dirichlet")}

model = Model("k * (dxxT)", "T(x)", parameters="k", boundary_conditions=bc)

valuepixelX=1 #In meter

nbrpixelX=40

x = np.linspace(0, valuepixelX*nbrpixelX, nbrpixelX) #Initialize the size of the window
T = [ 0 for i in range(nbrpixelX) ] #Initialise the field with 0
#T[int(nbrpixelX/2)]=1 #Initialise the middle point of the field
T[0]=1 #Initialise the extreme left point of the field

initial_fields = model.Fields(x=x, T=T, k=10) #Initialise the field, k is diffusion coefficient m/s ?
#initial_fields["T"].plot()
simulation = Simulation(model, initial_fields, dt=0.5, tmax=50) #Time in sec ?
container = simulation.attach_container()
for t, fields in simulation:
    print("time: %g, T mean value: %g" %(t, fields["T"].mean()))
    #fig = pl.figure()
    #fields["T"].plot()

#fig = pl.figure()
#fields["T"].plot()

hmap = hv.Dataset(container.data.T).to(hv.Curve, ["x"])
hv.renderer('bokeh').save(hmap, 'result3', fmt='scrubber')
#last_fields["T"].plot()

```

## Example 2 - Diffusion 2D

#### ▼ script A

```

# -*- coding: utf-8 -*-
"""
Created on Wed Apr  8 14:06:49 2020

@author: matth
"""
import pylab as pl
import numpy as np
from skfdiff import Model, Simulation

bc = {"T", "x": ("dirichlet", "dirichlet"), ("T", "y"): ("dirichlet", "dirichlet")}

model = Model("k * (dxxT + dyyT)", "T(x, y)", parameters="k", boundary_conditions=bc)

```

```

valuepixelX=1
valuepixelY=1
nbrpixelX=40
nbrpixelY=40

x = np.linspace(0, valuepixelX*nbrpixelX, nbrpixelX) #Initialize the size of the window
y = np.linspace(0, valuepixelY*nbrpixelY, nbrpixelY) #Initialize the size of the window

T = [ [ 0 for j in range(nbrpixelY) ] for i in range(nbrpixelX) ] #Initialise the field with 0
T[int(nbrpixelX/2)][int(nbrpixelY/2)]=1 #Initialise the middle point of the field

initial_fields = model.Fields(x=x, y=y, T=T, k=10) #Initialise the field
#initial_fields["T"].plot()
simulation = Simulation(model, initial_fields, dt=1, tmax=10)
for t, fields in simulation:
    print("time: %g, T mean value: %g" %(t, fields["T"].mean()))
    #fig = pl.figure()
    #fields["T"].plot()

fig = pl.figure()
fields["T"].plot()
#last_fields["T"].plot()

```

## 2.2.5.OptoBox (or Light Plate Apparatus)

Authors: Matthias Le Bec, Sylvain Pouzet, Erwan Eriau

Related publication:

<https://github.com/taborlab/LPA-hardware>

<https://www.nature.com/articles/srep35363>

<http://taborlab.github.io/iris/>

The LPA or Optobox is a device that can perform light activation experiments on 24-well plate. You can have maximum 2 different LEDs per well (top and bottom). You can not go below 1s of time resolution.

**To convert the input in irradiance (exemple):  $4000 \times 0,0007 = 2,8\text{mW/cm}^2$**

▼ How to build and set up the Optobox (more details are in the original publication)

- 3D printed parts can be found in the original publication.
- Place all the LED sockets in the "LEDSpacer" 3D pinte part
- Solder the LED sockets to the board
- 5V should be used every time.

▼ Program the board:

You need a "AVR microcontroller programmer". We use a "AVRISP mkII programmer"

You have two options to flash the board: use the precompiled file (.elf) or compile your own file (you will have to do it to calibrate the clock of the microcontroller but its optional)

▼ Compile your own file (optional, you can use the precompiled version)

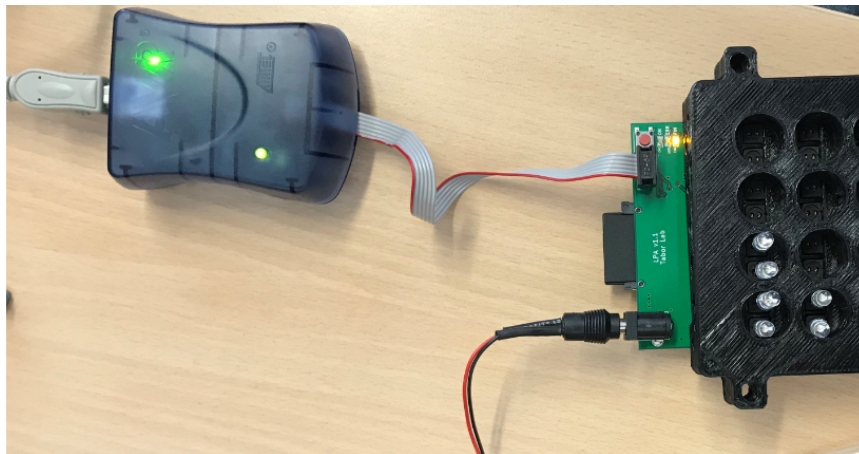
Use an old Arduino IDE: 1.6.0 works !!!

▼ Flash the board

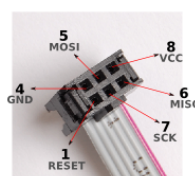
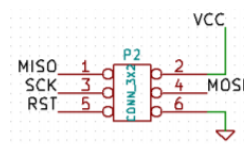
1. Install Atmel Studio (if not already done) (now it's called "Microchip Studio")

<https://www.microchip.com/en-us/development-tools-tools-and-software/microchip-studio-for-avr-and-sam-devices#Downloads>

2. Connect your programmer to your computer and the Optobox board. Power the Optobox too.

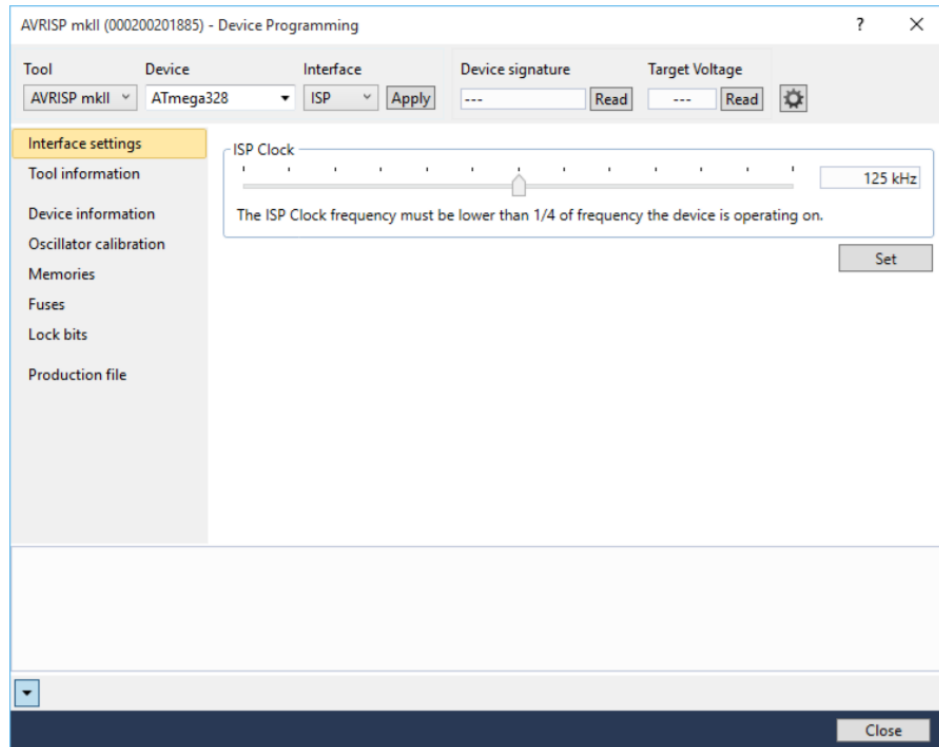


▼ Details



- On Atmel Studio, go to Tools -> Device Programming. Select "AVRISP mkII" under "programmer", select "ATmega328" under "Device" and "ISP" under "Interface". Click on the "Apply"

▼ Details



- Click on the "Read" button, the "Device signature" box should be filled, the "Target voltage" should be 3.3V.
- If it's the first time the new device is programmed: select "Fuses" from the list. Disable CKDIV8, enable CKOUT, set SUT\_CKSEL box to EXTOSC\_8MHZ\_XX\_1KCK\_14CK\_65MS. Click on the "Program". Fuse warning window is ok, click on "continue"
- Select "Production file" from the list, click on the "..." button, locate you file "firmware.elf".
- Activate "Flash", "Erase memory before programming", and "Verify programmed content" checkboxes, and click on the "Program" button.
- The messages "Erasing device... OK", "Programming Flash...OK", and "Verifying Flash...OK" should appear below.  
If not: just try a second time to click on "Program" and/or on "Verify"

We had this error message: "Verifying Flash...Failed! address=0x0000 expected=0x0c actual=0x00" but we just clicked on "Program" a second time and it worked.

#### ▼ Calibrating LEDs

LED compensation is achieved by setting the grayscale and dot correction for each LED. Grayscale and dot correction values are stored on the device's SD card as files "gcal.txt" and "dc.txt", respectively, and must be space delimited integers from 0-255 and 0-63, respectively.

Coarse adjustments can be made by setting the LED dot correction (useful during calibration to set ALL LEDs to the range of the spectrometer), while

fine

adjustments can be made setting the gray scale value (use to calibrate each LED independently).

There are different methods:

Image analysis method or Probe spectrometer method.

At the end you will need to measure the photon flux with the Probe spectrometer for both.

Or we can use a power meter.

### For simplicity we use the thorlabs power meter + S120C sensor

You should use a 3D printed adaptor to make the sensor alignment more reproducible

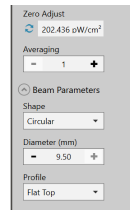
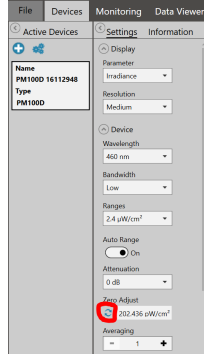
The basic idea is to trace irradiance= $f(\text{LED input})$  for each LED and get the rate. Then we will modify the dcal.txt depending on the rate of each LED. The following procedure is semi-automated in order to go faster.

To do so you need to create a protocol in the iris software so all the top LEDs increase in intensity every seconde in the following order: 10,50,100,300,600,1000,2000,3000,4000 (you will do the same for the bottom LEDs independently)

Load your optobox with the file

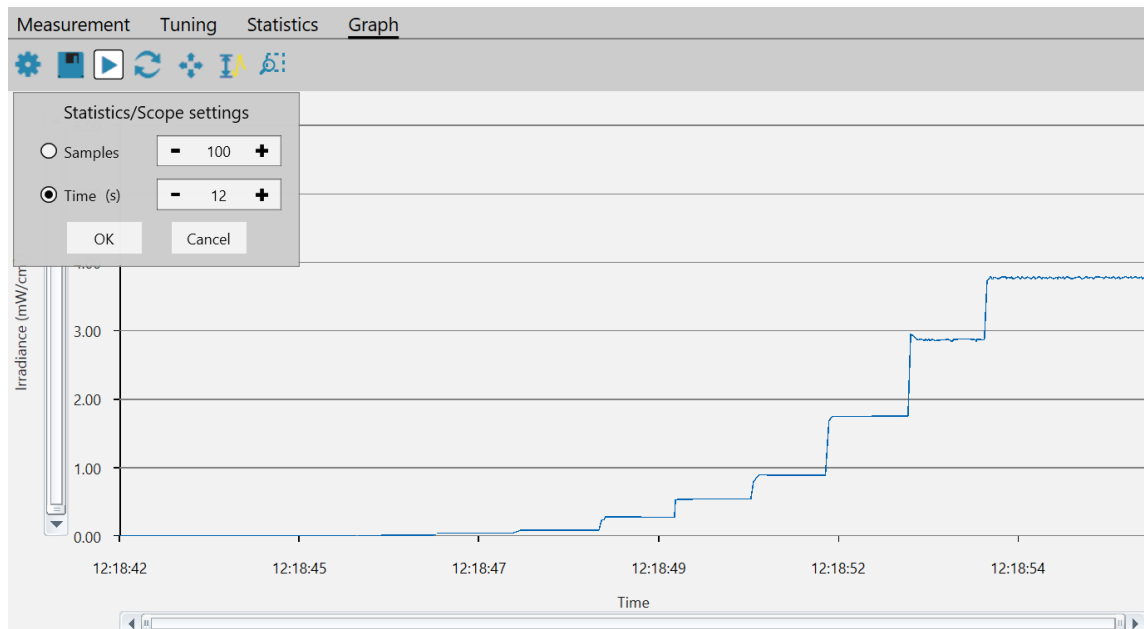
Power meter parameters:

- Install Thorlabs software : [https://www.thorlabs.com/software\\_pages/ViewSoftwarePage.cfm?Code=OPM](https://www.thorlabs.com/software_pages/ViewSoftwarePage.cfm?Code=OPM)
  - Plug the S120C sensor in the PM100D, and plug the PM100D to your computer.
  - Close the sensor and set the zero, and use the following parameters:
- ▼ Parameters



On the software

In Device, go to Graph  
set 12s (gear icon):



Put the sensor in the adaptor

Push the reset button on the optobox, 1 sec later reset the Graph measurement

After 12 sec stop the measure (make sure to have a similar profil see above) and save with the name of the LED, ex: "TA5" top A5, "BD6" bottom D6

→ Play with play, pause (when the graph is in the frame), save, reset on optobox, play, pause, save, reset etc.

When you have done every LED (24 top then 24 bottom):

- ▼ Python script

```

import pandas as pd
from scipy import stats
import numpy as np

"""t0=df['Time'][0]
print(t0[6:19])
t0sec=float(t0[6:19])+60*float(t0[3:5])
print(t0sec)"""

TopLED=[None]*6,[None]*6,[None]*6,[None]*6
BottomLED=[None]*6,[None]*6,[None]*6,[None]*6
TopLEDnorm=[None]*6,[None]*6,[None]*6,[None]*6
BottomLEDnorm=[None]*6,[None]*6,[None]*6,[None]*6
L=''
ligne=0
for L in 'ABCD':#the 4 rows of the optobox
    file=''
    ligne+=1
    column=1
    for column in range(1,7):#the 6 column of the optobox
        file='T'+L+str(column)+'.csv'
        print(file)
        df = pd.read_csv(file, sep=';', header=4, names=['Date', 'Time', 'Irradiance'])
        #header=4 is used to ignore the 4 first row
        #names= is used to rename the columns
        i=0
        v1=.0
        v2=.0
        valreel=[]
        last=.0
        for i in range(0,1100,5):#read in the file every 5 value
            v2=v1
            v1=float(df['Irradiance'][i])#read the value
            if v1>:.1:#this will round the value to get only 2 significant digits
                v1=round(v1,1)
            elif v1>0.1:
                v1=round(v1,2)
            elif v1>0.01:
                v1=round(v1,3)
            if v1==v2 and (v1>(last+0.2*last) or v1<(last-0.2*last)):#compare 2 values, and check if it hasn't been already stored
                valreel+=float(df['Irradiance'][i])#store the irradiance value
                last=v1

        print(valreel)
        lr = stats.linregress([10,50,100,300,600,1000,2000,3000,4000], valreel)#do a linear regression between the LED input and the stored irradiance values
        TopLED[ligne-1][column-1]=lr[0]#store the rate
        print(lr)
        if lr[2]<0.95:#check is the regression is correct
            print('Bad fit ',file,', r2=',lr[2])
    ligne=0
    for L in 'ABCD':#the 4 rows of the optobox
        file=''
        ligne+=1
        column=1
        for column in range(1,7):#the 6 column of the optobox
            file='B'+L+str(column)+'.csv'
            print(file)
            df = pd.read_csv(file, sep=';', header=4, names=['Date', 'Time', 'Irradiance'])
            #header=4 is used to ignore the 4 first row
            #names= is used to rename the columns
            i=0
            v1=.0
            v2=.0
            valreel=[]
            last=.0
            for i in range(0,1100,5):#read in the file every 5 value
                v2=v1
                v1=float(df['Irradiance'][i])#read the value
                if v1>:.1:#this will round the value to get only 2 significant digits
                    v1=round(v1,1)
                elif v1>0.1:
                    v1=round(v1,2)
                elif v1>0.01:
                    v1=round(v1,3)
                if v1==v2 and (v1>(last+0.2*last) or v1<(last-0.2*last)):#compare 2 values, and check if it hasn't been already stored
                    valreel+=float(df['Irradiance'][i])#store the irradiance value
                    last=v1

            print(valreel)
            lr = stats.linregress([10,50,100,300,600,1000,2000,3000,4000], valreel)#do a linear regression between the LED input and the stored irradiance values
            BottomLED[ligne-1][column-1]=lr[0]#store the rate
            print(lr)
            if lr[2]<0.95:#check is the regression is correct
                print('Bad fit ',file,', r2=',lr[2])

print('TOP:',TopLED)
print('BOTTOM:',BottomLED)

#A1=pd.DataFrame({'Irr':valreel})
#A1.to_csv('valreel.csv')

#Compute value (255 etc) for Normalisation
#minimum=min([item for sublist in [[item for sublist in TopLED for item in sublist], [item for sublist in BottomLED for item in sublist]]
# for item in sublist]) #Finds the minimum value in bottom&top #[item for sublist in ttop for item in sublist] #min()

minimum=0.0007 #we choose this rate value to calibrate all optobox
#a=minimum*255
#TopLEDnorm=[a/x for x in TopLED]
#BottomLEDnorm=[a/x for x in BottomLED]
de = pd.read_csv('gcal.txt', sep='\t', header=-1)
ligne=0
column=0
for ligne in range(0,4):#the 4 rows of the optobox
    for column in range(0,6):#the 6 column of the optobox
        t=minimum*de[column*2][ligne]
        b=minimum*de[column*2+1][ligne]
        TopLEDnorm[ligne][column]=int(round(t/TopLED[ligne][column]))
        BottomLEDnorm[ligne][column]=int(round(b/BottomLED[ligne][column]))

```

```
#testt=[[i[0] for i in TopLEDnorm], [i[0] for i in BottomLEDnorm]]
testt=[]
for x in [0,1,2,3,4,5]:
    testt.extend([[i[x] for i in TopLEDnorm], [i[x] for i in BottomLEDnorm]])
testt=list(map(list, zip(*testt)))#invert the matrix
np.savetxt("newgcal.txt", testt, delimiter="\t", newline='\r\n', fmt='%s')
# /!\ RAJOUTER 3 CARRIAGE RETURNS A LA MAIN APRES DANS LE FICHIER LA OU LES CHIFFRES N ONT PAS ETE SEPARES
```

If the script does not work, try to modify the range function according to the lowest column number in your excel files. Furthermore, if it the matrix does not fit, you should increase the range because you are missing values. Remember to modify it for the bottom analysing code too. CHECK IF YOUR .CSV ARE SAVED IN mW and not in  $\mu$ W

Run the python script in the same folder as your 48 files, it will automatically create a newgcal.txt file.

In the script, you should typically find a rate (slopes) of  $\sim 0.0009$ . Some LED should be over or under this value. We calibrated each LED to get a final rate of 0.0007. To do so we simply did  $(0.0007 \times 255) / (\text{rate calculated by script}) = \text{new value of grayscale entered in the new gcal.txt file}$ .

You should get  $\sim 2.1 \text{mW}$  at 4000

Detector diameter=0.95cm || Area = 0.71cm<sup>2</sup>

Figure to help you:

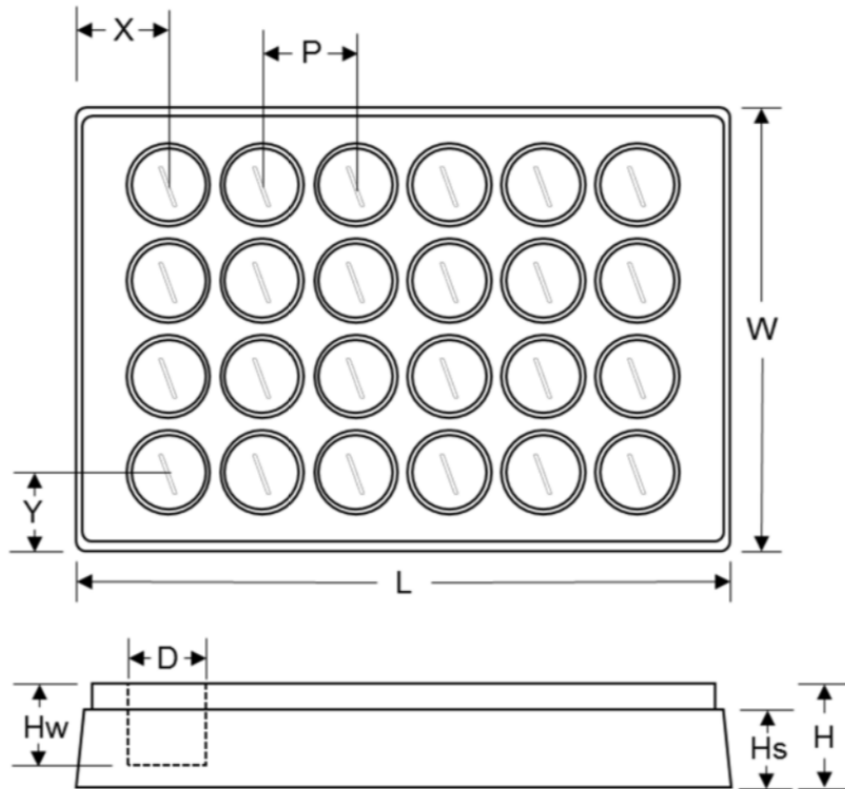
Fichier	Edition	Format	Affichage	?										
255	255	255	255	255	255	255	255	255	255	255	255	255	255	A
255	255	255	255	255	255	255	255	255	255	255	255	255	255	B
255	255	255	255	255	255	255	255	255	255	255	255	255	255	C
255	255	255	255	255	255	255	255	255	255	255	255	255	255	D
TOP Bottom		TOP Bottom		TOP Bottom		TOP Bottom		TOP Bottom		TOP Bottom		TOP Bottom		
1		2		3		4		5		6				

▼ Time calibration

(We checked two optoboxes for  $\sim 20$ h and the time was already calibrated)

▼ Which well plate ?

- The sup data of the optobox paper recommend the 24-well culture plate (AWLS-303008, ArcticWhite LLC). But they're shipped from the US, expensive and too much shipping fees.
  - Required dimensions



$X = 19.00 \pm 0.05$	$Y = 16.00 \pm 0.05$	$Hw = 18.45 \pm 0.05$
$P = 18.00 \pm 0.05$	$L = 127.90 \pm 0.1$	$Hs = 15.00 \pm 0.1$
$W = 85.85 \pm 0.1$	$D = 15.00 \pm 0.05$	$H = 20.00 \pm 0.05$

- We are using eppendorf ones, but they stopped to produce this model.

(Plastic film bottom instead of a coverglass bottom)

▼ Dimensions

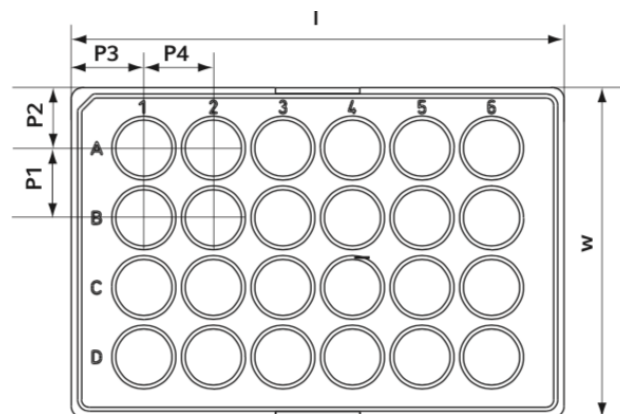




**Plate dimensions [mm]**

Length		Width		Height			
l	l1	w	w1	h	h1	fh	
127.8	124.2	85.5	82.0	15.0	0,4	9.3	
Well dimensions [mm]				Positions of well center [mm]			
Diameter		Thickness	Depth				
d	d1	bt	h2	P1	P2	P3	P4
14.5	13.2	Glass: 0.17 Foil: 0.025	14.6	18.0	15.7	18.9	18.0

## ▼ Launch an experiment:

<http://taborlab.github.io/iris/>

Iris then generates a zip file containing i) a device-readable binary file (.lpf) used to run the LPA, ii) a session file for reloading a program into Iris at a later time, and iii) a CSV file containing user-readable well randomization information.

The .lpf is then transferred to an SD card, which is inserted into the LPA (Optobox), and the Reset Button is pressed to run the light program.

## 3.2. Modelling script

# YeastOnSucroseAgar(1D)\_Coop-Cheat

This script use a PDE solver (scikit-fdiff) to resolve numerically the 1D diffusion equation. For the sucrose degradation, we use an hook in the PDE solver to acces and modify the concentration while the simulation run. There are no cell movement.

To run this script, you need several packages (skfdiff,numpy,holoviews,csv). You can also use the Anaconda environment containing all the necessary packages: <https://anaconda.org/matthias.lebec/CellModeling/files> (<https://anaconda.org/matthias.lebec/CellModeling/files>).

## Import packages

In [ ]:

```
import numpy as np
from skfdiff import Model, Simulation
from skfdiff import display_fields, enable_notebook #for display in realtime
from skfdiff import Container #to retrieve from disk
import holoviews as hv
enable_notebook()
import csv
```

## Define variables

In [ ]:

```
pixelvalue=0.0001 #0.1mm [m]
sizeX=0.045 #[m]
nbrpixelX=int(sizeX/pixelvalue)

sizeZ=0.00235 #[m]
toplayerthickness=0.00067 #[m] 0.67mm
ratiolayers=toplayerthickness/sizeZ

tol=1e1 #error tolerance for numerical method
deltat=2 #in sec ; time step for numerical resolution
tmax=60*60*85 #in sec ; total time to compute
containerpath="D:/Matthias_LE_BEC/Modelling/Python/" #path to save the simulation results
containerid="TestGitHub_1" #name for the simulation
```

In [ ]:

```
#Diffusion coefficient in water: at 30°C
kM=7.6e-10 #m²/s
kS=6.1e-10 #m²/s

KmE=0.026 #Km of Invertase
Kcat=4700 #Kcat of Invertase
umax=0.27 #/h ; maximal yeast growth rate
umax = umax/3600 #in sec
Ks=0.00012 #Monod constant for yeast
Kalpha=0.00001 #Arbitrary Hill coeff for Invertase production
Death = 0 #Death rate
Vmax1=(167e-6/60)*(15e-12) #Mich.Ment. coeff for glucose consumption
Vmax2=(104e-6/60)*(15e-12) #Mich.Ment. coeff for glucose consumption
Km1=0.0008 #Mich.Ment. coeff for glucose consumption
Km2=0.021 #Mich.Ment. coeff for glucose consumption

print("Stability evaluation: delta t=",deltat," should be < " , pixelvalue*pixelvalue/k
M)
```

In [ ]:

```
M0=0.00000001 #[M] ; Initial monomers concentration(Glu+Fruct) 0.005% = 0.00027M
S0=0.02921 #[M] ; Initial sucrose concentration 1% = 0.029M
E0=1e-35 #[M] ; Initial enzyme concentration
alphacheat=1.5e-25 #Invertase production rate[mol/s/cell] this is typically 1e-24 in WT
alphacoop=1.8e-24 #Invertase production rate[mol/s/cell] this is typically 1e-24 in WT

S0=S0*(1-ratiolayers) #take into account that sucrose is not in the whole thickness

CellD=1e13 #initial number of cell per m³
CellD0=CellD/1000 #initial number of cell per L
CellD0=CellD0*ratiolayers #take into account that cell are not in the whole thickness
```

In [ ]:

```
#Initialising the fields
x = np.linspace(0, pixelvalue*(nbrpixelX-1), nbrpixelX) #Initialize the size of the window
M = [ M0 for i in range(nbrpixelX) ] #Initialise the field M with M0
S = [ S0 for i in range(nbrpixelX) ] #Initialise the field S with S0
En = [ E0 for i in range(nbrpixelX) ] #Initialise the field E with E0
alpha = [ alphacheat for i in range(nbrpixelX) ] #Initialise the field alpha with alpha cheat
d = np.zeros(x.size)#Initialise the field with 0
Q= np.zeros(x.size)#Initialise the field with 0
I= np.zeros(x.size)#Initialise the field with 0
tracker= np.zeros(x.size)#Initialise the field with 0
for i in range(nbrpixelX):
    d[i]=CellID0

#Create the location of the cooperators:
listcoop=[]
center=int((nbrpixelX-1)/2)
ratioCoop=0.25 # area ratio of cooperator
pixelDMDsize=0.35e-3 #in meter ; size of one DMD pixel when projected on the surface
Wavelength=16*pixelDMDsize #in meter ; the light pattern wavelength
wl=Wavelength/pixelvalue #in pixel ; the light pattern wavelength

LightIntensity=1 #between 0 and 1
alphacoop=alphacheat+(alphacoop-alphacheat)*LightIntensity #compute alphacoop based on the light intensity: linearly

#Setup the light pattern
#Fill the listcoop
linecount=0
for i in range(nbrpixelX): # this is basically the blue pattern
    j=i-linecount*wl #This shift i depending on the number of the pattern
    if (j>(1-ratioCoop)*wl)&(j<=wl):
        listcoop+= [i]
    if (j>wl):
        linecount+=1

#Fill the illuminated pixel with the invertase production rate alphacoop
for i in listcoop:
    alpha[i]=alphacoop
```

## Define PDE model

In [ ]:

```
model = Model(["kM * (dxxM) - Q + 2*I",
              "kS * (dxxS) - I",
              "alpha* (M/(Kalpha+M))*d",
              "umax * (M/(Ks+M)) * d - Death*d"],
              ["M(x)", "S(x)", "En(x)", "d(x)"],
              parameters=["kM", "kS", "umax", "Ks", "Kalpha", "Death", "Q(x)", "I(x)", "alpha(x)"],
              boundary_conditions="noflux")
```

## Hook

In [ ]:

```
def degrad_hook(t, fields):
    fields["M"] = ("x"), np.where(fields.M <= 0, 0, fields.M) #This prevent M to go negative
    fields["S"] = ("x"), np.where(fields.S <= 0, 0, fields.S) #This prevent S to go negative
    fields["En"] = ("x"), np.where(fields.En <= 0, 0, fields.En) #This prevent En to go negative
    fields["d"] = ("x"), np.where(fields.d <= 0, 0, fields.d) #This prevent d to go negative
    fields["Q"] = ("x"), (Vmax1*fields.M/(Km1+fields.M)+Vmax2*fields.M/(Km2+fields.M))*
    fields.d #Computing the glucose consumption
    fields["I"] = ("x"), fields.En*Kcat*fields.S/(KmE+fields.S) #Computing the invertase activity
    return fields
```

## Initialize simulation

In [ ]:

```
initial_fields = model.Fields(x=x, M=M, S=S, d=d, kM=kM, kS=kS, umax=umax, Ks=Ks, Kalpha=Kalpha,
    Death=Death, Q=Q, I=I, En=En, alpha=alpha) #Initialise the field, k is diffusion coefficient m/s ?

###Here you have the tolerance setting, very important for the script computation time
simulation = Simulation(model, initial_fields, dt=deltat, tmax=tmax, hook=degrad_hook, scheme="Theta",
    theta=0.5, time_stepping=True, tol=tol, id=containerid)
container = simulation.attach_container(containerpath, force=True)
```

## If you want to plot in real time while simulation is running

In [ ]:

```
enable_notebook()
#display_fields(simulation)
```

## Run the simulation

In [ ]:

```
for t, fields in simulation:
    print("- time step:", t/3600, "hour, S mean:" , float(fields["S"].mean()), ", M mean:" ,
    float(fields["M"].mean()))
    print("Q mean:" , float(fields["Q"].mean()), "I mean:" , float(fields["I"].mean()))
    print("time since simulation start:", simulation.timer.total)
    #fig = pl.figure()
    #fields["C"].plot()
```

In [ ]:

```
simulation.timer.total #Print the total computation time
```

In [ ]:

```
container = Container.retrieve(containerpath+containerid) #Recover the container data stored in the disk
```

## Plot the result

In [ ]:

```
from xarray import concat, open_dataset, open_mfdataset
from path import Path
```

In [ ]:

```
path=Path(containerpath+containerid)
```

### For very big data:

In [ ]:

```
# listdataset=[]
# previousframe=0

# i=0
# for filename in path.files("data*.nc"):
#     print(filename)

#     listdataset+= [open_dataset(filename).isel(t=[0])] #This take only the first timepoint of each data*.nc file
```

### For normal data:

In [ ]:

```
listdataset=[]
previousframe=0

i=0
for filename in path.files("data*.nc"):
    #print(filename)

    listdataset+= [open_dataset(filename)]
```

In [ ]:

```
alldata = concat(listdataset,dim="t").sortby("t")
```

In [ ]:

```
skipframe=1000# the number of time frame you want to skip for the plotting in addition o
f the first sampling
start=0
end=150000
```

In [ ]:

```
hv.output(max_frames=1001) #Tune this "protection"
data=alldata.isel(t=slice(start,end,skipframe))
```

## Plotting:

In [ ]:

```
skipx=10 # the number of x position you want to skip for the plotting
```

In [ ]:

```
dprofil = hv.Dataset(data.d).to(hv.Curve, ["x"])
dprofil
```

In [ ]:

```
dcurve = hv.Dataset(data.d.sel(x=data.x[range(0,len(data.x),skipx)])).to(hv.Curve, ["t"
])
dcurve
```

In [ ]:

```
Mcurve = hv.Dataset(data.M.sel(x=data.x[range(0,len(data.x),skipx)] )).to(hv.Curve, [
"t"])
Mcurve
```

In [ ]:

```
Sprofil = hv.Dataset(data.S).to(hv.Curve, ["x"])
Sprofil
```

In [ ]:

```
Mprofil = hv.Dataset(data.M).to(hv.Curve, ["x"])
Mprofil
```

## Save the result in holoview

In [ ]:

```
AllPlot_t=(Sprofil+Mprofil+dprofil).cols(3)
AllPlot_x=(Mcurve+dcurve).cols(2)
hv.renderer('bokeh').save(AllPlot_t, containerid+'AllPlot_t', fmt='scrubber')
hv.renderer('bokeh').save(AllPlot_x, containerid+'AllPlot_x', fmt='scrubber')
```



## Save the result in csv

In [ ]:

```
path = Path('C:/Users/Mathias/Documents/Python Scripts/SucroseGrowthYeast/'+containerid
)
try:
    path.mkdir()
except:
    print("already existing folder")
```

In [ ]:

```
###d

variablename="d"
with open(path+"/"+containerid+"_"+variablename+".csv", mode='w',newline='') as csv_file:
    csv_writer = csv.writer(csv_file, delimiter=',', quotechar='')
    listx=[]
    for x in data.x.values:
        listx+=x
    csv_writer.writerow(["time"]+listx)
    c=0
    for i in data.t.values:
        listinx=[]
        for j in data.d.sel(t=i).values:
            listinx+=j
        csv_writer.writerow([i]+listinx)
        c+=1
```

In [ ]:

```
###M

variablename="M"
with open(path+"/"+containerid+"_"+variablename+".csv", mode='w',newline='') as csv_file:
    csv_writer = csv.writer(csv_file, delimiter=',', quotechar='')
    listx=[]
    for x in data.x.values:
        listx+=x
    csv_writer.writerow(["time"]+listx)
    c=0
    for i in data.t.values:
        listinx=[]
        for j in data.M.sel(t=i).values:
            listinx+=j
        csv_writer.writerow([i]+listinx)
        c+=1
```

In [ ]:

```
###S
variablename="S"
with open(path+"/"+containerid+"_"+variablename+".csv", mode='w',newline='') as csv_file:
    csv_writer = csv.writer(csv_file, delimiter=',', quotechar='')
    listx=[]
    for x in data.x.values:
        listx+=x
    csv_writer.writerow(["time"]+listx)
    c=0
    for i in data.t.values:
        listinx=[]
        for j in data.S.sel(t=i).values:
            listinx+=j
        csv_writer.writerow([i]+listinx)
        c+=1
```

In [ ]: